
JSCSEN 77(4)407–567(2012)

ISSN 1820-7421 (Online)

Journal of the Serbian Chemical Society



VOLUME 77

No 4

BELGRADE 2012

Available on line at



www.shd.org.rs/JSCS/

The full search of JSCS

is available through

DOAJ DIRECTORY OF

OPEN ACCESS

JOURNALS

www.doaj.org



CONTENTS

Organic Chemistry

- K. Tabatabaeian, H. Heidari, A. Khorshidi, M. Mamaghani and N. O. Mahmoodi: Synthesis of biscoumarin derivatives by the reaction of aldehydes and 4-hydroxycoumarin using ruthenium(III) chloride hydrate as a versatile homogeneous catalyst ... 407
M. Nasr-Esfahani, M. Montazerozohori and N. Filvan: Ultrasound-assisted catalytic synthesis of acyclic imides in the presence of *p*-toluenesulfonic acid under solvent-free conditions (Short communication) ... 415

Biochemistry and Biotechnology

- T. Riaz, M. A. Abbasi, A.-Ur-Rehman, T. Shahzadi, M. Ajaib and K. M. Khan: Phytochemical screening, free radical scavenging, antioxidant activity and phenolic content of *Dodonaea viscosa* Jacq. ... 423
L. Zeng and L. L. P. Vrijmoed: Antioxidant activities and phenolic constituents of *Cephalotaxus oliveri* Mast. aerial parts ... 437

Inorganic Chemistry

- G. H. Bindu and G. N. Rao: Mixed ligand complexes of essential metal ions with L-glutamine and succinic acid in sodium dodecyl sulfate–water mixtures ... 453

Physical Chemistry

- J. Mitrović, M. Radović, D. Bojić, T. Andelković, M. Purenović and A. Bojić: Decolorization of the textile azo dye Reactive Orange 16 by the UV/H₂O₂ process ... 465

Electrochemistry

- L.-H. Liu, C.-Q. Duan and Z.-N. Gao: Electrochemical behavior and electrochemical determination of carbamazepine at an ionic liquid modified carbon paste electrode in the presence of sodium dodecyl sulfate ... 483

Materials

- Č. Jovalekić, A. S. Nikolić, M. Gruden-Pavlović and M. B. Pavlović: Mechano-chemical synthesis of stoichiometric nickel and nickel–zinc ferrite powders with Nicolson–Ross analysis of the absorption coefficients ... 497

Thermodynamics

- M. V. Rathnam, S. Mohite and M. S. Kumar: Volumetric, viscometric and optical study of molecular interactions in binary mixtures of diethyl malonate with ketones at 303.15, 308.15 and 313.15 K ... 507

Chemical Engineering

- M. Vasić, Z. Radojević and Ž. Grbavčić: Calculation of the effective diffusion coefficient during the drying of clay samples ... 523

Environmental

- B. P. Dojčinović, G. M. Roglić, B. M. Obradović, M. M. Kuraica, T. B. Tosti, M. D. Maršović and D. D. Manojlović: Decolorization of Reactive Black 5 using a dielectric barrier discharge in the presence of inorganic salts ... 535

- K. Tálos, T. Pernyeszi, C. Majdik, A. Hegedűsóva and C. Páger: Cadmium biosorption by baker's yeast in aqueous suspensions ... 549

- EuCheMS News* ... 563

Published by the Serbian Chemical Society
Karnegijeva 4/III, 11000 Belgrade, Serbia

Printed by the Faculty of Technology and Metallurgy
Karnegijeva 4, P.O. Box 35-03, 11120 Belgrade, Serbia



Synthesis of biscoumarin derivatives by the reaction of aldehydes and 4-hydroxycoumarin using ruthenium(III) chloride hydrate as a versatile homogeneous catalyst

KHALIL TABATABAEIAN*, HANNANEH HEIDARI, ALIREZA KHORSHIDI,
MANOUCHEHR MAMAGHANI and NOSRAT O. MAHMOODI

Department of Chemistry, Faculty of Sciences, University of Guilan,
P. O. Box 41335-1914, Iran

(Received 27 April, revised 6 October 2011)

Abstract: The one-pot domino Knoevenagel-type condensation/Michael reaction of aromatic, heteroaromatic and aliphatic aldehydes with 4-hydroxycoumarin in aqueous media in the presence of ruthenium salt as homogeneous catalyst was investigated. It was found that 5 mol % of $\text{RuCl}_3 \cdot n\text{H}_2\text{O}$ catalyzes biscoumarin synthesis in high yields (70–95 %) under optimized, mild, green and environmentally benign reaction conditions in short times (25–35 min).

Keywords: ruthenium; biscoumarin; aldehyde; 4-hydroxycoumarin; homogeneous catalyst; condensation reaction.

INTRODUCTION

Coumarin derivatives have received considerable attention because of their biological importance and numerous pharmacological activities. Some coumarin derivatives, in general, and biscoumarins, in particular, are known for their anti-fungal, anti-HIV, anticancer, antithrombotic, anticoagulant, antimicrobial and antioxidant,^{1–4} urease inhibitory,⁵ cytotoxicity and enzyme inhibitory activities.⁶ In addition, their optical and fluorescence emission properties have already been studied.^{7,8} Although some types of these compounds could be isolated from plants, for example 7,7'-dihydroxy-6,6'-dimethoxy-3,3'-biscoumarin from *Erycibe obtusifolia*,⁹ attempts have been made to use alternative catalysts for biscoumarin synthesis. In 1999, Hagiwara *et al.* reported the use of Et_2AlCl as a Lewis acid for the condensation of 4-hydroxycoumarin and aldehydes in acetonitrile or dichloromethane at room temperature in moderate to good yields (40–80 %).¹⁰ Later, other researchers reported a similar reaction using piperidine,⁵ molecular iodine,¹¹ tetrabutylammonium bromide (TBAB),¹² heteropolyacids,¹³ phospho-

* Corresponding author. E-mail: Taba@gilan.ac.ir
doi: 10.2298/JSC110427189T

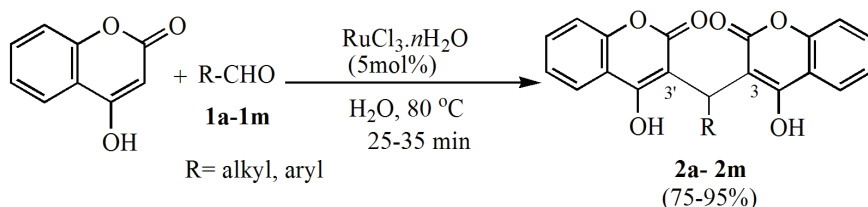
tungstic acid¹⁴ and sodium dodecyl sulfate (SDS)¹⁵ as catalysts. A number of catalyst-free condensation reactions under thermal and microwave irradiation,^{1d,16–18} heating in ionic liquid 1-butyl-3-methylimidazolium tetrafluoroborate ([bmim]BF₄)¹⁹ and sonochemical condition²⁰ were also developed. However, each of the above procedures has its own disadvantages, such as long reaction time, the use of large excess of reagents, low yield and so forth. Due to their wide application, further development of an efficient and useful method for the synthesis of biscoumarin derivatives was considered advantageous.

On the other hand, transition metal and especially ruthenium compounds are favorable materials having useful characteristics, including low redox potential, high electron transfer ability and high coordination ability to heteroatoms. They have been employed as catalyst for various organic syntheses.^{21,22} RuCl₃·nH₂O has shown suitable homogenous catalytic activity in diverse organic transformations, such as in the generation of hydrogen from isopropanol,²³ deoxygenation of aromatic N-oxides,²⁴ direct arylation of arenes,²⁵ etc. Hence, investigation of ruthenium chemistry has attracted the interest of our group.^{26–31}

To the best of our knowledge, Ru(III) salts have never been used as a water-soluble transition metal catalyst for the condensation reaction of 4-hydroxycoumarins with aromatic, heteroaromatic and aliphatic aldehydes for the synthesis of biscoumarin compounds.

RESULTS AND DISCUSSION

Details of the condensation reaction between 4-hydroxycoumarin and various aldehydes are summarized in Scheme 1. In order to optimize the reaction conditions, the effect of various parameters were studied.



Scheme 1. RuCl₃·nH₂O catalyzed synthesis of biscoumarins.

Upon treatment of 4-hydroxycoumarin and 3,4-dimethoxybenzaldehyde as a model reaction in the presence of RuCl₃·nH₂O (5 mol %) in refluxing EtOH, 3,3'-(3,4-dimethoxybenzylidene)-bis(4-hydroxycoumarin) (**2a**) was formed within 30 min as a white precipitate in 46 % yield (Table I, reaction conditions 2). When water was used as the solvent, surprisingly, the yield improved and the best results were obtained using 5 mol % RuCl₃·nH₂O in this solvent; other polar solvents such as EtOH, MeOH and CH₃CN gave lower yields. As is shown in Table II, the temperature had a critical effect on the reaction yield and at room tem-

perature, no reaction occurred even after four hours of stirring the reaction mixture. However, heating the reaction mixture at 80 °C afforded the product in 84 % yield (reaction conditions 3). For yield improvement, the effect of the catalyst loading was also studied (Table III). Increasing the catalyst loading from 5 to 10 mol % did not significantly affect the yield, while the reaction in the absence of RuCl₃·nH₂O in water at 80 °C, gave the product in only 30 % yield after 10 h.¹⁴

TABLE I. Optimization of the solvent for the synthesis of 3,3'-(3,4-dimethoxybenzylidene)-bis(4-hydroxycoumarin); reaction conditions: 4-hydroxycoumarin, 2 mmol, 3,4-dimethoxybenzaldehyde, 1 mmol, RuCl₃·nH₂O, 5 mmol, solvent, 5 mL, temperature: 80 °C

Reaction condition	Solvent	τ / min	Yield, %
1	H ₂ O	30	84
2	EtOH	30	46
3	CH ₃ OH	30	50
4	CH ₃ CN	30	30

TABLE II. Optimization of the temperature for the synthesis of 3,3'-(3,4-dimethoxybenzylidene)-bis(4-hydroxycoumarin); reaction conditions: 4-hydroxycoumarin, 2 mmol, 3,4-dimethoxybenzaldehyde, 1 mmol, RuCl₃·nH₂O, 5 mmol, water, 5 mL

Reaction condition	t / °C	τ / min	Yield, %
1	RT	30–240	—
2	50	30	42
3	80	30	84
4	100	30	84

TABLE III. Optimization of the amount of RuCl₃·nH₂O for the synthesis of 3,3'-(3,4-dimethoxybenzylidene)-bis(4-hydroxycoumarin); reaction conditions: 4-hydroxycoumarin, 2 mmol, 3,4-dimethoxybenzaldehyde, 1 mmol, 80 °C, water, 5 mL

Reaction condition	Amount of catalyst, mol %	τ / min	Yield, %
1	2	30	80
2	5	30	84
3	10	30	82
4	15	30	84

With the optimized conditions in hand, an array of aldehydes were treated with 4-hydroxycoumarin using 5 mol % RuCl₃·nH₂O at 80 °C whereby the desired products were afforded in good to excellent yields (75–95 %) (Table IV). Aromatic aldehydes, however, provided better yields in comparison with their aliphatic counterparts. With regard to the substituents, both aldehydes with electron withdrawing and electron donating groups participated in the reaction, but the former were better. It should be mentioned that the reaction with amides such as *N*-formylpiperidine failed. Even after several modifications such as a four-fold increase in the catalyst loading, prolonged reaction times and changing solvent,



no traceable amount of the desired product was obtained (Table IV, reaction condition 6).

TABLE IV. Ru(III)-catalyzed synthesis of biscoumarins by condensation of 4-hydroxycoumarin and aldehydes (all products were characterized by ^1H -NMR, ^{13}C -NMR and IR data)

Reaction condition	R	τ / min	Product	Yield ^a , %	M.p. ^b , °C
1	3,4-(CH ₃ O) ₂ C ₆ H ₃	30	2a	84	264–266 ^c
2	2-NO ₂ CH=CHC ₆ H ₄	30	2b	90	190–192
3	2-OH,3-CH ₃ OC ₆ H ₃	33	2c	84	268–270
4	3F,4-FC ₆ H ₃	25	2d	90	262–264
5	2-Cl,6-FC ₆ H ₃	25	2e	92	288–290
6	<i>N</i> -Formylpiperidine	60	2f	NR ^c	—
7	3-C ₆ H ₅ OC ₆ H ₄	30	2g	90	218–220
8	3-Indolyl	30	2h	90	238–240 ^c
9	Ph	25	2i	84	227–229 ^c
10	4-ClC ₆ H ₄	25	2j	85	252–254 ^c
11	4-CH ₃ OC ₆ H ₄	30	2k	92	242–244 ^c
12	CH ₃ CH ₂	35	2l	75	144–146
13	4-CNC ₆ H ₄	25	2m	95	240–242

^aIsolated yields; ^bm.p. are matched as given in the literature;^{25,28} ^cno reaction

The condensation products **2a** and **2h–k** (Table IV) are known compounds and their spectroscopic data were consistent with those reported in the literature.^{5,14,16,17a} Selected characterization data for the newly synthesized compounds (**2c–e**, **2g** and **2l–m**) are given in the Supplementary material to this paper.

A proposed mechanistic route for the condensation of aldehydes and 4-hydroxycoumarin that rationalizes the formation of the products is exhibited in Scheme 2. As is shown, nucleophilic attack of 4-hydroxycoumarin to the activated aldehyde (by Ru coordination), followed by H₂O elimination provides intermediate “A” that is further activated by Ru. This in turn, undergoes a second nucleophilic attack by another 4-hydroxycoumarin to provide the final product.

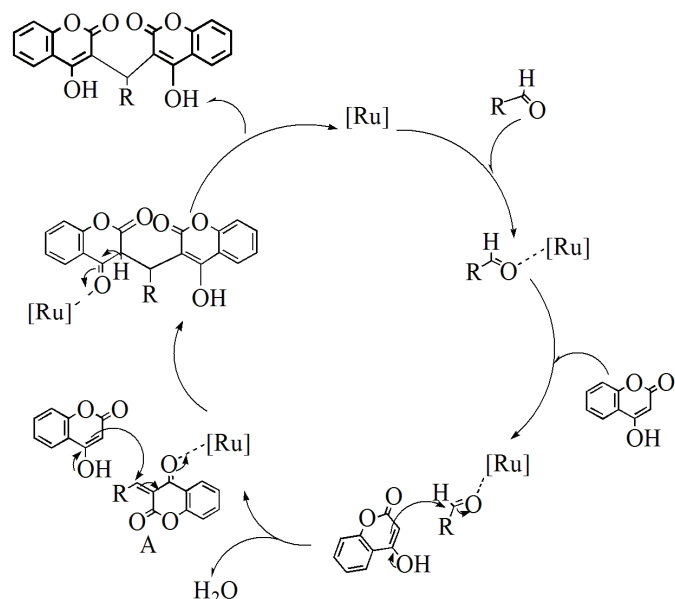
In order to evaluate the reusability of the catalyst, after the first run, the product was separated from the reaction mixture by filtration and substrates were added to the filtrate and tested again. It was found that the reused catalyst maintained its activity after successive runs, as is shown in Table V; after six runs, the reused catalyst showed only 8 % decrease in the yield of the biscoumarin product. Thus, the operational simplicity and reusability of the catalyst cover the expensive cost of ruthenium chloride hydrate.

EXPERIMENTAL

All reactions were followed by thin layer chromatography (TLC) with detection by UV light. The IR spectra were obtained in KBr discs on a Shimadzu IR-470 spectrometer. The ^1H -NMR spectra were obtained on a Bruker DRX-500 Avance spectrometer and the ^{13}C -NMR spectra were obtained on a Bruker DRX-125 or DRX-100 Avance spectrometers. Samples



were analyzed in CDCl_3 or $\text{DMSO}-d_6$, and the chemical shift values are reported in ppm relative to TMS (tetramethylsilane) as the internal reference. Melting points were measured on an electrothermal apparatus and are uncorrected. Elemental analyses were realized using a Carlo-Erba EA1110 CNNO-S analyzer and agreed with the calculated values. The mass spectra of representative compounds were recorded on a HP 5973 network mass selective detector.



Scheme 2. Proposed mechanism for the Ru(III)-catalyzed synthesis of biscoumarins.

TABLE V. Reusability of $\text{RuCl}_3 \cdot n\text{H}_2\text{O}$ in successive runs

Run No.	Yield, %
1	84
2	84
3	82
4	78
5	76
6	76

Materials

4-Hydroxycoumarin, the aldehydes, $\text{RuCl}_3 \cdot n\text{H}_2\text{O}$ and solvents were purchased from Merck and used without further purification.

General procedure for the synthesis of biscoumarins

The catalytic process was performed in a liquid phase. In a typical reaction, 4-hydroxycoumarin (2.0 mmol, 324 mg), the corresponding aldehyde (1.0 mmol), H_2O (5.0 ml) and $\text{RuCl}_3 \cdot n\text{H}_2\text{O}$ (5.0 mmol, 10.7 mg) were taken in a 50 mL round-bottom flask. The reaction mixture was heated at 80 °C in an oil bath and stirred magnetically. After completion of the reaction, as shown by TLC, the mixture was cooled until a solid appeared. The precipitate was

filtered and washed with aqueous ethanol. The crude products were recrystallized from EtOH to yield the pure products. When testing the reusability of the catalyst, hot ethanol was added after completion of the reaction. As the product was insoluble in the cool reaction media, after separation of the solid product, the excess solvent was evaporated from the filtrate. The same substrates were again added to the filtrate including the aqueous medium and catalyst without further purification and reused in the next run.

CONCLUSION

In summary, this study presents a simple experimental procedure under mild reaction conditions, which provides the desired products in short reaction times and high yields. Easy working up, use of water as an eco-friendly solvent, reusability of the catalyst, and availability of the Ru(III) salt are other highlights of this work. This protocol extends the applications of $\text{RuCl}_3 \cdot n\text{H}_2\text{O}$ to clean synthetic methodologies for preparation of pharmaceutically important biscoumarins.

SUPPLEMENTARY MATERIAL

Selected characterization data of the newly synthesized compounds are available electronically from <http://www.shd.org.rs/JSCS/>, or from the corresponding author on request.

Acknowledgement. The authors thank the Research Council of University of Guilan for the partial support of this study.

ИЗВОД

СИНТЕЗА ДЕРИВАТА БИСКУМАРИНА РЕАКЦИЈОМ АЛДЕХИДА И 4-ХИДРОСИКУМАРИНА ПОМОЋУ ХИДРАТИСАНОГ РУТЕНИЈУМ(III)-ХЛОРИДА КАО УНИВЕРЗАЛНОГ ХОМОГЕНОГ КАТАЛИЗATORА

KHALIL TABATABAEIAN, HANNANEH HEIDARI, ALIREZA KHORSHIDI, MANOUCHEHR MAMAGHANI
и NOSRAT O. MAHMOODI

Department of Chemistry, Faculty of Sciences, University of Guilan, P. O. Box 41335-1914, Iran

Испитивана је секвенција домино реакција Knovenagel-ова кондензација/Michael-ова адција ароматичних, хетероароматичних и алифатичних алдехида са 4-хидроксикумарином, у воденој средини, у присуству рутенијумових соли као хомогених катализатора. Утврђено је да 5 mol % $\text{RuCl}_3 \cdot n\text{H}_2\text{O}$ катализује синтезу бискумарина у високом приносу (70–95 %) под оптимизованим, благим и еколошки прихватљивим условима, у кратком реакционом времену (25–35 min).

(Примљено 27 априла, ревидирано 6. октобра 2011)

REFERENCES

1. a) F. Borges, F. Roleira, N. Milhazes, L. Santana, E. Uriarte, *Curr. Med. Chem.* **12** (2005) 887; b) I. Manolov, N. Danchev, *Arch. Pharm. Pharm. Med. Chem.* **2** (2003) 83; c) J. C. Jung, O. S. Park, *Molecules* **14** (2009) 4790; (d) I. Manolov, C. Maichle-Moessmer, N. Danchev, *Eur. J. Med. Chem.* **41** (2006) 882
2. a) C. X. Su, J. F. Mouscadet, C. C. Chiang, H. J. Tsai, L. Y. Hsu, *Chem. Pharm. Bull.* **54** (2006) 682; b) H. Zhao, N. Neamati, H. Hong, A. Mazumder, S. Wang, S. Sunder, G. W. A. Milne, Y. Pommier, T. R. Burke Jr., *J. Med. Chem.* **40** (1997) 242



3. K. A. Nolan, H. Zhao, P. F. Faulder, A. D. Frenkel, J. D. Timson, D. Siegel, D. Ross, T. R. Burke Jr., I. J. Stratford, A. R. Bryce, *J. Med. Chem.* **5** (2007) 6316
4. a) N. Hamdi, M. C. Puerta, P. Valerga, *Eur. J. Med. Chem.* **43** (2008) 2541; b) V. D. Kancheva, V. P. Boranova, J. Nechev, I. I. Manolov, *Biochimie* **92** (2010) 1138
5. K. M. Khan, S. Iqbal, M. A. Lodhi, G. M. Maharvi, Zia-Ullah, M. I. Choudhary, Atta-ur-Rahman, S. Perveen, *Bioorg. Med. Chem.* **12** (2004) 1963
6. a) M. Choudhary, N. Fatima, K. M. Khan, S. Jalil, S. Iqbal, Atta-ur-Rahman, *Bioorg. Med. Chem.* **14** (2006) 8066; b) I. Kostova, G. Momekov, M. Zaharieva, M. Karaivanova, *Eur. J. Med. Chem.* **40** (2005) 542
7. a) H. Ammar, S. Abid, S. Fery-Forgues, *Dyes Pigm.* **78** (2008) 1; b) A. Chandrasekhar, S. Padmanabhan, S. Seshadri, *Dyes Pigm.* **7** (1986) 13
8. B. D. Wagner, *Molecules* **14** (2009) 210
9. J. Liu, Z. Feng, J. Xu, Y. Wang, Z. Peicheng, *Phytochemistry* **68** (2007) 1775
10. H. Hagiwara, S. Miya, T. Suzuki, M. Ando, I. Yamamoto, M. Kato, *Heterocycles* **51** (1999) 493
11. M. Kidwai, V. Bansal, P. Mothsra, S. Saxena, R. K. Somvanshi, S. Dey, T. P. Singh, *J. Mol. Catal., A* **268** (2007) 76
12. J. M. Khurana, S. Kumar, *Tetrahedron Lett.* **50** (2009) 4125
13. M. M. Heravi, S. Sadjadi, N. Mokhtari Haj, H. Oskooie, F. F. Bamoharram, *Catal. Commun.* **10** (2009) 1643
14. P. Singh, P. Kumar, A. Katyal, R. Karla, S. K. Dass, S. Prakash, R. Chandra, *Catal. Lett.* **134** (2010) 303
15. H. Mehrabi, H. Abusaidi, *J. Iran. Chem. Soc.* **7** (2010) 890
16. S. Kadir, A. A. Dar, K. Z. Khan, *Synth. Commun.* **38** (2008) 3490
17. a) G. X. Gong, J. F. Zhou, L. T. An, X. L. Duan, S. J. Ji, *Synth. Commun.* **39** (2009) 497; b) J. F. Zhou, G. X. Gong, L. An, X. Sun, F. Zhu, *Chin. J. Org. Chem.* **29** (2009) 1988
18. H. Shaterian, M. Honarmand, *Chin. J. Chem.* **27** (2009) 1795
19. J. M. Khurana, S. Kumar, *Monatsh. Chem.* **141** (2010) 561
20. G. Cravotto, G. M. Nano, G. Palmisano, S. Tagliapietra, *Synthesis* (2003) 1286
21. S. I. Murahashi, *Ruthenium in Organic Synthesis*, Wiley-VCH, New York, 2004
22. C. Bruneau, P. H. Dixneuf, *Ruthenium Catalysts and Fine Chemistry*, Springer, Berlin, 2004
23. H. Junge, M. Beller, *Tetrahedron Lett.* **46** (2005) 1031
24. S. Kumar, A. Saini, J. S. Sandhu, *Tetrahedron Lett.* **46** (2005) 8737
25. N. Luo, Z. Yu, *Chem. Eur. J.* **16** (2010) 787
26. K. Tabatabaeian, M. Mamaghani, N. O. Mahmoodi, A. Khorshidi, *Synth. Commun.* **40** (2010) 1677
27. K. Tabatabaeian, M. Mamaghani, N. O. Mahmoodi, A. Khorshidi, *Can. J. Chem.* **87** (2009) 1213
28. K. Tabatabaeian, M. Mamaghani, N. O. Mahmoodi, A. Khorshidi, *Tetrahedron Lett.* **49** (2008) 1450
29. K. Tabatabaeian, M. Mamaghani, N. O. Mahmoodi, A. Khorshidi, *Catal. Commun.* **9** (2008) 416
30. K. Tabatabaeian, M. Mamaghani, N. O. Mahmoodi, A. Khorshidi, *J. Mol. Catal., A* **270** (2007) 112
31. K. Tabatabaeian, M. Mamaghani, N. O. Mahmoodi, A. Khorshidi, *Can. J. Chem.* **84** (2006) 1541.





SUPPLEMENTARY MATERIAL TO
**Synthesis of biscoumarin derivatives by the reaction of
aldehydes and 4-hydroxycoumarin using ruthenium(III)
chloride hydrate as a versatile homogeneous catalyst**

KHALIL TABATABAEIAN*, HANNANEH HEIDARI, ALIREZA KHORSHIDI,
MANOUCHEHR MAMAGHANI and NOSRAT O. MAHMOODI

*Department of Chemistry, Faculty of Sciences, University of Guilan,
P. O. Box 41335-1914, Iran*

J. Serb. Chem. Soc. 77 (4) (2012) 407–413

SELECTED CHARACTERIZATION DATA OF THE NEWLY
SYNTHESIZED COMPOUNDS

3,3'-(2-Nitrocinnamylidene)bis(4-hydroxycoumarin) (2b). Yellow solid; yield: 90 %; m.p. 190–192 °C; Anal. Calcd. for C₂₇H₁₇NO₈: C, 67.08; H, 3.54; N, 2.90 %. Found: C, 67.02; H, 3.46; N, 2.99 %; IR (KBr, cm⁻¹): 3400 (OH), 2950 (C–H stretching), 1700 (–C=O stretching of –COOR group), 1650, 1600 (–C=C stretching), 1550 (asymmetric stretching of NO₂), 1390 (symmetric stretching of NO₂), 760 (C–H out of plane bending); ¹H-NMR (500 MHz, CDCl₃, δ / ppm): 11.79 (1H, s, OH), 11.40 (1H, s, OH), 8.03–8.08 (2H, m, ArH), 7.98 (1H, dd, J = 1.1, 8.1 Hz, ArH), 7.74 (1H, d, J = 7.1 Hz, ArH), 7.67–7.42 (8H, m, ArH), 7.07 (1H, dd, J = 2.2, 15.9 Hz, –CH=CH), 6.71 (1H, dd, J = 4.1, 15.9 Hz, –CH=CH), 5.59 (1H, dd, J = 2.4, 4 Hz, –CH aliphatic); ¹³C-NMR (125 MHz, DMSO-d₆, δ / ppm): 165.66 (C–OH), 164.80 (C=O), 153.04 (C=), 148.17 (C–NO₂), 137.09 (CH=), 134.17 (C=C), 132.89 (C=), 132.67 (CH=), 129.09 (CH=), 128.85 (CH=), 125.03 (CH=), 124.67 (CH=), 124.55 (C=C), 123.31 (CH=), 118.75 (CH=), 116.79 (C=), 104.99 (C=), 35.97 (CH); MS (m/z, (relative abundance, %)): 483 (M⁺, 0.39), 481 (1.6), 393, 304, 274, 162, 121 (100), 92.

3,3'-(2-Hydroxy-3-methoxybenzylidene)bis(4-hydroxycoumarin) (2c). Yellow solid; yield: 84 %; m.p. 268–270 °C; Anal. Calcd. for C₂₆H₁₈O₈: C, 68.12; H, 3.86 %. Found: C, 68.34; H, 3.66 %; IR (KBr, cm⁻¹): 3100 (OH), 2800 (C–H stretching), 1710 (–C=O stretching of –COOR group), 1600 (C=C– stretching of olefin), 1550, 1500 (C=C– stretching of aromatic ring), 1200 (C–O–C, ester), 1100 (C–O ether), 750 (C–H out of plane bending); ¹H-NMR (500 MHz, CDCl₃, δ / ppm): 10.6 (1H, br, OH), 8.11 (1H, d, J = 7.7 Hz, ArH), 7.96 (1H, d, J = 7.1

*Corresponding author. E-mail: Taba@gilan.ac.ir

Hz, ArH), 7.39–7.53 (2H, *m*, ArH), 7.34 (1H, *t*, *J* = 7.8 Hz, ArH), 7.28 (1H, *t*, *J* = 10.4 Hz, ArH), 7.12–7.24 (2H, *m*, ArH), 6.95 (1H, *t*, *J* = 7.9 Hz, ArH), 6.79 (1H, *d*, *J* = 10.4 Hz, ArH), 6.73 (1H, *d*, *J* = 7.4 Hz, ArH), 5.61 (1H, *s*, CH aliphatic), 3.91 (3H, *s*, OCH₃); ¹³C-NMR (125 MHz, DMSO-*d*₆, δ / ppm): 159.10 (C=OH), 158.35 (C=O), 146.89 (C—OCH₃), 143.58 (C=), 143.41 (C=OH), 135.80 (CH=), 131.32 (CH=), 129.67 (CH=), 125.31(C=), 124.05 (CH=), 121.25 (CH=), 119.82 (CH=), 119.48 (C=), 117.49 (CH=), 115.94 (C=), 56.67 (OCH₃), 31.18 (CH aliphatic); MS (*m/z*, (relative abundance, %)): 458 (M⁺, 0.07), 440 (M—H₂O, 35.9), 319, 279 (100), 236, 121.

3,3'-(3,4-Difluorobenzylidene)bis(4-hydroxycoumarin) (2d). White solid; yield: 90 %, m.p. 262–264 °C; Anal. Calcd. for C₂₅H₁₄F₂O₆: C, 66.97; H, 3.15 %. Found: C, 66.79; H, 3.11 %; IR (KBr, cm⁻¹): 3500 (OH), 3080, 2850 (C—H stretching), 1640 (—C=O stretching of —COOR group), 1610, 1500 (C=C— stretching of aromatic ring), 1360, 1300 (C—F), 1095 (C—O ether), 770 (C—H out of plane bending); ¹H-NMR (500 MHz, CDCl₃, δ / ppm): 11.63 (1H, *s*, OH), 11.35 (1H, *s*, OH), 8.12 (1H, *d*, *J* = 7.8 Hz, ArH), 8.05 (1H, *d*, *J* = 7.7 Hz, ArH), 7.69 (2H, *m*, ArH), 7.43–7.47 (4H, *m*, ArH), 7.15–6.98 (3H, *m*, ArH), 6.07 (1H, *s*, CH aliphatic); ¹³C-NMR (100 MHz, DMSO-*d*₆, δ / ppm): 167.22 (C=OH), 165.10 (C=O), 152.87 (C=), 144.03 (C—F), 143.57 (C—F), 133.58 (C=), 125.46 (CH=), 124.88 (CH=), 122.93 (CH=), 117.86 (CH=), 117.72 (CH=), 117.17 (CH=), 116.40 (C=), 116.22 (CH=), 103.96 (C=), 36.08 (CH aliphatic); MS (*m/z*, (relative abundance, %)): 448 (M⁺, 39.1), 327, 285, 162, 120, 92 (100).

3,3'-(2-Chloro-6-fluorobenzylidene)bis(4-hydroxycoumarin) (2e). White solid; yield: 92 %, m.p. 288–290 °C; Anal. Calcd. for C₂₅H₁₄ClFO₆: C, 64.60; H, 3.04 %. Found: C 64.71; H 3.10 %; IR (KBr, cm⁻¹): 3100 (OH), 2700 (C—H stretching), 1660 (—C=O stretching of —COOR group), 1600 (C=C— stretching of olefine), 1550, 1500 (C=C— stretching of aromatic ring), 1350, 1110 (C—F), 760 (C—H out of plane bending); ¹H-NMR (500 MHz, CDCl₃, δ / ppm): 10.6 (1H, *br*, OH), 8.06 (1H, *dd*, *J* = 1.5, 8.0 Hz, ArH), 8.02 (1H, *dd*, *J* = 1.4, 7.9 Hz, ArH), 7.45 (1H, *t*, *J* = 7.8 Hz, ArH), 7.45 (1H, *t*, *J* = 7.8 Hz, ArH), 7.38 (1H, *t*, *J* = 7.2 Hz, ArH), 7.33 (1H, *t*, *J* = 8.2 Hz, ArH), 7.12–7.27 (5H, *m*, ArH), 5.50 (1H, *s*, CH aliphatic); ¹³C-NMR (125 MHz, DMSO-*d*₆, δ / ppm): 161.72 (C—F), 161.00 (C=OH), 153.21 (C=O), 152.84 (C=), 133.56 (C—Cl), 133.11(CH=), 130.03 (CH=), 126.75 (CH=), 125.45 (CH=), 124.82 (C=), 123.58 (C=), 117.35 (CH=), 117 (C=), 116.20 (CH=), 114.33 (C=), 28.98 (CH aliphatic), MS (*m/z*, (relative abundance, %)): 463 (M⁺, 0.07), 444 (M—HF, 41.7), 409, 283 (100), 163, 121.

3,3'-(3-Phenoxybenzylidene)bis(4-hydroxycoumarin) (2g). White solid; yield: 90 %, m.p. 218–220 °C; Anal. Calcd. for C₃₁H₂₀O₇: C, 73.80; H, 3.99 %. Found: C, 73.59; H, 3.84 %; IR (KBr, cm⁻¹): 3100 (OH), 2750 (C—H stretching), 1660 (—C=O stretching of —COOR group), 1600 (C=C— stretching of olefin), 1550, 1500 (C=C— stretching of aromatic ring), 1200 (C—O—C ester), 1110 (C—O



ether), 760 (C–H out of plane bending); $^1\text{H-NMR}$ (500 MHz, CDCl_3 , δ / ppm): 11.66 (1H, *s*, OH), 11.33 (1H, *s*, OH), 8.10 (1H, *d*, J = 7.7 Hz, ArH), 8.04 (1H, *d*, J = 7.7 Hz, ArH), 7.65–7.68 (2H, *m*, ArH), 7.29–7.34 (3H, *m*, ArH), 6.92–7.07 (6H, *m*, ArH), 6.12 (1H, *s*, CH aliphatic); $^{13}\text{C-NMR}$ (100 MHz, $\text{DMSO}-d_6$, δ / ppm) 166.39 (C–OH), 165.14 (C=O), 157.24, 156.56, 152.75, 143.58, 143.46, 132.22, 130.25, 129.99, 124.45, 124.05, 123.37, 122.51, 118.87, 118.77, 118.41, 118.00, 116.33, 116.27, 104.23 (aromatic), 36.50 (CH aliphatic); MS (*m/z*, (relative abundance, %)): 504 (M^+ , 15.3), 342, 274, 249, 162, 120, 92 (100), 63.

3,3'-Propylidenebis(4-hydroxycoumarin) (2l). Yellow solid; yield: 75 %; m.p. 144–146 °C; Anal. Calcd. for $\text{C}_{21}\text{H}_{16}\text{O}_6$: C, 69.23; H, 4.43 %. Found: C, 69.18; H, 4.39 %; IR (KBr, cm^{-1}): 3100 (OH), 2900 (C–H stretching), 1650 (–C=O stretching of –COOR group), 1600, 1540, 1480 (C=C– stretching of aromatic ring), 1110 (C–O), 750 (C–H out of plane bending); $^1\text{H-NMR}$ (500 MHz, CDCl_3 , δ / ppm): 12.03 (1H, *s*, OH), 11.22 (1H, *s*, OH), 8.04 (2H, *d*, J = 8.4 Hz, ArH), 7.60–7.65 (2H, *m*, ArH), 7.38–7.42 (4H, *m*, ArH), 4.44 (1H, *t*, –CH–CH₂, J = 8 Hz), 2.41–2.51 (2H, *m*, CH–CH₂–CH₃), 1.01 (3H, *t*, –CH₂–CH₃, J = 7.4 Hz); $^{13}\text{C-NMR}$ (125 MHz, $\text{DMSO}-d_6$, δ / ppm): 165.36 (C–OH), 164.69 (C=O), 152.50 (C=), 132.85 (CH=), 125.12 (CH=), 124.45 (CH=), 117.60 (CH=), 116.91 (C=), 106.02 (C=), 35.28 (CH), 22.13 (CH₂), 13.60 (CH₃); MS (*m/z*, (relative abundance, %)): 364 (M^+ , 24.4), 335, 279, 241, 202, 176, 149, 121 (100), 92.

3,3'-(4-Cyanobenzylidene)bis(4-hydroxycoumarin) (2m). White solid; yield: 95 %; m.p. 240–242 °C; Anal. Calcd. for $\text{C}_{26}\text{H}_{15}\text{NO}_6$: C, 71.39; H, 3.45; N, 3.20 %. Found: C, 71.29; H, 3.32; N, 3.25 %; IR (KBr, cm^{-1}): 3400 (OH), 3000 (C–H stretching), 2200 (–C≡N), 1660 (–C=O stretching of –COOR group), 1620 (C=C– stretching of olefin), 1560 (C=C– stretching of aromatic ring), 1340, 1080 (C–O ether), 780, 750, (C–H out of plane bending); $^1\text{H-NMR}$ (500 MHz, CDCl_3 , δ / ppm): 11.57 (1H, *s*, OH), 11.39 (1H, *s*, OH), 8.13 (1H, *d*, ArH, J = 7.7 Hz), 8.04 (1H, *d*, ArH, J = 7.7 Hz), 7.67–7.72 (4H, *m*, ArH), 7.44–7.51 (4H, *m*, ArH), 7.40 (2H, *d*, J = 7.9 Hz, ArH), 6.14 (1H, *s*, C–H aliphatic); $^{13}\text{C-NMR}$ (100 MHz, $\text{DMSO}-d_6$, δ / ppm): 167.50 (C–OH), 164.89 (C=O), 152.94 (C=), 148.71 (C=), 132.34 (CH=), 131.96 (CH=), 128.29 (CH=), 124.56 (CH=), 123.76 (CH=), 119.69 (CH=), 119.52 (C=), 116.20 (–C≡N), 108.39 (C=), 103.44 (C=), 37.14 (CH aliphatic); MS (*m/z*, (relative abundance, %)): 437 (M^+ , 0.58), 342, 249, 165, 120, 92 (100).





SHORT COMMUNICATION

Ultrasound-assisted catalytic synthesis of acyclic imides in the presence of *p*-toluenesulfonic acid under solvent-free conditions

MASOUD NASR-ESFAHANI*, MORTEZA MONTAZEROZOHORI
and NAJMEH FILVAN

Department of Chemistry, Yasouj University, Yasouj, Iran

(Received 11 May, revised 29 June 2011)

Abstract: A rapid and convenient preparation of acyclic imides by the reaction of aliphatic and aromatic nitriles with acyclic carboxylic anhydride in the presence of catalytic amounts of *p*-toluenesulfonic acid under thermal or ultrasonic conditions is reported. The advantages of this procedure are moderate reaction times, good to excellent yields, and use of an inexpensive and eco-friendly catalyst. The reaction of nitriles with aliphatic anhydrides proceeds under thermal conditions, while they are accelerated by the use of ultrasound irradiation.

Keywords: linear carboxylic anhydride; unsymmetrical acyclic imide; nitrile; *p*-toluenesulfonic acid; ultrasound.

INTRODUCTION

The imide group is an interesting functionality due to its wide presence in natural products and pharmacologically active compounds. Mixed acyclic imide functionality is shared by a growing class of natural products with diverse activities, such as dolastatin 15, a cytotoxic anticancer agent,¹ althiomycin, a potent antibiotic,² and antifeedant.³ Acyclic imides have also been used in the diastereoselective intramolecular photocycloaddition reactions,⁴ as bleach activators⁵ and asymmetric oxetane synthesis.⁶

Classically, imides are prepared by the reaction of amides with acyl chlorides, anhydrides and carboxylic esters or acids.⁷ However, these methods are not as straightforward as they may seem to be at first sight, and several side reactions, such as elimination to nitriles, formation of triacyl amides, or acyl group scrambling, can occur. The best yields were reported for acid-catalyzed reactions of anhydrides with amides. Other procedures for the synthesis of acyclic imides

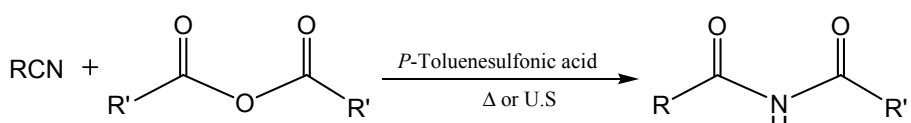
*Corresponding author. E-mail: manas@mail.yu.ac.ir
doi: 10.2298/JSC110511168N

involve aminocarbonylation of aryl bromides,⁸ and reaction of pentafluorophenyl esters with deprotonated amides.⁹ The available methods for the synthesis of unsymmetrical acyclic imides suffer from low yields, high temperature or scrambling of the groups to give symmetrical imides.

The use of ultrasonic waves in organic synthesis has been elevated during the last few years.^{10–17} Most of the observed effects are due to cavitation, the formation, growth and collapse of bubbles in an irradiated liquid, which makes sonochemistry unique. Cavitation induces very high local temperatures and pressures or strong electric fields^{13,18} inside the bubbles (cavities) and enhances mass transfer and turbulent flow in the liquid.¹⁹ Their specificity has been exhibited in homogeneous and heterogeneous reactions.^{15,16} They are defined as acoustic waves with frequencies in the 20 kHz to 100 MHz range.¹¹ Ultrasound is known to accelerate different types of organic reactions and it is established as an important technique in organic synthesis.^{13,20,21}

p-Toluenesulfonic acid (*p*-TSA) is a strong organic acid, about a million times stronger than benzoic acid. It is one of the few strong acids that are solid and, hence, conveniently weighed. In addition, unlike some of the strong mineral acids (especially nitric acid, sulfuric acid, and perchloric acid), *p*-TSA is non-oxidizing. The application of *p*-toluenesulfonic acid is feasible because of its easy preparation, easy handling, stability and good activity, and it is inexpensive and eco-friendly.

Herein, an efficient procedure for the catalytic synthesis of unsymmetrical acyclic imides using *p*-toluenesulfonic acid under thermal or ultrasound irradiation conditions is presented (Scheme 1).



Scheme 1. Reaction for the catalytic synthesis of unsymmetrical acyclic imides using *p*-toluenesulfonic acid under thermal or ultrasound irradiation conditions.

EXPERIMENTAL

All chemicals were purchased from Merck, Fluka or Sigma-Aldrich chemical companies. The reactions were monitored by thin layer chromatography (TLC). The products were isolated and identified by comparison of their physical and spectral data with authentic samples. Sonication was performed in Bandelin Sonorex D12207 type: RK 1028H ultrasonic cleaner (with a frequency of 35 kHz and a power of 1000 W). The IR spectra were recorded on a JASCO-680 FT-IR instrument, the ¹H-NMR spectra were obtained on a Bruker-Avance AQS 300 MHz or a Bruker 400 Ultrasheild (400 MHz) instrument. The melting points were measured on a Barnstead Electrothermal (BI 9300) apparatus.

General procedure for liquid nitriles

A mixture of nitrile (1.0 mmol), carboxylic anhydride (1.0 mmol), and *p*-toluenesulfonic acid monohydrate (30 mol %, equal to 0.30 mmol H⁺) was heated in a 10 mL round-bottomed flask at 70–80°C with concomitant stirring (or ultrasound irradiation). The reactions were completed within 30–120 min, as monitored by TLC (eluent, EtOAc:*n*-hexane, 1:2). After completion of the reaction, diethyl ether (15 mL) was added, the solid catalyst was separated, and then the pure crude products were obtained by short column chromatography.

General procedure for solid nitriles

The solid nitrile (1 mmol), carboxylic anhydride (2 mmol) and *p*-TSA monohydrate (50 mol %) were mixed thoroughly in a round-bottomed flask. The flask was heated at 80 °C with concomitant stirring (or ultrasound irradiation). After completion of the reaction, confirmed by TLC (eluent: EtOAc/*n*-hexane, 1:6), EtOAc (15 mL) was added and the solution was filtered to separate the solid catalyst. Then the pure products were obtained by column chromatography. The products were characterized by IR, ¹H-NMR, ¹³C-NMR and *via* comparison of their melting points with reported ones.

RESULTS AND DISCUSSION

The amidation of alcohols with nitriles in the presence of acidic catalyst is known as the Ritter reaction.⁹ By careful investigation of this reaction, this method was simulated for the one-pot synthesis of a wide variety of linear imides in fair to excellent yields using acid anhydrides instead of alcohols under thermal conditions or ultrasound irradiation (Scheme 1).

For investigation of the effect of different amounts of *p*-TSA monohydrate in the synthesis of unsymmetrical acyclic imides, various amounts of catalyst were used and it was found that 0.057 g (equal to 30 mol %) of *p*-TSA monohydrate for liquid nitriles and 0.095 g (equal to 50 mol %) for solid nitriles were the best amounts of the catalyst. These amounts were used to study the effects of various parameters on the reaction yields.

Synthesis of unsymmetrical acyclic imides catalyzed by p-toluenesulfonic acid

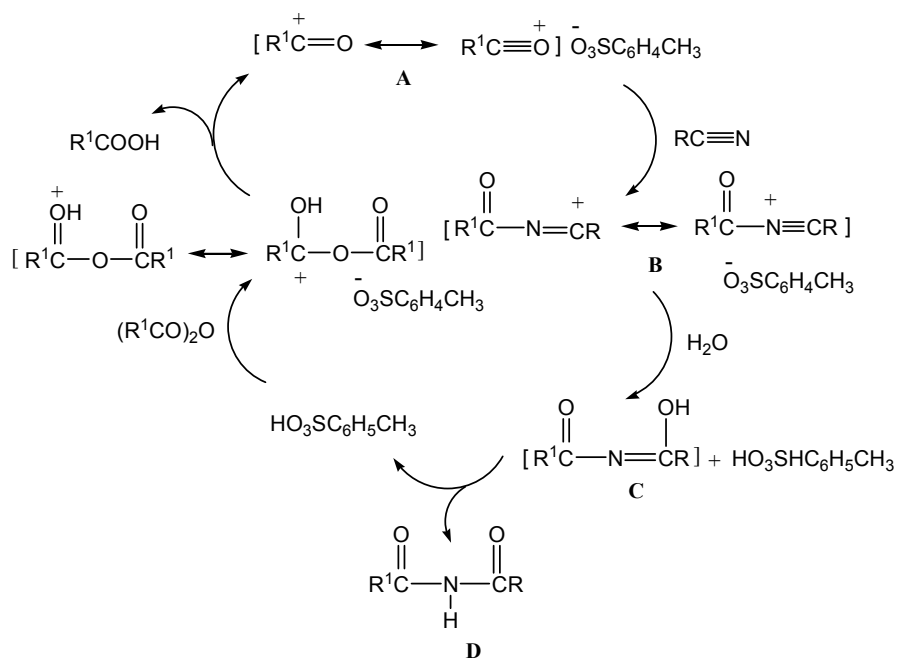
These reaction conditions were extended to a series of aromatic and aliphatic nitriles with acyclic carboxylic anhydrides under solvent-free conditions in the presence of *p*-TSA as an active reagent. The results from the reaction of various nitriles and carboxylic anhydrides in the presence of the optimized amount of *p*-TSA are summarized in Table I. As shown, good to excellent yields were obtained in the reaction of aromatic nitriles (Entries 4–16). The reaction of the nitriles with the aliphatic anhydrides proceeded within 30–120 min in the presence of *p*-TSA under thermal conditions, while by employment of ultrasound irradiation, these reactions were accelerated to within 5–28 min.

A plausible mechanism for the formation of acyclic imides is shown in Scheme 2. The mechanism may involve acylinium ion (A) from protonated carboxylic anhydride. On further reaction with nitrile, it affords the corresponding acylinium cation (B) that will react with water to afford the intermediate acylinol (C), which then yields the acyclic imide (D).

TABLE I. Products from reaction of nitriles and anhydrides under thermal or ultrasonic conditions

Entry	R	R'	Thermal	Ultrasonic	m.p. ^a / °C	
			Time, min	Time, min	Found	Reported
			Yield ^b , %	Yield, %		
1	CH ₃	CH ₃	100/80	20/90	72–73	73–74
2	CH ₃	CH ₃ CH ₂	120/82	25/92	88–89	85–86
3	CH ₃	CH ₃ CH ₂ CH ₂	120/75	25/90	107–108	109–110
4	2-Thiophene	CH ₃ CH ₂	80/85	13/92	135–137	137–138
5	C ₆ H ₅	CH ₃	35/88	5/97	110–112	112–114
6	(CH ₃) ₂ CH	CH ₃ CH ₂	80/86	8/95	110–111	124–126
7	4-ClC ₆ H ₄	CH ₃	30/86	6/94	133–135	136–137
8	4-ClC ₆ H ₄	CH ₃ CH ₂	50/87	10/96	155–157	157–158
9	4-CH ₃ OC ₆ H ₄	CH ₃	40/78	7/85	111–113	119–119.5
10	4-CH ₃ OC ₆ H ₄	CH ₃ CH ₂	35/75	5/78	137–139	133–134
11	4-CH ₃ OC ₆ H ₄	CH ₃ CH ₂ CH ₂	40/82	8/90	162–163	—
12	4-FC ₆ H ₄	CH ₃	85/84	15/93	112–113	111–112
13	4-FC ₆ H ₄	CH ₃ CH ₂	80/82	15/90	113–115	115
14	4-FC ₆ H ₄	CH ₃ CH ₂ CH ₂	70/75	12/83	106–108	108–109
15	3-NO ₂ C ₆ H ₄	CH ₃	120/65	23/80	197–198	195–196
16	3-NO ₂ C ₆ H ₄	CH ₃ CH ₂ CH ₂	150/68	28/85	107–109	108–110

^aAll products were fully characterized by their IR, ¹H-NMR and physical data and comparison with these reported in the literature;^{22–26} ^byields of pure isolated products



Scheme 2. A plausible mechanism for the formation of acyclic imides by the proposed method.

Spectral and physical data for the synthesized compounds

2-Methyl-N-propionylpropionamide (entry 6). White solid, m.p.: 110–111 °C; Anal. Calcd. for C₇H₁₃NO₂: C, 58.72; H, 9.15; N, 9.78 %. Found: C, 68.6; H, 9.20; N, 9.70 %; IR (KBr, cm⁻¹): 3266, 3180, 2969, 2930, 1734, 1273, 1174; ¹H-NMR (400 MHz, CDCl₃, δ / ppm): 0.91 (6H, d, J = 6.5 Hz), 1.42 (3H, t, J = 7.0 Hz), 2.76 (2H, q, J = 7.2 Hz), 4.20–4.23 (1H, m), 8.4 (1H, brs).

N-Acetyl-4-methoxybenzamide (entry 9). White solid, m.p.: 111–113 °C; Anal. Calcd. for C₁₀H₁₁NO₃: C, 62.17; H, 5.74; N, 7.25 %. Found: C, 62.3; H, 5.80; N, 7.20 %; IR (KBr, cm⁻¹): 3240, 3140, 2940, 1720, 1690, 1605; ¹H-NMR (400 MHz, CDCl₃, δ / ppm): 2.62 (3H, s), 3.89 (3H, s), 6.98 (2H, d, J = 7.8 Hz), 7.88 (2H, d, J = 7.5 Hz), 9.04 (1H, brs); ¹³C-NMR (100 MHz, CDCl₃, δ / ppm): 25.52, 55.55, 114.21, 125.00, 129.94, 132.21, 165.12, 173.03.

4-Methoxy-N-propionylbenzamide (entry 10). White solid, m.p.: 137–139 °C; Anal. Calcd. for C₁₁H₁₃NO₃: C, 63.76; H, 6.32; N, 6.76 %. Found: C, 63.8; H, 6.2; N, 6.9 %; IR (KBr, cm⁻¹): 3280, 3160, 2930, 1710, 1685, 1600, 1250; ¹H-NMR (500 MHz, CDCl₃, δ / ppm): 1.23 (3H, t, J = 6.8 Hz), 3.04 (2H, q, J = 7.2 Hz), 3.89 (3H, s), 6.98 (2H, d, J = 7.5 Hz), 7.87 (2H, d, J = 7.6 Hz), 8.88 (1H, brs); ¹³C-NMR (100 MHz, CDCl₃, δ / ppm): 18.28, 31.07, 55.54, 114.17, 124.91, 128.10, 129.86, 163.56, 177.42.

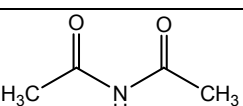
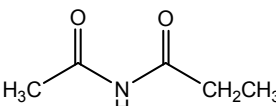
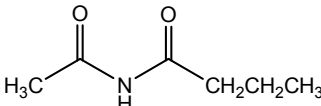
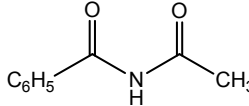
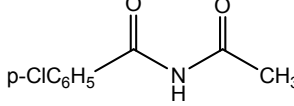
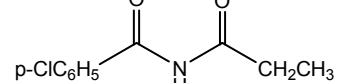
N-Butyryl-4-methoxybenzamide (entry 11). White solid, m.p.: 162–163 °C; Anal. Calcd. for C₁₂H₁₅NO₃: C, 65.14; H, 6.83; N, 6.33 %. Found: C, 65.20; H, 6.90; N, 6.40 %; IR (KBr, cm⁻¹): 3285, 2960, 2930, 1710, 1680, 1610, 1470, 1265; ¹H-NMR (400 MHz, CDCl₃, δ / ppm): 1.03 (3H, t, J = 7.6 Hz), 1.74–1.80 (2H, m), 3.01 (2H, t, J = 7.4 Hz), 3.89 (3H, s), 7.89 (2H, d, J = 7.6 Hz), 8.08 (2H, d, J = 7.2 Hz), 9.06 (1H, brs); ¹³C-NMR (100 MHz, CDCl₃, δ / ppm): 13.74, 17.66, 39.40, 55.46, 113.72, 114.17, 129.95, 132.30, 163.96, 177.01.

Comparative results

In order to show the ability of the employed method with respect to those previously reported, some of the present results in comparison to some other methods are summarized in Table II. As can be seen, the yield/time ratio of the present method is better than or comparable with the other reported results.

In conclusion, an efficient, inexpensive and straightforward procedure for a one-pot synthesis of unsymmetrical acyclic imides using *p*-TSA as catalyst has been found. To the best of our knowledge, this is one of the simplest procedures for the preparation of a wide variety of imides as a valuable class of organic compounds.

TABLE II. Comparison of some of the results obtained in the present study with those reported in the literature (values refer to yield (in %)/time (in min for A and C and in h for B) ratios. In the methods A, B and C, different catalysts were used with the same substrates. A: the present method with *p*-toluenesulfonic acid as catalyst under ultrasonic conditions. B: silica sulfuric acid at 60–70 °C,²² and C: tungstophosphoric acid as an acidic catalyst at 70 °C²³)

Entry	Product	A	B	C
1		90/20	96/5.9	96/40
2		92/25	93/5.9	94/50
3		90/25	92/6.1	89/50
4		97/5	35/7.1	73/40
5		94/6	—	86/85
6		96/10	—	81/80

Acknowledgment. The partial support of this work by Yasouj University is acknowledged.

ИЗВОД

СИНТЕЗА АЦИКЛИЧНИХ ИМИДА У ПРИСУСТВУ *p*-ТОЛУЕНСУЛФОНСКЕ КИСЕЛИНЕ БЕЗ РАСТВАРАЧА ПОД УСЛОВИМА ОЗРАЧИВАЊА УЛТРАЗВУКОМ

MASOUD NASR-ESFAHANI, MORTEZA MONTAZEROZOHOI и NAJMEH FILVAN

Department of Chemistry, Yasouj University, Yasouj, Iran

Приказана је брза синтеза ациклиничких имида реакцијом алифатичних и ароматичних нитрила и анхидрида ациклиничких карбоксилиних киселина у присуству *p*-толуенсулфонске киселине под термалним и ултразвучним условима. Предности описане методе су релативно кратко реакционо време, добар до одличан принос и употреба еколошких и јефтиних катализатора. Реакција нитрила и алифатичних анхидрида одвија се и под термичким условима, али је убрзана уколико се врши озрачивање ултразвуком.

(Примљено 11. маја, ревидирано 29. јуна 2011)

REFERENCES

1. G. R. Pettit, Y. Kamano, C. Dufresne, R. L. Cerny, C. L. Herald, J. M. Schmidt, *J. Org. Chem.* **54** (1989) 6005
2. H. Nakamura, Y. Iitaka, H. Sakakibara, H. Umezawa, *J. Antibiot.* **27** (1974) 894
3. D. G. Nagle, V. J. Paul, M. A. Roberts, *Tetrahedron Lett.* **7** (1996) 6263
4. S. Kohmoto, H. Masu, C. Tatsuno, K. Kishikawa, M. Yamamoto, K. Yamaguchi, *J. Chem. Soc., Perkin Trans. 1* (2000) 4464
5. U.S. patent PCT/US97/13195, WO 98/04664, 5 February 1998
6. M. Sakamoto, M. Takahashi, T. Fujita, S. Watanabe, I. Iida, T. Nishio, H. Aoyama, *J. Org. Chem.* **58** (1993) 3476
7. O. H. Wheeler, O. Rosado, *The Chemistry of Amides*, J. Zabichy, Ed., Wiley, New York, 1970, p. 335
8. A. Schnyder, A. F. Indolese, *J. Org. Chem.* **67** (2002) 594
9. M. B. Andrus, W. Li, R. F. Keyes, *Tetrahedron Lett.* **39** (1998) 5465
10. G. Cravotto, G. Palmisano, S. Tollari, G. M. Nano, A. Penoni, *Ultrason. Sonochem.* **12** (2005) 91
11. F. Alonso, I. P. Beletskaya, M. Yus, *Tetrahedron* **61** (2005) 11771
12. S. Tangestaninejad, M. Moghadam, V. Mirkhani, H. Kargar, *Ultrason. Sonochem.* **13** (2006) 32
13. T. J. Mason, J. P. Lorimer, *Applied Sonochemistry: The Uses of Power Ultrasound in Chemistry and Processing*, Wiley–VCH, Berlin, Y2002
14. G. Cravotto, M. Beggiato, A. Penoni, G. Palmisano, S. Tollari, J. M. Leveque, W. Bonrath, *Tetrahedron Lett.* **46** (2005) 2267
15. S. Moon, L. Duchin, J. V. Cooney, *Tetrahedron Lett.* **20** (1979) 3917
16. J. L. Luche, *Synthetic Organic Sonochemistry*, Plenum Press, New York, 1998
17. J. L. Luche, C. Einhorn, J. Einhorn, J. V. Sinisterra-Gago, *Tetrahedron Lett.* **31** (1990) 4125
18. T. Lepoint, F. Mullie, *Ultrason. Sonochem.* **1** (1994) S13
19. G. Cravotto, P. Cintas, *Chem. Soc. Rev.* **35** (2006) 180
20. B. S. Bhatkhande, M. V. Adhikari, S. D. Samant, *Ultrason. Sonochem.* **9** (2002) 31
21. G. V. Ambulgekar, S. D. Samant, A. B. Pandit, *Ultrason. Sonochem.* **12** (2005) 85
22. Z. Habibi, P. Salehi, M. A. Zolfogol, M. A. Yousefi, *Synlett* **5** (2007) 812
23. I. Mohammadpoor-Baltork, M. Nasr-Esfahani, *J. Iran. Chem. Soc.* 2012, in press
24. K. Tanaka, *Chem. Pharm. Bull.* **35** (1987) 364
25. Q. E. Thompson, *J. Am. Chem. Soc.* **73** (1951) 5841
26. F. Wang, *Adv. Synth. Catal.* **351** (2009) 246.



Phytochemical screening, free radical scavenging, antioxidant activity and phenolic content of *Dodonaea viscosa* Jacq.

TAUHEEDA RIAZ¹, MUHAMMAD ATHAR ABBASI^{1*}, AZIZ-UR-REHMAN¹,
TAYYABA SHAHZADI¹, MUHAMMAD AJAIB² and KHALID MOHAMMED KHAN³

¹Department of Chemistry, Government College University, Lahore-54000, Pakistan,

²Department of Botany, Government College University, Lahore-54000, Pakistan and

³HEJ Research Institute of Chemistry, International Centre for Chemical and Biological Sciences, University of Karachi, Karachi-75270, Pakistan

(Received 21 June, revised 9 September 2011)

Abstract: The purpose of this study was to evaluate the antioxidant potential of *Dodonaea viscosa* Jacq. A methanolic extract of the plant was dissolved in distilled water and sequentially partitioned with *n*-hexane, chloroform, ethyl acetate and *n*-butanol. Phytochemical screening showed the presence of phenolics, flavonoids and cardiac glycosides in large amounts in the chloroform, ethyl acetate and *n*-butanol fraction. The antioxidant potential of all these fractions and remaining aqueous fraction was evaluated by four methods: 1,1-diphenyl-2-picrylhydrazyl (DPPH) free radical scavenging activity, total antioxidant activity, the Ferric reducing antioxidant power (FRAP) assay and ferric thiocyanate assay along with the determination of their total phenolics. The results revealed that the ethyl acetate soluble fraction exhibited the highest percent inhibition of the DPPH radical as compared to the other fractions. It showed $81.14 \pm 1.38\%$ inhibition of the DPPH radical at a concentration of $60 \mu\text{g ml}^{-1}$. The concentration of this fraction leading to 50 % inhibition of the DPPH radical (IC_{50}) was found to be $33.95 \pm 0.58 \mu\text{g ml}^{-1}$, relative to butylated hydroxytoluene (BHT), having an IC_{50} of $12.54 \pm 0.89 \mu\text{g ml}^{-1}$. It also showed the highest FRAP value ($380.53 \pm 0.74 \mu\text{M}$ of trolox equivalents) as well as the highest total phenolic contents ($208.58 \pm 1.83 \text{ gallic acid equivalent (GAE) } \mu\text{g g}^{-1}$) and highest value of inhibition of lipid peroxidation ($58.11 \pm 1.49\%$ at a concentration of $500 \mu\text{g ml}^{-1}$) as compared to the other studied fractions. The chloroform fraction showed the highest total antioxidant activity, *i.e.*, 1.078 ± 0.59 (eq. to BHT).

Keywords: *Dodonaea viscosa* Jacq.; phytochemical screening; DPPH assay; total antioxidant activity; FRAP value; total phenolics; inhibition of lipid peroxidation.

*Corresponding author. E-mail: atrabbasi@yahoo.com
doi: 10.2298/JSC110621183R

INTRODUCTION

Medicinal plants constitute the major constituents of most indigenous medicines and a large number of Western medical preparations contain one or more component(s) of plant origin. The medicines that are in use today are definitely not the same as those that were used in ancient times or even in the recent past. Several modifications, improvement, sophistication and newer discoveries have continuously contributed to the type, quality, presentation and concept of medicinal preparation. In the development of human knowledge for therapeutic use, scientists endeavoured to isolate different chemical constituents from plants, subjected them to biological and pharmacological tests and then used them to prepare modern medicines.¹ There is increasing interest in the measurement and use of plant antioxidants for scientific research as well as for industrial (dietary, pharmaceutical and cosmetics) purposes. This is mainly due to their strong biological activity, excluding those of many synthetic antioxidants, which have possible activity as promoters of carcinogenesis. Therefore, the need exists for safe, economic, powerful and natural antioxidants to replace these synthetic ones. Obviously, there has been an increasing demand to evaluate directly the antioxidant properties of plant extracts.²

Many antioxidant compounds, naturally occurring in plant sources, have been identified as free radical or active oxygen scavengers.³ A number of plants have been investigated for their biological activities and antioxidant properties.^{4,5} Recently, interest has increased considerably in finding naturally occurring antioxidants for use in foods or medicinal materials to replace synthetic antioxidants.⁶ In addition, natural antioxidants have the capacity to improve food quality and stability and also act as nutraceuticals to terminate free radical chain reaction in biological systems, and thus may provide additional health benefits to consumers. Recent studies have highlighted the role of polyphenolic compounds of higher plants,⁷ such as flavonols⁸ and anthraquinones.⁹

In the search of plants as a source of natural antioxidants, some medicinal plants and fruits have been extensively studied for their antioxidant activity and radical scavenging in the last few decades.¹⁰ Some antioxidant compounds are extracted from easy sources, such as agricultural and horticultural crops, or medicinal plants. Among them, medicinal plants are taking the main role for providing a large number of pure antioxidants. *Dodonaea viscosa* Jacq. is a traditional medicinal plant belonging to the family Sapindaceae. Plants of this family are utilized in folklore medicine in Pakistan for the treatment of various fungal skin diseases, such as *Tinea capitis*, *T. pedis*, *T. manum*, *T. corporis*, etc. The powdered leaves of *D. viscosa* applied over burn and scald wounds were found to possess febrifuge properties and to be useful for different skin diseases.¹¹ It is commonly used for skin diseases in Ethiopia.¹² Investigation of the aerial parts of *D. viscosa* led to the isolation of a new *ent*-labdane (*ent*-15,16-epoxy-9 α H-labda-

-13(16),14-diene-3 β ,8 α -diol) and a novel *p*-coumaric acid ester of 1-L-*myo*-inositol (1-L-1-*O*-methyl-2-acetyl-3-*p*-coumaryl-*myo*-inositol).¹³ Many flavonoids,^{14–16} saponins,¹⁷ and diterpenes¹⁸ have also been isolated from *D. viscosa*. Notable among these compounds are pinocembrin, santin, penduletin, alizarin, 5-hydroxy-3,6,7,4'-tetramethoxyflavone, 5,7,4'-trihydroxy-3,6-dimethoxyflavone, isorhamnetin-3-rhamnosylgalactoside, 5,7-dihydroxy-3'-(4-hydroxy-3-methylbutyl)-3,6,4'-trimethoxyflavones,¹⁴ 5,6,4'-trihydroxy-3,7-dimethoxyflavone,¹⁶ viscosol,¹⁵ hautriwaic acid,^{16,18,19} dehydrohautriwaic acid, methyl dodonates,¹⁸ dodonoside A, dodonoside B,¹⁷ 5,7,4'-trihydroxy-3',5'-bis(3-methylbut-2-enyl)-3,6-dimethoxyflavone, and 5,7,4'-trihydroxy-3'-(4-hydroxy-3-methylbutyl)-50-(3-methylbut-2-enyl)-3,6-dimethoxyflavone, dodonic acid, hautriwaic lactone, (+)-hardwickiic acid, 5 α -hydroxy-1,2-dehydro-5,10-dihydroprintzianic acid methyl ester, strictic acid, dodonolide, alizarin,¹⁹ 3,5,7-trihydroxy-4'-methoxyflavone and 5-hydroxy-3,7,4'-trimethoxyflavone, 3,4',5,7-tetrahydroxyflavone (kaempferol),²⁰ and sakuranetin.^{21,22}

D. viscosa Jacq. is a popular medicinal plant. It is used in folk medicine as a remedy for fever, rheumatism and gout. The crude extract has inhibitory effects against *Staphylococcus aureus*, *Streptococcus pyogenes* and *Corynebacterium diphtheriae*, but no activity against *Escherichia coli* and *Pseudomonas aeruginosa*, thereby suggesting potential against notable Gram positive organisms.²³ Its leaves are used as anti-inflammatory, anti-ulcer, antibacterial and antifungal agents and in the treatment of bone fractures.²⁴

To the best of our knowledge, no work has been performed on the comparative antioxidant potential of various fractions of *D. viscosa* Jacq. Therefore, the present study was undertaken to investigate the *in vitro* antioxidant potential of various fractions of this plant.

EXPERIMENTAL

Plant material

The plant *D. viscosa* Jacq. was collected from Kotli, Azad Kashmir in February 2010, and identified by Mr. Muhammad Ajaib (taxonomist), Department of Botany, Government College University, Lahore. A Voucher specimen (G. C. Herb. Bot. 965) has been deposited in the Herbarium of the Botany Department of the same university.

Extraction and fractionation of the antioxidants

The shade-dried ground whole plant (0.8 kg) was exhaustively extracted with methanol (5 L) on a Soxhlet apparatus. The extract was evaporated in rotary evaporator Laborta 4000-efficient (Heidolph) at 40 °C under vacuum to yield the residue (126 g), which was dissolved in distilled water (1 L) and partitioned with *n*-hexane (4×1 L), chloroform (4×1 L), ethyl acetate (4×1 L) and *n*-butanol (4×1 L). These four organic fractions and the remaining water fraction were concentrated separately on rotary evaporator (*n*-hexane at 34 °C, chloroform at 38 °C, ethyl acetate at 45 °C, *n*-butanol at 50 °C and water at 60 °C under vacuum) and the thus obtained residues were used to evaluate their *in vitro* antioxidant potential.



Chemicals and standards

1,1-Diphenyl-2-picrylhydrazyl (DPPH) radical, 2,4,6-trypyridyl-*s*-triazine (TPTZ), trolox, gallic acid, Folin–Ciocalteu phenol reagent and butylated hydroxytoluene (BHT) were obtained from the Sigma Chemical Company Ltd. (USA) and the organic solvents (*n*-hexane, chloroform, ethyl acetate, *n*-butanol), and other employed chemicals were from Merck (Pvt.) Ltd. (Germany).

Phytochemical screening

Qualitative phytochemical screening of all five crude extracts, *i.e.*, the *n*-hexane soluble fraction, the chloroform soluble fraction, the ethyl acetate soluble fraction, the *n*-butanol soluble fraction and the remaining aqueous fractions, was performed to identify the phytochemical constituents, *i.e.*, alkaloids, terpenoids, saponins, tannins, sugars, phenolics, flavonoids and cardiac glycosides, using standard procedures.^{25–27}

Antioxidant assays

The following antioxidant assays were performed on all the studied fractions.

DPPH radical scavenging activity

The DPPH radical scavenging activities of each crude extract of plant were examined by comparison with that of a known antioxidant (BHT), using a reported method.²⁸ Briefly, various amounts of the samples (1000, 500, 250, 125, 60, 30, 15 and 8 µg mL⁻¹) were mixed with 3 ml of methanolic solution of DPPH (0.1 mM). The mixture was shaken vigorously and allowed to stand at room temperature for 1 h. Then, the absorbance was measured at 517 nm against methanol as a blank in a spectrophotometer (CECIL Instruments CE 7200, Cambridge, UK). The lower the absorbance of the reaction mixture, the higher was the free radical scavenging activity.

The percent of DPPH decolouration of the samples was calculated according to the formula:

$$\text{Antiradical activity (\%)} = (A_{\text{control}} - A_{\text{sample}})/A_{\text{control}} \times 100$$

Each sample was assayed in triplicate and the mean values were calculated.

Total antioxidant activity by the phosphomolybdenum method

The total antioxidant activities of various fractions of the plant were evaluated by the phosphomolybdenum complex formation method.²⁹ Briefly, 500 µg mL⁻¹ of each crude extract was mixed with 4 mL of reagent solution (0.6 M sulphuric acid, 28 mM sodium phosphate and 4 mM ammonium molybdate) in sample vials. The blank solution contained 4 mL of reagent solution. The vials were capped and incubated in water bath at 95 °C for 90 minutes. After the samples had been cooled to room temperature, the absorbance of mixture was measured at 695 nm against the blank. The antioxidant activity is expressed relative to that of BHT. All determinations were assayed in triplicate and mean values were calculated.

Ferric reducing antioxidant power (FRAP) assay

The FRAP assay was performed according to Benzie and Strain³⁰ with some modifications. The stock solutions included 300 mM acetate buffer (pH 3.6), 10 mM TPTZ solution in 40 mM hydrochloric acid, and 20 mM ferric chloride hexahydrate solution. The fresh working solution was prepared by mixing 25 mL acetate buffer, 2.5 mL TPTZ solution and 2.5 mL ferric chloride hexahydrate solution, which was then warmed to 37 °C before use. The solutions of plant samples and that of trolox were prepared in methanol (250 µg mL⁻¹). 10 µL of each of crude extracts was taken in separate test tubes and 2990 µL of FRAP solution was

added to each to make a total volume of 3 mL. The plant crude extracts were allowed to react with the FRAP solution in the dark for 30 min. The absorbance of the coloured product (ferrous tripyridyltriazine complex) was checked at 593 nm. The FRAP values are expressed as micromoles of trolox equivalents (TE) per mg of the sample using the standard curve constructed for different concentrations of trolox. The results are expressed in $\mu\text{mol TE mL}^{-1}$.

Total content of phenolics

The total phenolics of the various fractions of plant were determined by a reported method.³¹ An aliquot of 0.1 mL of each crude extract (0.5 mg mL^{-1}) was combined with 2.8 mL of 10 % sodium carbonate and 0.1 mL of 2 M Folin–Ciocalteu reagent. After 40 min, the absorbance at 725 nm was measured using a UV-visible spectrophotometer. The total phenolics are expressed as micrograms of gallic acid equivalents (GAE) per gram of sample using a standard calibration curve constructed for different concentrations of gallic acid. The curve was linear between 50 and 400 $\mu\text{g mL}^{-1}$ of gallic acid. The results are expressed in $\mu\text{g GAE g}^{-1}$.

Ferric thiocyanate (FTC) assay

The antioxidant activities of the various fractions of the plant on the inhibition of linoleic acid peroxidation were assayed by the thiocyanate method.³² Each crude extract (0.1 ml, 0.5 mg mL^{-1}) was mixed with 2.5 mL of linoleic acid emulsion (0.02 M, pH 7.0) and 2.0 mL of phosphate buffer (0.02 M, pH 7.0). The linoleic emulsion was prepared by mixing 0.28 g of linoleic acid, 0.28 g of Tween-20 as emulsifier and 50.0 mL of phosphate buffer. The reaction mixture was incubated for 5 days at 40 °C. The mixture without extract was used as the control. A 0.1 mL aliquot of the mixture was taken and mixed with 5.0 mL of 75 % ethanol, 0.1 mL of 30 % ammonium thiocyanate and 0.1 mL of 20 mM ferrous chloride in 3.5 % hydrochloric acid and allowed to stand at room temperature. Precisely 3 min after the addition of ferrous chloride to the reaction mixture, the absorbance was recorded at 500 nm. The antioxidant activity is expressed as follows:

$$\text{Inhibition of lipid peroxidation (\%)} = \{1 - (A_{\text{sample}})/(A_{\text{control}})\} \times 100$$

The antioxidant activity of BHT as reference standard was assayed for comparison.

Statistical analysis

All the measurements were performed in triplicate and statistical analysis was realised by statistical software. All the data are expressed as $\pm \text{SEM}$. Statistical analyses were determined using one way analysis of variance (ANOVA) followed by the *post-hoc* Tukey test.

RESULTS AND DISCUSSION

Phytochemical screening

Phytochemical screening was performed on all the studied fractions and results are given in Table I. It can be observed from the results that the chloroform fraction, ethyl acetate fraction, *n*-butanol fraction and aqueous fraction contained phenolics and flavonoids, while the *n*-hexane fraction showed absence of these compounds. Cardiac glycosides were absent in all the fractions. Terpenes were detected in all the fractions except the aqueous fraction. Alkaloids were detected only in the chloroform fraction and the ethyl acetate fraction. Tannins and sugars were present in the ethyl acetate fraction, the *n*-butanol fraction and the aqueous



fraction but were not detected in the *n*-hexane fraction and chloroform fraction. Saponins were present in all the fractions except the *n*-hexane fraction.

TABLE I. Phytochemical constituents of the various fractions of *D. viscosa* Jacq. ("+" represents presence and "—" represents absence)

Test	<i>n</i> -Hexane soluble fraction	Chloroform soluble fraction	Ethyl acetate soluble fraction	<i>n</i> -Butanol soluble fraction	Remaining aqueous fraction
Alkaloids	—	++	+	—	—
Terpenoids	+	++	++	+	—
Saponins	—	++	++++	+++	++
Tannins	—	—	++	++	++
Sugars	—	—	++	++	++
Phenolics	—	+	++	+	+
Flavonoids	—	+	++	+	+
Cardiac glycosides	—	—	—	—	—

DPPH scavenging activity

This method is based on the reaction of DPPH that is characterized as a pre-formed stable free radical with a deep violet colour and any substance that can donate a hydrogen atom to DPPH reduces it to a stable diamagnetic molecule.²⁸ The effects of phenolic compounds on DPPH scavenging are thought to be due to their hydrogen donating ability.³³ It was reported that the decrease in the absorbance of the DPPH caused by phenolic compound is due to scavenging of the radical by hydrogen donation, which is visualized as a discoloration from purple to yellow.³⁴ The reduction of the DPPH was followed *via* the decrease in absorbance at 517 nm. The various fractions of *D. viscosa* significantly reduced the DPPH. The values of percent scavenging of DPPH are presented in Table II. It was observed that activity increased with increasing concentration of the fractions in the assay. For the various concentrations of ethyl acetate, soluble fraction exhibited the highest percent inhibition of the DPPH as compared to the other fractions. This fraction showed $81.14 \pm 1.38\%$ inhibition of DPPH at a concentration of $60 \mu\text{g ml}^{-1}$. The various concentrations of the fractions which showed percent inhibition greater than 50 % the activities were found to be significant ($p < 0.05$).

The IC_{50} value is defined as the concentration of a substrate that causes 50 % loss of the DPPH activity and was calculated by linear regression of plots of the percentage antiradical activity against the concentration of the tested compounds.¹ The IC_{50} values of all the fractions were calculated and the results are given in Table III. The lower the IC_{50} value, the higher is the scavenging potential. The ethyl acetate soluble fraction exhibited the lowest IC_{50} value, *i.e.*, $33.95 \pm 0.58 \mu\text{g ml}^{-1}$ as compared to the other studied fractions. The chloroform soluble fraction and the *n*-butanol soluble fraction showed very similar IC_{50} va-

lues, *i.e.*, 79.42 ± 0.97 and $78.48 \pm 0.47 \mu\text{g ml}^{-1}$, respectively. The IC_{50} values of the *n*-hexane soluble fraction and the aqueous fraction were found to be 238.30 ± 1.89 and $189.28 \pm 1.59 \mu\text{g ml}^{-1}$, respectively.

TABLE II. 1,1-Diphenyl-2-picrylhydrazyl radical (DPPH) scavenging activity of the various fractions of *D. viscosa* Jacq.

Sr. No.	Sample	Concentration in the assay $\mu\text{g ml}^{-1}$	Scavenging of DPPH $\pm SEM^a$ %
1	<i>n</i> -Hexane soluble fraction	500	67.14 ± 1.72^b
		250	54.29 ± 1.25^b
		125	40.01 ± 0.81
		60	30.71 ± 1.68
2	Chloroform soluble fraction	125	78.14 ± 1.67^b
		60	33.57 ± 1.22
		30	23.47 ± 1.81
3	Ethyl acetate soluble fraction	60	81.14 ± 1.38^b
		30	52.85 ± 1.55^b
		15	22.14 ± 1.79
4	<i>n</i> -Butanol soluble fraction	125	75.71 ± 1.87^b
		60	40.62 ± 0.99
		30	22.12 ± 1.21
5	Remaining aqueous fraction	250	57.85 ± 1.69^b
		125	45.01 ± 0.81
		60	27.14 ± 0.46
6	BHT ^c	60	91.35 ± 0.14^b
		30	75.46 ± 0.08^b
		15	42.57 ± 0.05
		8	23.47 ± 0.34

^aAll results are presented as mean \pm standard mean error of three assays; ^b $p < 0.05$ when compared with the negative control, *i.e.*, blank/solvent ($p < 0.05$ is taken as significant); ^cstandard antioxidant

The results are expressed relative to butylated hydroxytoluene (BHT), a reference standard having IC_{50} of $12.54 \pm 0.89 \mu\text{g ml}^{-1}$. The IC_{50} values of the chloroform soluble fraction, the ethyl acetate soluble fraction, the *n*-butanol soluble fraction and the aqueous fraction were found to be significant ($p < 0.05$) while that of the *n*-hexane soluble fraction was found to be non-significant ($p > 0.05$) when compared with BHT.

Total antioxidant activity

The total antioxidant activity of the studied fractions was measured by the phosphomolybdenum complex formation method. This method is based on the reduction of molybdenum(VI) to molybdenum(V) by the antioxidants and the subsequent formation of a green phosphate Mo(V) complex at acidic pH values. Electron transfer occurs in this assay which depends on the structure of the antioxidant.²⁹ The phosphomolybdenum method usually detects antioxidants such as



ascorbic acid, some phenolics, tocopherols and carotenoids. The total antioxidant activities of these fractions were compared with the standard antioxidant BHT and the results are given in Table III. The results revealed that the chloroform fraction showed the highest total antioxidant activity, *i.e.*, 1.078 ± 0.59 , as compared to the other fractions. The total antioxidant activities of ethyl acetate, *n*-butanol and aqueous fraction were found to be 0.941 ± 0.17 , 0.636 ± 0.32 and 0.375 ± 0.29 , respectively. The *n*-hexane fraction showed lowest total antioxidant activity (0.356 ± 0.21). The results were compared with BHT, a reference standard having total antioxidant activity 1.219 ± 0.37 . The total antioxidant activity shown by the chloroform soluble fraction, the ethyl acetate soluble fraction and the *n*-butanol soluble fraction were found to be significant ($p < 0.05$), while those of the *n*-hexane and aqueous fraction were found to be non-significant ($p > 0.05$) when compared with BHT.

TABLE III. IC_{50} , total phenolics, total antioxidant activity, FRAP values and lipid peroxidation inhibition values of the different fractions of *D. viscosa* Jacq.

Sr. No.	Sample	DPPH-radical scavenging $IC_{50} / \mu\text{g L}^{-1}$	Total antioxidant activity (eq. to BHT)	FRAP value $\mu\text{mol TE mL}^{-1}$	Total phenolics $\mu\text{g GAE g}^{-1}$	Lipid peroxidation inhibition ^a %
1	<i>n</i> -Hexane soluble fraction	238.30 ± 1.89	0.356 ± 0.21	40.81 ± 0.48	28.23 ± 0.36	17.66 ± 0.87
2	Chloroform soluble fraction	79.42 ± 0.97^b	1.078 ± 0.59^b	278.45 ± 0.72^c	140.55 ± 1.21^c	49.37 ± 0.99^b
3	Ethyl acetate soluble fraction	33.95 ± 0.58^b	0.941 ± 0.17^b	380.53 ± 0.74^c	208.58 ± 1.83^c	58.11 ± 1.49^b
4	<i>n</i> -Butanol soluble fraction	78.48 ± 0.47^b	0.636 ± 0.32^b	234.40 ± 1.28^c	132.76 ± 1.53^c	41.50 ± 0.46^b
5	Remaining aqueous fraction	189.28 ± 1.59^b	0.375 ± 0.29	89.54 ± 0.98^c	95.17 ± 1.95^c	22.12 ± 0.76
6	BHT ^d	12.54 ± 0.89	1.219 ± 0.37	—	—	62.73 ± 0.96

^atested concentration at $500 \mu\text{g mL}^{-1}$; ^b $p < 0.05$ when compared with the reference standard (BHT); ^c $p < 0.05$ when compared with negative controls, *i.e.* blank/solvent ($p < 0.05$ is taken as significant); ^d expressed relative to BHT

Ferric reducing antioxidant power (FRAP)

The ferric reducing antioxidant power (FRAP) assay measures the reducing ability of antioxidants against the oxidative effects of reactive oxygen species. Electron donating antioxidants can be described as reductants and inactivation of



oxidants by reductants can be described as redox reactions. This assay is based on the ability of antioxidants to reduce Fe^{3+} to Fe^{2+} in the presence of tripyridyltriazine (TPTZ), whereby an intense blue Fe^{2+} -TPTZ complex with an absorbance maximum at 593 nm is formed.³⁰ Increasing absorbance indicates an increase in reductive ability. The FRAP values of the studied fractions were calculated and the results are presented in Table III. Among all the fractions, the ethyl acetate fraction showed the highest FRAP value ($380.53 \pm 0.74 \mu\text{mol TE mL}^{-1}$). The chloroform fraction, the *n*-butanol fraction and the aqueous fraction exhibited FRAP values of 278.45 ± 0.72 , 234.40 ± 1.28 and $89.54 \pm 0.98 \mu\text{mol TE mL}^{-1}$, respectively, while the *n*-hexane fraction showed a very low FRAP value, *i.e.*, $40.81 \pm 0.48 \mu\text{mol TE mL}^{-1}$. The high FRAP values obtained for the polar solvent fractions may be partially ascribed to the presence of phenolics and flavonoids. The FRAP values of the chloroform soluble fraction, the ethyl acetate soluble fraction, the *n*-butanol soluble fraction and the aqueous fraction were found to be significant ($p < 0.05$), while that of the *n*-hexane soluble fraction was found to be non-significant ($p > 0.05$) when compared with the blank.

Chemical composition of the fractions

Phenolic compounds and flavonoids are very important plant secondary metabolites. These compounds have numerous defence functions in plants, and thus, several environmental factors, such as light, temperature and humidity, and internal factors, including genetic differences, nutrients, hormones, *etc.*, contribute to their synthesis.³⁵ Similarly, other factors, such as germination, degree of ripening, variety, processing and storage also influence the content of plant phenolics.³⁶ It was reported that the phenolics are responsible for the variation in the antioxidant activity of plants.³⁷ They exhibit antioxidant activity by deactivating lipid free radicals or preventing decomposition of hydroperoxides into free radicals,^{38,39} or chelate metal ions and protect against pathogens and predators.⁴⁰ The most frequently encountered flavonoids are flavonols, quercetin, flavanols and anthocyanins.

The concentrations of phenolics in the different fractions, expressed as micrograms of gallic acid equivalents (GAEs) per gram of fraction, are given in Table III. Among the studied fractions, the ethyl acetate soluble fraction showed the highest amount of total phenolic compounds, *i.e.*, $208.58 \pm 1.83 \mu\text{g GAE g}^{-1}$. The chloroform fraction and the *n*-butanol fraction showed very similar values of total phenolic content (140.55 ± 1.21 and $132.76 \pm 1.53 \mu\text{g GAE g}^{-1}$, respectively). The total contents of phenolics in the *n*-hexane soluble fraction and the aqueous fraction were found to be 28.23 ± 0.36 , and $95.17 \pm 1.95 \mu\text{g GAE g}^{-1}$, respectively. The results for the total phenolics contents in the chloroform soluble fraction, the ethyl acetate soluble fraction, the *n*-butanol soluble fraction and the aqueous frac-

tion were found to be significant ($p < 0.05$), while that of the *n*-hexane soluble fraction was found to be non-significant ($p > 0.05$) when compared with the blank.

Oxygen reacts with unsaturated double bonds on lipids, which results in the generation of free radicals and lipid hydroperoxides. Peroxidation of lipids occurs both *in vivo* and *in vitro* and gives rise to cytotoxic and reactive products. These products disturb the normal functioning of the cell and can give rise to damaged or modified DNA. Hydrogen-donating antioxidants can react with lipid peroxy radicals and break the generation cycle of new radicals. The ferric thiocyanate assay, in which peroxide reacts with ferrous chloride to form ferric ions, is used to measure the amount of peroxide at the beginning of lipid peroxidation. The ferric ions then unite with ammonium thiocyanate and produce ferric thiocyanate, a reddish pigment.⁴¹ The various fractions of the plant were tested by this assay and the results are given in Table III. Significantly lower absorbances, as compared to the control, were observed for the chloroform fraction, the ethyl acetate fraction and the *n*-butanol fraction, which indicated that these fractions had greater antioxidant activities than the others. The fractions which showed greater values of percent inhibition of lipid peroxidation might contain primary antioxidant compounds, which are able to react aggressively with free radicals, particularly hydroxyl radicals, thereby terminating the radical-chain reaction and retarding the formation of hydroperoxides.⁴² The highest percentage inhibition of lipid peroxidation was exhibited by the ethyl acetate fraction ($58.11 \pm 1.49\%$) at a concentration of $500 \mu\text{g ml}^{-1}$, while the *n*-hexane soluble fraction showed the lowest percentage of inhibition of lipid peroxidation ($17.66 \pm 0.87\%$). The chloroform, *n*-butanol and aqueous fractions exhibited percent inhibition of lipid peroxidation of $49.37 \pm 0.99\%$, $41.50 \pm 0.46\%$ and $22.12 \pm 0.76\%$, respectively. The inhibition of lipid peroxidation by BHT (standard) was found to be $62.73 \pm 0.96\%$. The results for percent inhibition of lipid peroxidation of the chloroform soluble fraction, the ethyl acetate soluble fraction and the *n*-butanol soluble fraction were found to be significant ($p < 0.05$) while that of the *n*-hexane soluble fraction and the aqueous fraction were found to be non-significant ($p > 0.05$) when compared with BHT.

CONCLUSIONS

The obtained results showed that the chloroform fraction, the ethyl acetate fraction, the *n*-butanol fraction and the aqueous fraction contained phenolics and flavonoids, while the *n*-hexane fraction showed an absence of these compounds. Due to the presence of such compounds, the chloroform fraction, the ethyl acetate fraction and the *n*-butanol fraction showed good antioxidant activity, the aqueous fraction showed moderate activity due to lower amounts of such compounds while the *n*-hexane fraction showed no activity because of the absence of all these compounds. The ethyl acetate soluble fraction exhibited the highest

percent inhibition of the DPPH radical as compared to the other fractions. It showed 81.14 ± 1.38 % inhibition of the DPPH radical at a concentration of $60 \mu\text{g ml}^{-1}$. The IC_{50} of this fraction was $33.95\pm0.58 \mu\text{g ml}^{-1}$, relative to butylated hydroxytoluene (BHT), having an IC_{50} of $12.54\pm0.89 \mu\text{g ml}^{-1}$. It also showed the highest FRAP value ($380.53\pm0.74 \mu\text{g trolox equivalents}$) as well as the highest total phenolic content (208.58 ± 1.83) and the highest value of inhibition of lipid peroxidation (58.11 ± 1.49 % at a concentration of $500 \mu\text{g ml}^{-1}$) as compared to the other studied fractions. The chloroform fraction showed the highest total antioxidant activity (1.078 ± 0.59). Hence, it was concluded that chloroform fraction, ethyl acetate fraction and *n*-butanol fraction are rich in strong antioxidants. These fractions are potentially valuable sources of natural antioxidants and bioactive materials, which would be expected to increase shelf life of foods and fortify against peroxidative damage in living systems in relation to aging and carcinogenesis.

Acknowledgment. The authors are thankful to Higher Education Commission of Pakistan for financial support.

ИЗВОД

ФИТОХЕМИЈСКА АНАЛИЗА, АНТИОКСИДАТИВНА АКТИВНОСТ И САДРЖАЈ ФЕНОЛА У БИЉЦИ *Dodonaea viscosa*

TAUHEEDA RIAZ¹, MUHAMMAD ATHAR ABBAS¹, AZIZ-UR-REHMAN¹, TAYYABA SHAHZADI¹,
MUHAMMAD AJAIB² и KHALID MOHAMMED KHAN³

¹Department of Chemistry, Government College University, Lahore-54000, Pakistan, ²Department of Botany, Government College University, Lahore-54000, Pakistan и ³HEJ Research Institute of Chemistry, International Centre for Chemical and Biological Sciences, University of Karachi, Karachi-75270, Pakistan

Циљ студије је био утврђивање антиоксидативне активности биљке *Dodonaea viscosa* Jacq. Метанолском екстракту биљке је додата вода и извршена је екстракција *n*-хексаном, хлороформом, етил-ацетатом и *n*-бутанолом. Фитохемијском анализом је утврђено значајно присуство фенола, флавоноида и срчаних гликозида у хлороформском, етилацетатном и *n*-бутанолном екстракту. Антиоксидативни потенцијал ових фракција и заостале водене фракције је утврђен применом четири методе: DPPH, укупна антиоксидативна активност, FRAP тест и тест за одређивање укупних фенола. Етилацетатна фракција је била најпотентнији инхибитор DPPH радикала, у односу на друге фракције. Инхибиција је била 81.14 ± 1.38 % при концентрацији $60 \mu\text{g ml}^{-1}$. IC_{50} вредност ове фракције је била $33.95\pm0.58 \mu\text{g ml}^{-1}$. Ова фракција је имала највећу FRAP вредност ($380.53\pm0.74 \mu\text{M}$ тролокс еквивалента), највећи садржај фенола ($208.58\pm1.83 \text{ GAE } \mu\text{g g}^{-1}$) и најизраженију инхибицију липидне пероксидације (58.11 ± 1.49 % у концентрацији $500 \mu\text{g ml}^{-1}$). Хлороформска фракција је имала највећу укупну антиоксидативну активност, 1.078 ± 0.59 (апсорбација на 695 nm).

(Примљено 21. јуна, ревидирано 9. септембра 2011)

REFERENCES

1. G. Nahak, R. K. Sahu, *J. Am. Sci.* **6** (2010) 123
2. J. McClements, E. A. Decker, *J. Food Sci.* **65** (2000) 1270



3. W. Zheng, S. Y. Wang, *J. Agric. Food Chem.* **49** (2001) 5165
4. O. Baris, M. Golloce, R. Sahin, H. Ozer, *Turk. J. Biol.* **30** (2006) 65
5. A. Saleem, M. Ahotupa, K. Pihlaja, *Z. Naturforsch.* **56** (2001) 973
6. N. Ito, S. Fukushima, A. Hasegawa, M. Shibata, T. Ogiso, *J. Natl. Cancer Inst.* **70** (1983) 343
7. M. G. L. Hertog, E. J. M. Feskeens, C. H. Hollman, M. B. Katan, D. Kromhout, *Lancet* **342** (1993) 1007
8. N. Salah, N. J. Miller, G. Pagana, L. Tijburg, G. P. Bolwell, C. Rice-Evans, *Arch. Biochem. Biophys.* **2** (1995) 339
9. G. C. Yen, P. D. Duh, D. Y. Chuang, *J. Am. Oil Chem. Soc.* **70** (2000) 383.
10. R. P. Singh, K. N. C. Murthy, G. K. Jayaprakasha, *J. Agric. Food Chem.* **50** (2002) 81
11. A. J. Pirzada, W. Shaikh, K. Usmanghani, E. Mohiuddin, *Pak. J. Pharm. Sci.* **23** (2010) 337
12. T. Kefale, G. M. Tsige, K. Asres, E. Engidawork, *Phytother. Res.* **24** (2010) 60
13. R. Mata, J. L. Contreras, D. Crisanto, R. Peredmiranda, P. Castaneda, F. Delrio, *J. Nat. Prod.* **54** (1991) 913
14. K. Sachdev; D. K. Kulshreshtha, *Phytochemistry* **22** (1983) 1253
15. K. Sachdev, D. K. Kulshreshtha, *Phytochemistry* **25** (1986) 1967
16. A. Rojas, L. Hernandez, R. Pereda-Miranda, R. Mata, *J. Ethnopharmacol.* **35** (1992) 275
17. H. Wagner, C. Ludwig, L. Grotjahn, M. S. Y. Khan, *Phytochemistry* **26** (1987) 697
18. A. Ortega, P. E. Garcia, J. Cardenas, C. Mancera, S. Marquina, M. L. D. C. Garduño, E. Maldonado, *Tetrahedron* **57** (2001) 2981
19. H. M. Niu, D. Q. Zeng, C. L. Long, Y. H. Peng, Y. H. Wang, J. F. Luo, H. S. Wang, Y. N. Shi, G. H. Tang, F. W. Zhao, *J. Asian Nat. Prod. Res.* **12** (2010) 7
20. L. S. Teffo, M. A. Aderogba, J. N. Eloff, *Afr. J. Bot.* **76** (2010) 25
21. A. Rojas, S. Cruz, H. Ponce Monter, R. Mata, *Planta Med.* **62** (1996) 154
22. Hemlata, S. B. Kalidhar, *J. Indian Chem. Soc.* **71** (1994) 213
23. M. Getie, T. Gebre-Mariam, R. Rietz, C. Hohne, C. Huschka, M. Schmidtke, A. Abate, R. H. H. Neubert, *Fitoterapia* **74** (2003) 139
24. S. Yentakesh, Y. S. R. Reddy, M. Ramesh, M. M. Swamy, N. Mahadevan, B. Suresh, *Afr. J. Pharm. Pharmacol.* **2** (2008) 83
25. A. Sofowora, *Medicinal Plants and Traditional Medicine in Africa*, Spectrum Books, Ibadan, Nigeria, 1993, p. 150
26. G. E. Trease, W. C. Evans, *Pharmacognosy* 13th ed., Bailliere Tindall, London, 1989, p. 176
27. G. A. Ayoola, H. A. B. Coker, S. A. Adesegun, A. A. Adepoju-Bello, K. Obaweya, E. C. Ezennia, T. O. Atangbayila, *Trop. J. Pharm. Res.* **7** (2008) 1019
28. K. Lee, T. Shibamoto, *Food Chem.* **74** (2001) 443.
29. P. Prieto, M. Pineda, M. Aguilar, *Anal. Biochem.* **269** (1999) 337
30. I. F. F. Benzie, J. J. Strain, *Anal. Biochem.* **239** (1996) 70
31. H. P. S. Makkar, M. Bluemmeli, N. K. Borowy, K. Becker, *J. Sci. Food Agric.* **61** (1993) 161
32. P. Valentao, E. Fernandes, F. Carvalho, P. B. Andrade, R. M. Seabra, M. L. Bastos, *J. Agric. Food Chem.* **50** (2002) 4989
33. M. N. Siddaraju, S. M. Dharmesh, *J. Agric. Food Chem.* **55** (2007) 7377
34. S. J. Meir, B. Kanner, S. P. H. Akiri, *J. Agric. Food Chem.* **43** (1995) 1813



35. D. Strack, in *Plant Biochemistry*, P. M. Dey, J. B. Harborne, Eds., Academic Press, San Diego, CA, 1997, p. 387
36. L. Bravo, *Nutr. Rev.* **56** (1998) 317
37. Y. Cai, Q. Luo, M. Sun, H. Corke, *Life Sci.* **74** (2004) 2157
38. J. Pokorny, N. Yanishlieva, M. H. Gordon, Eds., *Antioxidants in food: practical applications*, Woodhead Publishing Limited, Cambridge, UK, 2001, p. 1
39. M. Pitchaon, M. Suttajit, R. Pongsawatmanit, *Food Chem.* **100** (2007) 1409
40. N. Balasundram, K. Sundram, S. Samman, *Food Chem.* **99** (2006) 191
41. F. Aqil, I. Ahmad, Z. Mehmood, *Turk. J. Biol.* **30** (2006) 177
42. H. I. Ismail, K. W. Chan, A. A. Mariod, M. Ismail, *Food Chem.* **119** (2010) 643.





Antioxidant activities and phenolic constituents of *Cephalotaxus oliveri* Mast. aerial parts

LINGBIN ZENG* and LILIAN L. P. VRIJMOED

Department of Biology and Chemistry, City University of Hong Kong, 83 Tat Chee Avenue,
Kowloon Tong, Hong Kong SAR, China

(Received 1 August, revised 28 October 2011)

Abstract: The antioxidant activity and the responsible chemical constituents in *Cephalotaxus oliveri* Mast. aerial parts were analyzed in the present study. The DPPH (2,2-diphenyl-1-picrylhydrazyl), ABTS (2,2'-azinobis(3-ethyl-benzothiazoline-6-sulfonic acid)), reducing power and total phenolic content assays indicated that the methanol extract of the aerial parts was the most potent radical-scavenger and reducing agent and had the highest content of phenolics among the tested extracts. The high positive linear correlations implied that the four assays had a similar capacity to predict the antioxidant potential of the aerial parts and that the present phenolic compounds contribute significantly to the DPPH and ABTS radical scavenging activities and to the reducing power of the extracts. The plant also displayed considerable superoxide anion radical scavenging activity. LC-MS/MS and GC-MS analyses resulted in the identification of 22 compounds in the methanol extract, of which 15 were phenolic compounds. The total amount of the phenolic compounds in the methanol extract determined by the HPLC method was more than 5.62 mg g⁻¹ dry weight. The considerable antioxidant potential and a high content of phenolic antioxidants suggest that *C. oliveri* aerial parts are a potential source of natural antioxidants.

Keywords: radical scavenging activity; reducing power; total phenolic content; LC-MS/MS; HPLC; GC-MS.

INTRODUCTION

Cephalotaxus is the single genus of the coniferous Cephalotaxaceae.¹ *Cephalotaxus* plants have been used in traditional Chinese medicine for the treatment of human malignant tumors, rheumatism, dyspepsia, abdominal distension and the like.² Among the *Cephalotaxus* species, *Cephalotaxus oliveri* Mast. is endemic to the subtropical forests of China, which have a scattered distribution.¹ Hitherto, a total of eight compounds, including three cephalotaxine-type alka-

* Correspondence: chnah@163.com (Lingbin Zeng), blililian@cityu.edu.hk (L. L. P. Vrijmoed)
doi: 10.2298/JSC110801204Z

loids, three bisflavones and two homoerythrina alkaloids, have been demonstrated to be present in *C. oliveri*.^{3–5} The plant is rich in two anticancer cephalotaxine-type alkaloids, *i.e.*, harringtonine and homoharringtonine.³ Harringtonine and homoharringtonine are clinical drugs in use in China for the treatment of acute non-lymphocytic leukemia and chronic myelogenous leukemia.^{3,5} Moreover, homoharringtonine is in clinic trials in the USA for the treatment of chronic myelogenous leukemia and other cancers.⁶

ROS (reactive oxygen species) include both oxygen radicals, such as superoxide, hydroxyl, peroxy and hydroperoxy radicals, and some non-radical oxidizing agents, such as hydrogen peroxide, hypochlorous acid and ozone.⁷ At normal physiological levels, ROS function as “redox messengers” in intracellular signaling and regulation, whereas excessive ROS damage cellular macromolecules, such as lipids, proteins, and nucleic acids, through inducing oxidative modification and promote cell death.⁷ As results, they cause inflammation or lesions on various organs and are associated with diseases such as atherosclerosis, arthritis and cancers.⁸ Together with endogenous defense systems, regular supplements of exogenous antioxidants limit or prevent the dangerous effects caused by excessive ROS.⁹ Due to the severe side effects of synthetic antioxidants, such as butylated hydroxyanisole (BHA), natural antioxidants from medicinal plants, vegetables, and fruits have received increasing attention and are considered as better alternatives to synthetic antioxidants.

The aerial parts (*i.e.*, branches with leaves) of *C. oliveri* are normally discarded as waste during pruning. To maximize the exploitation of the limited plant resources, it is necessary to evaluate the bioactive potential and analyze the chemical profile of the waste aerial parts. To the best of our knowledge, no data on the antioxidant activities and responsible components of *C. oliveri* aerial parts are hitherto available. Thus, in this study, the antioxidant activities of *C. oliveri* aerial parts were evaluated. The chemical constituents responsible for the activities were also analyzed.

EXPERIMENTAL

Plant materials and chemicals

The aerial parts of *C. oliveri* were collected from the South China Botanical Garden, Guangzhou, China, on January 25, 2008, and identified by Mr. Qiang Wei, a senior engineer from the Garden.

BHA (butylated hydroxyanisole), BHT (butylated hydroxytoluene), DPPH (2,2-diphenyl-1-picrylhydrazyl), ABTS (2,2'-azinobis(3-ethyl-benzothiazoline-6-sulfonic acid)), Trolox (6-hydroxy-2,5,7,8-tetramethylchroman-2-carboxylic acid), Folin-Ciocalteu reagent, gallic acid, trichloroacetic acid, ferric chloride, potassium persulfate, potassium ferricyanide, NADH (β -nicotinamide adenine dinucleotide), NBT (nitroblue tetrazolium), PMS (phenazin methosulfate), protocatechuic acid, gentisic acid, catechin, vanillic acid, epicatechin, caffeic acid, syringic acid, epicatechin gallate, *p*-coumaric acid, taxifolin, apigenin, and emodin were pur-

chased from Sigma-Aldrich (St. Louis, MO). All other reagents were of analytical or HPLC grade.

Sample preparation

The collected plant materials were washed, air-dried at room temperature (*ca.* 23 °C), then ground to a powder and passed through a 20-mesh sieve. The sieved powder was extracted exhaustively with water, methanol, acetone, ethyl acetate, chloroform and hexane (3:50, w/v), respectively, at 220 rpm in a shaker at room temperature and filtered through Whatman No. 1 filter paper (Advantec, Tokyo). All obtained extracts were lyophilized and kept in the dark at –20 °C until use.

The method described by Neo *et al.*¹⁰ with some modification was used to treat the plant material for the chemical constituent analysis by the LC-MS/MS and HPLC methods. In brief, 20 ml of supernatant after centrifugation following the methanol extraction was mixed well with 5 ml water and then evaporated at 50 °C under vacuum to a smaller volume to remove the methanol. The residual aqueous phase was centrifuged to remove the insoluble components. The supernatant was extracted three times with hexane to remove the possibly present free fatty acids and other lipid contaminants. After the removal of hexane at 50 °C under vacuum, the free phenolics (soluble free phenolics, SFP) in the aqueous phase were extracted exhaustively with diethyl ether–ethyl acetate (1:1, v/v) with a solvent to aqueous phase ratio of 1:1 (v/v). The diethyl ether–ethyl acetate extracts were pooled and treated with anhydrous sodium sulfate to remove moisture, filtered, evaporated to dryness under vacuum and finally re-dissolved in 2.25 ml methanol. The precipitate pellet was added into 12 ml water and 5 ml 10 M NaOH and then shaken at 220 rpm overnight. The hydrolyzed solution was adjusted to pH 2. The released phenolics (esterified phenolics, EFP) were extracted exhaustively with diethyl ether–ethyl acetate (1:1, v/v). The diethyl ether–ethyl acetate extracts were combined, evaporated to dryness, and dissolved into 0.75 ml of methanol. The treatment procedure of the methanol extract for chemical analyses by LC-MS/MS and HPLC is schematically presented in Fig. 1.

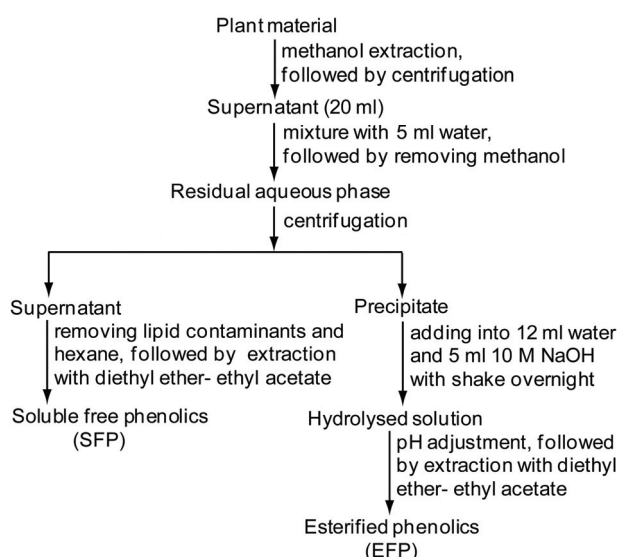


Fig. 1. Treatment scheme of the methanol extract of *C. oliveri* aerial parts for chemical component analyses by LC-MS/MS and HPLC.

DPPH radical scavenging activity

The DPPH radical scavenging effect of the *C. oliveri* extracts was assessed according to the method described by Zeng *et al.*¹¹ with slight modification. In brief, 0.1 ml of the extract solutions or the positive controls BHA and BHT were mixed with 2 ml freshly prepared DPPH solution in ethanol and then incubated for 30 min at room temperature. The DPPH radical scavenging activities were assayed spectrophotometrically in a microplate reader (PowerWave XS, BioTek Instruments, Inc.) at 517 nm. The DPPH radical scavenging activity is reported in µmol of Trolox equivalents per gram extract (µmol TE g⁻¹ dry matter) and as the IC_{50} value (defined as the concentration in mg ml⁻¹ that caused a 50 % inhibition of the DPPH radical).

ABTS radical scavenging activity

The ABTS radical scavenging activity was assayed using the method described by Zeng *et al.*¹¹ with some modifications. Briefly, ABTS radicals were generated in a mixture of 7 mM ABTS and 2.45 mM potassium persulfate in water at room temperature in the dark during 12–16 h. An aliquot of 0.10 ml extract solution or the reference compounds BHA and BHT was introduced into 2.6 ml of diluted ABTS radical solution with absorbance of 0.8 at 734 nm and mixed thoroughly. The reactive mixture was allowed to stand at room temperature for 6 min and absorbance was recorded immediately afterwards at 734 nm in a microplate reader (PowerWave XS). ABTS radical scavenging activity of the extracts is expressed in term of TEAC (Trolox equivalent antioxidant capacity, µmol TE g⁻¹ dry extract). The scavenging activity is also reported as the IC_{50} value (defined as the concentration in µg ml⁻¹ that caused a 50 % inhibition of the ABTS radical).

Reducing power

The reducing power of the extracts was determined by the method of Zeng *et al.*¹¹. Extract solution or the positive controls BHA and BHT (80 µl), sodium phosphate buffer (200 µl, 0.2 M, pH 6.6) and potassium ferricyanide (200 µl, 10 mg ml⁻¹) were mixed and incubated at 50 °C for 20 min. The mixture was then placed into a refrigerator at 4 °C to rapidly lower its temperature. Then, trichloroacetic acid (200 µl, 100 mg ml⁻¹) was added and incubated for 5 min to stop the reaction. Afterwards, the resultant mixture (680 µl) was mixed with 680 µl distilled water and 68 µl ferric chloride (10 mg ml⁻¹). Finally, the absorbance of the resulting mixture was measured in a microplate reader (PowerWave XS). A higher absorbance indicates a stronger reducing power.

Superoxide anion radical scavenging activity

Superoxide anion radical scavenging activity of the extracts of *C. oliveri* was measured by the method of Zhang *et al.*¹² with a slight modification. Briefly, 3 ml of 16 mM Tris-HCl buffer (pH 8.0), containing 1 ml of NBT (150 µM) solution, 1 ml of NADH (468 µM) solution and 1 ml of extract solution or the positive control gallic acid at 0.10 mg ml⁻¹ were mixed at room temperature and the mixture was measured as the blank. Then, 1 ml of PMS solution (60 µM) was added. After incubation at room temperature for 5 min, the absorbance of the resulting mixture was measured at 560 nm. Superoxide radical scavenging activity was calculated as scavenging activity (%) = (absorbance of control – absorbance of sample)/(absorbance of control – absorbance of blank)×100.

Total phenolic content

Total phenolic content of *C. oliveri* extracts was estimated by the Folin-Ciocalteu colorimetric assay according to the method described by Zeng *et al.*¹¹ Briefly, 1.0 ml of extract

solution was mixed with 5 ml of 0.20 M Folin–Ciocalteu reagent. After incubation at room temperature for 6 min, 4 ml of sodium carbonate (75 g l^{-1}) was added. Absorbance of the resulting blue-colored solution was measured in a microplate reader (PowerWave XS) at 760 nm after incubation at room temperature for 2 h with intermittent shaking. The amount of total phenolic content was calculated as gallic acid equivalents (GAE, mg g^{-1} dry extract).

Phenolic constituents in methanol extract analyzed by LC–MS/MS

LC–MS/MS under the negative ion multiple reaction monitoring (MRM) mode was used for the phenolic analysis of the methanol extract using an Agilent 1200 series LC (Agilent, Santa Clara, USA) instrument fitted with a binary pump, an on-line degasser and an Applied Biosystem API 2000 mass spectrometer (Life Technologies Corporation, California, USA) equipped with an ESI (electrospray ionization) interface. The whole LC–MS/MS system was controlled by Analyst software (Life Technologies Corporation, California, USA). The HPLC separation was performed on a reverse-phase Zorbax C18 column ($250 \text{ mm} \times \text{i.d. } 4.6 \text{ mm}, 5 \mu\text{m}$, Agilent, Santa Clara, CA).

The employed mobile phases A and B were acidified water (0.1 % acetic acid, v/v) and methanol, respectively. For the analysis of the SFP fraction, the gradient elution was programmed as follows: from 5 to 35 % B in 10 min; from 35 to 45 % B in 25 min; from 45 to 60 % B in 10 min; from 60 to 70 % B in 10 min and from 70 to 100 % B in 5 min and kept at 100 % B for 10 min. To analyze the EFP fraction, the gradient elution was programmed as follows: from 5 to 10 % B in 2 min and kept at 10 % B for 3 min; from 10 to 40 % B in 10 min; from 40 to 50 % B in 5 min; from 50 to 90 % B in 25 min and from 90 to 100 % B in 10 min and kept at 100 % B for 10 min. The flow rate was 1 ml min^{-1} and the injection volume was $10 \mu\text{L}$. A T-type phase separator was used to split the effluent from the HPLC column into the mass spectrometer. The conditions for the MS analysis were the same as those used by Zeng *et al.*¹¹. The collision energy for each compound was optimized. Nitrogen was used as the nebulizing and collision gas in the MS analysis.

The phenolic compounds in the methanol extract of *C. oliveri* aerial parts were characterized and identified by MS/MS by comparison with the MS data and the LC retention times of authentic standards.

Phenolic content determination by HPLC analysis

The content of phenolic compounds in the methanol extract was determined by the HPLC method using a Waters HPLC system with a 600 pump, a 600 controller, a 2487 dual-wavelength absorbance detector, an in-line degasser and Empower software (Waters Corporation, Massachusetts, USA). The LC conditions for the separation of the component on a reverse-phase Zorbax C18 column ($250 \text{ mm} \times \text{i.d. } 4.6 \text{ mm}, 5 \mu\text{m}$, Agilent, Santa Clara, CA) were the same as for the LC part in the LC–MS/MS analysis. The quantification was performed using the external standard method with the wavelength set at 280 nm. The amount of phenolic compounds is expressed as $\mu\text{g g}^{-1}$ dry extract.

GC–MS determination of the chemical constituents in the methanol extract

The chemical constituents in the methanol extract of *C. oliveri* aerial parts were also analyzed by the GC–MS method, which was realized using an Agilent 7890A GC system (Agilent, Palo Alto) together with an Agilent 5975C mass spectrometer operating in the EI mode and equipped with an HP-5MS capillary column ($30 \text{ m} \times 0.25 \text{ mm} \times 0.25 \mu\text{m}$).

The electron energy was set at 70 eV with a mass range at m/z 25–800. The GC injector temperature and the MS source temperature were set at 280 and 230 °C, respectively. Helium was used as the carrier gas at a flow rate of 1 ml min^{-1} . The oven temperature was pro-



grammed from 60 to 120 °C at a rate of 3 °C min⁻¹, held isothermal for 5 min, raised to 155 °C at 5 °C min⁻¹, held isothermal for 10 min; raised to 170 °C at 3 °C min⁻¹, held for 5 min; raised to 200 °C at 3 °C min⁻¹, held for 10 min; raised to 250 °C at 5 °C min⁻¹, held for 10 min; to 270 °C at 10 °C min⁻¹ and then held for 15 min. An aliquot of 1.0 µl methanol extract dissolved in acetone was injected automatically in the splitless mode.

The components were identified based on a comparison of their gas chromatographic retention indices and mass spectra to those from NIST05 MS library and from the literature. Retention indices were calculated for each separate component against *n*-alkane standards (C8–C40, Sigma–Aldrich, Switzerland) on the HP-5MS column.

Statistical analysis

All data are presented as means ± SD. Differences at $p < 0.05$ were considered statistically significant. All the statistical analyses were performed with Origin 6.0 (Microcal Software, Inc., Northampton) or Excel 2003 (Microsoft Corporation, Redmond, WA).

RESULTS

DPPH radical scavenging activity

The DPPH radical scavenging effect of *C. oliveri* extracts compared with BHA and BHT is presented in Fig. 2. Water extract (WE) and methanol extract (ME) exhibited a similarly strong ability to quench the DPPH radical ($p > 0.05$) with IC_{50} values of 0.96 and 0.82 mg ml⁻¹, respectively. These values are comparable to the IC_{50} value of BHT (0.55 mg ml⁻¹). In contrast, the hexane extract (HE) showed the weakest scavenging effect ($p < 0.01$), with only about 10 % activity at 10 mg ml⁻¹. The DPPH radical scavenging activity expressed as Trolox equivalents of the extracts were 316.1±1.0, 331.7±4.8, 250.0±2.6, 60.3±1.8, 45.3±2.1 and 12.8±1.8 µmol TE g⁻¹ for WE, ME, acetone extract (AE), ethyl acetate extract (EE), chloroform extract (CE) and HE, respectively. The TEAC values of WE and ME were more than 24 times that of HE. The results showed the order of DPPH radical scavenging activities of the extracts as ME > WE > AE > EE > CE > HE ($p < 0.01$).

ABTS radical scavenging activity

The ABTS radical scavenging activity of the extracts and BHT and BHA are shown in Fig. 3. For CE and HE, when the assay concentrations were > 2.5 mg ml⁻¹, the absorbance of the extract solutions *per se* at 734 nm apparently affected the results. They had only very weak ABTS radical scavenging activity with inhibition of only 27.3±0.2 and 10.4±0.6 %, respectively, at 2.5 mg ml⁻¹. The respective IC_{50} values of WE, ME, AE and EE were 0.76, 0.49, 0.82 and 3.36 mg ml⁻¹, while the respective values of BHA and BHT were 0.054 and 0.080 mg ml⁻¹. These result suggested that the extracts had only weak or moderate ABTS radical scavenging activity. In addition, the TEAC values of the extracts ranged from 22.5±1.7 to 621.6±1.7 µmol TE g⁻¹ dry weight. ME had the strongest ABTS scavenging activity with a TEAC value 27 times higher than that of HE. The results

indicated that the order of ABTS radical scavenging activity of the extracts was ME > WE > AE > EE > CE > HE ($p < 0.01$).

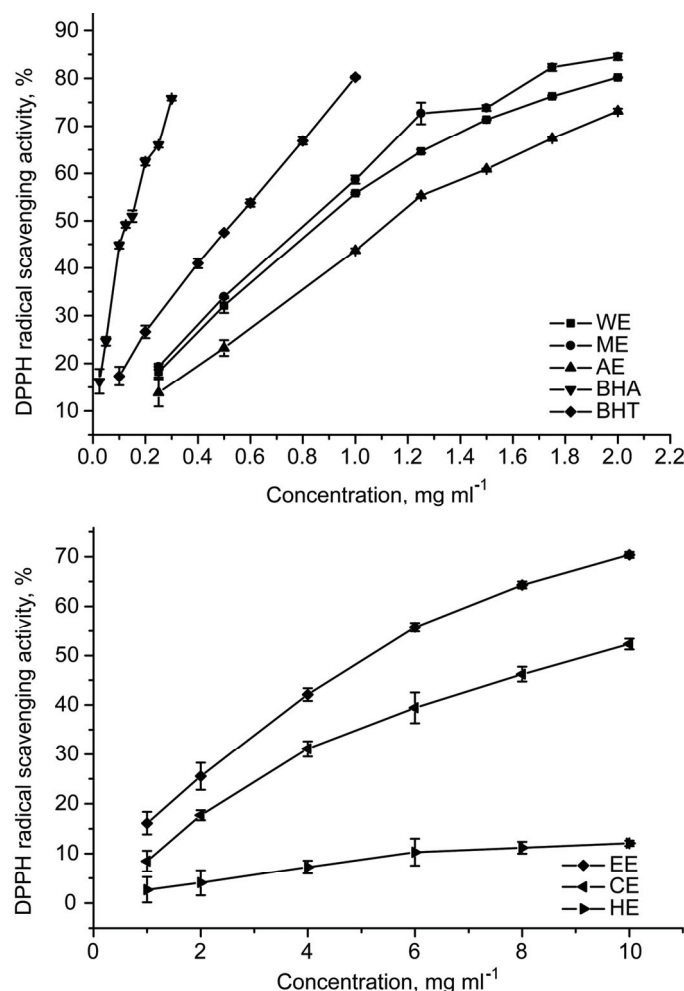


Fig. 2. DPPH radical scavenging activities of different extracts of *C. oliveri* aerial parts and positive controls. WE, water extract; ME, methanol extract; AE, acetone extract; EE, ethyl acetate extract; CE, chloroform extract; HE, hexane extract. The values are the mean of three determinations $\pm SD$ (standard deviation).

Reducing power

The reducing powers of the extracts of *C. oliveri* aerial parts are indicated in Fig. 4. Two-way ANOVA analysis suggested that the order of reducing power of the extracts ME > WE > AE > EE > CE > HE, which is consistent with the results in the DPPH and ABTS assays. At the concentrations of 0.8 mg ml⁻¹ for

ME and 1.5 mg ml⁻¹ for WE, their reducing power was equal to that of BHT. However, CE and HE had very weak reducing power.

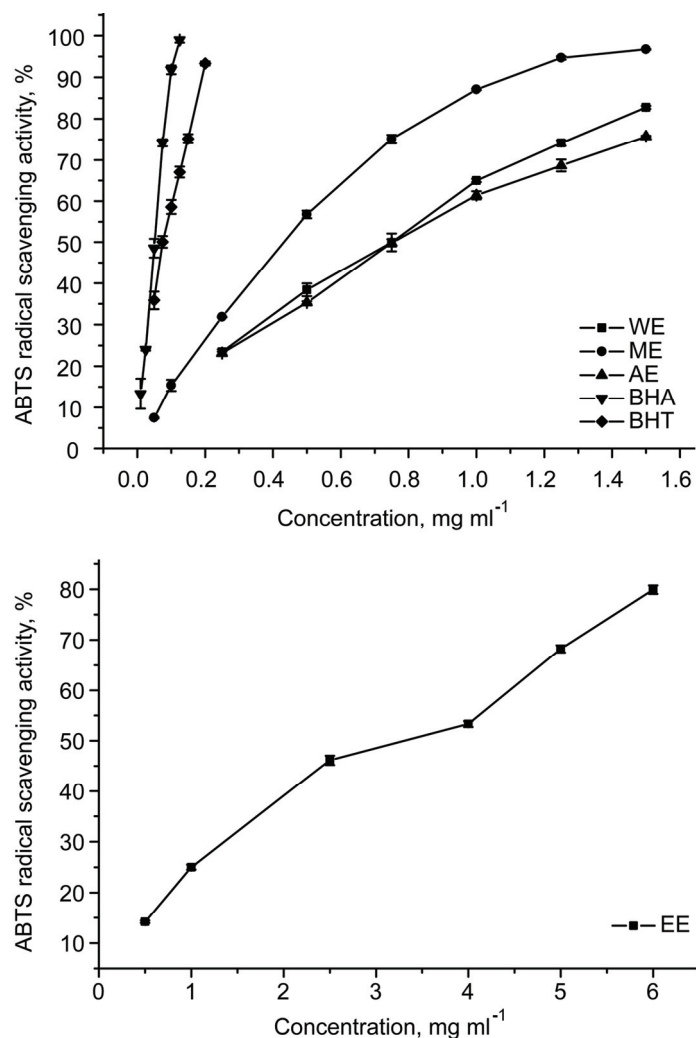


Fig. 3. ABTS radical scavenging activities of different extracts of *Cephalotaxus oliveri* aerial parts and positive controls. WE, water extract; ME, methanol extract; AE, acetone extract; EE, ethyl acetate extract. The values are the mean of three determinations $\pm SD$ (standard deviation).

Superoxide anion radical scavenging activity

Superoxide anion radical scavenging activities of the extracts at 0.1 mg ml⁻¹ are shown in Fig. 5. Two-sample *t*-tests suggested that the descending order of the scavenging activity of the extracts is EE ($49.5 \pm 1.2\%$) > CE ($44.9 \pm 1.3\%$) >

HE ($41.6 \pm 0.6\%$) > ME ($33.2 \pm 0.6\%$) \geq AE ($32.6 \pm 0.8\%$) > WE ($29.4 \pm 1.0\%$), while the activity of gallic acid was $57.5 \pm 0.3\%$. This means that EE had the strongest superoxide anion scavenging activity, which was comparable to that of gallic acid.

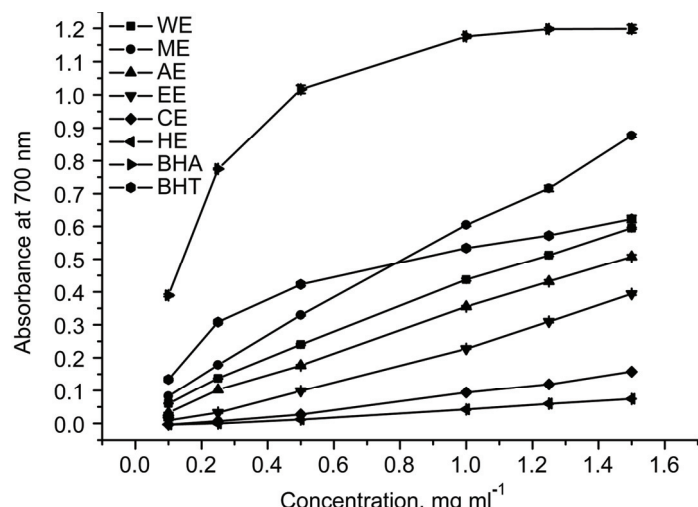


Fig. 4. Reducing power of different extracts of *C. oliveri* aerial parts and positive controls.
WE, water extract; ME, methanol extract; AE, acetone extract; EE, ethyl acetate extract;
CE, chloroform extract; HE, hexane extract. The values are the mean of three
determinations $\pm SD$ (standard deviation).

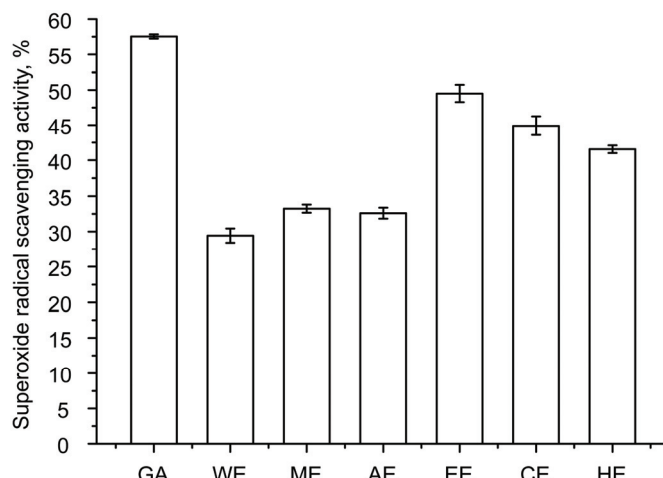


Fig. 5. Superoxide radical scavenging activities of different extracts of *C. oliveri* aerial parts and positive control at 0.1 mg ml^{-1} . GA, gallic acid; WE, water extract; ME, methanol extract; AE, acetone extract; EE, ethyl acetate extract; CE, chloroform extract; HE, hexane extract.
The values are the mean of three determinations $\pm SD$ (standard deviation).

Total phenolics content

The total phenolic content of the six extracts are presented in Table I, which varied extensively ($p < 0.01$) from 7.2 ± 0.2 to 96.1 ± 1.8 mg GAE g⁻¹ dry weight. ME had the highest total phenolic content at 96.1 ± 1.8 mg GAE g⁻¹ dry weight, followed by WE, AE, EE, CE and HE in descending order. The total phenolic content of ME was about 13 and four times larger than those of HE and CE, respectively.

TABLE I. Total phenolics content (GAE, mg g⁻¹) in the extracts of *C. oliveri* aerial parts (means of three replicates $\pm SD$ (standard deviation) as mg g⁻¹ dried extract)

WE ^a	ME ^b	AE ^c	EE ^d	CE ^e	HE ^f
78.23 ± 1.48	96.07 ± 1.85	68.98 ± 2.66	47.96 ± 0.44	23.65 ± 0.43	7.21 ± 0.23

^aWater extract; ^bmethanol extract; ^cacetone extract; ^dethyl acetate extract; ^echloroform extract; ^fhexane extract

Phenolic components in the methanol extract determined by LC-MS/MS and HPLC

In total, 12 phenolic compounds were identified in the methanol extract of *C. oliveri* aerial parts by LC-MS/MS analysis and their MS data and content are given in Table II. All the 12 compounds were detected in the SFP fraction but only three in the EFP fraction. Apigenin, *p*-coumaric acid, and emodin were present in both the SFP and EFP fractions. The content of most of the individual

TABLE II. Phenolic compounds in the methanol extract of *C. oliveri* aerial parts identified by ESI-MS/MS and their content determined by HPLC

No.	Compound	M m/z [M-H] ⁻	MS/MS m/z	Retention time min ^a		Content ^b , µg g ⁻¹		
				SFP	EFP	SFP	EFP	Total ^c
1	Protocatechuic acid	153	109, 108, 91	10.01	— ^d	54.0 ± 0.2	—	54.01
2	Gentisic acid	153	109	10.98	—	602.1 ± 6.8	—	602
3	Catechin	289	221, 245, 203	11.62	—	256.0 ± 3.6	—	256
4	Vanilllic acid	167	108, 123, 152	14.19	—	184.6 ± 2.2	—	185
5	Epicatechin	289	221, 245, 109	14.27	—	2205.8 ± 9.9	—	2206
6	Caffeic acid	179	135	14.40	—	87.8 ± 1.7	—	87.8
7	Syringic acid	197	182, 167, 123	14.83	—	Trace	—	Trace
8	Epicatechin gallate	441	169	16.43	—	ND ^e	—	ND ^e
9	<i>p</i> -Coumaric acid	163	119	18.54	20.52	129.9 ± 5.3	110.9 ± 3.5	240
10	Taxifolin	303	125, 285	19.07	—	2349 ± 3.3	—	235
11	Apigenin	269	117, 149, 151	49.48	32.33	817.5 ± 5.3	677.4 ± 3.5	1495
12	Emodin	269	225, 241	63.18	45.73	14.9 ± 0.6	247.0 ± 2.1	262
Total ^f								5620

^aRetention time in LC-MS/MS analysis; ^bmeans of three replicates $\pm SD$ as µg g⁻¹ dry methanol extract; ^csum of content of phenolic compounds in both SFP and EFP fractions; ^dabsent in the fraction; ^eContent not determined; ^fsum of content of all identified phenolic compounds



phenolic compounds was larger than $100 \mu\text{g g}^{-1}$ dry methanol extract, especially epicatechin and apigenin, the contents of which were larger than 1.0 mg g^{-1} dried methanol extract. The total amount of the phenolic compounds identified was more than 56.2 mg g^{-1} dried methanol extract.

Chemical components detected by GC–MS analysis

Based on the comparison of the retention indices and mass spectra to those from NIST05 MS library and the literature, ten compounds as shown in Table III were identified in the methanol extract of *C. oliveri* aerial parts by GC–MS analysis. The identified compounds are characterized by the presence of three phenolic compounds, *i.e.*, ferruginol, 2,5-bis(1,1-dimethylethyl)phenol and α -tocopherol. In addition, an important phytosterol, *i.e.*, β -sitosterol, was also detected in the methanol extract.

TABLE III. Chemical components in the methanol extract of *C. oliveri* aerial parts analyzed by GC–MS

No.	R _t ^a / min	Compound	R _I ^b
1	13.305	1-(4-Methylphenyl)ethanone	1188
2	28.580	2,4-Bis(1,1-dimethylethyl)phenol	1516
3	28.931	Dihydroactinidiolide	1526
4	43.855	6,10,14-Trimethyl-2-pentadecanone	1846
5	48.507	Hexadecanoic acid, methyl ester	1922
6	51.432	Hexadecanoic acid	1969
7	69.720	Ferruginol	2330
8	70.482	4,8,12,16-Tetramethylheptadecan-4-oxide	2342
9	95.559	α -Tocopherol	3119
10	100.709	β -Sitosterol	3291

^aRetention time of elution from HP-5MS column; ^bRetention index on an HP-5MS column in reference to C8–C40 *n*-alkanes

DISCUSSION

Antioxidant potential

Foods or extracts of medicinal plants are mixtures with multi-functions. It is easily understood that multiple reaction characteristics and mechanisms, and different phase localizations are usually involved, hence any single method will be not accurate and comprehensive enough to reflect the antioxidant profile of a mixed or complex system.¹³ Therefore, more than two different methods are typically used. In the present study, DPPH, ABTS, superoxide anion scavenging, reducing power and the Folin–Ciocalteu colorimetric assays were used to test the antioxidant potential of extracts from *C. oliveri* aerial parts. They are chemical methods associated with electron donation or hydrogen donation and can be spectrophotometrically assessed.¹⁴



DPPH and ABTS radicals are two artificial free radicals that are widely used to test the antioxidant potential of plant extracts or food materials. The antioxidant effect is determined by measuring the reduction of the radicals in the test systems. The most widely and commonly used method recently to evaluate the DPPH and ABTS radicals scavenging activities is to monitor the decrease of UV absorption at 517 and 734 nm, respectively, with a UV spectrophotometer.¹⁴ The results obtained in this study implied that the DPPH and ABTS scavenging activities of all the extracts were dose-dependent, as is the case with BHA and BHT. Generally, except water, the solvents with higher polarity showed better extractability of the antioxidants scavenging DPPH and ABTS radicals from *C. oliveri* aerial parts. For each solvent extract, the TEAC value in the ABTS test was overtly higher than that in the DPPH test. One of the reasons for this may be the color interference by some components, such as anthocyanins (λ_{max} 475–485 nm), with DPPH chromogen,¹⁵ which resulted in lower measured TEAC values.

The reducing power was measured by direct electron donation to reduce the Fe³⁺/ferricyanide complex to ferrous products, while electron-donating activity is an important mechanism of phenolic antioxidant action. Ferrous ions can be monitored spectrophotometrically at 700 nm. Increased absorbance at 700 nm indicates increased reducing power. The reducing power of all the extracts of *C. oliveri* aerial parts was dose-dependent. The reducing powers of WE and ME were strong and comparable to that of BHT.

Superoxide anion radical contributes to tissue damage and various diseases. In this study, superoxide anion radical was generated by the non-enzymatic PMS–NADH–NBT system. EE had the strongest superoxide anion radical scavenging activity with *ca.* 50 % inhibition at a concentration of 0.1 mg ml⁻¹.

Phenolic compounds are ubiquitous secondary metabolites in plants. It has been well demonstrated that the antioxidant activity of plant materials is well correlated with the content of phenolic compounds they produce. In the present study, except HE, all the five other extracts had a high total phenolic content (GAE > 20 mg g⁻¹ dry extract).¹⁶ The results implied that *C. oliveri* aerial parts contain a high level of phenolic compounds and that ME had the highest antioxidant potential, whereas HE had the lowest potential. This result suggested that high polarity organic solvents extract the phenolic compounds better from *C. oliveri* aerial parts than those of lower polarity.

Correlations of the assays determining the antioxidant potential of the extracts

Highly positive linear correlations between the total phenolic content and DPPH radical scavenging activity ($R = 0.9466$), ABTS radical scavenging capacity ($R = 0.9914$) and reducing power ($R = 0.9870$) suggest that the phenolic compounds are significantly responsible for the antioxidant ability, the scavenging of DPPH and ABTS radicals and the reducing power of the extracts, which is

consistent with previous results showing the antioxidant activity of *C. sinensis*.¹⁷ Highly positive linear correlations were also present between the reducing power assay and the DPPH ($R = 0.9609$) and ABTS assays ($R = 0.9977$), which implies that the constituents present in the extracts scavenging DPPH and ABTS radicals are also able to reduce ferric ions and that the reducing ability seems contributive to the free radical-scavenging capacity of the extracts. In addition, the highly positive linear relationship between DPPH and ABTS radicals scavenging activity ($R = 0.9883$) shows that the two methods have similar predictive capacities for the antioxidant activity of *C. oliveri* extracts. However, such relationships did not exist between superoxide radical scavenging activity and total phenolic content and other antioxidant activities of the extracts. Such different behaviors may be due to differences in the main active components and mechanisms of the action of scavenging different radicals and reaction with the test probes.¹⁸

Chemical components

For the first time, the chemical profile of *C. oliveri* using the LC–MS/MS and GC–MS methods is reported. Phenolic compounds are the characteristic components in the chemical profile. The LC–MS/MS analysis resulted in the identification of 12 phenolic compounds in the methanol extract of *C. oliveri* aerial parts, including four hydroxybenzoic acids (*i.e.*, protocatechuic acid, gentisic acid, vanillic acid and syringic acid), two hydroxycinnamic acids (*i.e.*, caffeic acid and *p*-coumaric acid), three flavan-3-ols (*i.e.*, catechin, epicatechin and epicatechin gallate), two flavanones (*i.e.*, taxifolin and apigenin) and one phenolic anthraquinone (*i.e.*, emodin). Except *p*-coumaric acid, apigenin and emodin, all the other identified phenolic compounds were detected only in the SFP fraction, which means that they were present in the soluble free form in the methanol extract. Apigenin and *p*-coumaric acid were present in both the soluble free form and bound form, while emodin had a much higher content in the EFP fraction than in the SFP fraction, which means that most of emodin in the methanol extract of *C. oliveri* was present in the bound form. The GC–MS analysis suggested the presence of ten organic compounds in the methanol extract of *C. oliveri* aerial parts, of which three were phenolic compounds. As a result, a total of 15 phenolic compounds were identified in the methanol extract by both the LC–MS/MS and GC–MS methods.

Due to the reactivity of phenol moiety (hydroxyl substituent on the aromatic ring), most phenolic compounds can behave as antioxidants. The presence of at least 15 phenolic compounds implies *C. oliveri* should have antioxidant potential. Phenolic acids are ubiquitous in plant food (*e.g.*, fruits, vegetables and coffee)¹⁹ and are the main phenols consumed by humans. The phenolic acids identified in this research are all prominent naturally occurring ones and their role as dietary antioxidants has received increasing attention.²⁰ They possess various potent an-

tioxidant activities.^{20,21} The other phenolic compounds also have potent antioxidant activities. For example, of the tocopherols and tocotrienols in the vitamin E group found in food, only α -tocopherol meets human vitamin E requirements. α -Tocopherol is the most powerful soluble lipid natural antioxidant known.²² It scavenges peroxy radicals extremely rapidly, which maintains the integrity of long-chain polyunsaturated fatty acids in the membranes of cells and thus maintains their bioactivity.^{22,23} Moreover, it possibly plays a role in the prevention of cancer and atherosclerosis.²² In addition, β -sitosterol is one of the most abundant phytosterols, which has demonstrated, to some extent, DPPH and hydrogen peroxide scavenging activity and strong nitric oxide radical-scavenging activity. It also inhibits the autoxidation of methyl linoleate and polyunsaturated fatty acid oxygenation.²⁴ The presence of the components with antioxidant potency confirms and contributes to the antioxidant activities of the *C. oliveri* extracts.

CONCLUSIONS

Some natural antioxidants have remarkable pharmaceutical and therapeutic potentials. They are in the central area in the development of functional foods and can be used as food additives to prevent the lipid oxidation of foods. The considerable antioxidant activities and the presence of important phenolic antioxidants imply that the aerial parts of *C. oliveri*, usually cut off as waste, could be a source of natural antioxidants.

Acknowledgements. The authors gratefully thank the School of Graduate Studies of the City University of Hong Kong for a PhD studentship to the first author Lingbin Zeng, the South China Botanical Garden, Guangzhou, China for providing the plant material and Mr. Qiang Wei for identification of the plant.

ИЗВОД

АНТИОКСИДАТИВНА АКТИВНОСТ И САДРЖАЈ ФЕНОЛА У НАДЗЕМНИМ ДЕЛОВИМА БИЉКЕ *Cephalotaxus oliveri* MAST.

LINGBIN ZENG и LILIAN L. P. VRIJMOED

Department of Biology and Chemistry, City University of Hong Kong, 83 Tat Chee Avenue, Kowloon Tong, Hong Kong SAR, China

У овој студији је анализирана антиоксидативна активност и хемијски састав надземних делова биљке *Cephalotaxus oliveri* Mast. Тестови са DPPH (2,2-дифенил-1-пикрилхидразил) и ABTS (2,2'-азинобис(3-етил-бензотиазолин-6-сулфонска киселина)), као и тестови за одређивање редукујућег потенцијала и садржаја фенола су показали да метанолни екстракт надземних делова биљке има највећи потенцијал за хватање радикала и редукцију, због велике концентрације фенола. Велика позитивна корелација између четири теста указује на сличне могућности тестова у процени антиоксидативног потенцијала. Биљка је, такође, показала да има значајан капацитет хватања супероксид анјонског радикала. Методама LC-MS/MS и GC-MS идентификована су 22 једињења у метанолном екстракту, од којих су 15 фенолна јединења. Укупни садржај фенола у метанолном екстракту је одређиван методом HPLC и чинио је више од 56,2 mg g⁻¹ суве масе. Значајан антиоксидативни потенцијал и висок садржај

фенолних антиоксиданаса указују да би надземни делови *C. oliveri* могли бити коришћени као извор природних антиоксиданаса.

(Примљено 1. августа, ревидирано 28. октобра 2011)

REFERENCES

1. L. G. Fu, N. Li, R. R. Mill, in *Flora of China*, Z. Y. Wu, P. H. Raven, Eds., Science Press, Beijing and Missouri Botanical Garden Press, St. Louis, 2000, p. 85
2. Editorial Board of China Herbal, State Administration of Traditional Chinese Medicine, China, *China Herbal*, Vol. 4, Shanghai Science and Technology Press, Shanghai, China, 1999, p. 335
3. T. P. Chu, *Acta Phytotaxon. Sin.* **17** (1979) 7
4. Z. W. Ma, G. F. He, W. F. Yin, *Acta Bot. Sin.* **28** (1986) 641
5. F. X. Zhang, Z. H. Wang, W. D. Pan, Y. J. Li, J. Q. Mai, J. Q. Sun, G. E. Ma, *Acta Bot. Sin.* **2** (1978) 129
6. H. Itokawa, X. Wang, K. H. Lee, 2005. in *Anticancer Agents from Natural Products*, G. M. Cragg, D. G. I. Kingston, D. J. Newman, Eds., Brunner-Routledge Psychology Press, Boca Raton, FL, p. 47
7. M. L. Circu, T. Y. Aw, *Free Radical Biol. Med.* **48** (2010) 749
8. C. Balsano, A. Alisi, *Curr. Pharm. Des.* **15** (2009) 3063
9. I. P. Kaur, T. Geetha, *Mini Rev. Med. Chem.* **6** (2006) 305
10. Y. P. Neo, A. Ariffin, C. P. Tan, Y. A. Tan, *Food Chem.* **122** (2010) 353
11. L. B. Zeng, Z. R. Zhang, Z. H. Luo, J. X. Zhu, *Food Chem.* **125** (2011) 456
12. Q. F. Zhang, Z. R. Zhang, H. Y. Cheung, *Food Chem.* **115** (2009) 297
13. R. L. Prior, X. L. Wu, K. Schacht, *J. Agric. Food Chem.* **53** (2005) 4290
14. J. K. Moon, T. Shibamoto, *J. Agric. Food Chem.* **57** (2009) 1655
15. J. M. Awika, L. W. Rooney, X. Wu, R. L. Prior, L. Cisneros-Zevallos, *J. Agric. Food Chem.* **51** (2003) 6657
16. K. Tawaha, F. Q. Alali, M. Gharaibeh, M. Mohammad, T. El-Elimat, *Food Chem.* **104** (2007) 1372
17. M. K. Saeed, Y. L. Deng, Z. Parveen, R. J. Dai, W. Ahmad, Y. H. Yu, in *Proceeding of IEEE/ICME International Conference on Complex Medical Engineering 2007*, Beijing, China, 2007, p. 1651
18. A. Cakir, A. Mavi, A. Yildirim, M. E. Duru, M. Harmandar, C. Kazaz, *J. Ethnopharmacol.* **87** (2003) 73
19. K. Herrmann, *Crit. Rev. Food Sci. Nutr.* **28** (1989) 315
20. R. J. Robbins, *J. Agric. Food Chem.* **51** (2003) 2866
21. F. Natella, M. Nardini, M. D. Felice, C. Scaccini, *J. Agric. Food Chem.* **47** (1999) 1453
22. C. Schneider, *Mol. Nutr. Food Res.* **49** (2005) 7
23. M. G. Traber, J. Atkinson, *Free Radical Biol. Med.* **43** (2007) 4
24. G. Cefarelli, B. D'Abrosca, A. Fiorentino, A. Izzo, C. Mastellone, S. Pacifico, V. Piscopo, *J. Agric. Food Chem.* **54** (2006) 803.





Mixed ligand complexes of essential metal ions with L-glutamine and succinic acid in sodium dodecyl sulfate–water mixtures

GANDHAM HIMA BINDU¹ and GOLLAPALLI NAGESWARA RAO^{2*}

¹Department of Engineering Chemistry, Andhra University, India and ²Department of Inorganic and Analytical Chemistry, Andhra University, Visakhapatnam-530 003, India

(Received 1 February, revised 25 July 2011)

Abstract: Speciation of mixed ligand complexes of Co(II), Ni(II) and Cu(II) with L-glutamine and succinic acid was studied in varying amounts (0.0–2.5 %, w/v) of sodium dodecyl sulfate (SDS) in aqueous solutions while maintaining an ionic strength of 0.16 mol L⁻¹ (NaCl) at 303.0 K. Titrations were performed in the presence of different relative concentrations (M:L:X = 1:2:2, 1:4:2 and 1:2:4) of metal (M) to L-glutamine (L) to succinic acid (X) using sodium hydroxide. The stability constants of the ternary complexes were refined with MINIQUAD75. The best-fit chemical models were selected based on statistical parameters and residual analysis. The species detected were ML₂X, MLX, MLXH and MLXH₂ for Co(II), Ni(II) and Cu(II). The increased stability of the ternary complexes compared to their binary complexes was believed to be due to electrostatic interactions of the side chains of the ligands, charge neutralization, chelate effect, stacking interactions and hydrogen bonding. The species distribution with pH at different compositions of SDS and plausible equilibria for the formation of the species are also presented.

Keywords: speciation; mixed ligand complexes; L-glutamine; succinic acid; SDS.

INTRODUCTION

The specificity and selectivity of enzyme–substrate reactions are achieved by manipulating the equivalent solution dielectric constants at the active site. Knowledge of the equivalent solution dielectric constant can throw light on the mechanism of the reaction. Furthermore, intramolecular and ligand–ligand stacking interactions in mixed ligand complexes are favored in water–organic media, which reduce the dielectric constant of the solution. Hence, modeling studies involving ternary complexes have gained popularity in different aqua–organic mixtures with varying dielectric constants.^{1–4} L-Glutamine (Gln) serves as a vehicle for transporting ammonia in a nontoxic form from peripheral tissues to visceral or-

* Corresponding author. E-mail: gollapallinr@yahoo.com
doi: 10.2298/JSC110201177B

gans where the ammonia can be excreted as ammonium ions (kidneys) or converted to urea (liver).⁵ Gln is utilized in the brain for respiration and biosynthesis of substances related to neuronal functions, such as γ -aminobutyric acid, GABA. It is also utilized for the growth and differentiation of the neural cells.⁶ It is often depleted in stress states, such as malignancy.⁷ Gln has a possible therapeutic role in the prevention of damage to normal tissues, including peripheral nerves, during chemotherapy.⁸

Succinic acid (Suc) is involved in the citric acid or tricarboxylic acid (TCA) cycle and the glyoxalate cycle. It is synthesized in almost all microbial, plant, and animal cells.⁹ The concentration of Suc in human blood plasma is 1.0–6.0 mg L⁻¹. Suc can be used for the manufacture of medicaments or nutritional supplements effective for the treatment of insulin resistance in mammals, preferably in non-insulin dependent diabetic humans.¹⁰ On the other hand, recent analysis showed that the fermentative production of Suc from renewable resources could be more cost-effective than the petroleum-based processes.¹¹ Suc is a bidentate ligand. In coordination chemistry, it forms strong complexes with many metal ions. The mixed ligand complexes of Gln and Suc with calcium and magnesium in acetonitrile–water and ethylene glycol–water and of cobalt and nickel in urea–water and DMF–water media were reported earlier.^{1,12–14} In this study, speciation of ternary complexes of Co(II), Ni(II) and Cu(II) with Gln and Suc in SDS–water mixtures was investigated.

EXPERIMENTAL

Solutions of Co(II), Ni(II) and Cu(II) chlorides (0.1 mol L⁻¹) were prepared by dissolving GR Grade (Merck, India) salts in triple distilled water. Aqueous solutions of Gln and Suc (Merck, India) were also prepared. To increase the solubility of Gln and Suc and to suppress hydrolysis of the metal salts, the mineral acid concentration in the above solutions was maintained at 0.05 mol L⁻¹. SDS (Merck, India) was used as received. A 0.2 mol L⁻¹ hydrochloric acid (Qualigens, India) solution and a 0.4 mol L⁻¹ sodium hydroxide (Qualigens, India) were prepared. A 2 mol L⁻¹ sodium chloride (Qualigens, India) solution was prepared to maintain the ionic strength in the titrand. To assess the errors that might have crept into the determination of the concentrations, the data were subjected to analysis of variance of one-way classification (ANOVA). The strength of the alkali was determined using the Gran plot method.¹⁵

Apparatus

The titrations were performed in media containing varying concentrations of SDS maintaining an ionic strength of 0.16 mol L⁻¹ with sodium chloride at 303.0±0.1 K. A sytronics μ pH system (model 362) (readability 0.001) was used. The glass electrode was equilibrated in a well-stirred SDS–water mixture containing inert electrolyte. The effect of variations in asymmetry, liquid junction potential, activity coefficient, sodium ion error and dissolved carbon dioxide on the response of glass electrode were accounted for in the form of a correction factor, which was computed from simulated acid–base titration data calculated by the SCPHD program.^{16,17} A correction was applied to the pH meter dial reading by using a correction factor. Titrations of a strong acid with alkali were performed at regular intervals to check the complete equilibration of the electrode. The calomel electrode was refilled with an SDS–water

mixture of equivalent composition to that of the titrand. In each of the titrations, the titrand consisted of 1–3 mmol of mineral acid in a total volume of 50 cm³. The titrations were performed in the presence of different relative concentrations (1:2:2, 1:4:2 and 1:2:4) of metal (M) to Gln (L) and Suc (X) with 0.4 mol L⁻¹ NaOH.

Modeling strategy

The best-fit chemical models consisting of stoichiometric coefficients and logarithm of stability constants ($\log \beta$) were arrived at using the computer program Miniquad 75.¹⁸ Some heuristics were followed in refining stability constants and validating models.^{19,20} The formation constants for acid–base equilibria and those for binary metal complexes of Gln and Suc were fixed in the refinement of the mixed ligand stability constants using MINIQUAD75.

RESULTS AND DISCUSSION

Complex equilibria

A preliminary investigation of alkalimetric titrations of mixtures containing different mole ratios of Gln and Suc in the presence of a mineral acid and an inert electrolyte inferred that MLXH, MLX, ML₂X and MLXH₂ species are formed for Co(II), Ni(II) and Cu(II). The parameters of the best-fit models and statistical parameters are given in Table I.²¹ The very low standard deviation in the $\log \beta$ values indicates the precision of these parameters. The small values of U_{corr} indi-

TABLE I. Best fit chemical models of Co(II), Ni(II) and Cu(II)–L-glutamine–succinic acid complexes in SDS–water mixtures. Temperature: 303 K; ionic strength: 0.16 mol L⁻¹

SDS % w/v	log β_{mlxh} (SD)				NP	$U_{\text{corr}} \times 10^8$	Skew- ness	Kurto- sis	χ^2	R Factor
	1110	1111	1112	1210						
Co(II) (pH range 2.0–9.0)										
0.0	8.12(13)	14.13(30)	18.99(21)	11.88(10)	152	14.27	1.40	15.43	169.24	0.013
0.5	7.94(23)	14.85(15)	18.85(39)	11.90(13)	177	25.05	4.50	43.64	416.27	0.016
1.0	7.69(25)	14.23(30)	18.54(47)	11.65(13)	177	28.64	3.62	35.50	333.20	0.018
1.5	7.78(29)	14.47(29)	19.17(21)	11.85(11)	182	18.93	7.15	76.51	744.57	0.014
2.0	7.78(26)	14.05(52)	19.26(17)	11.81(11)	177	28.14	3.82	37.05	236.59	0.017
2.5	7.15(25)	14.15(14)	18.82(12)	11.06(12)	182	14.13	6.28	64.73	593.91	0.012
Ni(II) (pH range 2.0–9.0)										
0.0	9.09(19)	14.71(20)	19.79(10)	13.40(13)	168	18.03	-0.71	6.06	136.79	0.014
0.5	8.80(16)	14.17(24)	18.66(20)	13.00(11)	168	11.15	-0.09	12.45	313.38	0.011
1.0	8.79(13)	13.99(34)	18.68(19)	13.02(12)	167	16.09	-0.81	10.55	323.43	0.013
1.5	8.06(14)	13.83(23)	18.80(11)	11.95(20)	176	17.95	-1.01	8.50	289.27	0.013
2.0	8.14(15)	13.73(26)	18.69(12)	12.27(16)	173	20.39	-0.37	8.17	173.85	0.015
2.5	7.99(13)	13.51(24)	18.46(9)	11.66(44)	181	10.92	0.38	8.30	40.02	0.010
Cu(II) (pH range 2.0–6.0)										
0.0	11.73(7)	16.33(8)	20.13(10)	17.79(7)	153	2.73	-0.60	3.80	23.08	0.005
0.5	11.69(6)	15.99(6)	19.67(8)	17.58(6)	149	4.68	-1.69	9.91	138.36	0.007
1.0	11.18(8)	15.78(4)	19.23(7)	17.97(4)	161	4.21	-0.55	7.71	74.41	0.006
1.5	12.40(9)	16.39(14)	20.59(7)	18.07(13)	150	15.08	0.03	4.75	53.41	0.012
2.0	11.03(16)	15.29(19)	19.52(7)	17.31(7)	157	6.38	-0.91	5.67	29.30	0.008
2.5	12.30(8)	15.75(28)	19.98(8)	18.31(11)	156	11.48	-0.24	3.20	1.69	0.010



cate that the model is consistent with the experimental data.²² For most of the systems, the kurtosis values were around 3 and, hence, the residuals form a mesokurtic pattern. For very few systems are the kurtosis values more than 3 (lepto-kurtic pattern). The values of skewness between -1.69 and 7.15 show that the residuals form a part of a normal distribution and hence the least squares method can be applied to the present data. The sufficiency of the model is further evident from the low crystallographic *R*-factor values, which indicate the need for inclusion of additional species in the model. χ^2 is a special case of a γ -distribution that measures the probability of residuals forming a part of standard normal distribution.

The linear variation (Fig. 1) of the stability constants of the Gln and Suc complexes of Co(II), Ni(II) and Cu(II) in SDS–water mixtures with mole fraction indicates that electrostatic forces dominate the equilibrium process under the employed experimental conditions. The stability of a complex depends on the charge of the Stern layer,²³ polarity of the medium and the electrostatic attraction or

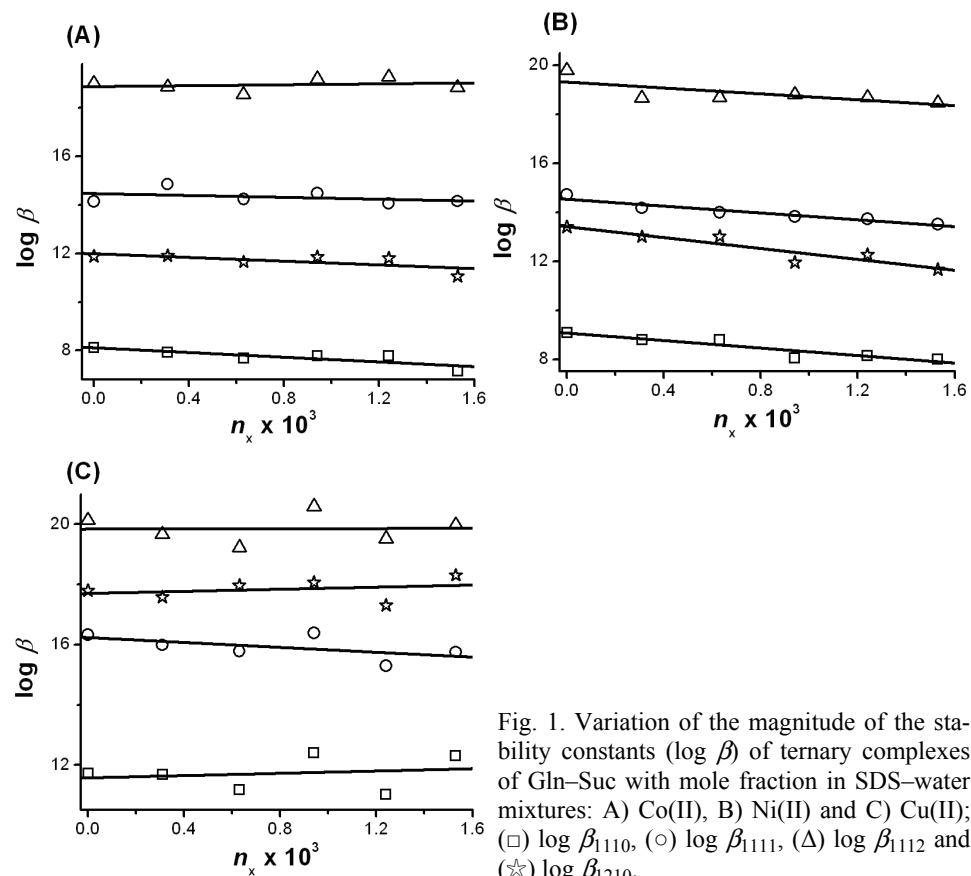


Fig. 1. Variation of the magnitude of the stability constants ($\log \beta$) of ternary complexes of Gln–Suc with mole fraction in SDS–water mixtures: A) Co(II), B) Ni(II) and C) Cu(II); (\square) $\log \beta_{1110}$, (\circ) $\log \beta_{1111}$, (Δ) $\log \beta_{1112}$ and (\star) $\log \beta_{1210}$.

repulsive forces operating between the complex species and the micellar surface. This linear decrease²⁴ is due to the decreasing dielectric constant of the medium with increasing surfactant content.²⁵ The charged species will be destabilized due to the decreased dielectric constant of the medium with increasing surfactant concentration. The stability of the neutral mixed complexes (Fig. 1) is not influenced by SDS. SDS acts as a denaturant of macromolecules by interacting with the peptide groups. Hence, the stability of the species decreases with increasing SDS content. Another reason for the decreased stability of the ternary complexes is the ligation power of SDS.

Stability of the ternary complexes

The change in the stability of the ternary complexes as compared to their binary analogues was quantified.^{26,27} In one of the approaches, the difference in stability ($\Delta \log K$) for the two reactions ML with X and M(aq) with X is compared with that calculated purely on statistical grounds. Eq. (1) can be formulated based on the properties of the cyclic systems reported earlier, from which it is clear that both the ligands in the ternary complex mutually influence to the same extent.^{28,29}

$$\begin{aligned} \Delta \log K &= \log K_{MLX}^{ML} - \log K_{MX}^M = \log K_{MLX}^{MX} - \log K_{ML}^M = \\ &= \log K_{MLX}^M - \log K_{ML}^M - \log K_{MX}^M \end{aligned} \quad (1)$$

Both the electrostatic theory of binary complex formation and statistical arguments clearly indicate that, in the case of a given multivalent hydrated metal ion, more coordination positions will be available for the first ligand than for the second one. Hence, the order of stability $K_{ML}^M > K_{ML_2}^{ML}$ holds well. This leads to the natural expectation for $\Delta \log K$ to be negative, although several exceptions have been found.^{26,30} The statistical values of $\Delta \log K$ for bidentate L and X are -0.4 and -0.6 for octahedral and square planar complexes, respectively, whereas for distorted octahedral complexes, the values vary between -0.9 and -0.3 . Negative values of $\Delta \log K$ can be understood as the secondary ligand forms a more stable complex with the hydrated metal ion than with ML, which does not mean that the ternary complex is absent.

Whenever the experimental value of $\Delta \log K$ exceeds the statistical value, it can be inferred that the ternary complex is formed as a result of interaction of ML with X or MX with L. Sigel postulated that $\Delta \log K$ values of ternary complexes containing bipyridyl as the primary ligand were positive for O-donors (malonic acid, pyrocatechol, etc.), negative for N-donors (ethylene diamine) and intermediate or many times a small negative values for amino acids with both N and O coordination sites.^{26,31,32} However, a very high negative value (-2.3) for Cu(en)(iminodiacetic acid) and a positive value (0.82) in the case of Cu(o phen)-(6,7-dihydroxynaphthalene-2-sulfonate) were also observed.²⁶

The formulae for the calculation of $\Delta \log K$ values are given in Table II. The $\Delta \log K$ values calculated for the binary and ternary complexes are incorporated in Table II. Co(II), Ni(II) and Cu(II) ions form octahedral complexes with Gln and Suc. For most of the systems given in Table II, the values of $\Delta \log K$ are found to be higher than those expected on statistical grounds (-0.4). The increased stability of the ternary complexes might be due to the interactions outside the coordination sphere, such as the formation of hydrogen bonds between the coordinated ligands. In addition, a similar stabilizing effect may likewise be exerted by electrostatic interactions between non-coordinated, charged groups of the ligands, such as the $-\text{NH}_3^+$ of Gln and the $-\text{COO}^-$ of Suc.²

TABLE II. Variation of stability of ternary complexes of Gln–Suc in SDS–water mixtures.
 $\Delta \log K_{1110} = \log \beta_{1110} - \log \beta_{1100} - \log \beta_{1010}$; $\Delta \log K_{1111} = \log \beta_{1111} - \log \beta_{1100} - \log \beta_{1011}$;
 $\Delta \log K_{1112} = \log \beta_{1112} - \log \beta_{1101} - \log \beta_{1011}$; $\Delta \log K_{1210} = \log \beta_{1210} - \log \beta_{1200} - \log \beta_{1010}$;
 $\log X_{1110} = 2 \log \beta_{1110} - \log \beta_{1200} - \log \beta_{1020}$

SDS, % w/v	$\Delta \log K_{1110}$	$\Delta \log K_{1111}$	$\Delta \log K_{1112}$	$\Delta \log K_{1210}$	$\log X_{1110}$
Co(II)					
0.0	1.1	1.87	0.06	1.36	2.72
0.5	0.72	2.7	-0.42	0.68	1.93
1.0	2.38	3.77	1.72	2.56	3.33
1.5	-0.54	1.78	-0.34	-0.04	1.02
2.0	1.17	3.33	1.87	1.32	2.57
2.5	0.47	3.22	1.19	0.29	0.49
Ni(II)					
0.0	0.84	1.56	1.0	0.37	2.52
0.5	1.89	1.93	0.41	1.12	2.88
1.0	0.83	1.06	0.19	0.48	1.93
1.5	0.49	1.56	1.93	-0.38	1.47
2.0	—	1.74	0.73	—	1.42
2.5	1.26	2.06	0.99	-0.43	0.82
Cu(II)					
0.0	-0.47	-0.58	-0.15	-1.16	1.85
0.5	—	0.38	0.39	—	2.97
1.0	—	1.42	1.4	—	3.5
1.5	1.78	1.44	2.07	0.78	4.48
2.0	-0.77	-0.55	0.07	-1.1	0.34
2.5	1.8	0.72	1.61	0.57	3.56

Effect of influential parameters on stability constants

Any variation in the parameters (the concentrations of the chemicals) affects the magnitudes of the equilibrium constants. Such parameters are called influential parameters. In order to rely on the best-fit chemical model for critical evaluation and application under varied experimental conditions with different accuracies of data acquisition, an investigation was undertaken by introducing possi-

mistic errors in the concentrations of alkali, acid, ligands, metal ions and correction factor. The results in Table III emphasize that the errors in the concentrations of alkali and acid affect the stability constant more than the errors of the ligands and the metal ion.

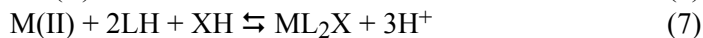
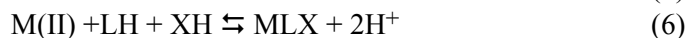
TABLE III. Effect of errors in the influential parameters on stability constants of ternary complexes of Ni(II) with Gln–Suc in a 1.5 % w/v SDS–water mixture

Component	Error, %	$\log \beta (SD)$			
		1110	1111	1112	1210
Alkali	0	8.06 (14)	13.83 (23)	18.80 (11)	11.95 (20)
	-5	Rejected	Rejected	19.55 (12)	Rejected
	-2	7.15 (41)	Rejected	18.92 (08)	Rejected
	+2	9.54 (12)	15.25 (12)	19.71 (9)	13.99 (16)
	+5	10.99 (18)	16.14 (18)	20.30 (13)	16.06 (24)
Acid	-5	10.79 (13)	16.34 (12)	20.59 (9)	15.39 (16)
	-2	9.46 (12)	15.32 (11)	19.88 (8)	13.68 (15)
	+2	7.33 (24)	Rejected	18.63 (9)	Rejected
	+5	Rejected	Rejected	18.84 (12)	Rejected
Gln	-5	7.90 (15)	13.50 (36)	18.57 (13)	11.98 (17)
	-2	7.99 (14)	13.69 (27)	18.70 (12)	11.95 (19)
	+2	8.14 (13)	13.97 (20)	18.91 (10)	11.96 (21)
	+5	8.33 (13)	14.23 (16)	19.13 (9)	12.07 (21)
Suc	-5	8.80 (13)	14.38 (15)	18.87 (14)	13.23 (16)
	-2	8.36 (13)	14.09 (17)	18.80 (12)	12.53 (16)
	+2	7.71 (17)	13.41 (45)	18.84 (10)	Rejected
	+5	7.68 (19)	13.86 (23)	19.24 (8)	Rejected
Metal	-5	8.18 (14)	14.02 (19)	18.90 (11)	12.24 (17)
	-2	8.10 (14)	13.90 (21)	18.84 (11)	12.06 (19)
	+2	8.02 (14)	13.75 (25)	18.77 (11)	11.82 (22)
	+5	7.96 (14)	13.65 (28)	18.73 (11)	11.62 (26)

Distribution diagrams

A perusal of the distribution diagrams (Fig. 2) reveals that at very low pH values, the concentrations of the mixed ligand complexes are lower than those of protonated ligands. The concentrations of the ternary species increased with increasing pH. The protonated ternary species, $MLXH$ and $MLXH_2$ are distributed at lower pH values and the unprotonated ternary species, MLX and ML_2X at higher pH values. Higher concentrations of the ternary species than those of binary species indicate the higher stability of the former. The ternary species exist in the pH range 2.0–9.0 for Co(II), Ni(II) and 2.0–6.0 for Cu(II), respectively. The formation of the complex species can be represented by the following equilibria. The charges of the species are omitted for clarity.





The protonated ligands LH_2 and XH_2 interact with the metal ion to form $MLXH_2$ (Eq. (2)), which successively loses protons to form $MLXH$ (Eq. (3)) and MLX (Eq. (5)). $MLXH$ species may also be formed due to (Eq. (4)). LH and XH interact with the metal ion to form MLX (Eq. (7)). ML_2X is formed by (Eq. (6)). $MLXH_2$ may be formed by the interaction of MXH and LH_2 (Eq. (8)) and/or MLH and XH_2 (Eq. (9)). MXH and LH interact to form $MLXH$ (Eq. (10)). The possible structures of these ternary complexes are proposed in Fig. 3. The exis-

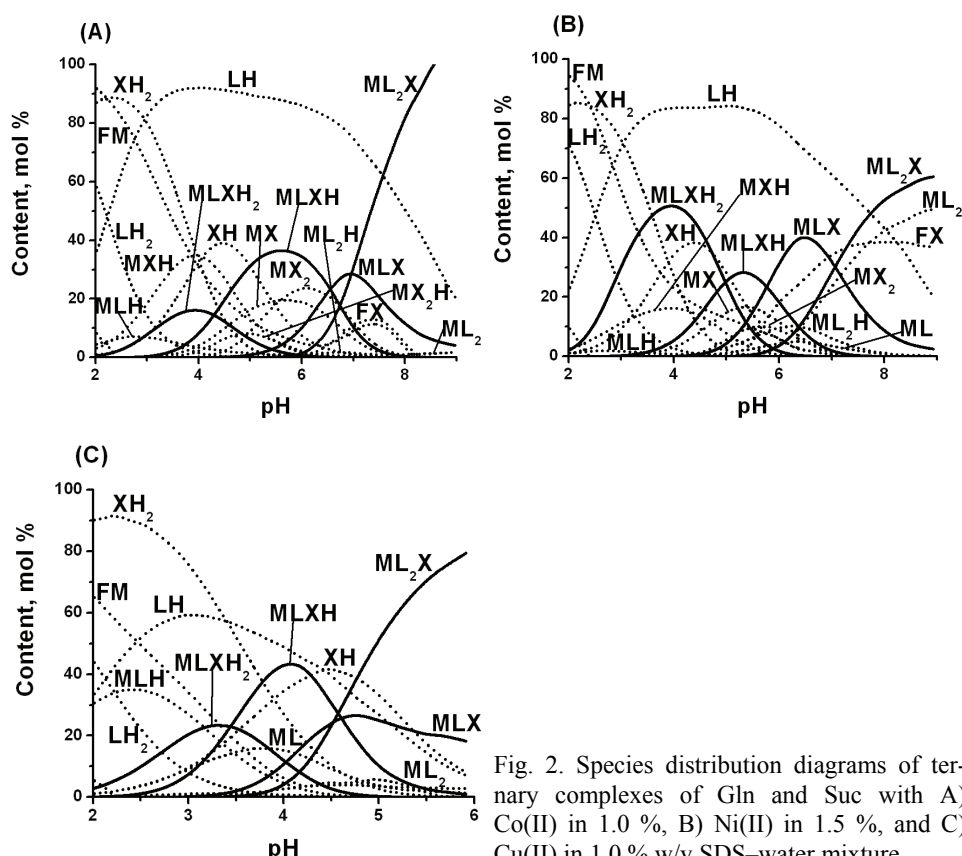


Fig. 2. Species distribution diagrams of ternary complexes of Gln and Suc with A) Co(II) in 1.0 %, B) Ni(II) in 1.5 %, and C) Cu(II) in 1.0 % w/v SDS–water mixture.

tence of ML_2X and the absence of MLX_2 are due to the higher affinity of LH than XH towards the metal ion.

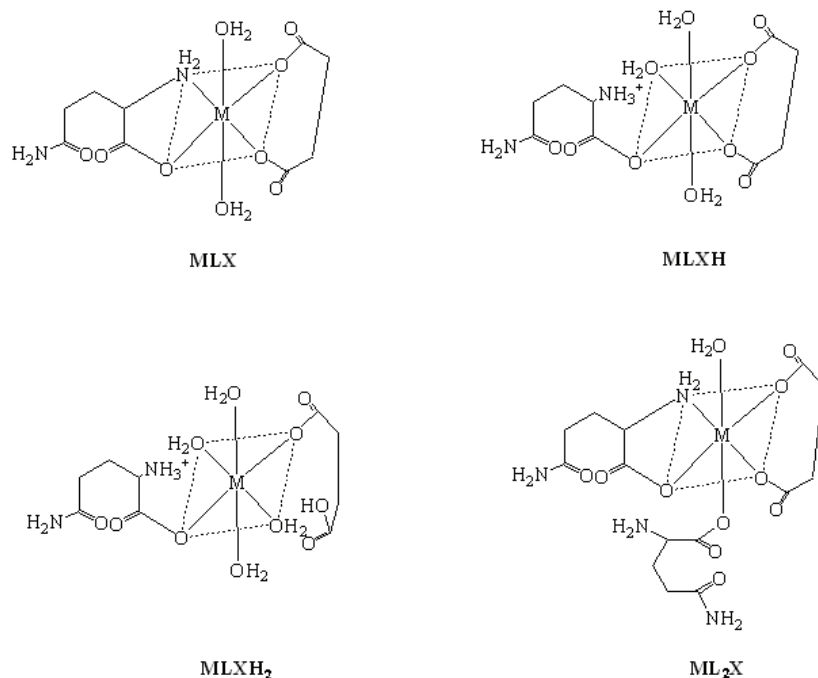


Fig. 3. Structures of ternary complexes of Co(II), Ni(II), Cu(II) with Gln and Suc.

Biological relevance of the present study

The presence of SDS considerably decreases the dielectric constant of the aqueous solution and creates compartmentalization due to the formation of micelles. Thus, the surfactant solution is expected to mimic the physiological conditions of the active site cavities with low dielectric constants and the concept of equivalent solution dielectric constant in the active site cavities is invoked. The stability constants determined and the species predicted under these mimicked conditions can be extrapolated to those expected to be present in the active site cavities of biomolecules. Such studies are useful to understand: *i*) the role played by the active site cavities in biological molecules, *ii*) the type of complex formed by the metal ion, *iii*) the bonding behavior of protein residues with a metal ion, and *iv*) the greater significance of the concentrations of complex chemical species than the total concentrations of essential metals in soils and water in predicting their bioavailability. The species refined and their relative concentrations under the present experimental conditions represent the possible forms of Co(II),

Ni(II) and Cu(II) ions in biological fluids and the speciation represents the biological activity of these metals in the presence of glutamine and succinate residues.

CONCLUSIONS

The following conclusions have been drawn from the modeling studies of the speciation of ternary complexes of Co(II), Ni(II) and Cu(II) with Gln and Suc in SDS–water media.

The species detected were MLX, MLXH, MLXH₂ and ML₂X for Co(II), Ni(II) and Cu(II).

The linear variation of the $\log \beta$ values with mole fraction of the medium indicates the dominance of electrostatic forces over non-electrostatic forces.

The change in the stability of the ternary complexes as compared to their binary analogues shows that the ternary complexes are more stable than the binary complexes due to the interactions outside the coordination sphere.

The existence of ML₂X and the absence of MLX₂ are due to the higher affinity of LH than XH towards the metal ion.

This study also gives an insight into the bioavailability/bioaccumulation of these metals. The ternary complexes are more amenable for metal transport because of their extra stability while the binary complexes make the metal bioavailable due to their decreased stability.

ИЗВОД

ФОРМИРАЊЕ КОМПЛЕКСА ЕСЕНЦИЈАЛНИХ ЈОНА МЕТАЛА СА МЕШОВИТИМ
ЛИГАНДИМА Л-ГЛУТАМИНОМ И ЂИЛИБАРНОМ КИСЕЛИНОМ У СМЕШИ
НАТРИЈУМ-ДОДЕЦИЛ-СУЛФАТА (SDS) И ВОДЕ КАО РАСТВАРАЧА

GANDHAM HIMA BINDU¹ и GOLLAPALLI NAGESWARA RAO²

¹Department of Engineering Chemistry, Andhra University и ²Department of Inorganic & Analytical Chemistry, Andhra University, Visakhapatnam-530 003, India

У различитим односима натријум-додецил-сулфата и воде као растварача (0,0–2,5%, m/v) и јонској јачини од 0,16 mol L⁻¹ (NaCl), на температури од 303,0 K, изучавано је формирање комплекса Co(II), Ni(II) и Cu(II) са мешовитим лигандима L-глутамином и ђилибарном киселином. Титрације су вршene раствором натријум-хидроксида при различитим односима концентрација метала (M), L-глутамина (L) и ђилибарне киселине (X) (M:L:X = 1:2:2, 1:4:2 и 1:2:4). Константе стабилности су израчунате помоћу Miniquad 75 програма, док је најбоље слагање хемијских модела добијено на основу статистичких параметара и методом резидуалних анализа. Нађено је да у раствору постоје комплекси са следећим општим формулама: ML₂X, MLX, MLXH и MLXH₂ за Co(II), Ni(II) и Cu(II). Већа стабилност тернарних у односу на одговарајуће бинарне комплексе се објашњава електростатичким интеракцијама бочних ланаца лиганада, хелатним ефектом, неутрализацијом наелектрисања, као и постојањем одређених интеракција налегања и водоничних веза.

(Примљено 1. фебруара, ревидирано 25. јула 2011)

REFERENCES

1. S. B. Ronald, G. N. Rao, *Proc. Natl. Acad. Sci. India, A* **72** (2002) 301
2. M. S. Babu, G. N. Rao, K. V. Ramana, M. S. P. Rao, *Proc. Natl. Acad. Sci. India, A* **73** (2003) 173
3. B. B. V. Sailaja, T. Kebede, G. N. Rao, M. S. P. Rao, *Proc. Natl. Acad. Sci. India, A* **74** (2004) 399
4. G. N. Rao, K. G. Sudarsan, *Chem. Speciation Bioavailability* **18** (2006) 71
5. W. Wiley, M. D. Souba, *Ann. Surgery* **218** (1993) 715
6. M. Tetsuya, M. Nobuhiko, *Med. Sci. Res.* **17** (1989) 425
7. J. M. Lacey, D. W. Wilmore, *Nutr. Rev.* **48** (1990) 297
8. W. S. Wang, J. K. Lin, T. C. Lin, W. S. Chen, J. K. Jiang, H. S. Wang, T. J. Chiou, J. H. Liu, C. C. Yen, P. M. Chen, *Oncologist* **12** (2007) 312
9. H. Song, S. Y. Lee, *Enzyme Microb. Technol.* **39** (2006) 352
10. I. A. Pomytkin, O. E. Kolesova, T. J. Ukhanova, *PCT Int. Appl. Wo* **28** (2000) 944
11. T. Willke, K. D. Vorlop, *Appl. Microbiol. Biotechnol.* **66** (2004) 131
12. S. B. Ronald, G. N. Rao, *J. Indian Chem. Soc.* **79** (2002) 799
13. G. N. Rao, A. Ramakrishna, *J. Indian Chem. Soc.* **83** (2006) 332
14. A. Ramakrishna, G. N. Rao, *Proc. Natl. Acad. Sci. India, A* **77** (2007) 21
15. G. Gran, *Anal. Chim. Acta* **206** (1988) 111
16. M. S. Babu, G. N. Rao, K. V. Ramana, M. S. P. Rao, *Indian J. Chem., A* **40** (2001) 1334
17. G. N. Rao, *PhD Thesis*, Andhra University, Visakhapatnam, India, 1989
18. P. Gans, A. Sabatini, A. Vacca, *Inorg. Chim. Acta* **18** (1976) 237
19. G. N. Rao, R. S. Rao, *J. Indian Council Chem.* **8** (1992) 12
20. B. B. V. Sailaja, T. Kebede, G. N. Rao, M. S. P. Rao, *J. Indian Chem. Soc.* **79** (2002) 155
21. R. S. Rao, G. N. Rao, *Computer Applications in Chemistry*, Himalaya Publishing House, Mumbai, India, 2005, p. 302
22. G. N. Rao, V. L. S. N. Murthy, *J. Indian Chem. Soc.* **81** (2004) 424
23. C. A. Bunton, G. Cerichelli, Y. Ihara, L. Supulveda, *J. Am. Chem. Soc.* **101** (1979) 2429
24. A. K. Singh, D. Manjula, *J. Indian Chem. Soc.* **71** (2001) 635
25. E. H. Cordes, *Pure Appl. Chem.* **50** (1978) 617
26. R. Griesser, H. Sigel, *Inorg. Chem.* **9** (1970) 1238
27. R. B. Martin, R. Prados, *J. Inorg. Nucl. Chem.* **36** (1974) 1665
28. H. Sigel, *Chimia* **21** (1967) 489
29. H. Sigel, K. Becker, D. B. McCormick, *Biochim. Biophys. Acta* **148** (1967) 655
30. H. Sigel, *Angew. Chem. Int. Ed. Engl.* **14** (1975) 394
31. H. Sigel, R. Griesser, *Helv. Chim. Acta* **50** (1967) 1842
32. H. Sigel, *Angew. Chem. Int. Ed. Engl.* **7** (1968) 137.





J. Serb. Chem. Soc. 77 (4) 465–481 (2012)
JSCS-4283

Journal of the Serbian Chemical Society

JSCS-info@shd.org.rs • www.shd.org.rs/JSCS

UDC 677.027.233+677.027.562.6+

667.281+546.215:54-76

Original scientific paper

Decolorization of the textile azo dye Reactive Orange 16 by the UV/H₂O₂ process

JELENA MITROVIĆ*, MILJANA RADOVIĆ#, DANIJELA BOJIĆ, TATJANA
ANĐELOVIĆ#, MILOVAN PURENOVIĆ and ALEKSANDAR BOJIĆ#

*Department of Chemistry, Faculty of Sciences and Mathematics,
University of Niš, Višegradska 33, 18 000 Niš, Serbia*

(Received 16 February, revised 3 August 2011)

Abstract: The photochemical decolorization of C.I. Reactive Orange 16 (RO16), a reactive textile azo dye, by the UV/H₂O₂ process was studied using a batch photoreactor with UV lamps emitting at 253.7 nm. Complete decolorization of 50.0 mg dm⁻³ initial dye concentration was achieved in less than 6 min under optimal conditions (25 mM initial peroxide concentration, at pH 7.0 and with a UV light intensity of 1950 µW cm⁻²). The effects of experimental variables, such as initial pH, initial concentration of H₂O₂, initial dye concentration, and the intensity of UV light were studied. The highest decolorization rates were realized at a peroxide concentration in range from 20 to 40 mM, above which decolorization was inhibited by the scavenging effect of the peroxide. The decolorization was more efficient in neutral pH values. The efficiency of the process was improved with lower initial dye concentrations and at higher intensities of UV light.

Keywords: Reactive Orange 16; UV/H₂O₂ process; decolorization.

INTRODUCTION

Colored effluent from the textile industry is becoming more and more apparent as one of the major environmental problems associated with this industry. It is estimated that 15 % of total production of colorants may be released to wastewater during synthesis and processing operations.¹ Dyes in wastewaters cause aesthetic problems, absorb and scatter sunlight and thus affect the aquatic ecosystem.² Azo compounds represent the largest group of colorants with respect to both the number and production volume. These compounds contain one or more azo groups (–N=N–), mostly linked to benzene or naphthalene rings.¹ Some azo dyes, via metabolic cleavage of the azo linkage, can produce potentially car-

* Corresponding author. E-mail: jelenam81@gmail.com

Serbian Chemical Society member.

doi: 10.2298/JSC110216187M

cinogenic aromatic amines.³ This is one more reason for the open concern about the release of azo dyes to the environment. According to their mode of application, textile dyes can be classified as acid, reactive, metal complex, disperse, vat, mordant, direct, basic and sulfur dyes.⁴ The research on textile effluent decolorization has focused on fiber reactive dyes for the following reasons. Reactive dyes are most commonly in use today, especially for dyeing cellulosic fibers, such as cotton and wool. Reactive azo dyes possess a low fixation rate and up to 50 % of the applied reactive dye is usually discharged as a deeply colored effluent.⁴ In the reactive dyeing process, ten times more water is consumed on average for the preparation, dyeing, washing, and rinsing stages than during dyeing with other dye types.⁴ Therefore, it is necessary to remove reactive azo dyes from effluents before their discharge.

Conventional methods for water treatment (activated carbon adsorption, coagulation, flocculation, reverse osmosis and ultrafiltration) are non-destructive and just transfer contaminants from one phase to another and form secondary waste.⁵ Recently, advanced oxidation processes (AOPs) have been used as techniques which are alternative to physico-chemical phase transfer methods. These techniques are successfully applied for the complete mineralization of organic pollutants in water.^{6–8} AOPs involve different processes, such as H₂O₂/UV, O₃/UV, H₂O₂/O₃/UV, TiO₂/UV, H₂O₂/Fe²⁺, UV/H₂O₂/Fe²⁺, H₂O₂/Fe³⁺, Fe²⁺/oxalate/UV, H₂O₂/Fe³⁺/oxalate, H₂O₂/Fe³⁺/oxalate/UV, Mn²⁺/oxalic acid/O₃ and H₂O₂/Fe²⁺/Fe³⁺/UV. In these processes, a complex set of reactions occur, which imply generation of oxidizing species, such as •OH radicals and hydroperoxyl radicals.⁹ These species, especially radicals that have an oxidation potential of 2.8 V, are powerful oxidizing agents able to degrade a variety of organic water contaminants.¹⁰ Some of the advantages of use of UV/H₂O₂ in comparison to other AOPs are a considerably safe and easy operation, a reduction of the chemical oxygen demand (COD) and a short reaction time.¹¹ The reaction of hydroxyl radicals, generated by photolysis of H₂O₂, with organic contaminant includes three different mechanisms: hydrogen abstraction, electrophilic addition, and electron transfer.¹⁰

The aim of this study was to investigate the efficiency of decolorization of the widely used textile azo dye C.I. Reactive Orange 16 (RO16) with UV radiation in the presence of H₂O₂. The decolorization rate of this process depends on many parameters, such as initial pH, initial azo dye concentration, initial H₂O₂ concentration, UV light intensity, which were varied in order to determine the optimal operating conditions.

EXPERIMENTAL

Reagents

The azo reactive dye Reactive Orange 16 (50 %) was obtained from Farbotex (Italy) and used without further purification. The H₂O₂ solution (30 %), analytical grade, was purchased

from Merck (Germany). All other used reagents were of analytical grade. All solutions were prepared with deionized water.

Photoreactor

All photochemical experiments were performed in a batch photoreactor, schematically shown in Fig. 1. Low-pressure mercury vapor lamps, with a maximum emission primarily at 253.7 nm (28 W, UV-C, Philips, Holland), were used as the light source. Ten UV lamps were fixed parallel in a reflector at the top of the photoreactor. An air cooling system, with electrical fans, was used to vent the heat outside of the reactor and to prevent the lamps from overheating. The interior surface of the photoreactor was made of highly polished stainless steel, because of light reflection. Intensity of UV radiation was measured by a UV radiometer Solarmeter model 8.0 UVC (Solartech, USA). The total UV intensity was controlled by turning on a different number of UV lamps, from 2 up to 10 lamps, which gave intensity from 730 up to 1950 $\mu\text{W cm}^{-2}$ (with all ten UV lamps on) at the distance of 220 mm from the working solution surface. Some of the experiments were conducted using the lowest UV light intensity in order to reduce the decolorization rate of the dye for a better observation of the effects of some parameters.

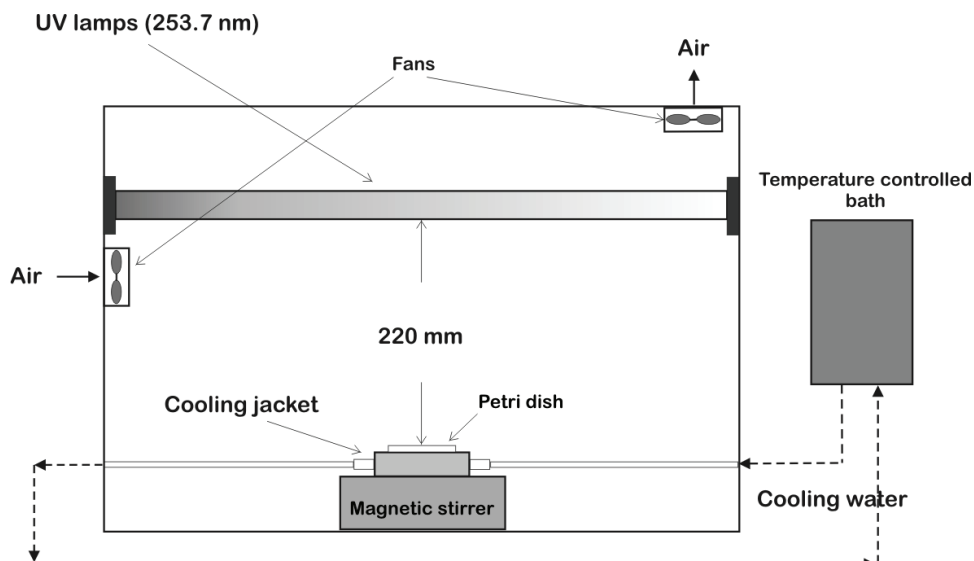


Fig. 1. Scheme of the batch photoreactor.

Procedure

In each experiment, 100 ml of dye solution of the desired initial concentrations of dye and H_2O_2 and appropriate pH value was irradiated. During the irradiation, the solution was magnetically stirred at a constant rate and the temperature was maintained at $25 \pm 0.5^\circ\text{C}$ by thermostating. The pH of the solution was measured using a HACH SensIon3 pH meter and adjusted by the addition of aqueous NaOH or dilute mineral acids. Simultaneously, the photolysis of a blank sample containing the same amount of peroxide and at the same pH but without dye was carried out. This was done in order to avoid interference due to H_2O_2 , which may absorb light in the range from 190 to 450 nm. At certain reaction intervals, a 5 ml aliquot

was withdrawn, analyzed by UV–Vis spectrophotometry (Carry 50, Varian) and returned back to the photoreactor. Dye concentrations were calculated from the calibration curve established by relating the concentration to the absorbance measured at 494 nm. The absorbance at 494 nm is due to the color of the dye solution ($n \rightarrow \pi^*$ transition in $-N=N-$) and it was used to monitor the decolorization of the dye. All experiments were performed at least in triplicate and the results are presented as mean value $\pm SD$.

RESULTS AND DISCUSSION

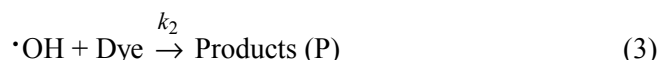
Three preliminary experiments were performed in order to investigate the effect of UV radiation only, hydrogen peroxide without UV radiation, and UV irradiation plus H_2O_2 . The solution of RO16 dye (50.0 mg dm^{-3}) without peroxide was irradiated for 24 h to examine the effect of UV light radiation alone. When the irradiation of dye solution was performed in the absence of H_2O_2 there was no observable decrease of the residual dye concentration (results not shown). This indicated that the direct photolysis of RO16 dye by UV irradiation was slow (reaction (1)):



A solution with only peroxide was left in the dark for 24 h. The dye removal efficiency in this case was also negligible (results not shown). However, if hydrogen peroxide was applied in combination with UV radiation, the residual dye concentration rapidly decreases (Fig. 2). Complete decolorization was obtained in less than 6 min, with an initial dye concentration of 50.0 mg dm^{-3} in the presence of $25 \text{ mM } H_2O_2$ and under $1950 \mu\text{W cm}^{-2}$ light intensity. This can be related to the generation of highly reactive $\cdot OH$ radicals by direct photolysis of the added hydrogen peroxide, as shown by reaction (2):



These radicals undergo radical-chain reactions with the aromatic rings and probably also with the $-N=N-$ double bond of the azo dye RO16, thereby forming new products (reaction (3)):



The new products also have high reactivity towards the $\cdot OH$ radicals as the starting compound (reaction (4)):



According to reaction (3), the kinetic expression for the decolorization of the azo dye RO16 can be presented as:

$$-\frac{dc_d}{dt} = k c_{OH} c_d \quad (5)$$



where c_d is the initial dye concentration; c_{OH} is the hydroxyl radical concentration; k is the second order rate constant and t is the reaction time.

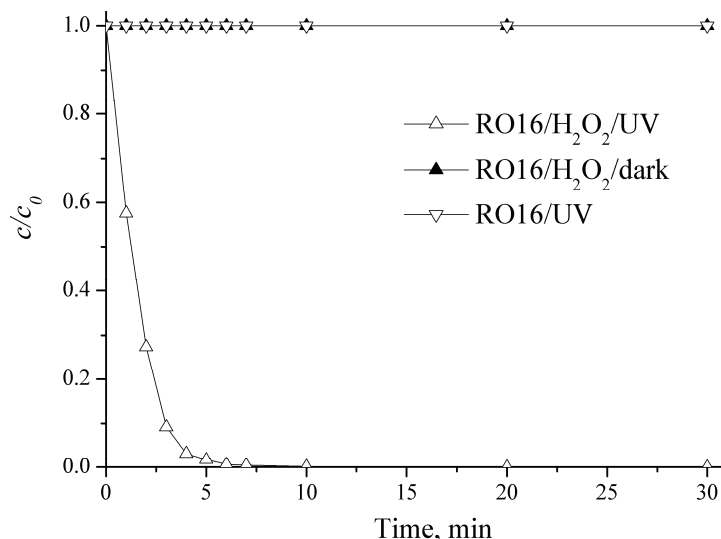


Fig. 2. Effect of UV radiation, H_2O_2 and $\text{UV}/\text{H}_2\text{O}_2$ on the decolorization of RO16.
 $c_0(\text{RO16}) = 50.0 \text{ mg dm}^{-3}$, $c_0(\text{H}_2\text{O}_2) = 25.0 \text{ mmol dm}^{-3}$, pH 7.0 ± 0.2 , UV light intensity:
 $1950 \mu\text{W cm}^{-2}$, temperature: $25 \pm 0.5^\circ\text{C}$.

Many models have been postulated to describe the kinetics of these reactions using the steady-state approximation, in which the concentration of hydroxyl radicals does not change with the reaction time.^{12,13} In this way, the non-measurable concentration of the radicals was correlated as a function of hydrogen peroxide concentration.

According to the steady-state approach, the assumption that the rate of production of an intermediate ($\bullet\text{OH}$) is equal to the rate of its consumption can be used (reaction (6)):¹⁴

$$k_1 c_{\text{H}_2\text{O}_2} = k_2 c_{\text{OH}} c_d + k_3 c_p c_{\text{OH}} \quad (6)$$

From Eq. (6), the steady state concentration of $\bullet\text{OH}$ radicals is obtained:

$$c_{\text{OH}} = \frac{k_1 c_{\text{H}_2\text{O}_2}}{k_2 c_d + k_3 c_p} \quad (7)$$

If the reactivity of $\bullet\text{OH}$ towards the different organic compounds present in solution is assumed to be approximately of the same order of magnitude and if a large quantity of H_2O_2 compared to dye was used so that the change in peroxide concentration is insignificant, after integration the exponential time dependence is obtained:

$$\ln(c_t/c_0) = -k_{\text{app}}t \quad (8)$$

where c_t is the concentration of dye after irradiation time t , c_0 is the dye concentration at $t = 0$ and k_{app} (min^{-1}) is the apparent pseudo-first order rate constant. The apparent reaction rate constants k_{app} for the decolorization of RO16 were calculated from semi-logarithmic graphs of $\ln(c_t/c_0)$ vs. time, using the linear regression method. For all the experimental results, the values of the square of the relative correlation coefficients (R^2) were higher than 0.98, which confirmed the proposed kinetic model.

UV-Vis spectral changes

The typical spectrum of RO16 is characterized by two bands in the visible region, with their maxima at 494 and 386 nm, and by two bands in the ultraviolet region, located at 297 and 254 nm. The absorbance peaks at 254 and 297 nm are due to $\pi \rightarrow \pi^*$ transitions in the benzene and naphthalene rings of RO16, respectively,¹⁵ and decreases in the absorbance in this region indicate degradation of the aromatic part of the dye. The two bands in the visible region are due to $n \rightarrow \pi^*$ transitions in the azo linkage and are attributed to the presence of two forms of the dye molecules, the azo and the hydrazone form. The band at 386 nm corresponds to the azo form, while the band at 494 nm is linked to the hydrazone form of the azo dye, which is favored by water.¹⁶ These forms originate from intramolecular hydrogen bonding tautomeric interaction between the oxygen of the naphthyl group and the β -hydrogen of the corresponding azo-linkage. The disappearance of absorption peaks in the visible region indicates that the main chromophores of the dye were destroyed and for this reason, dye solutions become decolorized. The changes in the UV-Vis absorption spectra of RO16 solutions during UV irradiation in presence of H_2O_2 at different irradiation time are shown in Fig. 3. It is obvious that the intensity of peaks in the visible region, as well as the intensity of peaks in the ultraviolet region, rapidly decreased with irradiation time and after 6 min of irradiation, no absorption peaks were observed. Thus, the UV/ H_2O_2 process provides not only decolorization of the azo dye RO16, but also an appreciable degree of decomposition of the aromatic rings in the dye molecules.

Changes of pH and conductivity in the UV/ H_2O_2 process

The changes in the pH of dye solutions as a function of the irradiation time for different initial pH values are shown in Fig. 4. After 40 min of irradiation, the pH decreased from 6.86 to 4.31 in neutral medium, from 5.36 to 3.69 in weak acidic medium and from 8.86 to 6.92 in weak basic medium. However, in strong basic (pH 10.12) and strong acidic media (pH 2.08 and 3.2), no significant changes in pH were observed after 40 min of irradiation. Previous reports^{17,18} indicated that low molecular weight organic acids, such as oxalic, acetic, formic, ma-

leic, malonic, fumaric and succinic acid, are formed during UV irradiation of dyes. Hence, the significant drops of the solution pH in neutral medium by 2.5 pH units and in weak acidic and basic medium by almost 2 pH units are probably due to the formation of organic and inorganic acids as degradation products of RO16. The effect of these degradation products on the solution pH was more prominent in neutral and weak acidic medium, which could be expected. On the other hand, in strong basic medium, weak organic acids were not formed in sufficient amounts for neutralization of the base.

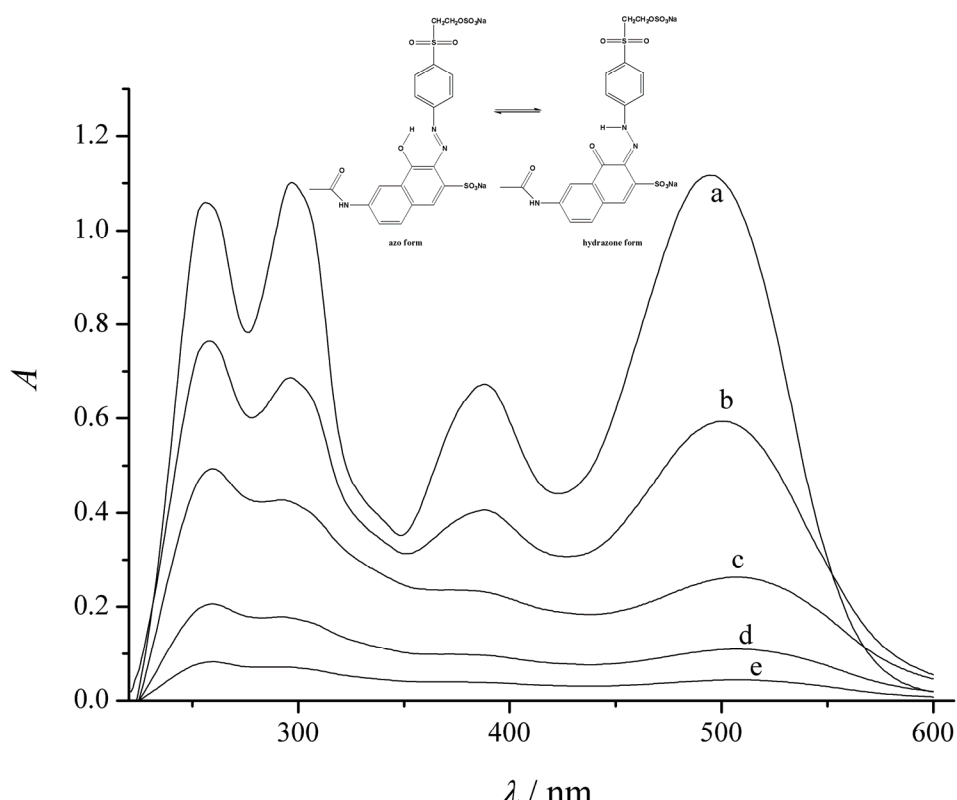


Fig. 3. UV-Vis spectral changes of RO16 as a function of irradiation time: a) 0, b) 1, c) 2, d) 3 and e) 4 min. $c_0(\text{RO16}) = 50.0 \text{ mg dm}^{-3}$, $c_0(\text{H}_2\text{O}_2) = 25.0 \text{ mmol dm}^{-3}$, pH 7.0 ± 0.2 , UV light intensity: $1950 \mu\text{W cm}^{-2}$, temperature: $25 \pm 0.5^\circ\text{C}$. Inset: tautomeric forms of RO16.

The conductivity of the dye solution was found to increase progressively during the irradiation from 39 to $102 \mu\text{S cm}^{-1}$ (Fig. 5). In the first 4 min of irradiation, when the dye solution was still colored, the conductivity slightly increased from 39 to $42.3 \mu\text{S cm}^{-1}$; however, after complete decolorization had been achieved (about 6 min) and the main chromophore ($-\text{N}=\text{N}-$) in the dye mo-

olecules destroyed, the conductivity rapidly increased and reached a value of 102 $\mu\text{S cm}^{-1}$ at the end of the experiment. The increase of conductivity with time can also be associated with the formation of the above-mentioned acid products in solution as well as with the formation of other mineralization products, such as NH_4^+ , NO_3^- , NO_2^- and SO_4^{2-} .¹⁸

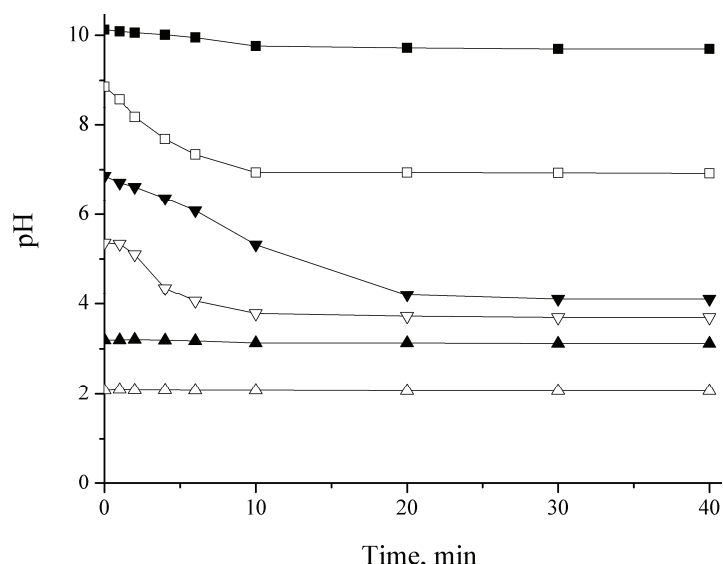


Fig. 4. Changes in pH during irradiation. $c_0(\text{RO16}) = 50.0 \text{ mg dm}^{-3}$, $c_0(\text{H}_2\text{O}_2) = 25.0 \text{ mmol dm}^{-3}$, UV light intensity: $1950 \mu\text{W cm}^{-2}$, temperature: $25 \pm 0.5^\circ\text{C}$.

The effect of the initial H_2O_2 concentration

The concentration of hydrogen peroxide is an important parameter that influences the efficiency of dye removal by the UV/ H_2O_2 process. Due to the low molar absorption coefficient of H_2O_2 at 254 nm ($18.6\text{--}19.6 \text{ L mol}^{-1} \text{ cm}^{-1}$),¹⁹ an excess of H_2O_2 is theoretically required to produce sufficient $\cdot\text{OH}$ radicals. Numerous authors have reported that the concentration of H_2O_2 may either enhance the photoreaction rate or inhibit it due to the scavenging action of peroxide, depending on the concentration.^{20–24} Therefore, an optimum concentration of H_2O_2 in the reaction course must be reached. In order to determine the effect of H_2O_2 concentration on the decolorization rate, doses of H_2O_2 in range of 10 up to 100 mM were added. The applied UV light intensity was $730 \mu\text{W cm}^{-2}$, because of the very fast decolorization at the maximal value ($1950 \mu\text{W cm}^{-2}$), which made the investigation of this operational parameter difficult. The other parameters were kept constant. The apparent rate constants vs. different initial concentrations of H_2O_2 are summarized in Fig. 6. This plot shows that k_{app} considerably in-

creased from 0.142 to 0.331 min⁻¹ with increasing hydrogen peroxide concentration from 10 to 20 mM. At the low concentration of H₂O₂, a relatively low concentration of hydroxyl radicals was formed for dye oxidation, which resulted in a low decolorization rate. However, with increasing peroxide concentration, more hydroxyl radicals were generated upon its photodissociation (reaction (2)). On further increasing of the peroxide concentration to 40 mM, the apparent constant rate reached a plateau and stayed almost unchangeable.

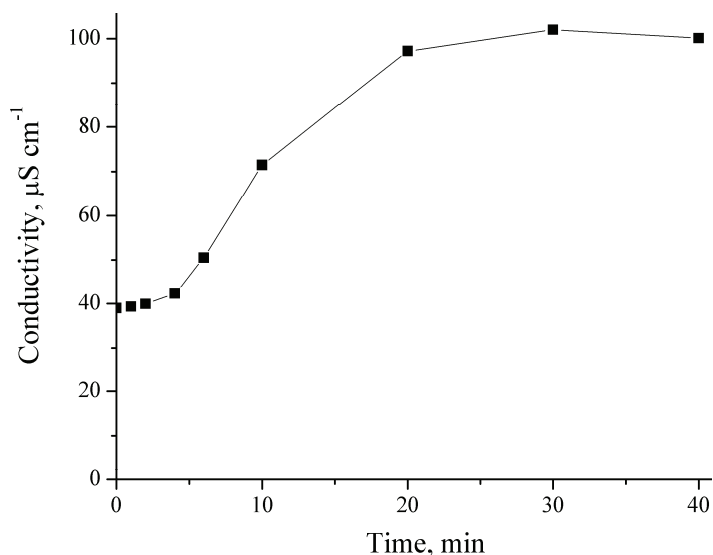
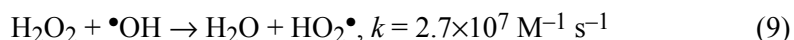
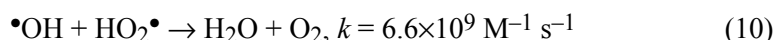


Fig. 5. Changes in conductivity during irradiation. $c_0(\text{RO16}) = 50.0 \text{ mg dm}^{-3}$, $c_0(\text{H}_2\text{O}_2) = 25.0 \text{ mmol dm}^{-3}$, UV light intensity: $1950 \mu\text{W cm}^{-2}$, pH 7.0 ± 0.2 , temperature: $25 \pm 0.5^\circ\text{C}$.

At an initial peroxide concentration above 40 mM, the apparent rate constant decreased from 0.329 to 0.18 min⁻¹ on decreasing the H₂O₂ dose from 40 to 100 mM. When the initial peroxide concentration was very high, the generated •OH radicals mostly reacted with the excess peroxide and produced hydroperoxyl radicals HO₂• (reaction (9)), which are less reactive than •OH, and the rate of dye removal decreased:²⁵



The generated •OH can also react with HO₂• and produce water and oxygen (reaction (10)) or dimerize to H₂O₂ (reaction (11)).^{25,26} In this way, the concentration of •OH available for dye degradation also decreased:



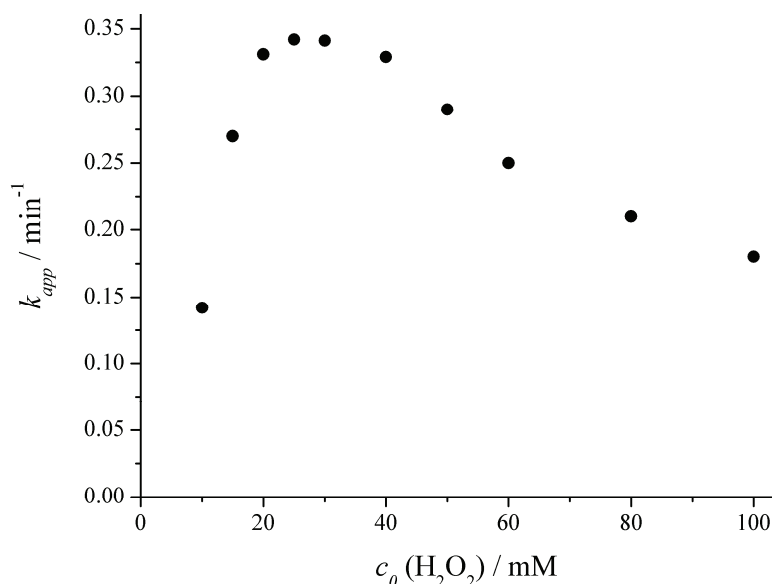


Fig. 6. The effect of the initial H_2O_2 concentration on the rate of RO16 decolorization.

$c_0(\text{RO16}) = 50.0 \text{ mg dm}^{-3}$, pH 7.0 ± 0.2 , UV light intensity: $730 \mu\text{W cm}^{-2}$, temperature: $25 \pm 0.5^\circ\text{C}$.

Therefore, the optimum range of the hydrogen peroxide concentration giving the maximum RO16 decolorization rate was from 20 to 40 mM. These values are related to the optimum value of relative molar ratio of the H_2O_2 concentration to that of the dye ($\text{H}_2\text{O}_2/\text{RO16}$) between 246 and 493. Many authors noticed the existence of an optimal molar ratio between peroxide and dye that leads to a faster decolorization rate. Muruganandham and Swaminahan²⁷ reported that the optimal initial peroxide concentration for the decolorization of the chlorotriazine reactive azo dye, Reactive Orange 4, in a batch photoreactor was about 20 mM ($[\text{H}_2\text{O}_2]_0/[\text{RO4}]_0 = 40$, $c(\text{RO4}) = 5 \times 10^{-4} \text{ mol L}^{-1}$, pH 3.0, UV light power: 64 W). Neamtu *et al.*²⁸ reported approximately the same optimal concentration of peroxide (24.5 mM) for the decolorization of 100 mg L^{-1} initial concentration of three reactive azo dyes, Reactive Red 120, Reactive Black 5 and Reactive Yellow 84 ($[\text{H}_2\text{O}_2]_0/[\text{RR120}]_0 = 360$, $[\text{H}_2\text{O}_2]_0/[\text{RB5}]_0 = 243$, $[\text{H}_2\text{O}_2]_0/[\text{RY14}]_0 = 470$, respectively) in a batch photoreactor. On the other hand, Aleboyeh *et al.*²² investigated the critical effect of the peroxide concentration in the decolorization of the three commercial dyes (Acid Orange 8, Methyl Orange, Acid Blue 74) in a continuous photoreactor and found that the optimal peroxide/dye molar ratio was different in each case ($[\text{H}_2\text{O}_2]_0/[\text{AO8}]_0 = 55$, $[\text{H}_2\text{O}_2]_0/[\text{MO}]_0 = 65$, $[\text{H}_2\text{O}_2]_0/[\text{AB74}]_0 = 70$). This confirms the importance of determining the optimal initial peroxide concentration for UV/ H_2O_2 decolorization for each dye and for every

experimental condition. In this study, an initial H_2O_2 concentration of 25 mmol dm^{-3} was used in all the subsequent experiments.

The effect of pH

The initial pH of dye solutions is also an important parameter for optimizing the operational conditions, since the colored effluent from textile industry could have different pH values. The influence of pH on the rate of decolorization of the RO16 azo dye by UV/ H_2O_2 process was investigated at seven different pH values: 2.0, 3.0, 4.0, 5.0, 7.0, 9.0, and 10.0 during 10 min of treatment time, using 50 mg dm^{-3} dye solutions and 25 mM H_2O_2 . The first tests run were realized by adjusting the acidic pH (2.0, 3.0, 4.0 and 5.0) with four inorganic acids (HCl , HNO_3 , H_2SO_4 and H_3PO_4) and the changes in the decolorization rate are shown in Fig. 7. In all cases, a decrease of the decolorization rate from pH 5 to 2 is evident. On acidification of the solution, amount of added conjugated bases increased (Cl^- , NO_3^- , SO_4^{2-} and PO_4^{3-}). These anions are able to react with hydroxyl radicals leading to inorganic radical ions which exhibit a much lower reactivity than $\cdot\text{OH}$, hence they did not participate in the dye decolorization. There is also a drastic competition between the dye and the anions with respect to $\cdot\text{OH}$:

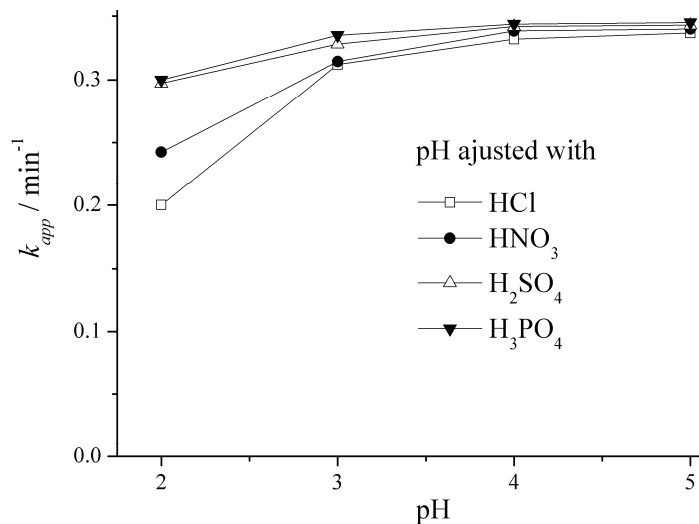
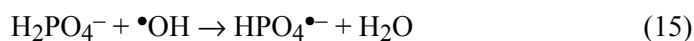
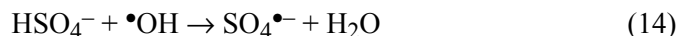


Fig. 7. Effect of pH adjustment with different mineral acids on the rate of RO16 decolorization. $c_0(\text{RO16}) = 50.0 \text{ mg dm}^{-3}$, $c_0(\text{H}_2\text{O}_2) = 25.0 \text{ mmol dm}^{-3}$, UV light intensity: $730 \mu\text{W cm}^{-2}$, temperature: $25 \pm 0.5^\circ\text{C}$.

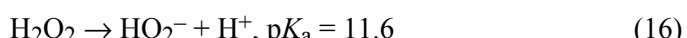
The lowest values of the apparent rate constant in all cases were obtained at pH 2, where the greatest concentration of inorganic anions was added to adjust the pH. On increasing the pH value from 3.0 to 5.0, the concentrations of added inorganic anions decreased and, as a result, the values of k_{app} increased slightly. Hence, the scavenging effect decreases with decreasing concentration of added inorganic anions. A comparison of the process efficiency in the pH range from 2 to 5 suggests the following increasing scavenging effect phosphate < sulfate < nitrate < chloride.

Jaysona *et al.*²⁹ reported that the rate constant for the interaction between •OH and Cl⁻ was $k = 4.3 \times 10^9 \text{ M}^{-1} \text{ s}^{-1}$ (reaction (12)). Katsumura *et al.*³⁰ investigated the reactivity of NO₃• and obtained a value for the rate constant for the reaction •OH with NO₃⁻ of $1.3 \times 10^8 \text{ M}^{-1} \text{ s}^{-1}$ (reaction (13)). The results of Jiang *et al.*³¹ and Maruthamuthu *et al.*³² showed that HSO₄⁻ and H₂PO₄⁻ react with •OH at a lower rate ($k = 4.7 \times 10^5 \text{ M}^{-1} \text{ s}^{-1}$ and $k = 2 \times 10^4 \text{ M}^{-1} \text{ s}^{-1}$, respectively) than NO₃⁻ (reactions (14) and (15)). Therefore, the obtained scavenging effects of the anions used in this study are in agreement with the values of the rate constants given in the mentioned literature.^{29–32}

On the other hand, in a study of Galindo *et al.*³³, which considers the photochemical degradation of Acid Blue 74, a different order of scavenging effects of the anions was shown. They found that the sulfate anion was the strongest •OH scavenger, followed by nitrate and phosphate anions, while the chlorides were the weakest scavenger. This decay in the rate of Acid Blue 74 degradation in the presence of sulfate anions was explained by possible aggregation of dye molecule, when a strong electrolyte such as sulfuric acid was added. •OH radicals show less affinity to aggregated dye than to single molecules. The results of the present investigation demonstrated that the scavenging effect of the anions was predominant, as no significant effect of aggregation of the dye molecules could be expected with the applied concentrations of the mineral acids.³⁴

The other test runs were performed by adjusting the pH with NaOH at 7.0, 9.0 and 10.0 (Fig. 8). A decline of apparent rate constants from 0.342 min^{-1} at pH 7 to 0.151 min^{-1} at pH 10.0 was observed, which can be a consequence of the following possible reasons.

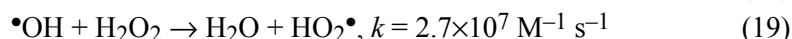
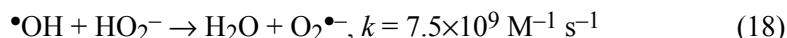
First, at alkaline pH, the concentration of the conjugate base of H₂O₂ increases (reaction (16)):



This anion (HO₂⁻) reacts with a non-dissociated molecule of H₂O₂, which leads to oxygen and water, instead of producing hydroxyl radicals under UV radiation (reaction (17)). Therefore, the instantaneous concentration of •OH is lower than expected:



Furthermore, the deactivation of $\cdot\text{OH}$ is more important when the pH of the solution is high. The reaction of $\cdot\text{OH}$ with HO_2^- is approximately 300 times faster than its reaction with H_2O_2 (reactions (18) and (19)).



The reactivity of $\text{O}_2^{\bullet-}$ and HO_2^{\bullet} with organic pollutants is much lower than that of $\cdot\text{OH}$. They preferentially disproportionate and produce hydrogen peroxide and dioxygen (reaction (20)):

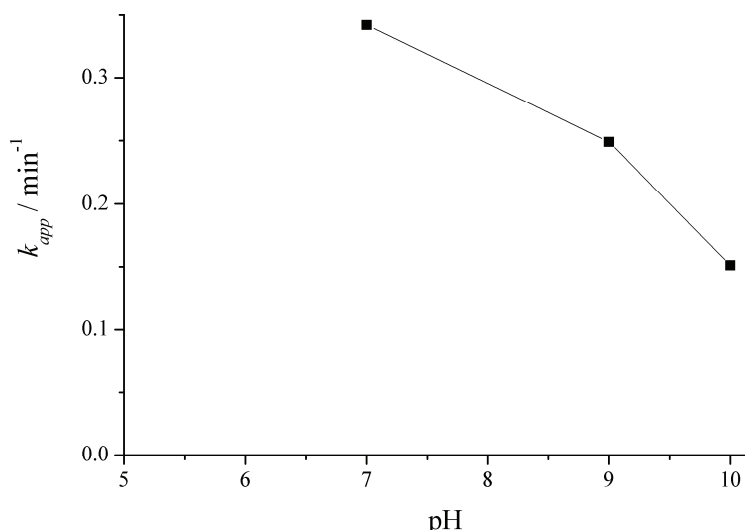
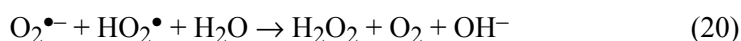


Fig. 8. Effect of pH on the rate of RO16 decolorization. $c_0(\text{RO16}) = 50.0 \text{ mg dm}^{-3}$, $c_0(\text{H}_2\text{O}_2) = 25.0 \text{ mmol dm}^{-3}$, UV light intensity: $730 \mu\text{W cm}^{-2}$, temperature: $25 \pm 0.5^\circ\text{C}$.

On the other hand, several authors have reported that the peroxide self-decomposition rate, which is strongly pH dependent, partly contributes to the decrease of the k_{app} values in alkaline medium (reaction (21)).^{27,35}



Chu³⁶ investigated the self-decomposition rate of peroxide and found that its first order self-decomposition constants are 2.29×10^{-2} and $7.4 \times 10^{-2} \text{ min}^{-1}$ at pH 7.0 and 10.5, respectively. The photodecomposition of peroxide by UV light at the same pH values was also investigated by this author. By comparing the results at alkaline pH values, it was concluded that the decrease of the H_2O_2 concentration was significantly caused by its self-decomposition; hence, a decay pathway not involving free radicals must occur.

Both of the two proposed peroxide decomposition pathways in alkaline medium, the first leading to the formation of the HO_2^- and the second the self decomposition of H_2O_2 leading to the formation of water and oxygen, can occur simultaneously, which results in a decrease in the $\cdot\text{OH}$ concentration and, consequently, a decrease in the dye decolorization rate.

It is important to note that the pH of the dye bath for reactive dyes depends on the textile fiber and in industrial applications, the dyeing of cellulosic fibers is performed in alkaline dye baths, while dye baths for wool are acidic. The results presented in this paper indicated that removal efficiency of RO16 dye is higher at neutral pH values; hence, effluents from the textile industry must be neutralized for treatment by the UV/ H_2O_2 process in order to achieve the maximal decolorization rate.

The effect of initial dye concentration

The effect of the initial RO16 concentration on the efficiency of dye degradation was investigated in the concentration range from 20–80 mg dm⁻³ and the results are presented in Fig. 9. It appears that with increasing initial dye concentration, the efficiency of dye removal almost linearly decreases. The results indicate that the apparent rate constant decreases from 0.382 min⁻¹ for a dye concen-

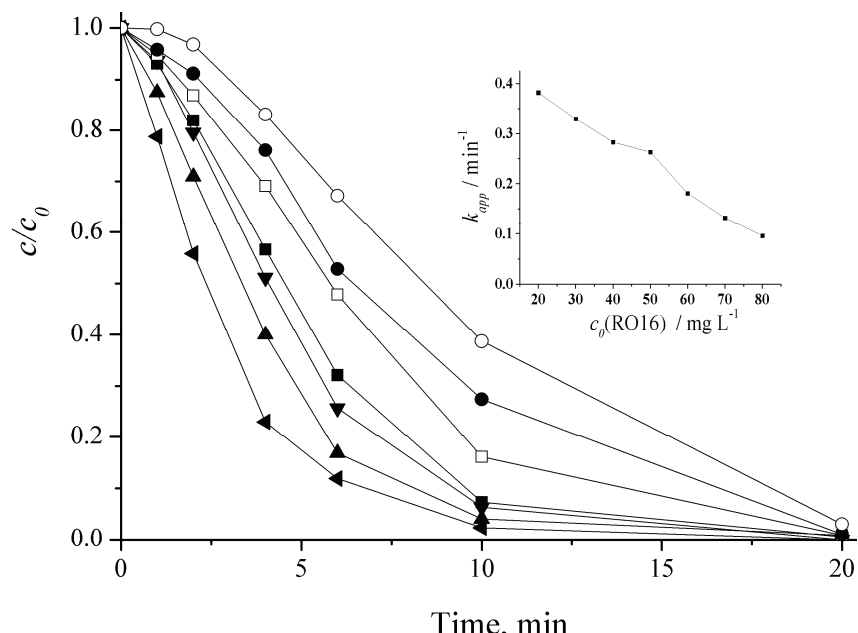


Fig. 9. Effect of the initial concentration of RO16, 20 (◀), 30 (▲), 40 (▼), 50 (■), 60 (□), 70 (●) and 80 mg dm⁻³ (○) on its decolorization. $c_0(\text{H}_2\text{O}_2) = 25.0 \text{ mmol dm}^{-3}$, pH 7.0±0.2, UV light intensity: 730 $\mu\text{W cm}^{-2}$, temperature: 25±0.5 °C. Inset represents k_{app} at different initial dye concentrations.

tration of 20 mg dm^{-3} to 0.096 min^{-1} for a dye concentration of 80 mg dm^{-3} . Similar results were already reported by Behnajady *et al.*³⁷ At high dye concentrations, most of the UV light was absorbed by the dye instead of by the peroxide because of its higher molar extinction coefficient at 253.7 nm . Hence, the dye solution becomes increasingly impermeable to UV light, which inhibits photolysis of the peroxide. This is very important from the application point of view and the $\text{UV}/\text{H}_2\text{O}_2$ system would be more effective for relatively dilute dye solutions.

The effect of UV light intensity

The influence of UV-light intensity on the decolorization of RO16 azo dye was monitored by varying the light intensity from 730 up to $1950 \mu\text{W cm}^{-2}$ and the results are shown in Fig. 10. It is evident that the apparent rate constant increased linearly with increasing UV light intensity. This result is consistent with those of previous studies, in which an increase in the decolorization rate with increasing UV light intensity was generally observed.³⁸ Such an effect is expected because photodissociation of peroxide is initiated by its absorption of UV light; hence, increases in the UV light intensity enhance the production of hydroxyl radicals.

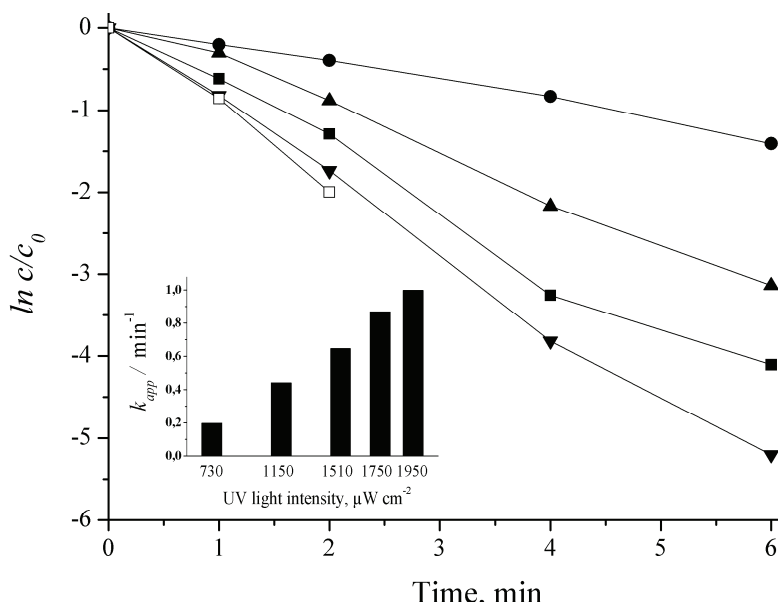


Fig. 10. Effect of UV light intensity, 730 (●), 1150 (▲), 1510 (■), 1750 (▼) and $1950 \mu\text{W cm}^{-2}$ (□) on the decolorization of RO16. $c_0(\text{RO16}) = 50.0 \text{ mg L}^{-1}$, $c_0(\text{H}_2\text{O}_2) = 25.0 \text{ mmol dm}^{-3}$, pH 7.0 ± 0.2 , temperature $25 \pm 0.5^\circ\text{C}$. Inset represents k_{app} at different UV light intensities.

CONCLUSIONS

The results presented in this paper showed that the UV/H₂O₂ process could be efficiently used for the decolorization of aqueous solutions of the azo dye Reactive Orange 16. It was found that the rate of decolorization is significantly affected by the initial pH, the initial hydrogen peroxide concentration, the initial dye concentration and the UV light intensity. The decolorization follows pseudo first order reaction kinetics. Peroxide concentrations in the range from 20 to 40 mM appear as optimal. Color removal was observed to be faster in neutral pH solutions than in acidic and basic ones. The hydroxyl radical scavenging effect of the examined inorganic anions increased in the order phosphate < sulfate < nitrate < chloride. Pseudo-rate constant (k_{app}) decreased as the initial dye concentration increased, but it increased linearly with increasing UV light intensity and attained a maximal value at the highest applied intensity. The complete removal of color, after selection of optimal operational parameters, was achieved within 6 min of UV irradiation, which indicates that it is a highly efficient process.

Acknowledgement. Authors would like to acknowledge the financial support of the Ministry of Education and Science of the Republic of Serbia (Project No. TR34008).

И З В О Д

ОБЕЗБОЈАВАЊЕ ТЕКСТИЛНЕ АЗО БОЈЕ РЕАКТИВНИ ОРАНЖ 16 UV/H₂O₂ ПРОЦЕСОМ

ЈЕЛЕНА МИТРОВИЋ, МИЉАНА РАДОВИЋ, ДАНИЈЕЛА БОЛИЋ, ТАТЈАНА АНЂЕЛКОВИЋ,
МИЛОВАН ПУРЕНОВИЋ и АЛЕКСАНДАР БОЛИЋ

Одсек за хемију, Природно-математички факултет, Универзитет у Нишу, Вишеградска 33, 18000 Ниш

У раду је проучавана ефикасност деколоризације реактивне азо боје реактивни оранж 16 (RO16) UV/H₂O₂ процесом у фотопректору са UV лампама максимума емисије на 253,7 nm. При оптималним условима (25 mM иницијална концентрација пероксида, pH 7, интензитет UV зрачења 1950 μW cm⁻²) потпуно уклањање иницијалне концентрације боје (50,0 mg dm⁻³) је постигнуто за мање од 6 min. Испитиван је утицај параметара UV/H₂O₂ процеса, као што су иницијална pH вредност, иницијална концентрација водоник-пероксида, иницијална концентрација боје и интензитет UV зрачења на ефикасност деколоризације боје. Највећа ефикасност процеса постигнута је при иницијалној концентрацији пероксида у распону од 20 до 40 mM, изнад које је процес инхибиран његовим ефектом хватача радикала. Процес деколоризације је ефикаснији у неутралној средини. Са повећањем иницијалне концентрације боје расте и ефикасност процеса као и са повећањем интензитета UV зрачења.

(Примљено 16. фебруара, ревидирано 3. августа 2011)

REFERENCES

1. H. Zollinger, *Color Chemistry: Syntheses, Properties and Applications of Organic Dyes and Pigments*, Wiley–VCH, Weinheim, Germany, 2003, p. 579
2. L. G. Devi, S. G. Kumar, K. M. Reddy, C. Munikrishappa, *J. Hazard. Mater.* **164** (2009) 459

3. M. H. Habibi, A. Hassanzadeh, S. Mahdavi, *J. Photochem. Photobiol., A* **172** (2005) 89
4. *Advanced oxidation processes for water and wastewater treatment*, S. Parsons, Ed., IWA Publishing, London, 2004, p. 302
5. M. A. Behnajady, N. Modirshahla, H. Fathi, *J. Hazard. Mater., B* **136** (2006) 816
6. M. Muruganandham, M. Swaminathan, *Dyes Pigm.* **68** (2006) 133
7. E. Kusvuran, O. Erbatur, *J. Hazard. Mater., B* **106** (2004) 115
8. K. H. Wong, S. Tao, R. Dawson, P. K. Wong, *J. Hazard. Mater., B* **109** (2004) 149
9. F. S. Garcia Einschlag, J. Lopez, L. Carlos, A. L. Capparelli, A. M. Braun, E. Oliveros, *Environ. Sci. Technol.* **36** (2002) 3936
10. O. Lergini, E. Oliveros, A. M. Braun, *Chem. Rev.* **93** (1993) 671
11. A. M. Marechal, Y. M. Slokar, T. Taufer, *Dyes Pigm.* **33** (1997) 281
12. A. M. El-Dein, J. A. Libra, U. Wiesmann, *Chemosphere* **52** (2003) 1069
13. X. Dong, W. Ding, X. Zhang, X. Liang, *Dyes Pigm.* **74** (2007) 470
14. A. Aleboyeh, Y. Moussa, H. Aleboyeh, *Sep. Purif. Technol.* **43** (2005) 143
15. S. M. Milosavljević, *Structural methods of instrumental analysis*, Faculty of Chemistry, Belgrade, 1994, p. 35 (in Serbian)
16. A. S. Ozen, P. Doruker, V. Aviyente, *J. Phys. Chem., A* **111** (2007) 13506
17. M. Styliidi, D. I. Kondarides, X. E. Verykios, *Appl. Catal., B* **47** (2004) 189
18. Z. He, L. Lin, S. Song, M. Xia, L. Xu, H. Ying, J. Chen, *Sep. Purif. Technol.* **62** (2008) 376
19. K. Li, D. R. Hokanson, J. C. Crittenden, R. R. Trussell, D. Minakata, *Water Res.* **42** (2008) 5045
20. W. Abdel-Alim Sadik, A. W. Nashed, *Chem. Eng. J.* **137** (2008) 525
21. D. Jiraroj, F. Unob, A. Hagege, *Water Res.* **40** (2006) 107
22. A. Aleboyeh, H. Aleboyeh, Y. Moussa, *Dyes Pigm.* **57** (2003) 67
23. N. Daneshvar, M. Rabbani, N. Modirshahla, M. A. Behnajady, *Chemosphere* **56** (2004) 895
24. N. H. Ince, *Water Res.* **33** (1999) 1080
25. G. V. Buxton, C. L. Greenstock, W. P. Helman, A. B. Ross, *J. Phys. Chem. Ref. Data* **17** (1988) 513
26. K. Schested, O. L. Rasmussen, H. Fricke, *J. Phys. Chem.* **72** (1968) 626
27. M. Muruganandham, M. Swaminathan, *Dyes Pigm.* **62** (2004) 269
28. M. Neamtu, I. Siminiceanu, A. Yediler, A. Kettrup, *Dyes Pigm.* **53** (2002) 93
29. G. G. Jayson, B. J. Parsons, A. J. Swallow, *J. Chem. Soc., Faraday Trans.* (1973) 1597
30. Y. Katsumura, P. Y. Jiang, R. Nagaishi, T. Oishi, K. Ishigure, *J. Phys. Chem.* **95** (1991) 4435
31. P. Y. Jiang, Y. Katsumura, R. Nagaishi, M. Domae, K. Ishikawa, K. Ishigure, Y. Yoshida, *J. Chem. Soc., Faraday Trans.* **88** (1992) 1653
32. P. Maruthamuthu, P. Neta, *J. Phys. Chem.* **82** (1978) 710
33. C. Galindo, P. Jacques, A. Kalt, *J. Photochem. Photobiol., A* **141** (2001) 47
34. M. H. Habibi, A. Hassanadeh, A. Z. Isfahani, *Dyes Pigm.* **69** (2006) 111
35. H.Y. Shu, M. C. Chang, *J. Hazard. Mater., B* **125** (2005) 96
36. W. Chu, *Chemosphere* **44** (2001) 935
37. M. A. Behnajady, N. Modirshahla, M. Shokri, *Chemosphere* **55** (2004) 129
38. M. W. Chang, C. C. Chung, J. M. Chern, T. S. Chen, *Chem. Eng. Sci.* **65** (2010) 135.





Electrochemical behavior and electrochemical determination of carbamazepine at an ionic liquid modified carbon paste electrode in the presence of sodium dodecyl sulfate

LI-HONG LIU^{1,2}, CHENG-QIAN DUAN^{1,3} and ZUO-NING GAO^{1*}

¹Key Lab of Energy Sources and Chemical Engineering, College of Chemistry and Chemical Engineering, Ningxia University, Yinchuan 750021, China, ²Department of Chemistry, Heihe College, Heihe 164300, China and ³Higher Vocational College, Ningxia Medical University, Yinchuan 750004, China

(Received 20 April, revised 9 October 2011)

Abstract: The electrochemical behavior and electrochemical determination of carbamazepine (CBZ) at a hydrophobic ionic liquid 1-benzyl-3-methylimidazole hexafluorophosphate ($[BnMIM]PF_6$) modified carbon paste electrode ($[BnMIM]PF_6/CPE$) in the presence of sodium dodecyl sulfate (SDS) were investigated. A well-defined and sensitive oxidation peak was observed at the $[BnMIM]PF_6/CPE$ in the presence of SDS and a 0.10 M phosphate buffer solution (pH 6.80). The oxidation peak current of CBZ increased significantly at the $[BnMIM]PF_6/CPE$ in the presence of SDS compared with that in the absence of SDS at the carbon paste electrode. It suggested that both SDS and $[BnMIM]PF_6/CPE$ show an obvious enhancing effect on the electrochemical oxidation of CBZ. The electrochemical kinetic parameters for CBZ at the $[BnMIM]PF_6/CPE$ in aqueous SDS solutions were also determined by chronocoulometry and chronoamperometry. Finally, the experimental conditions were optimized, and a new electrochemical method for the determination for CBZ was established. The oxidation peak current was linearly dependent on the CBZ concentration in the range 7.0 μ M to 0.7 mM, with a detection limit of 0.98 μ M (signal to noise ratio, $S/N = 3$). The relative standard deviation for six determinations of 0.10 mM CBZ was between 1.40 and 2.13 %. The proposed method was applied in the determination of CBZ in commercial tablet samples.

Keywords: carbamazepine; sodium dodecyl sulfate; ionic liquid modified carbon paste electrode; electrochemistry.

INTRODUCTION

Carbamazepine (5*H*-dibenz[*b,f*]azepine-5-carbox-amide, CBZ, structure presented in Fig. 1) has been extensively used in the treatment of epilepsy.¹ Now it

* Corresponding author. E-mail: gaozn@nxu.edu.cn
doi: 10.2298/JSC110420188L

is considered as the most frequently prescribed front-line anticonvulsant in complex partial seizures.² Due to its clinical importance, many analytical techniques have been developed for its determination and also its metabolite in biological fluids (plasma, urine), including high performance liquid chromatography (HPLC),^{3,4} HPLC with an electrochemical detector,⁵ liquid chromatography with mass spectrometry (LC–MS),⁶ gas chromatography,^{7,8} capillary electrokinetic chromatography,⁹ mass spectrometry,¹⁰ chemiluminescence,¹¹ spectrofluorimetry¹² and spectrophotometry.¹³ Electroanalytical techniques bring with them important advantages, such as high sensitivity, relative simplicity, low costs and portable field-based equipment. They therefore offer interesting alternatives to replace the methods that are currently in use. Voltammetric and polarographic methods have been reported for the determination of CBZ. These included polarography in which the electrochemical reduction of CBZ at a mercury drop electrode was studied,^{14,15} potentiometry with polymer membrane-based ion-selective electrodes,¹⁶ more recently, described by Garcia *et al.*¹⁷, the determination of carbamazepine in pharmaceutical solutions using differential-pulse adsorptive stripping voltammetry and the oxidation properties of the molecule with different modified and the unmodified carbon electrodes. Thus, Rodriguez *et al.*¹⁸ studied the electrochemical behavior and determination of carbamazepine on glassy carbon electrodes and microelectrodes. Teixeira *et al.*¹⁹ described the voltammetric determination of carbamazepine at a multi-walled carbon nanotubes (MWCNTs) film-coated glassy carbon electrode (GCE) and Jaldappagari *et al.*²⁰ investigated the electrochemical behavior of carbamazepine (CBZ) at a fullerene-C₆₀ modified glassy carbon electrode. However, its electrochemical behavior and electrochemical determination at an ionic liquid 1-benzyl-3-methylimidazole hexafluorophosphate modified carbon paste electrode ([BnMIM]PF₆/CPE) in the presence of sodium dodecyl sulfate (SDS) has, to the best of our knowledge, not been reported in the literature.

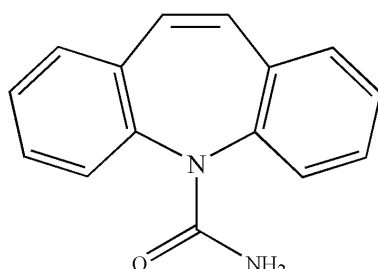


Fig. 1. Structure of carbamazepine.

Recently, the application of room temperature ionic liquids (RTILs) in the fields of analytical chemistry and electrochemical biosensors has attracted much attention. Ionic liquids (ILs) are composed of an organic cation and either an organic or an inorganic anion, preserved in the liquid state over a wide tem-

perature range.²¹ Due to their specific physicochemical characteristics, such as high chemical and thermal stability, good ionic conductivity, negligible vapor pressure and wider electrochemical windows,^{22–27} RTILs have been used as a new modifier on the surface of electrodes or binders to make a carbon ionic liquid electrode (CILE). For example, Safavi *et al.*^{28,29} fabricated an ionic liquid, *i.e.*, octylpyridinium hexafluorophosphate (OPFP), modified carbon paste electrode and investigated the electrochemical oxidation of some phenolic compounds. Zheng *et al.*³⁰ fabricated an ionic liquid, *i.e.*, 1-pentyl-3-methylimidazolium bromide modified carbon paste electrode and investigated the voltammetric determination of rutin. Liu *et al.*³¹ reported a CILE constructed of graphite powder mixed with the ionic liquid 1-butyl-3-methylimidazolium hexafluorophosphate (BMIMPF₆) and the electrode had an increased sensitivity of the response toward potassium ferricyanide. Sun *et al.*^{32–34} also combined butylpyridinium hexafluorophosphate (BPPF₆) with graphite powder to fabricate an ILs modified electrode and applied it in the electrochemical determination of different inorganic, organic and biomolecules.

As a continuation of previous work,^{35–38} in this study, the hydrophobic ionic liquid 1-benzyl-3-methylimidazole hexafluorophosphate ([BnMIM]PF₆) was used as a modifier to fabricate [BnMIM]PF₆/CPE and the electrochemical behavior and electrochemical kinetics of carbamazepine (CBZ) at [BnMIM]PF₆/CPE in the presence of sodium dodecyl sulfate (SDS) were investigated.

Surfactants are a kind of amphiphilic molecule with hydrophilic head on one side and a long hydrophobic tail on the other. They can be adsorbed at an electrode surface and alter the properties of the electrode/solution interface and subsequently influence the electrochemical processes of electroactive species.^{39,40} Now surfactants are extensively used in the fields of electrochemistry and electroanalytical chemistry.⁴¹ Hu and coworkers successfully employed surfactants for the analysis of some biomolecules,^{42,43} and found that the electrochemical responses of the analyzed compounds were remarkably enhanced in the presence of the surfactants. Moreover, they proposed a synergistic adsorption mechanism to interpret the enhancing effects of the surfactants. For example, surfactants might combine with the substrate in certain forms and strengthen their adsorption on the electrode surface, which facilitated the electron or the substance transfer between the electrode and the solution.^{44–47} Kaifer colleagues reported significant changes in the redox potentials and peak currents of methyl viologen in a sodium dodecyl sulfate (SDS) micellar solution.^{48,49}

In the present work, the oxidation peak currents of CBZ were found to increase greatly at [BnMIM]PF₆/CPE in the presence of SDS compared with those at bare CPE and [BnMIM]PF₆/CPE in the absence of SDS. The experimental results indicated that both [BnMIM]PF₆ and SDS can greatly enhance the electrochemical responses of CBZ. Simultaneously, a quantitative electroche-

mical determination method was developed which was successfully used to determine CBZ in commercial samples.

EXPERIMENTAL

Apparatus

All electrochemical experiments were performed using an electrochemistry workstation CHI660A (CH Instrument, USA). The working electrodes were a carbon paste electrode (CPE) and a 1-benzyl-3-methylimidazole hexafluorophosphate ([BnMIM]PF₆) modified carbon paste electrode ([BnMIM]PF₆/CPE). A CHI115 platinum wire and a CHI150 saturated calomel electrode (SCE) served as the auxiliary electrode and reference electrode, respectively. All potentials measured and reported in this work are *versus* a SCE.

Reagents

Carbamazepine was manufactured by China Drug and Biological Products Testing Organization and was used as received without further purification. Carbamazepine tablets were from FuDan FuHua Pharmaceutical Corporation (Shanghai, China), 1-benzyl-3-methylimidazole hexafluorophosphate ([BnMIM]PF₆) from Chengjie Chemical Reagent Ltd. (Shanghai, China, purity 99 %) and sodium dodecyl sulfate (SDS) from Beijing Chemistry Factory (Beijing, China, analytical grade). All solutions were prepared using deoxygenated and doubly distilled water. All other chemicals were of analytical grade and were used as received.

Preparation of CPE and [BnMIM]PF₆/CPE

The carbon paste electrode was prepared as follows: 1.50 g of graphite and 0.50 mL of paraffin oil were mixed in a mortar to form a homogeneous mixture. The mixture was pressed by hand into the end cavity of a polytetrafluoroethylene (PTFE) cylindrical electrode body and the surface was polished on a piece of weighing paper.

The BPPF₆/CPE was prepared as follows: 0.50 g of [BnMIM]PF₆ was first dissolved in 2.0 mL of DMF, and then added to 1.50 g of graphite powder in a mortar, ground until the DMF had entirely volatilized, and finally mixed with 0.50 mL of paraffin oil in the mortar. The mixture was pressed by hand into the end cavity of a PTFE cylindrical electrode body and the surface was polished on a piece of weighing paper.

Experimental procedure

The electrochemical experiments were performed in a conventional electrochemical cell, containing 0.10 M phosphate buffer solutions (PBS) as the supporting electrolyte and a certain concentration of CBZ and SDS. A 0.01 M ethanolic stock solution of CBZ was prepared in and diluted solutions were prepared daily with doubly distilled water just before use. All experiments were realized at room temperature.

RESULTS AND DISCUSSION

Cyclic voltammetric behavior of CBZ

The cyclic voltammetric behavior of 0.10 mM CBZ in 0.10 M PBS were investigated at the CPE and [BnMIM]PF₆/CPE in the absence and the presence of SDS at a scanning rate of 50 mV s⁻¹ over the potential range from 0.30 to 1.20 V. As shown in Fig. 2, a less sensitive electrochemical response was observed for 0.10 mM CBZ at CPE in the absence of SDS (curve *a*). Moreover, the oxidation peak potential shifted negatively by about 50 mV and the oxidation peak current



increased about two times of that at the [BnMIM]PF₆/CPE (curve *b*) in the absence of SDS. Due to the decrease of the oxidation peak potentials and the increase of the oxidation peak currents, the good enhancing effect on the electrochemical oxidation of CBZ was attributed to the specific advantages of RTILs, including high conductivity and the promotion of the electron transfer rate.³⁴ After the addition of 0.40 mM SDS, the oxidation peak potential shifted negatively by about 70 mV and the oxidation peak current increased to nearly four times that at the CPE (curve *c*) and the oxidation peak potential remained almost constant and the oxidation peak current increased to nearly three times that at [BnMIM]PF₆/CPE in the presence of SDS (curve *d*). It is well known that surfactants can be adsorbed on a hydrophobic surface to form a surfactant film,⁵⁰ which may alter the overvoltage of CBZ on the electrode surface and facilitate the electron transfer rate.⁵¹ Moreover, CBZ surface concentration on the CPE and [BnMIM]PF₆/CPE can be greatly increased in the presence of SDS, therefore, the oxidation peak current of CBZ significantly increased at both the CPE and the [BnMIM]PF₆ in the presence of SDS. Hence, the conclusion can be drawn from the comparisons that both CPE and [BnMIM]PF₆/CPE in the presence of SDS are more active to CBZ than that in the absence of SDS and can greatly enhance the electrochemical sensitivity. Therefore, both RTILs and SDS

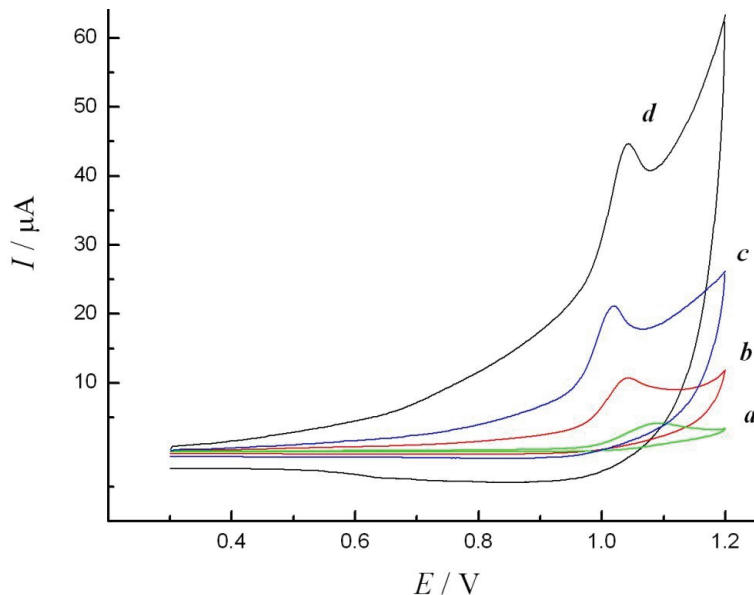


Fig. 2. Cyclic voltammograms of CBZ in 0.10 M PBS (pH 6.8) at the CPE in the absence (a) and the presence (c) of SDS, at the [BnMIM]PF₆/CPE in the absence (b) and the presence (d) of SDS. Scanning rate: 50 mV·s⁻¹, CBZ concentration: 0.10 mM, SDS concentration: 0.40 mM. Accumulation time: 160 s.

have synergistic effect on the CBZ electrochemical oxidation process. In addition, no corresponding reduction peak was observed in the reverse scanning, indicating the irreversibility of the electrochemical oxidation.

Furthermore, the effect of scanning rate on the electrochemical behavior of 0.10 mM CBZ at [BnMIM]PF₆/CPE in the presence of 0.40 mM SDS at different scan rates of 30 to 500 mV s⁻¹ were investigated by CV. With increasing potential scanning rate, the peak currents increased and the peak potentials shifted positively, which implied the irreversible nature of the electrode reaction processes. The oxidation peak currents versus the square roots of the scanning rate gave a straight line, as expected for a diffusion-limited electrode reaction process. The linear regression equation is expressed as I_{pa} (μ A) = -2.469 + 1.469 $v^{1/2}$ (where v is in mV s⁻¹), with a correlation coefficient (R) of 0.9977.

The effects of the experimental conditions on the oxidation peak currents and potentials

The effect of various media on the peak currents and potentials of CBZ could be easily observed from CV. The CV of CBZ at a scanning rate of 50 mV s⁻¹ in different electrolyte solutions, *i.e.*, aqueous NaCl, NaAc, NaNO₃, Na₂SO₄ and NaAc-HAc, Britton-Robinson buffer (B-R), Na₂HPO₄-NaH₂PO₄ (PBS) solutions containing NaCl were investigated. The experimental results showed that in an aqueous 0.10 M PBS solution, CBZ had a well-defined electrochemical behavior. Thus, a 0.10 M aqueous PBS solution was chosen as the supporting electrolyte.

The influence of the surfactant, *i.e.*, the anionic surfactants sodium dodecyl benzene-sulfonate (SDBS), sodium dodecyl sulfate (SDS) and the cationic surfactants cetyltrimethylammonium bromide (CTAB), cetylpyridine bromide (CPB), dodecyltrimethylammonium bromide (DTAB) on the oxidation peak current of CBZ were also examined. It was observed that all the anionic surfactants could improve the oxidation peak current of CBZ over a certain concentration range (below the critical micelle concentration (CMC)), but the degree of enhancement varied. Among these surfactants, the oxidation peak current of CBZ was the highest and the background current the smallest in the presence of SDS. The SDS concentration also affects the oxidation peak current of CBZ. Thus, the influence of the SDS concentration on the oxidation peak current of CBZ was examined, and the experimental results showed that with gradual increasing concentration of SDS from 0.01 to 0.40 mM, the oxidation peak current of CBZ also obviously increased, while on further increasing the SDS concentration from 0.40 to 0.90 mM, the oxidation peak currents remained almost constant. Therefore, the SDS concentration was chosen as 0.40 mM.

The effect of solution pH on the oxidation peak current and peak potential for CBZ at [BnMIM]PF₆/CPE were studied in 0.10 M PBS over the pH range from 2.0 to 9.0. It was found that the oxidation peak currents remained almost

constant from pH 2.0 to 7.5 and then decreased as the pH was further increased. Therefore, an aqueous PBS solution of pH 6.8 was chosen as the electrolyte. Furthermore, the peak potentials shifted only slightly in the pH range 2.0 to 9.0, suggesting that no proton was involved in the electrode reaction.

Accumulation potential and time

The effects of the accumulation potential on the oxidation peak current were investigated. When the accumulation potential was shifted from 0.10 to 0.80 V, the oxidation peak current of CBZ altered very slightly. This reveals that the accumulation potential has no obvious influence on the oxidation current of CBZ under these conditions.

The influences of the accumulation time from 20 to 200 s on the peak current were investigated and it was found that the peak current increase linearly with the accumulation time in the range of 20 to 160 s. However, the peak current did not increase, as when the accumulation time was extended beyond 160 s. Usually, an accumulation time of 160 s employed in this study.

Electrochemical kinetics

The charge-transfer coefficient α . According to the experimental results mentioned above, the oxidation of CBZ is a diffusion-limited electrochemical process at [BnMIM]PF₆/CPE in the presence of SDS. For an irreversible diffusion-controlled process, the peak potential (E_{pa}) is proportional to the logarithm of potential scanning rate (v) according to the equation:⁵²

$$E_{\text{pa}} = (b \log v)/2 + \text{constant} \quad (1)$$

Based on this equation, the slope of an E_{pa} vs. $\log v$ plot is $b/2$, in which b indicates the Tafel slope. The dependence of E_{pa} on $\log v$ for oxidation of CBZ at the [BnMIM]PF₆/CPE in the presence of SDS is shown in Fig. 3. Its linear regression equation is expressed as E_{pa} (mV) = 989.6 + 40.44 $\log v$, with a correlation coefficient (R) of 0.9970. Thus $b = 2\partial E_{\text{p}}/\partial(\log v) = 81$ mV was obtained. Thus, from the equation $b = 2.303 RT/n(1-\alpha)F$ ($n = 2$,^{15,16} $T = 298$ K, $F = 96485$ C mol⁻¹), the charge-transfer coefficient $\alpha = 0.63$.

The diffusion coefficient D. The apparent diffusion coefficient D of CBZ and the geometrical surface area of electrode were also determined in this work by chronocoulometry (CC):⁵³

$$Q = \frac{2nFAcD^{1/2}t^{1/2}}{\pi^{1/2}} + Q_{\text{dl}} + Q_{\text{ads}} \quad (2)$$

where Q is the total charge, n is number of electrons transferred in the electrochemical oxidation reaction. A is the electrode area (cm²), c is the concentration of the electroactive species, D is the diffusion coefficient (cm² s⁻¹) and t is the time (ms). The geometrical surface area of the modified electrode and CPE were

calculated from the slopes of Q vs. $t^{1/2}$ curves obtained using 5.0 mM of $\text{Fe}(\text{CN})_6^{3-}$ as a model compound. As the number of electron transferred of CBZ is 2,^{15,16} the surface area (A) of [BnMIM] PF_6 /CPE is 0.0686 cm^2 . For a CBZ concentration (C) of 0.10 mM, the diffusion coefficient (D) of CBZ in the presence of SDS was calculated to be $8.10 \times 10^{-4} \text{ cm}^2 \text{ s}^{-1}$.

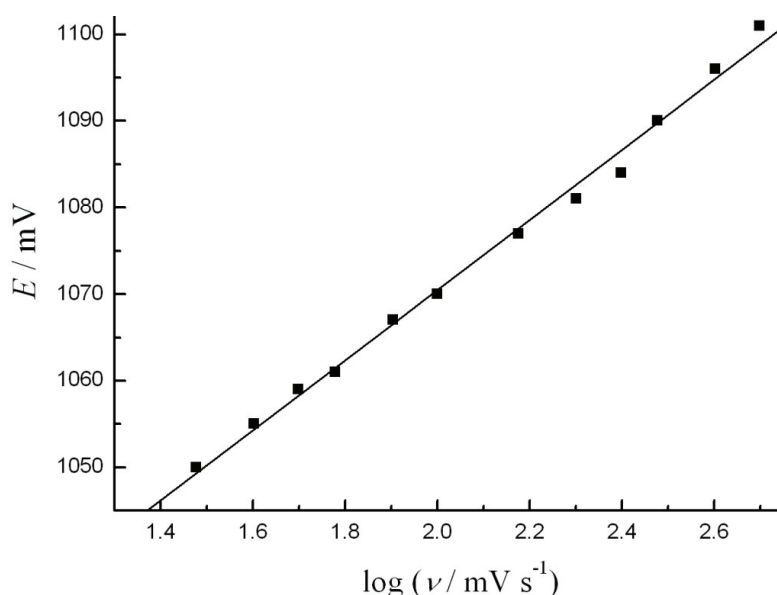


Fig. 3. Dependence of the voltammetric peak potentials on the logarithm of the scanning rate for CBZ oxidation at the [BnMIM] PF_6 /CPE in the presence of SDS.

The electrode reaction rate constant k_f . Due to the increase of the electrochemical oxidation of CBZ in the presence of SDS, it should obey the following chronoamperometric equation.^{36,54}

$$I_C / I_L = \lambda^{1/2} \left[\pi^{1/2} \operatorname{erf}(\lambda^{1/2}) + \exp(-\lambda) / \lambda^{1/2} \right] \quad (3)$$

The CA curves are shown in Fig. 4, where I_C is the catalytic current in the presence of SDS, I_L is the diffusion-limited current in the absence of SDS. $\lambda = kc_0t$ (k is the rate constant and c_0 is the bulk initial concentration of SDS) is the argument of the error function. In cases where λ exceeds 1.5, the error function is almost equal to unity and the reaction zone is in the pure kinetic region; hence, the above equation can be reduced to:

$$I_C / I_L = \pi^{1/2} \lambda^{1/2} = \pi^{1/2} (kc_0t)^{1/2} \quad (4)$$

This equation can be used to calculate the rate constant (k) of the oxidation process. Knowing that the value of I_C/I_L is proportional to $\lambda^{1/2}$, a plot of I_C/I_L vs.

$\lambda^{1/2}$ can be given by combining Eq. (3) with Eq. (4) and used as a working curve for chronoamperometry. In this way, $\lambda^{1/2}$ can be determined from the working curve after measuring I_C and I_L , and then the value of the electrode reaction rate constant k can simply be calculated from the slope if c_0 (a given concentration of SDS) and t are known. Both I_C and I_L were measured at $t = 17$ ms where $I_C/I_L > 1.5$, and the rate constant k was calculated to be $(1.07 \pm 0.10) \times 10^2 \text{ dm}^3 \text{ mol}^{-1} \text{ s}^{-1}$.

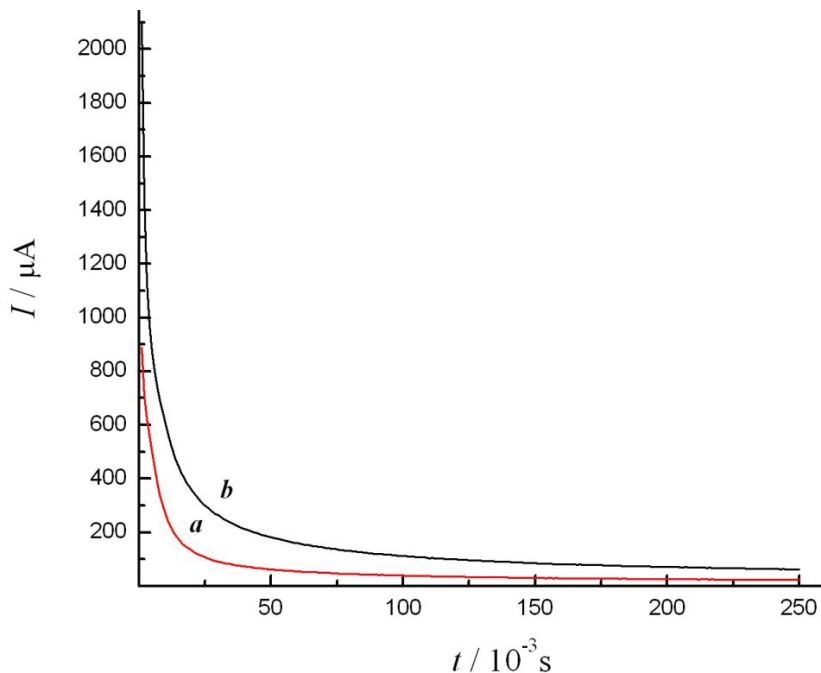


Fig. 4. Chronoamperometry plots of CBZ at the $[\text{BnMIM}] \text{PF}_6/\text{CPE}$ in the absence (a) and the presence (b) of 0.40 mM SDS.

Electrochemical reaction order. The cyclic voltammetric behavior of the oxidation of different concentrations of CBZ at the $[\text{BnMIM}] \text{PF}_6/\text{CPE}$ in the presence of SDS was examined. In the given concentration range, it was found that the logarithm of the peak current, I_{pa} , depended linearly on the logarithm of c_{CBZ} . The linear relationship equation was $\log I_{\text{pa}} = 22.261 + 0.9519 \log c_{\text{CBZ}}$ with a correlation coefficient (R) of 0.9958. The slope close to 1 implies that the electrochemical oxidation of CBZ obeys first-order kinetics with respect to CBZ.⁵⁵

Electrochemical determination of CBZ

Optimization of the operational parameters of differential pulse voltammetry. Differential pulse voltammetry (DPV) responses are markedly dependent on the parameters of the excitement signals. Therefore, optimization of the pulse width and amplitude, and the scan potential increment was performed. The de-

pendence of the oxidation peak current on the pulse amplitude was examined in the range 10–85 mV. Between 10 and 75 mV, the variation of the peak current with pulse amplitude was linear one, above 75 mV, the peak current remained almost constant. Thus, a pulse amplitude of 75 mV was chosen to improve the sensitivity without distortion of the peak. Using a pulse amplitude of 75 mV, the pulse width was varied in the range of 0.01 to 0.035 s. It was found that between 0.01 and 0.02 s, the peak current increased linearly with increasing pulse width, above 0.02 s, the variation of the peak current with the pulse width remained almost constant. A pulse width of 0.02 s was applied. In addition, using a pulse amplitude of 75 mV and a pulse width of 0.02 s, a scanning potential increment of 6 mV was found to develop a well-defined peak and a higher current response.

Differential pulse voltammetry of CBZ. The DPV behavior of 0.10 mM CBZ at the [BnMIM]PF₆/CPE in the presence of 0.40 mM SDS and 0.10 M aqueous PBS solution under the optimal experimental conditions (amplitude of 75 mV, pulse width of 0.02 s and scanning potential increment of 6 mV) is shown in Fig. 5. From the curves in Fig. 5, it can be seen that CBZ itself showed a weak DPV response at the CPE in the absence of SDS, but the electrochemical response was greatly enhanced using the [BnMIM]PF₆/CPE in the presence of SDS. The experimental result is in quite good agreement with that of CV.

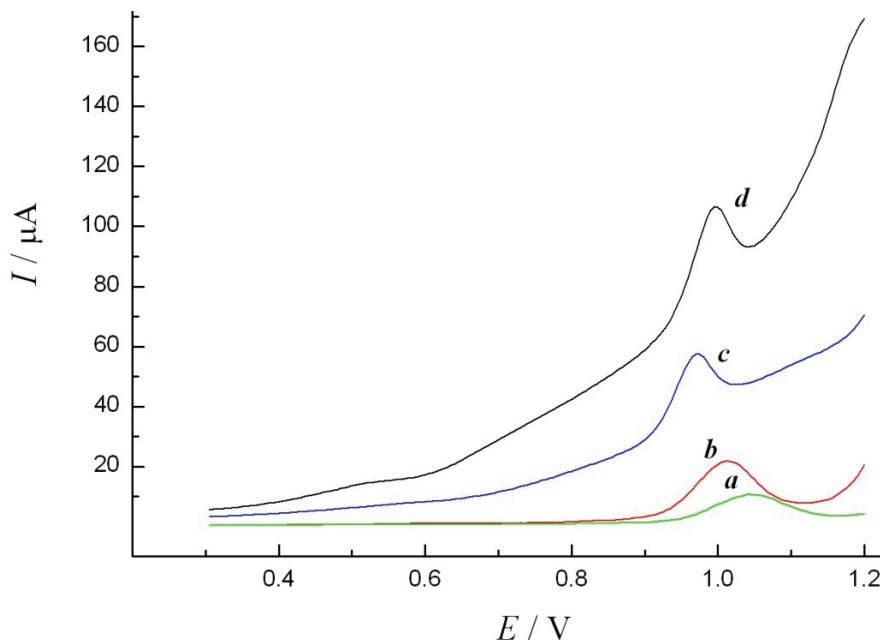


Fig. 5. DPV of 0.10 mM CBZ at the CPE in the absence (a) and the presence (c) of SDS, and at the [BnMIM]PF₆/CPE in the absence (b) and the presence (d) of 0.40 mM SDS.
Accumulation time 160 s.

The relationship between the anodic peak currents for CBZ and its concentration were investigated at the [BnMIM]PF₆/CPE in the presence of SDS. Linear calibration curves were obtained over the range 7.0 μM–0.70 mM in 0.10 M PBS solution (as shown in Fig. 6) with a linear fitting regression equation of I_{pa} (μA) = 3.337 + 161.11c, where c is in mM, with a correlation coefficient (R) of 0.9959. The detection limit defined as a signal-to-noise ratio of 3 ($S/N = 3$) was 0.98 μM for CBZ under the optimized experimental conditions.

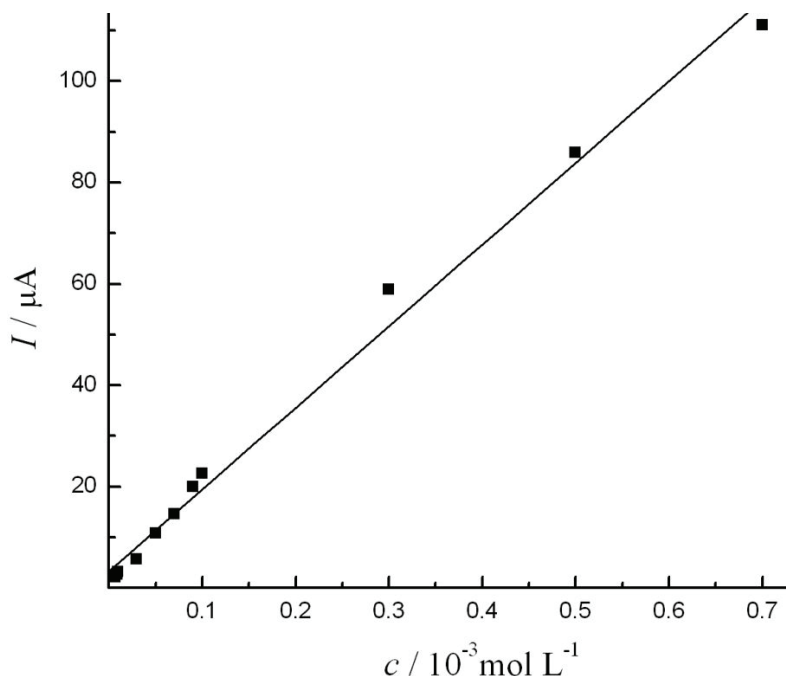


Fig. 6. The relationships between peak current and the CBZ concentration for CBZ oxidation at the [BnMIM]PF₆/CPE in the presence of SDS.

Interferences and reproducibility

The influences of various possible interferents were also studied by analyzing a standard solution of 0.10 mM CBZ in the presence of 0.40 mM SDS. The amount of the foreign species tolerated was that which caused a change in the responding signal of ±5 %. The interferences of some metal ions and organic compounds were examined. The experimental results showed that 1000-fold of the inorganic ions K⁺, Na⁺, Cl⁻, NO₃⁻ and SO₄²⁻, and 100-fold of glucose, saccharose, urea and tartaric acid did not affect the CBZ currents response.

In order to inspect the reproducibility of the electrode, ten sequential determination were made using the same electrode in the presence of 0.40 mM SDS, almost the same results were obtained. A relative standard deviation (RSD) value

of about 3.6 % was obtained by measuring the oxidation peak current for CBZ electrochemical oxidation with CV. The experimental results showed the good reproducibility of the modified electrode.

Sample determination

The proposed determination was successfully applied in the determination of CBZ in commercial pharmaceutical samples. A 1.0 mM CBZ sample was prepared in ethanol solutions, and 0.10 mM CBZ samples were analyzed using the proposed method. An acceptable reproducibility with a relative standard deviation (*RSD*) of 1.40–2.13 % was obtained for six parallel measurements. The determination was performed by standard addition. In addition, the recoveries based on this method were in the range of 101.2–103.7 %. The result indicates that the proposed determination could be used as an effective electrochemical determination of CBZ in commercial tablet samples.

CONCLUSIONS

In this work, the electrochemical behavior of CBZ in the presence of SDS at a [BnMIM]PF₆/CPE was investigated. It was found that the oxidation peak current of CBZ remarkably increased at the [BnMIM]PF₆/CPE in the presence of SDS. The results indicated that the electrochemical responses of CBZ were facilitated by SDS and the ionic liquid [BnMIM]PF₆. The electrochemical kinetic parameters were also determined. The proposed method is simple, rapid and inexpensive, which was demonstrated by its application in the determination of CBZ in commercial samples.

Acknowledgements. This work was financially supported by the Natural Science Foundation of Ningxia (NZ1147) and the Scientific Research Fund of Heilongjiang Provincial Education Department (12511348).

ИЗВОД

ЕЛЕКТРОХЕМИЈСКО ПОНАШАЊЕ И ОДРЕЂИВАЊЕ КАРБАМАЗЕПИНА У ПРИСУСТВУ НАТРИЈУМ-ДОДЕЦИЛСУЛФАТА НА ЕЛЕКТРОДИ ОД УГЉЕНИЧНЕ ПАСТЕ МОДИФИКОВАНОЈ ЈОНСКОМ ТЕЧНОШЋУ

LI-HONG LIU^{1,2}, CHENG-QIAN DUAN^{1,3} и ZUO-NING GAO¹

¹*Key Lab of Energy Sources and Chemical Engineering, College of Chemistry and Chemical Engineering, Ningxia University, Yinchuan 750021, China*, ²*Department of Chemistry, Heihe College, Heihe 164300, China* и ³*Higher Vocational College, Ningxia Medical University, Yinchuan 750004, China*

Испитивано је електрохемијско понашање и могућност електрохемијског одређивања карбамазепина (KBZ) на електроди од угљеничне пасте која је модификована хидрофобном јонском течношћу 1-бензил-3-метилимидазол хексафлуорофосфатом ([BnMIM]PF₆/CPE), у присуству натријум-додецил-сулфата (SDS). Добро дефинисан и осетљив струјни пик оксидације KBZ је запажен на [BnMIM]PF₆/CPE у присуству SDS у фосфатном пufferу вредности pH 6,80. Висина струјног пика у присуству SDS је била знатно већа него када он није био присутан на електроди. Претпостављено је да и SDS и [BnMIM]PF₆ значајно повећавају бр-

зину електрохемијске оксидације KBZ. Кинетички параметри оксидације KBZ на [BnMIM]PF₆/CPE у присуству SDS су одређени и хронокулонометријом и хроноамперометријом. Након оптимизације експерименталних параметара предложена је нова електрохемијска метода одређивања KBZ. Оксидациони пик је зависио линеарно од концетрације KBZ у опсегу од 7,0 μM до 0,7 mM уз границу детекције од 0,98 μM (однос сигнала и шума је 3). Релативна стандардна девијација одређивања у раствору 0,10 mM KBZ у 6 експеримената је износила од 1,40 до 2,13 %. Предложена метода је примењена и на одређивање KBZ у узорку комерцијалних таблета.

(Примљено 20. априла, ревидирано 9. октобра 2011)

REFERENCES

1. I. Bernus, R. G. Dickinson, W. D. Hooper, M. J. Eadie, *Epilepsy Res.* **24** (1996) 163
2. H. Breton, M. Cociglio, F. Bressolle, H. Peyriere, J. P. Blayac, D. Hillaire-Buys, *J. Chromatogr., B* **828** (2005) 80
3. R. G. Kelmann, G. Kuminek, H. F. Teixeira, L. S. Koester, *Chromatographia* **66** (2007) 427
4. M. Zhang, W. John, *Ther. Drug Monit.* **19** (1997) 92
5. F. S. Messiha, *Alcohol* **3** (1986) 135
6. G. F. V. Rooyen, D. Badenhorst, K. J. Swart, H. K. L. Hundt, T. Scanes, A. F. Hundt, *J. Chromatogr., B* **769** (2002) 1
7. J. T. Burke, J. P. Thenot, *J. Chromatogr., B* **340** (1985) 199
8. J. C. Duran-Alvarez, E. Becerril-Bravo, V. S. Castro, B. Jimenez, R. Gibson, *Talanta* **78** (2009) 1159
9. E. Marziali, M. A. Raggi, N. Komarova, E. Kenndler, *Electrophoresis* **23** (2002) 3020
10. J. L. Maggs, M. Pirmohamed, N. R. Kitteringham, B. K. Park, *Drug. Metab. Dispos.* **25** (1997) 275
11. S. H. Lee, M. Li, J. K. Suh, *Anal. Sci.* **19** (2003) 903
12. L. D. L. Pena, A. Gomez-Hens, D. Perez-Bendito, *Fresenius J. Anal. Chem.* **338** (1990) 821
13. Z. Rezaei, B. Hemmateenejad, S. Khahnadideh, M. Gorgin, *Talanta* **65** (2005) 21
14. Z. Q. Zhang, S. Z. Chen, W. L. Huang, F. Xu, *Acta Pharmacol. Sin.* **28** (1993) 312
15. U. Dunnbier, W. Jugelt, K. Hanig, B. Vieth, *Pharmazie* **41** (1986) 567
16. D. J. Turk, S. A. McClintock, W. C. Purdy, *Anal. Lett.* **18** (1985) 2605
17. M. A. García-García, O. Domínguez-Renedo, A. Alonso-Lomillo, M. J. Arcos-Martínez, *Sensor Lett.* **7** (2009) 586
18. S. Atkins, J. M. Sevilla, M. Blazquez, T. Pineda, J. Gonzalez-Rodriguez, *Electroanal.* **22** (2010) 2961
19. A. Veiga, A. Dordio, A. J. Palace Carvalho, D. M. Teixeiraa, J. G. Teixeira, *Anal. Chim Acta* **674** (2010) 182
20. S. S. Kalanur, S. Jaldappagari, S. Balakrishnan, *Electrochim. Acta* **56** (2011) 5295
21. Q. Zhang, W. Wei, G. C. Zhao, *Electroanal.* **20** (2008) 1002
22. M. Galinski, A. Lewandowski, I. Stepniak, *Electrochim. Acta* **51** (2006) 5567
23. D. R. McFarlane, J. Sun, J. Golding, P. Meakin, M. Forsyth, *Electrochim. Acta* **45** (2000) 1271
24. C. A. Brooks, A. P. Doherty, *Electrochim. Commun.* **6** (2004) 867
25. F. Zhao, X. Wu, M. Wang, Y. Liu, L. Gao, S. Dong, *Anal. Chem.* **76** (2004) 4960
26. P. He, H. T. Liu, Z. Y. Li, Y. Liu, X. D. Xu, J. H. Li, *Langmuir* **20** (2004) 10260
27. N. Nishi, S. Imakura, T. Kakiuchi, *Anal. Chem.* **78** (2006) 2726



28. A. Safavi, N. Maleki, O. Moradlou, F. Tajabadi, *Anal. Biochem.* **359** (2006) 224
29. A. Safavi, N. Maleki, F. Tajabadi, *Analyst* **132** (2007) 54
30. Y. Zhang, J. B. Zheng, *Talanta* **77** (2008) 325
31. H. T. Liu, P. He, Z. Y. Li, C. Y. Sun, L. H. Shi, Y. Liu, G. Y. Zhu, J. H. Li, *Electrochem. Commun.* **7** (2005) 1357
32. W. Sun, R. F. Gao, K. Jiao, *J. Phys. Chem. B.* **111** (2007) 4560
33. W. Sun, R. F. Gao, X. Q. Li, D. D. Wang, M. X. Yang, K. Jiao, *Electroanal.* **20** (2008) 1048
34. W. Sun , Y. Z. Li, Y. Y. Duan, K. Jiao, *Biosens. Bioelectron.* **24** (2008) 988
35. J. Peng, Z. N. Gao, *Anal. Bioanal. Chem.* **384** (2006) 1525
36. Z. N. Gao, J. Peng, X. X. Han, *Pol. J. Chem.* **81** (2007) 441
37. X. X. Han, Z. N. Gao, *Acta Pharmacol. Sin.* **42** (2007) 413
38. L. H. Liu, Z. N. Gao, *Chin. J. Pharm. Anal.* **30** (2010) 438
39. R. Vittal, H. Gomathi, K. J. Kim, *Adv. Colloid Interface Sci.* **119** (2006) 55
40. M. Plavsic, D. Krznaric, B. Cosovic, *Electroanal.* **6** (1994) 469
41. P. Manisankar, G. Selvanathan, C. Vedhi, *Talanta* **68** (2006) 686
42. P. P. Xie, X. X. Chen, F. Wang, C. G. Hu, S. S. Hu, *Colloids Surf., B* **48** (2006) 17
43. Q. He, X. P. Dang, C. G.. Hu, S. S. Hu, *Colloids Surf., B* **35** (2004) 93
44. S. S. Hu, Y. Q. Yan, Z. F. Zhao, *Anal. Chim. Acta* **248** (1991) 103
45. H. C. Yi, K. B. Wu, S. S. Hu, D. F. Cui, *Talanta* **55** (2001) 1205
46. S. H. Zhang, K. B. Wu, S. S. Hu, *Talanta* **58** (2002) 747
47. S. S. Hu, K. B. Wu, H. C. Yi, D. F. Cui, *Anal. Chim. Acta* **464** (2002) 209
48. A. E. Kaifer, A. J. Bard, *J. Phys .Chem.* **89** (1985) 4876
49. P. A. Quintela, A. Diaz, A. E. Kaifer, *Langmuir* **4** (1988) 663
50. T. F. Connors, J. F. Rusling, A. Owlia, *Anal. Chem.* **57** (1985) 170
51. J. B. Zheng, X. L. Zhou, *Bioelectrochem.* **70** (2007) 408
52. S. M. Golabi, H. R. Zare, *Electroanal.* **11** (1999) 1293
53. A. J. Bard, L. R. Faulkner, *Electrochemical Methods Fundamentals and Applications*, Wiley, New York, 1980, p. 200
54. Z. Galus, *Fundamentals of Electrochemical Analysis*, Ellis Horwood Press, New York, 1994, p. 398
55. H. H. Wu, *Electrochemistry*, Chemical Industry Press, Beijing, China, 2004, p. 84 (in Chinese).





Mechano-chemical synthesis of stoichiometric nickel and nickel-zinc ferrite powders with Nicolson-Ross analysis of the absorption coefficients

ČEDOMIR JOVALEKIĆ¹, ALEKSANDAR S. NIKOLIĆ^{2*}, MAJA GRUDEN-PAVLOVIĆ²
and MIODRAG B. PAVLOVIĆ³

¹Institute for Multidisciplinary Research, Kneza Višeslava 1a, 11001 Belgrade, Serbia,

²Faculty of Chemistry, Studentski trg 12–16, 11001 Belgrade, Serbia and ³Faculty of Electrical Engineering, B. Kralja Aleksandra 73, 11001 Belgrade, Serbia

(Received 2 March, revised 6 May 2011)

Abstract: The interest in finding new methods for the preparation of nickel ferrite (NiFe_2O_4) and nickel–zinc ferrite ($\text{Ni}_x\text{Zn}_{1-x}\text{Fe}_2\text{O}_4$) powders has recently increased, because the physical and chemical properties of these soft magnetic materials depend strongly on the preparation conditions. In this study, powder samples of ferrites were obtained by: 1) a classic sintering procedure ($\text{Ni}_x\text{Zn}_{1-x}\text{Fe}_2\text{O}_4$, $x = 0.9$) and 2) planetary mill synthesis (both NiFe_2O_4 and the $\text{Ni}_x\text{Zn}_{1-x}\text{Fe}_2\text{O}_4$). The mechano-chemical reaction leading to the formation of the spinel phase of $\text{Ni}_x\text{Zn}_{1-x}\text{Fe}_2\text{O}_4$ ($x = 1$ or 0.9) was monitored by scanning electron microscopy (SEM), transmission electron microscopy (TEM), and X-ray diffraction (XRD) analysis. The values of the real and imaginary parts of the permittivity and permeability were measured for the obtained nickel and nickel–zinc ferrite samples in the 7–12 GHz frequency range. Based on the obtained results, the electromagnetic radiation (EMR) absorption coefficients were calculated for all three types of sample. It was concluded that the method of preparation and the final particle size influence the EMR absorption coefficient of nickel and nickel–zinc ferrites.

Keywords: ferrites; nanocrystalline materials; mechano-chemistry; radar absorbers.

INTRODUCTION

It is well known that the properties of ferrite materials strongly depend on the preparation conditions. Consequently, different methods for the preparation of ferrite powders are described in the literature.^{1–3} By choosing a method that leads to a reduction of the particle size, the magnetic properties (such as coercive

*Corresponding author. E-mail: asn@chem.bg.ac.rs
doi: 10.2298/JSC110302186J

field, Curie temperature, saturation magnetization and absorption coefficients) may change significantly in comparison with those of the bulk material.

The basic structure of a spinel ferrite is $A_xB_{1-x}Fe_2O_4$, where A and B are divalent metal ions (*e.g.*, Mg, Mn, Ni, Zn, *etc.*). In a unit cell of the spinel lattice, there are eight tetrahedral and sixteen octahedral sites occupied by A, B and Fe^{3+} , while the oxygen anions are arranged in a cubic close-packed structure. Site occupancy may range from the normal spinel structure, in which the A and B cations occupy the tetrahedral sites and Fe^{3+} the octahedral ones, to the inverse spinel, in which half the Fe^{3+} cations occupy the tetrahedral sites, and three (A, B and Fe^{3+}) cations occupy the octahedral sites. In general, site occupancy in $NiFe_2O_4$ and $Ni_xZn_{1-x}Fe_2O_4$ may be expressed by rewriting its generic formula as $(Ni_{1-\lambda}Fe_\lambda)[NI_\lambda Fe_{1-\lambda}]O_4$ and $(Ni_xZn_{1-x})_{1-\lambda}Fe_\lambda][(Ni_xZn_{1-x})_\lambda Fe_{1-\lambda}]O_4$, where the parentheses and square brackets denote the tetrahedral and octahedral sites, respectively. λ represents the so-called degree of inversion, defined as the fraction of tetrahedral sites occupied by Fe^{3+} .

Interest in nanoparticle materials permanently increases because of the significant influence of large surface/volume ratio of nanoparticles on their physical properties, compared to their bulk counterpart.⁴ Recent investigations in the field of mechano-chemistry have resulted in the mechano-synthesis of stoichiometric and chemically pure nanoscale spinel ferrites,^{5–12} which were undertaken because this class of materials have significant permeability values over very narrow frequency ranges.^{13,14} In most cases, the complete formation of spinel ferrites was obtained only after milling followed by sintering, *i.e.*, by employing two processing steps. It was noted that the combined mechano-chemical-thermal treatment yielded a well-ordered spinel phase in ferrites at lower annealing temperatures and shorter durations, than those required for conventional ceramic methods.^{15,16} Herein, an improvement of the method in order to obtain ferrites with better properties, which can be employed in microwave electronics, is presented.

The request that an absorber of electromagnetic radiation (EMR) needs to be efficient can be satisfied by material with special properties. The material has to not only attenuate electromagnetic (EM) waves penetrating its volume, but also moreover present a good match to the incident waves at the air/material interface. Good absorption is provided with ϵ_r' , μ_r' , $\tan \delta_\mu$ and $\tan \delta_\epsilon$ as large as possible, while good matching at the interface requires $\mu_r' = \epsilon_r'$ and $\tan \delta_\mu = \tan \delta_\epsilon$.¹⁷ The present paper describes a technique for preparing nickel ferrite ($NiFe_2O_4$) and nickel-zinc ferrite ($Ni_{0.9}Zn_{0.1}Fe_2O_4$), based on planetary mill synthesis, which increases the absorption factor of ferrites obtained by the classical route, in the frequency range 7–12 GHz.^{18–21}

EXPERIMENTAL

Powder samples of NiFe_2O_4 and $\text{Ni}_{0.9}\text{Zn}_{0.1}\text{Fe}_2\text{O}_4$ soft ferrites were synthesized by classic sintering (sample **1** ($\text{Ni}_{0.9}\text{Zn}_{0.1}\text{Fe}_2\text{O}_4$), made in Ei Ferrite, Belgrade) and by planetary mill synthesis (sample **2** (NiFe_2O_4) and sample **3** ($\text{Ni}_{0.9}\text{Zn}_{0.1}\text{Fe}_2\text{O}_4$)).

In the classic sintering process, thermal diffusion occurs between NiO crystals (1–2 μm in size) and the hematite, and the final size of particles should be larger than the size of crystals in the starting components. The average particle size obtained by the conventional sintering method (sample **1**) was several microns.

Mixtures of crystalline powders of NiO and Fe_2O_3 for sample **2**, and NiO , ZnO and Fe_2O_3 (purity 99 %) for sample **3**, were used as the starting materials for the planetary mill syntheses. Mechano-chemical treatment was performed in a planetary ball mill (Fritsch Pulverisette 5). A hardened-steel vial (500 cm^3 volume) filled with 286 hardened-steel balls (8 mm in diameter) was used as the milling medium. The mass of the powders was 30 g and the balls-to-powder ratio was 20:1. Milling was performed for 50 h, in air, without any additives.

Sizes and shapes of polycrystalline powder particle of samples **2** and **3** were examined by scanning electron microscopy (SEM) (JEOL JSM-5200) and by combined field-emission (scanning) transmission electron microscopy (TEM) (the grid was dried overnight at room temperature and observed with a FEI Tecnai biotwin (120 kV)) and by X-ray diffraction (XRD) analysis. Prior to the SEM surveys, the particles were gold-sputtered in a JFC 1100 ionic sputter coater. Prior to the TEM investigations, the powders were crushed in a mortar, dispersed in ethanol and fixed on a copper-supported carbon film. The XRD analysis of samples **2** and **3** was performed on a Philips PW 1730 automatic diffractometer with CuK_α graphite-monochrome radiation ($\lambda = 0.1542 \text{ nm}$).

Values of the real and imaginary parts of the permittivity and permeability were measured for all three samples in the 7–12 GHz frequency range. Samples were prepared by pressing the powder into aluminum holders (27 mm×27 mm) without thermal treatment. The measurements were performed using a HP 8510 network analyzer system with simple-to-fabricate test fixtures, with the capability to measure simultaneously both μ_r and ϵ_r at up to 400 frequency points. Based on the values obtained for μ_r and ϵ_r , the EMR absorption coefficient was calculated.

RESULTS AND DISCUSSION

SEM Micrographs of powder samples of NiFe_2O_4 (sample **2**) and $\text{Ni}_{0.9}\text{Zn}_{0.1}\text{Fe}_2\text{O}_4$ (sample **3**) synthesized by the planetary mill procedure are shown in Fig. 1. It can be noticed that the nanoscale crystallites tend to agglomerate, because of the dipolar field of each crystallite. TEM Micrographs of samples **2** and **3**, presented in Fig. 2, show that the nanoscale crystallites form particles of average size 10–15 nm, which is consistent with the average crystallite size determined by XRD analysis. The shape of the majority of the crystallites appears to be spherical. Agglomerated crystallites form particles with sizes mostly up to 50 nm.

The X-ray diffractograms of samples **2** and **3** are presented in Fig. 3. They show that no peaks of the starting compounds were present after 50 h of milling, only the full spectrum of the characteristic peaks of NiFe_2O_4 in sample **2** and those of $\text{Ni}_{0.9}\text{Zn}_{0.1}\text{Fe}_2\text{O}_4$ in sample **3**. The calculated lattice parameters were

0.83369 ± 10^{-5} for NiFe_2O_4 and 0.83401 ± 10^{-5} nm for $\text{Ni}_{0.9}\text{Zn}_{0.1}\text{Fe}_2\text{O}_4$, which are consistent with the values obtained by other authors (ICPD 10-325; ICPD 22-1012).

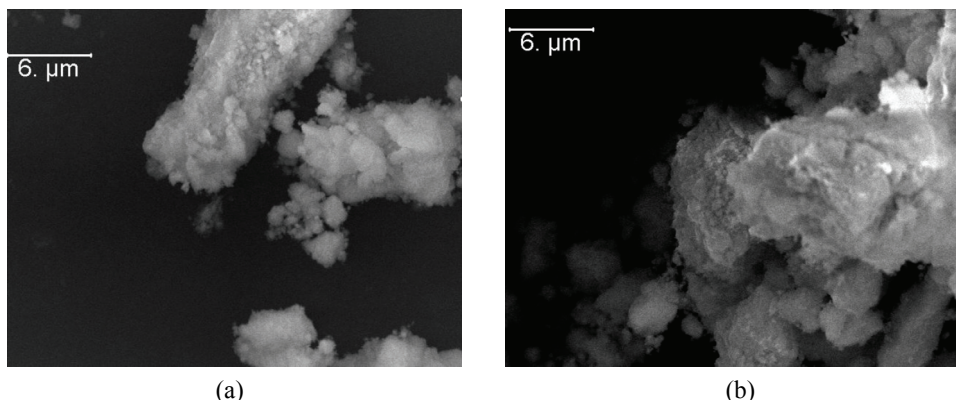


Fig. 1. SEM Images of the nanocrystalline mechano-synthesized samples after 50 h of milling:
a) sample 2 (NiFe_2O_4) and b) sample 3 ($\text{Ni}_{0.9}\text{Zn}_{0.1}\text{Fe}_2\text{O}_4$).

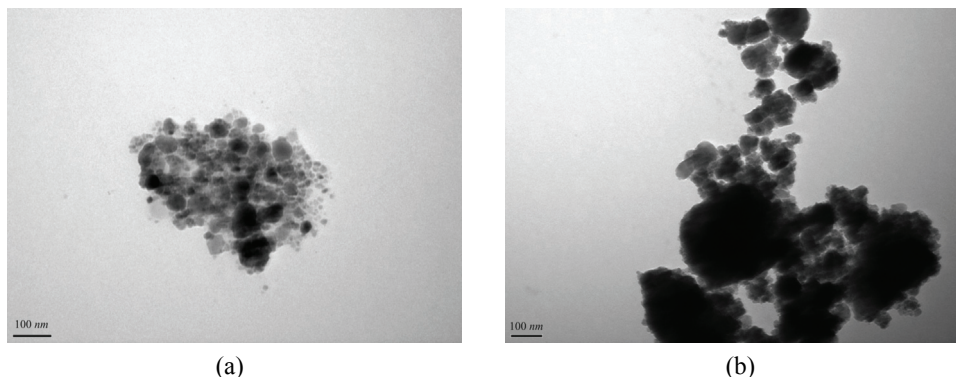


Fig. 2. TEM Images of the nanocrystalline mechano-synthesized samples after 50 h of milling: a) sample 2 (NiFe_2O_4) and b) sample 3 ($\text{Ni}_{0.9}\text{Zn}_{0.1}\text{Fe}_2\text{O}_4$).

Crystallite sizes of the powders were calculated from the XRD data by means of the Scherrer Equation:²²

$$S = \frac{0.9\lambda}{B \cos \theta_B} \quad (1)$$

where S is the crystallite grain size, λ is the wavelength of the X-ray source, θ_B is the Bragg angle of the considered XRD peaks, and B represents the full width at half maximum (FWHM) line broadening obtained as follows:

$$B^2 = B_m^2 - B_s^2 \quad (2)$$

where B_m is the FWHM line broadening of the material and B_s represents the FWHM line broadening of the internal standard (α -Al₂O₃). The resulting values of crystallite size obtained from the strongest (111) reflections were in the range of 10–15 nm for NiFe₂O₄ and Ni_{0.9}Zn_{0.1}Fe₂O₄.

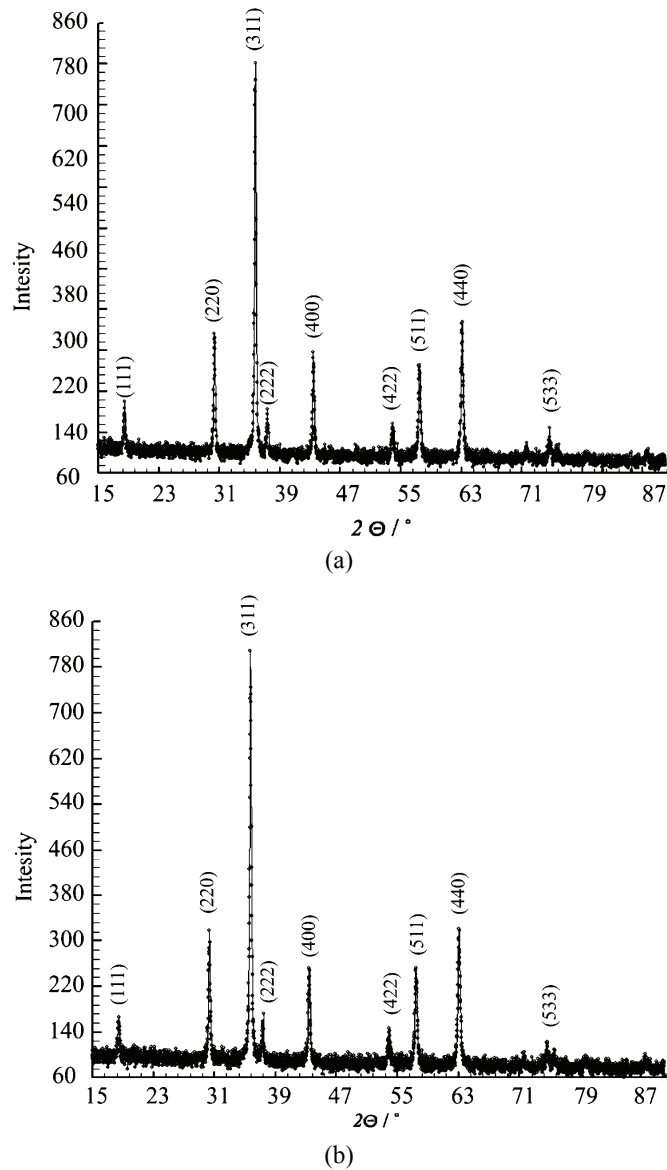


Fig. 3. XRD Patterns of the mechano-synthesized samples after 50 h of milling:
a) sample 2 (NiFe₂O₄) and b) sample 3 (Ni_{0.9}Zn_{0.1}Fe₂O₄).

The complex permittivity and permeability values of all ferrite samples were obtained from measurements conducted using an HP 8510 Network Analyzer system. From the obtained frequency dependence of the permittivity and permeability, the EMR attenuation coefficient α was calculated using the formula:

$$\alpha = 2\pi f \sqrt{\mu_0 \epsilon_0} \sqrt{\epsilon_r' \mu_r' / 2} \times \\ \times \sqrt{(\tan \delta_\mu \tan \delta_\epsilon - 1) + (1 + \tan^2 \delta_\mu \tan^2 \delta_\epsilon + \tan^2 \delta_\mu + \tan^2 \delta_\epsilon)^{1/2}} \quad (3)$$

where the loss tangents are defined by $\tan \delta_\mu = \mu_r''/\mu_r'$ and $\tan \delta_\epsilon = \epsilon_r''/\epsilon_r'$ (μ_r' and ϵ_r' being the real parts, and μ_r'' and ϵ_r'' the imaginary parts of the permeability and permittivity, respectively).

The real and complex parts of the permittivity exhibited frequency dependency in all three samples, but without any marked maximum values; hence all the examined materials could be used as wide-range absorbents. Samples **1** and **3** exhibited higher values of the real part of the permittivity than those of sample **2**. Conversely, sample **2** exhibited higher values of the imaginary part of the permittivity than the other two sample types (Fig. 4). The real part of the permeability was the highest in sample **3**, and the lowest in sample **2**. Sample **1** and sample **2** exhibited higher values of the imaginary part of permeability than those of sample **3** (Fig. 5).

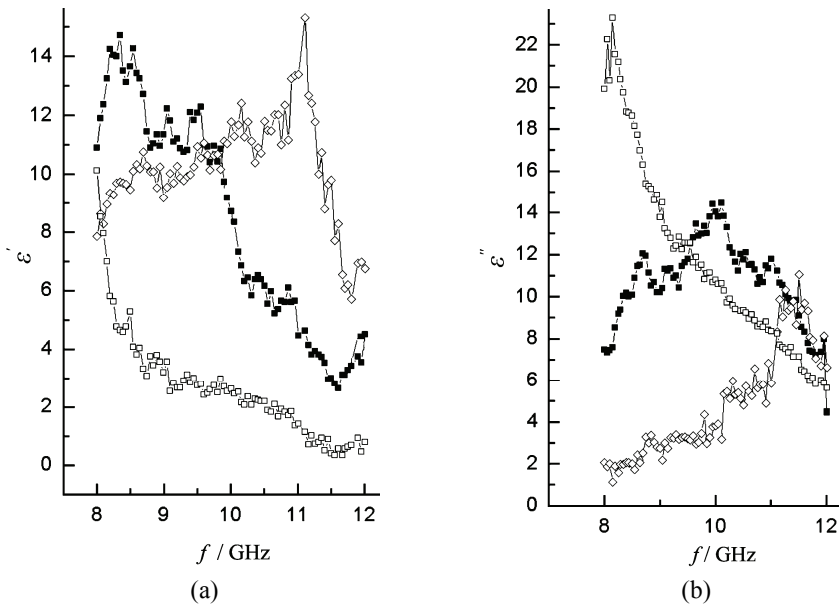


Fig. 4. Values of the real, ϵ_r' (a), and the imaginary part, ϵ_r'' (b), of permittivity for the ferrite samples: \diamond – $\text{Ni}_{0.1}\text{Zn}_{0.9}\text{Fe}_2\text{O}_4$ (sample **1**) obtained by the standard sintering route, \square – NiFe_2O_4 (sample **2**) and \blacksquare – $\text{Ni}_{0.1}\text{Zn}_{0.9}\text{Fe}_2\text{O}_4$ (sample **3**) obtained mechano-chemically.

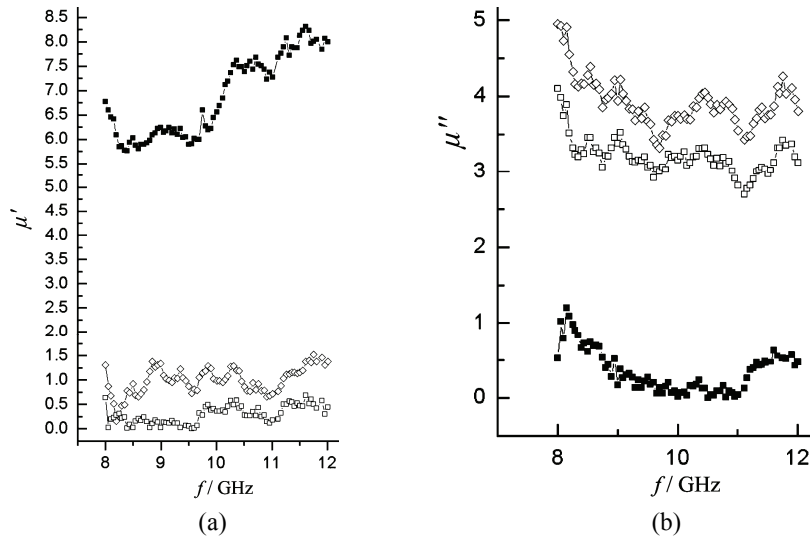


Fig. 5. Values of the real, μ'_r (a), and the imaginary part, μ''_r (b), of permeability for ferrite samples: \diamond – $\text{Ni}_{0.1}\text{Zn}_{0.9}\text{Fe}_2\text{O}_4$ (sample 1) obtained by the standard sintering route, \square – NiFe_2O_4 (sample 2) and \blacksquare – $\text{Ni}_{0.1}\text{Zn}_{0.9}\text{Fe}_2\text{O}_4$ (sample 3) obtained mechano-chemically.

The values of the EMR attenuation coefficient (α) calculated from expression (3) are presented in Fig. 6, in linear and log scales. It may be concluded that the EMR attenuation coefficient depended more on the method of preparation,

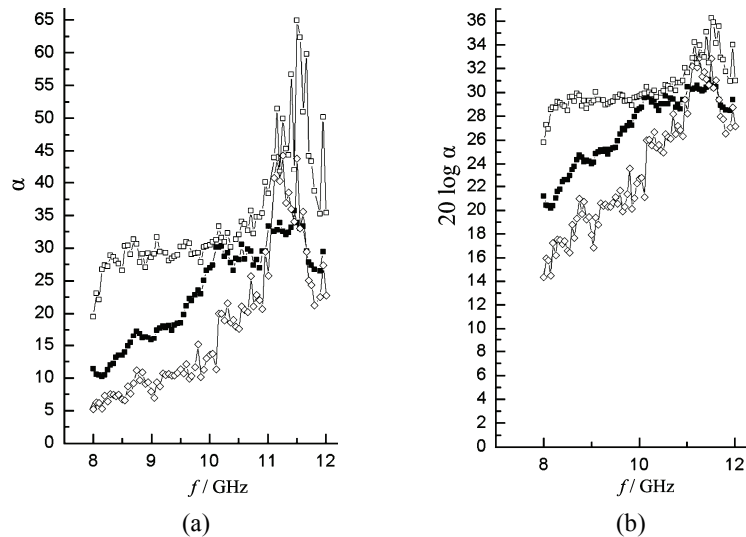


Fig. 6. Values of EMR attenuation coefficient (α) for \diamond – $\text{Ni}_{0.1}\text{Zn}_{0.9}\text{Fe}_2\text{O}_4$ (sample 1) obtained by the standard sintering route, \square – NiFe_2O_4 (sample 2) and \blacksquare – $\text{Ni}_{0.1}\text{Zn}_{0.9}\text{Fe}_2\text{O}_4$ (sample 3), presented in a) linear and b) logarithmic scale.

i.e., on powder particle morphology than on the chemical content of the samples. It can be seen in Figure 6b that the change of attenuation coefficient for sample **2** was within 30 dB, for sample **3** between 20 and 30 dB, and for sample **1** between 10 and 30 dB. The higher values of the EMR attenuation coefficient observed for samples **2** and **3**, obtained by the mechano-chemical process, are the result of the extremely high specific granule surface (granule-weight to granule-surface ratio), as well as of the large number of dislocations and impurities in the crystal structure concentrated at the granule surfaces, which is typical for powders obtained mechano-chemically. Larger granules present in sample **1** resulted in lower values of the EMR attenuation coefficient.

CONCLUSION

Based on the obtained results, it can be concluded that the nickel ferrite (NiFe_2O_4) produced by the mechano-chemical process gave better results with respect to EMR attenuation than the nickel–zinc ferrite obtained by both the classic and mechano-chemical sintering process. For the mechano-chemically prepared nickel ferrite samples, the EMR attenuation coefficient showed a practically constant value (within a 30 dB margin) over the whole frequency range (7–12 GHz), which places these soft ferrites among the most favorable wide-range microwave absorbents. The configuration of the soft ferrites obtained by this method is a single-layer one, as opposed to the complex multi-layer configurations applied hitherto. Final judgment on the applicability of these materials for wide-range radar absorbers demands an extension of this investigation toward higher frequencies.

Acknowledgements. The Ministry of Education and Science of the Republic of Serbia supported this work.

ИЗВОД

МЕХАНОХЕМИЈСКА СИНТЕЗА НИКАЛ И НИКАЛ–ЦИНК ФЕРИТНИХ ПРАХОВА СА
NICOLSON–ROSS АНАЛИЗОМ АБСОРПЦИОНИХ КОЕФИЦИЈЕНТА

ЧЕДОМИР ЈОВАЛЕКИЋ¹, АЛЕКСАНДАР С. НИКОЛИЋ², МАЈА ГРУДЕН-ПАВЛОВИЋ²
и МИОДРАГ Б. ПАВЛОВИЋ³

¹Институут за мултидисциплинарна истраживања, Кнеза Вишеслава 1а, 11001 Београд, ²Хемијски
факултет, Студентски трг 12–16, 11001 Београд и ³Електротехнички факултет,
Б. Краља Александра 73, 11001 Београд

У новије време повећан је интерес за проналажење нових метода за синтезу никал-ферита (NiFe_2O_4) и никал–цинк-феритних ($\text{Ni}_x\text{Zn}_{1-x}\text{Fe}_2\text{O}_4$) прахова, због чињенице да физичка и хемијска својства ових „меких“ магнетних материјала у многоме зависе од услова припреме. Добијени феритни прахови, описани у овом раду, синтетисани су: 1) класичном процедуром синтеровања ($\text{Ni}_x\text{Zn}_{1-x}\text{Fe}_2\text{O}_4$, $x = 0,9$ или 2) синтезом у планетарном млину (NiFe_2O_4 и $\text{Ni}_x\text{Zn}_{1-x}\text{Fe}_2\text{O}_4$). Просечна величина честица добијених првом методом износи 3–5 μm, док друга метода даје честице величине 10–12 nm. Карактеризација узорака праћена је скенирајућом електронском микроскопијом (SEM), трансмисионом електронском микро-

скопијом (TEM), као и дифракционом анализом X-зрацима (XRD). Реални и имагинарни делови коефицијената пермитивности и пермеабилности су мерени на добијеним узорцима никал и никал–цинк-ферита у фреквентном опсегу 7–12 GHz . На основу добијених резултата, израчунати су EMR апсорпциони коефицијенти за све добијене узорке. Закључено је да је начин припреме, као и добијена величина честица, утичу на EMR апсорпционе коефицијенте никал и никал–цинк-ферита.

(Примљено 2. марта, ревидирано 6. маја 2011)

REFERENCES

1. W. C. Kim, S. J. Kim, C. S. Kim, *J. Appl. Phys.* **91** (2002) 7607
2. C. Huang, E. Matijevic, *Solid State Ionics* **84** (1996) 249
3. A. Anwar, T. Fujiwara, S. Song, M. Yoshimura, *Solid State Ionics* **151** (2002) 419
4. F. Vetrone, J.-C. Boyer, J. A. Capobianco, A. Speghini, M. Bettinelli, *Nanotechnology* **15** (2004) 75
5. E. Manova, B. Kunev, D. Paneva, I. Mitov, L. Petrov, C. Estournes, C. D. Orleans, J.-L. Rehspringer, M. Kurmoo, *Chem. Mater.* **16** (2004) 5689
6. M. Muroi, R. Street, P. McCormick, G. Amighian, *J. Phys. Rev. B* **63** (2001) 184414
7. P. Druska, U. Steinike, V. Šepelak, *J. Solid State Chem.* **13** (1999) 146
8. V. Šepelak, S. Wissmann, K. D. Becker, *J. Magn. Magn. Mater.* **203** (1999) 135
9. V. G. Harris, D. J. Fatemi, J. O. Cross, E. E. Carpenter, V. M. Browning, J. P. Kirkland, A. Mohan, G. J. Long, *J. Appl. Phys.* **94** (2003) 496
10. R. N. Bhowmik, R. Ranganathan, *J. Mater. Sci.* **37** (2002) 4391
11. N. Guigue-Millot, S. Begin-Colin, Y. Champion, M. J. Hytch, G. Le Caer, P. Perriat, *J. Solid State Chem.* **170** (2003) 30
12. V. Šepelak, M. Menzel, I. Bergmann, M. Wiebcke, F. Krumeich, K. D. Becker, *J. Magn. Magn. Mater.* **1616** (2004) 272
13. H. Severin, P. J. Stoll, *Z. Angew. Phys.* **23** (1967) 209
14. B. Heck, *Magnetic Materials and their Applications*, Butterworths, London, UK, 1974
15. H. M. Yang, X. C. Zhang, A. D. Tang, G. Z. Qiu, *Chem. Lett.* **33** (2004) 826
16. G. Ennas, G. Marongiu, S. Marras, G. Piccaluga, *J. Nanopart. Res.* **6** (2004) 99
17. I. Nicolaescu, *J. Optoelectron. Adv. Mater.* **8** (2006) 333
18. Č. Jovalekić, M. Zdujić, A. Radaković, M. Mitić, *Mat. Lett.* **24** (1995) 365
19. M. Zdujić, Č. Jovalekić, Lj. Karanović, M. Mitić, D. Poleti, D. Skala, *Mater. Sci. Eng., A* **245** (1998) 109
20. M. Zdujić, Č. Jovalekić, Lj. Karanović, M. Mitić, *Mater. Sci. Eng., A* **266** (1999) 204
21. A. S. Nikolić, P. Osmoković, D. Manojlović, N. Šojić, M. B. Pavlović, *J. Optoelectron. Adv. Mater.* **10** (2008) 1390
22. B. E. Warren, *X-Ray Diffraction*, Addison-Wesley, Reading, MA, USA, 1969.





Volumetric, viscometric and optical study of molecular interactions in binary mixtures of diethyl malonate with ketones at 303.15, 308.15 and 313.15 K

MANAPRAGADA V. RATHNAM^{1*}, SUDHIR MOHITE¹
and MANAPRAGADA S. KUMAR²

¹Physical Chemistry Research Laboratory, B. N. Bandodkar College of Science, Thane – 400 601, India and ²Department of Chemistry, Zulal Bhilajirao Patil College, Deopur, Dhule – 424 002, India

(Received 12 July, revised 22 September 2011)

Abstract: Density, ρ , viscosity, η , and refractive index, n_D , were measured for binary mixtures of diethyl malonate with ketones (acetophenone, cyclopentanone, cyclohexanone and 3-pantanone) at temperatures of 303.15, 308.15 and 313.15 K over the entire composition range. The excess volume, V^E , deviation in viscosity, $\Delta\eta$, excess Gibb's free energy of activation for viscous flow, ΔG^E , and deviation in molar refraction, ΔR , were determined from the experimental data and the computed results were fitted to the Redlich–Kister polynomial equation. The values of V^E , $\Delta\eta$, ΔG^E , and ΔR were plotted against the mole fraction of diethyl malonate. The observed positive and negative values of the excess parameters for all the studied binary mixtures were explained based on the intermolecular interactions present in these mixtures. Furthermore, different empirical relations were used to correlate the binary mixture viscosities and refractive indices.

Keywords: density; diethyl malonate; ketones; molecular interactions; excess properties.

INTRODUCTION

Liquid–liquid mixtures due to their unusual behavior have attracted considerable attention.¹ The physico–chemical properties *viz.* density, viscosity, refractive index or speed of sound and the thermodynamic behavior of binary mixtures have been studied for various reasons. One of the most important of which is that these properties provide information about molecular interactions. Many engineering problems require quantitative data of the viscosity and density of liquid mixtures. Such data find extensive application in solution theory and

*Corresponding author. E-mail: mvrathnam58@rediffmail.com
doi: 10.2298/JSC110712198R

molecular dynamics.² Furthermore, these properties are used for the interpretation of data obtained from biochemical and kinetic studies.³

Diethyl malonate, a colorless, fragrant liquid boiling at 199 °C, is prepared by the reaction of monochloroacetic acid with methanol and carbon monoxide. It is used to synthesize barbiturates and vitamins B1 and B6 because of its typical structure consisting of two adjacent carbonyl groups. In the pharmaceutical industry, diethyl malonate is used for the synthesis of pharmaceuticals such as chloroquine. It can also be used in the pesticides, paint, spice industries, etc.

In general, ketoesters are highly polar and are known to self-associate through dipole–dipole interactions.⁴ Ketones are used as solvents for insecticides, fungicides and as intermediates in the synthesis of pharmaceuticals. In particular, acetophenone is most commonly used as a flavoring agent in many cherry-flavored sweets, drinks and in chewing gum.

Thermodynamic and transport properties of binary liquid mixtures involving various types of organic solvents are replete in the literature. However, only a few studies on ketones with esters are available.^{5–10} Pan *et al.*¹¹ studied the density and viscosity for binary mixtures containing diethyl oxalate, and dibutyl phthalate with normal alkanols at 303.15 K. Rodriguez *et al.*¹² reported the density and refractive index of and the speed of sound in binary mixtures (diethyl carbonate + alcohols) at several temperatures. Nayak *et al.*¹³ studied the density, viscosity and refractive index of and the speed of sound in diethyl oxalate, diethyl phthalate and dioctyl phthalate at 298.15, 303.15 and 308.15 K. Moreover, Baragi *et al.*¹⁴ studied the density, viscosity and refractive index of and speed of sound in binary mixtures of 1,4-dioxane with diethyl malonate. Likewise, thermodynamic and acoustic properties containing diethyl malonate with alcohols or hydrocarbons have been reported in the literature.^{15–19} In continuation of our research program involving the study of excess properties^{20–22} of binary liquid mixtures containing various types of esters, in this manuscript the experimental measurements of density, ρ , viscosity, η , and refractive index, n_D , for binary mixtures of diethyl malonate with ketones (acetophenone, cyclopentanone, cyclohexanone and 3-pentanone) at 303.15, 308.15 and 313.15 K and at atmospheric pressure are reported. The experimental values of ρ , η and n_D were used to calculate the excess volume, V^E , the deviation in viscosity, $\Delta\eta$, the excess Gibb's free energy of activation for viscous flow, ΔG^E , and the deviation in molar refraction, ΔR . These results were used to discuss the nature of the interactions between the unlike molecules in terms of dipole–dipole interactions and dispersion forces. The refractive index data was also predicted using some of the refractive index models of mixing rules and the results are discussed in terms of the average percentage deviation (APD) and the standard percentage deviation, $\sigma(\%)$. The agreement between the experimental and theoretical values was found to be satisfactory. Similarly, the McAllister four-body interaction model, the

Lobe and Jouyban–Acree model were used to correlate the viscosities of the binary liquid mixtures with the mole fraction.

EXPERIMENTAL

Materials

Diethyl malonate, acetophenone (Sigma-Aldrich) and cyclopentanone, cyclohexanone and 3-pentanone (all Merck) with mass fraction purities greater than 99.0 % were used without further purification. The purity of the solvents was ascertained by gas liquid chromatography (GLC) and the analysis indicated a mol % purity of > 99.0 %. The experimental results of density, viscosity and refractive index of the pure liquids at 303.15 K are compared with available literature data in Table I-S of the Supplementary material.

Methods

Binary mixtures were prepared by mass in airtight-stoppered glass bottles. The masses were recorded on a digital electronic balance (Mettler AE 240, Switzerland) to an uncertainty of ± 0.0001 g. To prevent the samples from preferential evaporation, the mixtures were prepared by transferring aliquots *via* syringes into stoppered bottles. The uncertainty in mole fraction was thus estimated to be less than ± 0.0001 . A set of nine binary mixtures was prepared for each system, and their physical properties were measured at the respective composition of the mole fraction varying from 0.1 to 0.9 in steps of 0.1.

The densities of the pure liquids and their binary mixtures were determined with a portable density meter (DMA 35 Anton Paar). The instrument was calibrated frequently before the start of the actual experiments using deionized water and dry air according to established standard procedures. The instrument has a temperature sensor that measures the sample temperature right at the measuring cell. The densities of all the binary mixtures were measured after achieving thermal equilibrium with successive increments of 5 K for the temperature range from 303.15 to 313.15 K. All measurements for each sample were made in triplicate; the average values are reported and considered for further analysis. The reproducibility of the density measurements was ± 0.0005 g cm⁻³ and the experimental uncertainty in the density measurements was approximately $\pm 3 \times 10^{-4}$.

The viscosities of the pure liquids and their mixtures were determined at atmospheric pressure and at temperatures 303.15, 308.15 and 313.15 K using an Ubbelhode viscometer. The viscometer bulb had a capacity of about 15 ml and the capillary tube had a length of about 90 mm with an internal diameter of 0.5 mm. The thoroughly cleaned and perfectly dried viscometer was filled with the sample liquid by fitting the viscometer to about 30° from the vertical and its limbs were closed with Teflon® caps to avoid the evaporation. The viscometer was kept in a transparent-walled bath with a thermal stability of ± 0.01 K for about 20 min to obtain thermal equilibrium. An electronic digital stopwatch with an uncertainty of ± 0.01 s was used for flow time measurements. At least three repetitions of each mixture reproducible to ± 0.05 s were obtained, and the results were averaged. The viscosity was calculated from measured efflux time, *t*, using the following relation:

$$\eta = \rho (At - B/t) \quad (1)$$

where ρ is the density and *A* and *B* are characteristic constants of the viscometer, which were determined by taking water and benzene as calibration liquids. The uncertainty in the thus estimated viscosity was found to be ± 0.008 mPa s.

Refractive indices were measured using a refractometer (RM40, Mettler Toledo, Switzerland) with an uncertainty of ± 0.0001 . The instrument had a built-in solid state thermostat



temperature range (5 to 100 °C) with an uncertainty of ± 0.1 °C. The instrument calibration was realized with doubly distilled water. The average of three measurements was taken for each sample.

RESULTS AND DISCUSSION

Experimental data and excess or deviation values

The densities, ρ , viscosities, η , and refractive indices n_D of the mixtures at 303.15, 308.15 and 313.15 K are listed as a function of mole fraction in Table II-S of the Supplementary material.

The density values were used to calculate the excess molar volumes, V^E , using the following relation:

$$V^E = (x_1 M_1 + x_2 M_2)/\rho - (x_1 M_1/\rho_1 + x_2 M_2/\rho_2) \quad (2)$$

where ρ is the density of the mixture and x_1 , M_1 and ρ_1 , and x_2 , M_2 and ρ_2 , are the mole fraction, molar mass, and density of pure components 1 and 2, respectively. The calculated excess molar volumes are included in Table II-S and graphically represented in Fig 1.

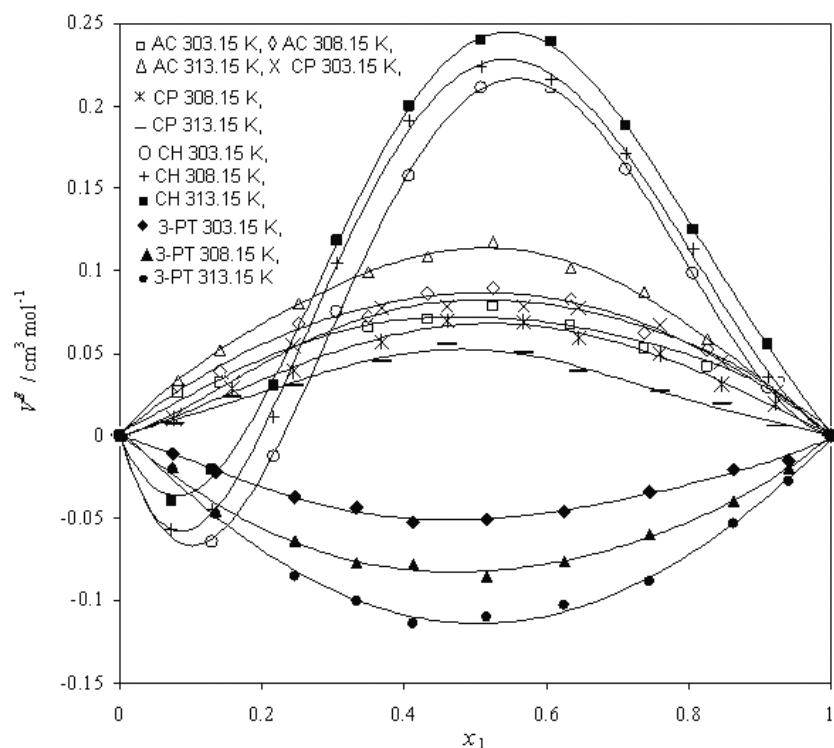


Fig. 1. Excess volume, V^E , as a function of diethyl malonate mole fraction, x_1 + acetophenone (AC); + cyclopentanone (CP); + cyclohexanone (CH); + 3-pentanone (3-PT).

The deviations in the viscosity, $\Delta\eta$, were calculated using the relation:

$$\Delta\eta = \eta - (x_1 \eta_1 + x_2 \eta_2) \quad (3)$$

where η is the absolute viscosity of the mixture, and η_1 and η_2 are the viscosities of the pure components 1 and 2, respectively. The $\Delta\eta$ data are graphically represented in Fig. 2.

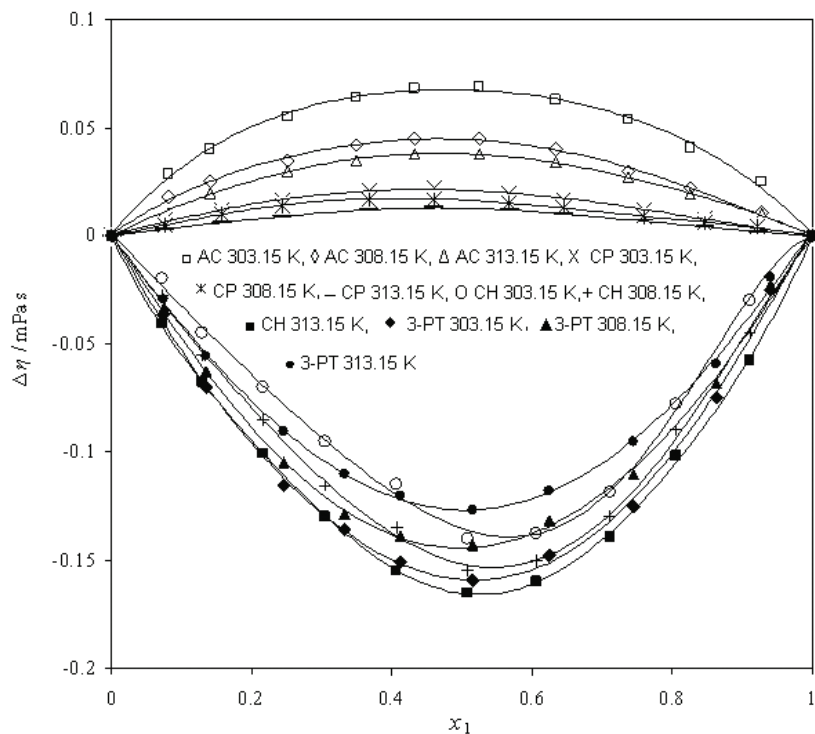


Fig. 2. Deviation in viscosity, $\Delta\eta$, as a function of diethyl malonate mole fraction, x_1 + acetophenone (AC); + cyclopentanone (CP); + cyclohexanone (CH); + 3-pentanone (3-PT).

The excess Gibb's energy of activation, ΔG^E , of viscous flow was obtained using the following relation:

$$\Delta G^E = RT(\ln(\eta V) - x_1 \ln(\eta_1 V_1) - x_2 \ln(\eta_2 V_2)) \quad (4)$$

where V is the molar volume of the mixture and V_1 and V_2 are the molar volumes of the pure components 1 and 2, respectively. The ΔG^E data are graphically represented in Fig. 3.

The refractive index values, n , were used to calculate the Lorentz–Lorentz molar refraction,²³ and deviations in the molar refraction were calculated as:

$$\Delta R = R_m - (x_1 R_1 + x_2 R_2) \quad (5)$$

where R_1 and R_2 are the molar refractivities of pure components 1 and 2, respectively, and R_m is the molar refractivity of the mixtures calculated by using the relation:

$$R_m = ((n^2 - 1) / (n^2 + 2)) / ((x_1 M_1 + x_2 M_2) / \rho) \quad (6)$$

The so-obtained ΔR data are graphically represented in Fig. 4.

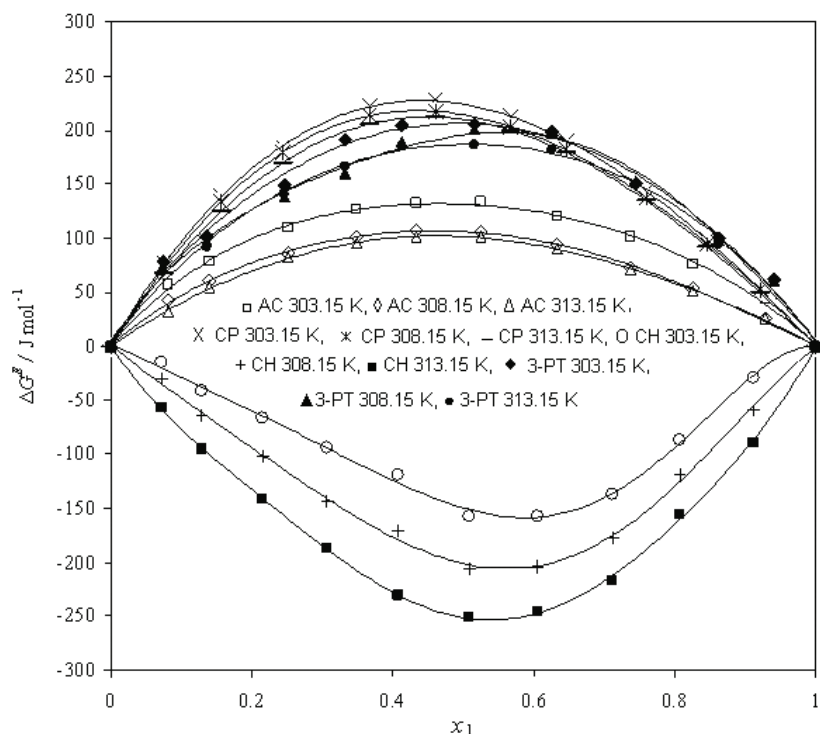


Fig. 3. Excess Gibbs Energy, ΔG^E , as a function of diethyl malonate mole fraction, x_1 + acetophenone (AC); + cyclopentanone (CP); + cyclohexanone (CH); + 3-pentanone (3-PT).

All of the quantities (V^E , $\Delta\eta$, ΔG^E and ΔR) were fitted to the Redlich-Kister²⁴ polynomial equation by the method of least squares to derive the binary coefficients:

$$\Delta y = x_1(1 - x_1) \sum_{i=0}^n A_i (2x_1 - 1)^i \quad (7)$$

The variation in standard deviation (σ) was calculated using the relation:

$$\sigma(y) = (\sum (y_{\text{obs}} - y_{\text{cal}})^2 / (n - m))^{1/2} \quad (8)$$

where n represents the number of data points and m is the number of coefficients. The calculated values of coefficients along with the standard deviations (σ) are given in Table I.

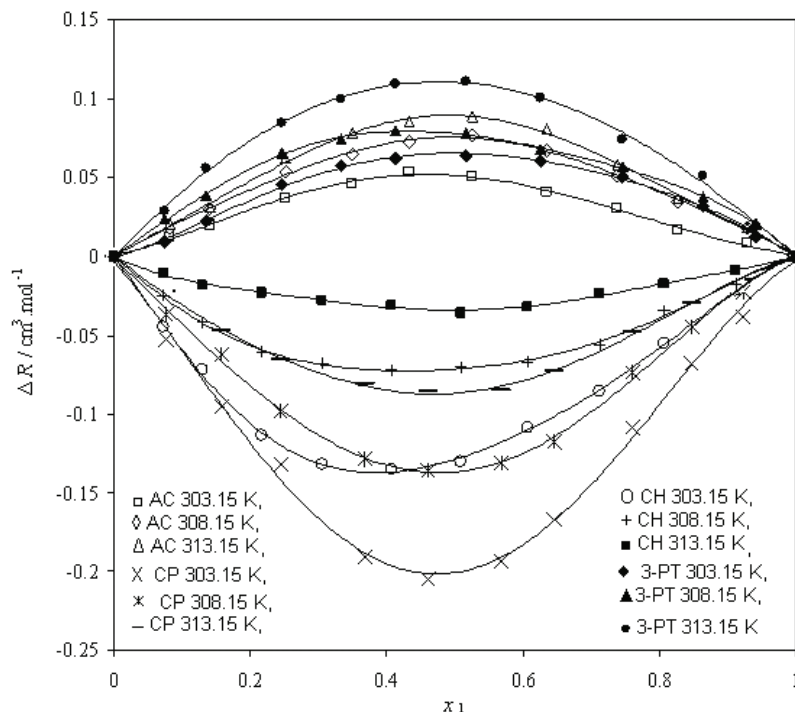


Fig. 4. Deviation in molar refraction, ΔR , as a function of diethyl malonate mole fraction, x_1 + acetophenone (AC); + cyclopentanone (CP); + cyclohexanone (CH); + 3-pentanone (3-PT).

TABLE I. Derived parameters of Eq. (7) for various functions and standard deviation (σ) of the binary mixtures at 303.15, 308.15 and 313.15 K

Function	T / K	A_0	A_1	A_2	A_3	σ
Diethyl malonate (1) + acetophenone (2)						
$\bar{\nu}^E$	303.15	0.2699	-0.0155	0.0981	-0.0084	0.002
	308.15	0.3453	0.0153	0.0076	-0.0333	0.004
	313.15	0.4504	0.0366	-0.0692	-0.1189	0.003
$\Delta\eta$	303.15	0.2699	-0.0155	0.0981	-0.0084	0.002
	308.15	0.1775	-0.0229	0.0039	-0.0345	0.001
	313.15	0.1517	-0.0227	-0.0079	0.0143	0.001
ΔR	303.15	0.2036	-0.0618	-0.1182	0.0500	0.002
	308.15	0.2979	-0.0175	-0.0898	0.0193	0.002
	313.15	0.3518	-0.0260	-0.1566	0.0275	0.003
ΔG^E	303.15	524.3250	-57.1088	163.6531	-27.5843	3.539
	308.15	422.6787	-66.2303	18.3785	-66.5172	5.551
	313.15	404.1643	-68.1976	-8.5612	23.7000	1.466

TABLE I. Continued

Function	T / K	A_0	A_1	A_2	A_3	σ
Diethyl malonate (1) + cyclopentanone (2)						
V^E	303.15	0.3304	0.0120	-0.0616	0.1423	0.003
	308.15	0.2703	0.0290	-0.1013	0.0249	0.003
	313.15	0.2052	-0.0338	-0.1370	0.0204	0.003
$\Delta\eta$	303.15	0.0846	-0.0238	-0.0191	0.0022	0.001
	308.15	0.0656	-0.0332	-0.0081	0.0290	0.000
	313.15	0.0505	-0.0125	-0.0250	0.0051	0.000
ΔR	303.15	-0.8002	0.1332	0.3718	-0.0028	0.007
	308.15	-0.5458	0.0791	0.2558	0.0616	0.004
	313.15	-0.3462	0.0611	0.1225	0.0404	0.002
ΔG^E	303.15	893.7855	-216.1805	13.3465	-1.8419	1.130
	308.15	856.6069	-228.7443	24.9172	51.6539	0.381
	313.15	836.9972	-182.8202	-19.9603	16.6195	0.401
Diethyl malonate (1) + cyclohexanone (2)						
V^E	303.15	0.8241	0.5942	-1.5870	0.1723	0.003
	308.15	0.8975	0.3965	-1.4937	0.4915	0.005
	313.15	0.9476	0.4495	-1.2831	0.3316	0.004
$\Delta\eta$	303.15	-0.5462	-0.2207	0.2528	0.3333	0.003
	308.15	-0.6070	-0.1422	0.1618	0.1496	0.003
	313.15	-0.6537	-0.0865	0.0319	0.0593	0.003
ΔR	303.15	-0.5224	0.2712	0.0495	-0.0556	0.003
	308.15	-0.2905	0.0613	-0.0117	0.0873	0.002
	313.15	-0.1338	0.0027	0.0172	0.0522	0.002
ΔG^E	303.15	-606.8685	-369.8802	375.6739	527.3885	5.562
	308.15	-804.4342	-295.0760	288.3852	300.8933	5.448
	313.15	-990.5262	-219.4471	108.3232	146.5062	5.365
Diethyl malonate (1) + 3-pentanone (2)						
V^E	303.15	-0.2039	0.0412	0.0346	-0.0952	0.002
	308.15	-0.3303	0.0391	-0.0235	-0.0562	0.004
	313.15	-0.4549	0.05565	0.0368	-0.2077	0.003
$\Delta\eta$	303.15	-0.6370	-0.0554	0.0660	0.0845	0.004
	308.15	-0.5786	0.0052	0.0676	-0.0248	0.004
	313.15	-0.5071	-0.0271	0.0676	0.0578	0.003
ΔR	303.15	0.2608	-0.0043	-0.0575	0.0992	0.002
	308.15	0.3112	-0.0878	0.0389	0.1473	0.001
	313.15	0.4423	-0.0568	-0.0319	0.0299	0.003
ΔG^E	303.15	821.9431	-18.5135	124.3100	-9.8292	10.572
	308.15	777.7993	165.4446	144.2818	-309.9339	9.692
	313.15	746.4863	34.3000	166.5115	-37.4047	7.395

The excess molar volume curves (Fig. 1) are not symmetric. The V^E values for the systems diethyl malonate + acetophenone and + cyclopentanone are completely positive, the maximum values of isotherms fall around the mole fraction $x_1 = 0.5$, while for diethyl malonate + 3-pentanone, they are completely negative over the entire composition range, having minima at $x_1 = 0.5$. However, for the

system diethyl malonate + cyclohexanone, the V^E values are negative in the lower composition of ester ($x_1 = 0.2$) at 303.15, 308.15 and 313.15 K, and the V^E values become positive as the composition of ester increases. The positive values of V^E suggest the dominance of dispersion forces while the negative values of V^E suggest specific interactions between the unlike molecules of the binary liquid systems.^{25,26} In the present study, the unusual behavior as observed for diethyl malonate + cyclohexanone indicates that the strengths of the specific or dispersion forces are not the only factor influencing the excess volume of the liquid mixtures but the molecular size and shape of the component also play a dominant role in deciding the deviation from ideality. Moreover, it was observed in many binary systems that there is no simple correlation between strength of the interactions and the observed properties. Accordingly, Rastogi *et al.*²⁷ suggested that the observed excess property is a combination of an interaction and non-interaction part, the non interaction part being the size effect, *i.e.*:

$$X^E_{\text{(observed)}} = X^E_{\text{(interaction)}} + X^E_{\text{(size effect)}}$$

where X^E refers to the excess or deviation in the property.

A perusal of (Fig. 2) reveals that the $\Delta\eta$ values for the binary mixtures of diethyl malonate with acetophenone and with cyclopentanone are completely positive, while for diethyl malonate + cyclohexanone and + 3-pentanone, the $\Delta\eta$ values are completely negative over the entire range of composition at all the studied temperatures. The positive $\Delta\eta$ values decrease with increasing temperature. The negative $\Delta\eta$ values become more negative as the temperature increases for diethyl malonate + cyclohexanone, whereas less negative for diethyl malonate + 3-pentanone. The positive $\Delta\eta$ values are indicative of specific interactions,^{28–30} while the negative $\Delta\eta$ values indicate that dispersion forces are dominant; furthermore, the existence of dispersion forces indicates that the component molecules have different molecular sizes and shapes.³¹

The values of ΔG^E (Fig. 3) for the binary mixtures of diethyl malonate with acetophenone, cyclopentanone and 3-pentanone are completely positive over the entire composition; while for the mixtures of with cyclohexanone, the values are completely negative all the studied temperatures. The positive ΔG^E values decrease with increasing temperature, whereas the negative ΔG^E values become more negative.

The dependences of the molar refraction, ΔR , on the mole fraction of diethyl malonate at 303.15, 308.15 and 313.15 K are presented in Fig. 4. It is observed that for the mixtures with acetophenone and 3-pentanone, ΔR is completely positive, while for the mixtures with cyclopentanone and cyclohexanone, the ΔR values are completely negative over the entire range of composition. The positive ΔR values increase with increasing temperature, whereas the negative ΔR values

become less negative. The plots are of parabolic shape and are characterized by the presence of well-defined minima/maxima.

Correlating models for mixture viscosities

The experimental viscosities of the binary mixtures of diethyl malonate with acetophenone, cyclopentanone, cyclohexanone and 3-pentanone at 303.15, 308.15 and 313.15 K were fitted to the two parameter Lobe,³² the three parameter McAllister four-body³³ and the three parameter Jouyban–Acree^{34,35} models.

The Lobe Equation involves the volume fraction of components Φ_1 and Φ_2 and was tested by fitting with two parameter, α_{12} and α_{21} , to the kinematic viscosity–mole fraction (ν, x_1) data pairs and is given by:

$$\nu = \Phi_1 \nu_1 \exp(\Phi_2 \alpha_{12} \ln(\nu_2/\nu_1)) + \Phi_2 \nu_2 \exp(\Phi_1 \alpha_{21} \ln(\nu_2/\nu_1)) \quad (9)$$

The McAllister (four-body) Model applied to correlate kinematic viscosities of binary liquid mixtures is given by:

$$\begin{aligned} \ln \nu = & x_1 \ln \nu_1 + 4x_1^3 x_2 \ln \nu_{1112} + 6x_1^2 x_2^2 \ln \nu_{1122} + 4x_1 x_2^3 \ln \nu_{2221} + x_2^4 \ln \nu_2 - \\ & - \ln [x_1 + (x_2 M_2/M_1)] + 4x_1^3 x_2 \ln \{[3 + (M_2/M_1)]/4\} + 6x_1^2 x_2^2 \times \\ & \times \ln \{[1 + (M_2/M_1)]/2\} + 4x_1 x_2^3 \ln \{[1 + (3M_2/M_1)]/4\} + x_2^4 \ln (M_2/M_1) \end{aligned} \quad (10)$$

where ν , ν_1 and ν_2 are the kinematic viscosities of the binary mixtures and the pure components 1 and 2, respectively. ν_{1112} , ν_{1122} and ν_{2221} are model parameters, which are obtained by non-linear regression.

The Jouyban–Acree Model is based on a theoretical consideration of two-body and three-body interactions between the various molecules in solution. The model could be used in practice for correlating the experimental viscosity data of different binary mixtures at various temperatures as:

$$\begin{aligned} \ln \eta = & x_1 \ln \eta_1 + x_2 \ln \eta_2 + A_0(x_1 x_2/T) + A_1(x_1 x_2(x_1 - x_2)/T) + \\ & + A_2(x_1 x_2(x_1 - x_2)^2/T) \end{aligned} \quad (11)$$

where A_0 , A_1 and A_2 are interaction parameters. η_1 and η_2 are the viscosity of the pure components at temperature T . The predictive ability of Eqs. (9)–(11) was tested by calculating the standard percentage deviation $\sigma(\%)$ as:

$$\sigma(\%) = (1/n - k \sum (100(Y_{\text{exp}} - Y_{\text{cal}})/Y_{\text{exp}})^2)^{1/2} \quad (12)$$

and the average percentage deviation (*APD*) using the relation:

$$APD = 100 \sum_{i=1}^n (|Y_{\text{exp}} - Y_{\text{cal}}|) / n \quad (13)$$

between the experimental and the calculated values; n represents the number of data points in each set and k the number of numerical coefficients in the equations, Y indicates the respective correlating property. The deviation values of Eqs. (12) and (13) obtained using the experimental viscosity data are given in Table II.



TABLE II. Adjustable parameters, standard percentage deviation, σ , and average percentage deviation (APD) of the correlations for the viscosities

<i>T</i> / K	Lobe		McAllister four-body model				Jouyban-Acree model							
	α_{12}	α_{21}	σ / %	<i>APD</i>	v_{1112}	v_{1122}	v_{2221}	σ / %	<i>APD</i>	A_0	A_1	A_2	σ / %	<i>APD</i>
Diethyl malonate (1) + acetophenone (2)														
303.15	2.53338	-3.6895	0.23	0.29	1.7012	1.6285	1.7565	0.13	0.11	51.8696	-7.0372	19.7008	0.36	0.15
308.15	0.1615	-1.0233	0.09	0.11	1.5106	1.4928	1.5635	0.10	0.09	39.0955	-9.6821	2.4985	0.16	0.11
313.15	2.5387	-3.2133	0.06	0.07	1.4074	1.3989	1.4538	0.05	0.04	36.4069	-6.0723	-1.1598	0.12	0.05
Diethyl malonate (1) + cyclopentanone(2)														
303.15	2.2762	-1.8436	0.08	0.10	1.5327	1.4164	1.4966	0.05	0.05	63.6068	-18.0848	0.2274	0.29	0.04
308.15	2.3538	-1.8730	0.08	0.08	1.4022	1.2984	1.3793	0.04	0.03	58.4043	-17.1637	1.7784	0.28	0.04
313.15	2.0911	-1.6750	0.10	0.10	1.3042	1.2148	1.2788	0.02	0.03	55.5530	-13.1099	-3.8643	0.23	0.01
Diethyl malonate (1) + cyclohexanone (2)														
303.15	-15.8419	5.5224	0.98	1.45	1.6873	1.2947	2.4875	0.71	0.55	-99.5588	-114.2321	196.5356	3.71	4.00
308.15	-6.9947	2.4203	0.19	0.41	1.4321	1.4048	1.8077	0.18	0.13	-117.109	-18.5453	26.3678	0.57	0.35
313.15	-6.8777	2.1691	0.27	0.90	1.3153	1.2982	1.6627	0.31	0.24	-133.787	-16.9713	18.8131	0.61	0.64
Diethyl malonate (1) + 3-pentanone (2)														
303.15	1.0578	-0.8175	0.39	0.26	1.3228	0.9806	0.8749	0.39	0.38	79.6830	-0.3868	14.5896	0.49	0.26
308.15	0.9304	-0.6452	0.45	0.25	1.2180	0.8947	0.8004	0.42	0.39	73.9628	8.8340	18.0103	0.53	0.28
313.15	1.0170	-0.7425	0.35	0.27	1.1437	0.8493	0.7771	0.27	0.25	70.5074	4.8170	19.7092	0.38	0.31



A close examination of these values reveals that the magnitude of these values remained almost same, with the exception for the Jouyban–Acree Model, for which the obtained *APD* values were much lower in comparison to the standard percentage deviation σ (%) values. While for the mixtures of diethyl malonate + 3-pentanone, the same trend was observed for all three studied models. Furthermore, it was observed that the McAllister four-body Model correlates the mixture viscosities excellently when compared to the Lobe and Jouyban–Acree Models.

Correlating models for refractive index

The experimental refractive index and density data of the studied binary mixtures were correlated using empirical/semi-empirical relations and models as reported earlier.³⁶ The experimental refractive index data were then compared with the corresponding Lorentz–Lorentz,^{37,38} Weiner,^{37,38} Heller,^{37,38} Eykman,³⁹ Newton,⁴⁰ Eyring–John⁴¹ and Dale–Gladstone⁴² relations.

The values of standard percentage deviation, σ (%), and average percentage deviation (*APD*) as obtained from Eqs. (12) and (13) are reported in Table III. Comparison of these values revealed that σ values were small in magnitude as compared to the values of *APD*. For diethyl malonate + 3-pentanone, the maximum *APD* (0.164) was obtained using the Eykman Relation while the minimum *APD* (0.024) was obtained using the Weiner relation. Whereas, for diethyl malonate + cyclopentanone system, the *APD* values are quite higher (maximum 0.274 by the Eykman and minimum 0.033 by the Weiner Relation) as compared to the

TABLE III. Average percentage deviation (*APD*) and standard percentage deviation, σ , in the refractive index from different mixing relations

<i>T</i> / K	Lorentz–Lorentz	Eykman	Weiner	Heller	Dale–Gladstone	Newton	Eyring–John	
	<i>APD</i>	σ / %	<i>APD</i>	σ / %	<i>APD</i>	σ / %	<i>APD</i>	σ / %
Diethyl malonate (1) + acetophenone (2)								
303.15	0.013	0.011	0.049	0.022	0.010	0.010	0.040	0.020
308.15	0.024	0.015	0.023	0.015	0.003	0.006	0.044	0.021
313.15	0.026	0.016	0.017	0.013	0.005	0.007	0.048	0.023
Diethyl malonate (1) + cyclopentanone (2)								
303.15	0.114	0.034	0.274	0.052	0.073	0.027	0.216	0.047
308.15	0.079	0.028	0.189	0.044	0.056	0.022	0.149	0.039
313.15	0.052	0.023	0.126	0.035	0.033	0.018	0.098	0.031
Diethyl malonate (1) + cyclohexanone (2)								
303.15	0.087	0.029	0.214	0.046	0.057	0.024	0.166	0.041
308.15	0.057	0.024	0.143	0.038	0.038	0.019	0.109	0.033
313.15	0.047	0.022	0.119	0.034	0.032	0.018	0.090	0.030
Diethyl malonate (1) + 3-pentanone (2)								
303.15	0.038	0.020	0.088	0.030	0.024	0.015	0.071	0.027
308.15	0.053	0.023	0.121	0.035	0.033	0.018	0.098	0.031
313.15	0.071	0.027	0.164	0.040	0.044	0.021	0.131	0.036



diethyl malonate + cyclohexanone system. For diethyl malonate + acetophenone, all the mixing rules, except the Newton Relation, exhibited low APD values with a maximum (0.065) by the Dale–Gladstone and the minimum (0.003) by Weiner Relation. Furthermore, it was observed that temperature has an effect on σ values. For the binary mixtures of diethyl malonate + cyclopentanone and diethyl malonate + cyclohexanone, the values were found to decrease with increasing temperature, while for the binary mixtures of diethyl malonate + 3-pentanone, the values increased with increasing temperature. However, for the binary mixtures of diethyl malonate + acetophenone, the values of σ and APD did not exhibit any systematic variation with temperature. Based on the present analysis, it could be concluded that all the studied mixing rules predicted the experimental refractive index data satisfactorily.

CONCLUSIONS

The density, viscosity and refractive index measurements for binary mixture of diethyl malonate + acetophenone, + cyclopentanone, + cyclohexanone and + 3-pentanone at 303.15, 308.15 and 313.15 K over the entire composition range were determined. From the experimental data, the excess volume, V^E , deviations in viscosity, $\Delta\eta$, molar refraction, ΔR , and excess Gibb's Free Energy of activation of flow, ΔG^E , were obtained. The reported excess properties showed both positive and negative deviations. These excess properties were correlated by the Redlich–Kister polynomial equation to derive the coefficients and standard deviations. The viscosity results were also analyzed using the empirical relations proposed by Lobe, McAllister and Jouyban–Acree. Furthermore, the refractive indices of the binary mixtures were correlated using various empirical/semi-empirical relations and models.

SUPPLEMENTARY MATERIAL

The comparison of experimental results and literature data (Tables I-S and II-S) are available electronically from <http://www.shd.org.rs/JSCS/>, or from the corresponding author on request.

Acknowledgement. One of the authors (M. V. Rathnam) sincerely acknowledges the University Grant Commission, New Delhi for financial assistance through the major research project (No 38-24/ 2009(SR) dated 21/12/2009.

ИЗВОД

СТУДИЈА ВОЛУМЕТРИЈСКИХ, ВИСКОЗИМЕТРИЈСКИХ И ОПТИЧКИХ СВОЈСТАВА И
МОЛЕКУЛСКИХ ИНТЕРАКЦИЈА У БИНАРНОЈ СМЕШИ ДИЕТИЛМАЛОНАТА И
КЕТОНА НА 303,15, 308,15 И 313,15 К

MANAPRAGADA V. RATHNAM¹, SUDHIR MOHITE¹ и MANAPRAGADA S. KUMAR²

¹Physical Chemistry Research Laboratory, B. N. Bandodkar College of Science, Thane – 400 601, India и

²Department of Chemistry, Zulal Bhilajirao Patil College, Deopur, Dhule – 424 002, India

Извршена су мерења густине, ρ , вискозности, η , и индекса рефракције, n_D , бинарних смеша диетилмалоната са кетонима (ацетофенон, циклопентанон, циклохексанон и 3-пентанон) на температурама 303,15, 308,15 и 313,15 К и у целом концентрационом опсегу. На основу експерименталних података, одређене су допунска запремина, V^E , промена вискозности при мешању, $\Delta\eta$, допунска Гибсова слободна енергија, ΔG^E , и промена моларне рефракције при мешању, ΔR . Добијене вредности су корелисане Редлих–Кистер-овим полиномом. Вредности V^E , $\Delta\eta$, ΔG^E и ΔR су приказане графички у зависности од молског удела диетилмалоната. Позитивне и негативне вредности допунских својстава за све испитиване бинарне смеше су објашњене на основу међумолекулских интеракција присутних у овим смешама. Поред тога, извршено је корелисање вискозности и индекса рефракције бинарних смеша преко различитих емпиријских корелација.

(Примљено 12. јула, ревидирано 22. септембра 2011)

REFERENCES

- M. B. Ewing, B. J. Levien, K. N. Marsh, R. H. Stokes, *J. Chem. Thermodyn.* **2** (1970) 689
- A. Mchaweh, A. Alsaygh, Kh. Nasrifar, M. Moshfeghian, *Fluid. Phase Equilib.* **224** (2004) 157
- C. M. Kinart, W. J Kinart, *Phys. Chem. Liq.* **38** (2000) 155
- A. C. Francis, *Organic Chemistry*, 4th ed., McGraw-Hill, New York, 2002, p. 619
- A. Qin, D. E. Hoffman, P. Munk, *J. Chem. Eng. Data* **37** (1992) 66
- J. N. Nayak, M. I. Aralaguppi, T. M. Aminabhavi, *J. Chem. Eng. Data* **48** (2003) 628
- T. S. Jyostana, N. Satyanarayana, *Indian J. Chem., A* **44** (2005) 1365
- A. Diwedi, M. Singh, *Indian J. Chem., A* **46** (2007) 789
- C. Gonzalez, J. M. Resa, R. G. Concha, J. M. Goenaga, *J. Food Eng.* **79** (2007) 1104
- W. L. Izonfuo, A. J. Kemeakegha, *Indian J. Chem., A* **48** (2009) 1242
- I. C. Pan, M. Tang, Y. P. Chen, *J. Chem. Eng. Data* **45** (2000) 1012
- A. Rodriguez, J. Canosa, J. Tojo, *J. Chem. Eng. Data* **46** (2001) 1506
- J. N. Nayak, M. I. Aralaguppi, T. M. Aminabhavi, *J. Chem. Eng. Data* **48** (2003) 1489
- J. G. Baragi, M. I. Aralaguppi, T. M. Aminabhavi, M. Y. Kariduraganvar, S. S. Kulkarni, *J. Chem. Eng. Data* **50** (2005) 917
- J. M. Monzon, S. Otin, C. G. Losa, *J. Chem. Thermodyn.* **13** (1981) 385
- S. Baluja, N. Pandaya, N. Kachhadia, A. Solanki, P. Inamdar, *Phys. Chem. Liq.* **43** (2005) 309
- S. L. Oswal, D. B. Gheewala, K. D. Prajapati, R. L. Gardas, N. Y. Ghel, S. P. Ijardar, *Thermochim. Acta* **426** (2005) 141
- Y. Wang, H. Gao, W. Yan, *J. Chem. Eng. Data* **55** (2010) 381
- Y. Wang, H. Gao, W. Yan, *Fluid. Phase Equilib.* **291** (2010) 8
- M. V. Rathnam, S. Mohite, M. S. S. Kumar, *J. Chem. Eng. Data* **54** (2009) 305



21. M. V. Rathnam, K. Jain, S. Mankumare, M. S. S. Kumar, *J. Chem. Eng. Data* **55** (2010) 3929
22. M. V. Rathnam, S. Mohite, M. S. S. Kumar, *J. Solution Chem.* **39** (2010) 1735
23. S. Glasstone, *Textbook of Physical Chemistry*, 2nd ed., D. Van Nostrand Co., London, 1949
24. O. Redlich, A. T. Kister, *Ind. Eng. Chem.* **40** (1948) 345
25. K. H. Chen, T. C. Hsiun, *J. Chem. Eng. Data* **50** (2005) 608
26. M. N. Roy, A. Sinha, B. Sinha, *J. Solution Chem.* **34** (2005) 1311
27. R. P. Rastogi, J. Nath, J. Misra, *J. Phys. Chem.* **71** (1967) 1277
28. R. J. Fort, W. R. Moore, *Trans. Faraday Soc.* **62** (1966) 1112
29. R. Palepu, J. Oliver, B. Mackinnon, *Can. J. Chem.* **63** (1985) 1024
30. T. M. Reed, T. E. Taylor, *J. Phys. Chem.* **63** (1959) 58
31. G. P. Dubey, M. Sharma, N. Dubey, *J. Chem. Thermodyn.* **40** (2008) 309
32. V. M. Lobe, *M.Sc. Thesis*, University of Rochester, Rochester, New York, 1973
33. R. A. McAllister, *AICHE J.* **6** (1960) 427
34. A. Jouyban, M. Khoubnasab Jafari, Z. Vaez-Ghamaleki Fekari, W. E. Acree Jr., *Chem. Pharm. Bull.* **53** (2005) 519
35. A. Jouyban, A. Fathi-Azarbay Jani, M. Khoubnasab Jafari, W. E. Acree Jr., *Indian J. Chem., A* **44** (2005) 1553
36. M. V. Rathnam, S. Mohite, M. S. S. Kumar, *J. Chem. Eng. Data* **55** (2010) 5946
37. T. M. Aminabhavi, H. T. S. Phayade, R. S. Khinnavar, B. Gopalkrishna, K. C. Hansen, *J. Chem. Eng. Data* **39** (1994) 251
38. A. Z. Tasic, B. D. Djordjevic, D. K. Grozdanic, N. Radojkovic, *J. Chem. Eng. Data* **37** (1992) 310
39. C. J. F. Bottcher, *Theory of Electric Polarization*; Elsevier, Amsterdam, 1952
40. S. S. Kurtz Jr., A. L. Ward, *J. Franklin Inst.* **222** (1936) 563
41. H. Eyring, M. S. John, *Significant Liquid Structures*, Wiley, New York, 1969
42. T. P. Dale, J. H. Gladstone, *Philos. Trans. R. Soc. London* **148** (1858) 887
43. J. A. Riddick, W. B. Bunger, T. K. Sakano, *Organic Solvents, Physical Properties and Methods of Purifications*, Vol. 2, Wiley-Interscience, New York, 1986
44. J. Timmermans, *Physico-Chemical Constants of Pure Organic Compounds*, Vol. I, Elsevier, Amsterdam, 1950
45. M. I. Aralaguppi, C. V. Jadav, T. M. Aminabhavi, *J. Chem. Eng. Data* **44** (1999) 435.



SUPPLEMENTARY MATERIAL TO
**Volumetric, viscometric and optical study of molecular
interactions in binary mixtures of diethyl malonate
with ketones at 303.15, 308.15 and 313.15 K**

MANAPRAGADA V. RATHNAM^{1*}, SUDHIR MOHITE¹
and MANAPRAGADA S. KUMAR²

¹Physical Chemistry Research Laboratory, B. N. Bandodkar College of Science,
Thane – 400 601, India and ²Department of Chemistry, Zulal Bhilajirao
Patil College, Deopur, Dhule – 424 002, India

J. Serb. Chem. Soc. 77 (4) (2012) 507–521

TABLE I-S. Comparison of experimental densities, ρ , viscosities, η , and refractive indices, n_D , of the pure components with the available literature values at 303.15, 308.15 and 313.15 K

Liquid	T / K	$\rho / \text{g cm}^{-3}$		$\eta / \text{mPa s}$		n_D	
		Exp.	Lit. ^a	Exp.	Lit.	Exp.	Lit.
Diethyl Malonate	303.15	1.0443	1.0446 ⁴³	1.728	1.721 ¹⁷	1.4095	1.4097 ⁴³
	308.15	1.0387	1.0388 ¹⁴	1.570	1.602 ¹⁴	1.4076	1.4085 ¹⁴
	313.15	1.0336	–	1.456	–	1.4055	–
Acetophenone	303.15	1.0199	1.0194 ⁴⁴	1.518	1.511 ⁴³	1.5294	1.5297 ⁴³
	308.15	1.0169	1.0172 ⁴³	1.378	–	1.5270	–
	313.15	1.0135	1.0139 ⁴³	1.291	–	1.5250	–
Cyclopentanone	303.15	0.9385	0.9390 ⁴³	0.999	0.995 ⁴³	1.4335	–
	308.15	0.9339	–	0.927	–	1.4310	–
	313.15	0.9290	–	0.865	–	1.4290	–
Cyclohexanone	303.15	0.9377	0.9376 ⁴³	1.816	1.810 ⁴³	1.4465	1.4463 ⁴⁵
	308.15	0.9328	–	1.657	1.635 ⁴⁵	1.4440	1.4439 ⁴⁵
	313.15	0.9282	–	1.542	–	1.4420	–
3-Pentanone	303.15	0.8057	0.8054 ⁴³	0.429	0.424 ⁴³	1.3879	1.3878 ⁴³
	308.15	0.8017	–	0.397	–	1.3857	–
	313.15	0.7977	–	0.388	0.380 ⁴³	1.3835	–

^aReference numbers relate to the Reference list in the original paper: J. Serb. Chem. Soc. 77 (4) (2012) 507–521

*Corresponding author. E-mail: mvrathnam58@rediffmail.com

TABLE II-S. Values of the density (ρ), excess volume (V^E), viscosity (η), and refractive index (n_D) for the binary liquid mixtures

x_1	$\rho / \text{g cm}^{-3}$	$V^E / \text{cm}^3 \text{ mol}^{-1}$	$\eta / \text{mPa s}$	n_D
Diethyl malonate (1) + acetophenone (2)				
$T = 303.15 \text{ K}$				
0.0000	1.0199	—	1.518	1.5294
0.0812	1.0222	0.026	1.564	1.5166
0.1401	1.0239	0.032	1.587	1.5078
0.2516	1.0269	0.053	1.626	1.4921
0.3486	1.0294	0.066	1.655	1.4793
0.4322	1.0315	0.070	1.677	1.4689
0.5248	1.0337	0.078	1.697	1.4579
0.6335	1.0363	0.067	1.714	1.4456
0.7384	1.0387	0.053	1.727	1.4345
0.8256	1.0406	0.042	1.732	1.4257
0.9278	1.0427	0.032	1.738	1.4160
1.0000	1.0443	—	1.728	1.4095
$T = 308.15 \text{ K}$				
0.0000	1.0169	—	1.378	1.5270
0.0812	1.0189	0.030	1.412	1.5143
0.1401	1.0204	0.039	1.430	1.5056
0.2516	1.0230	0.068	1.461	1.4900
0.3486	1.0253	0.072	1.487	1.4773
0.4322	1.0271	0.086	1.506	1.4669
0.5248	1.0291	0.089	1.524	1.4560
0.6335	1.0314	0.083	1.540	1.4438
0.7384	1.0336	0.062	1.550	1.4327
0.8256	1.0353	0.052	1.559	1.4239
0.9278	1.0373	0.025	1.567	1.4142
1.0000	1.0387	—	1.570	1.4076
$T = 313.15 \text{ K}$				
0.0000	1.0135	—	1.291	1.5250
0.0812	1.0153	0.034	1.315	1.5123
0.1401	1.0166	0.052	1.334	1.5035
0.2516	1.0190	0.080	1.363	1.4880
0.3486	1.0210	0.099	1.384	1.4753
0.4322	1.0227	0.108	1.400	1.4649
0.5248	1.0245	0.117	1.416	1.4540
0.6335	1.0267	0.101	1.430	1.4418
0.7384	1.0287	0.087	1.440	1.4306
0.8256	1.0304	0.058	1.446	1.4218
0.9278	1.0323	0.025	1.454	1.4121
1.0000	1.0336	—	1.456	1.4055



TABLE II-S. Continued

x_1	$\rho / \text{g cm}^{-3}$	$V^E / \text{cm}^3 \text{ mol}^{-1}$	$\eta / \text{mPa s}$	n_D
Diethyl malonate (1) + cyclopentanone(2)				
$T = 303.15 \text{ K}$				
0.0000	0.9385	—	0.999	1.4335
0.0758	0.9514	0.012	1.061	1.4294
0.1566	0.9637	0.032	1.125	1.4257
0.2437	0.9756	0.054	1.193	1.4223
0.3678	0.9906	0.078	1.288	1.4180
0.4601	1.0006	0.079	1.356	1.4157
0.5678	1.0111	0.078	1.433	1.4137
0.6456	1.0180	0.077	1.487	1.4127
0.7598	1.0273	0.067	1.565	1.4116
0.8459	1.0338	0.044	1.624	1.4108
0.9215	1.0391	0.026	1.675	1.4101
1.0000	1.0443	—	1.728	1.4095
$T = 308.15 \text{ K}$				
0.0000	0.9339	—	0.927	1.4310
0.0758	0.9467	0.010	0.981	1.4273
0.1566	0.9589	0.029	1.038	1.4240
0.2437	0.9708	0.039	1.098	1.4207
0.3678	0.9857	0.057	1.180	1.4169
0.4601	0.9955	0.070	1.240	1.4147
0.5678	1.0059	0.068	1.307	1.4126
0.6456	1.0128	0.059	1.355	1.4114
0.7598	1.0220	0.049	1.425	1.4101
0.8459	1.0284	0.031	1.477	1.4092
0.9215	1.0336	0.019	1.524	1.4084
1.0000	1.0387	—	1.570	1.4076
$T = 313.15 \text{ K}$				
0.0000	0.9290	—	0.865	1.4290
0.0758	0.9418	0.008	0.913	1.4256
0.1566	0.9540	0.024	0.964	1.4223
0.2437	0.9659	0.031	1.018	1.4193
0.3678	0.9808	0.045	1.094	1.4157
0.4601	0.9906	0.055	1.150	1.4135
0.5678	1.0010	0.051	1.213	1.4113
0.6456	1.0079	0.039	1.257	1.4100
0.7598	1.0171	0.026	1.321	1.4084
0.8459	1.0234	0.019	1.369	1.4073
0.9215	1.0286	0.006	1.412	1.4064
1.0000	1.0336	—	1.456	1.4055



TABLE II-S. Continued

x_1	$\rho / \text{g cm}^{-3}$	$V^E / \text{cm}^3 \text{ mol}^{-1}$	$\eta / \text{mPa s}$	n_D
Diethyl malonate (1) + cyclohexanone (2)				
$T = 303.15 \text{ K}$				
0.0000	0.9377	—	1.816	1.4465
0.0713	0.9490	-0.059	1.790	1.4422
0.1285	0.9572	-0.065	1.760	1.4389
0.2155	0.9684	-0.013	1.727	1.4340
0.3058	0.9789	0.075	1.694	1.4294
0.4070	0.9899	0.157	1.665	1.4251
0.5085	1.0003	0.211	1.631	1.4214
0.6055	1.0099	0.211	1.625	1.4185
0.7125	1.0201	0.162	1.635	1.4157
0.8065	1.0286	0.098	1.667	1.4136
0.9118	1.0375	0.029	1.706	1.4114
1.0000	1.0443	—	1.728	1.4095
$T = 308.15 \text{ K}$				
0.0000	0.9328	—	1.657	1.4440
0.0713	0.9440	-0.056	1.623	1.4401
0.1285	0.9520	-0.045	1.591	1.4370
0.2155	0.9631	0.012	1.553	1.4325
0.3058	0.9735	0.104	1.515	1.4281
0.4070	0.9844	0.191	1.487	1.4238
0.5085	0.9949	0.224	1.458	1.4201
0.6055	1.0045	0.216	1.454	1.4170
0.7125	1.0146	0.171	1.465	1.4141
0.8065	1.0230	0.113	1.497	1.4119
0.9118	1.0319	0.035	1.533	1.4095
1.0000	1.0387	—	1.570	1.4076
$T = 313.15 \text{ K}$				
0.0000	0.9282	—	1.542	1.4420
0.0713	0.9392	-0.040	1.495	1.4380
0.1285	0.9471	-0.020	1.463	1.4348
0.2155	0.9582	0.031	1.423	1.4304
0.3058	0.9686	0.118	1.386	1.4263
0.4070	0.9795	0.199	1.352	1.4222
0.5085	0.9899	0.239	1.333	1.4185
0.6055	0.9994	0.239	1.330	1.4154
0.7125	1.0095	0.188	1.341	1.4124
0.8065	1.0179	0.125	1.371	1.4100
0.9118	1.0267	0.055	1.406	1.4075
1.0000	1.0336	—	1.456	1.4055



TABLE II-S. Continued

x_1	$\rho / \text{g cm}^{-3}$	$V^E / \text{cm}^3 \text{ mol}^{-1}$	$\eta / \text{mPa s}$	n_D
Diethyl malonate (1) + 3-pentanone (2)				
$T = 303.15 \text{ K}$				
0.0000	0.8057	—	0.429	1.3879
0.0736	0.8302	-0.011	0.488	1.3903
0.1356	0.8497	-0.022	0.535	1.3923
0.2458	0.8820	-0.037	0.633	1.3956
0.3326	0.9055	-0.044	0.725	1.3979
0.4124	0.9258	-0.053	0.814	1.3998
0.5158	0.9503	-0.051	0.940	1.4020
0.6256	0.9744	-0.046	1.094	1.4041
0.7456	0.9987	-0.034	1.273	1.4061
0.8626	1.0206	-0.021	1.475	1.4078
0.9415	1.0345	-0.015	1.627	1.4088
1.0000	1.0443	—	1.728	1.4095
$T = 308.15 \text{ K}$				
0.0000	0.8017	—	0.397	1.3857
0.0736	0.8261	-0.019	0.450	1.3884
0.1356	0.8456	-0.046	0.493	1.3905
0.2458	0.8777	-0.063	0.580	1.3939
0.3326	0.9011	-0.078	0.658	1.3962
0.4124	0.9212	-0.078	0.742	1.3981
0.5158	0.9456	-0.085	0.859	1.4003
0.6256	0.9695	-0.076	0.999	1.4023
0.7456	0.9936	-0.060	1.162	1.4043
0.8626	1.0153	-0.040	1.341	1.4060
0.9415	1.0290	-0.020	1.478	1.4070
1.0000	1.0387	—	1.570	1.4076
$T = 313.15 \text{ K}$				
0.0000	0.7977	—	0.388	1.3835
0.0736	0.8220	-0.021	0.437	1.3863
0.1356	0.8414	-0.047	0.477	1.3886
0.2458	0.8735	-0.085	0.560	1.3921
0.3326	0.8968	-0.101	0.633	1.3945
0.4124	0.9169	-0.114	0.708	1.3965
0.5158	0.9411	-0.110	0.812	1.3987
0.6256	0.9649	-0.103	0.938	1.4007
0.7456	0.9889	-0.088	1.089	1.4025
0.8626	1.0104	-0.054	1.250	1.4041
0.9415	1.0240	-0.028	1.375	1.4049
1.0000	1.0336	—	1.456	1.4055





Calculation of the effective diffusion coefficient during the drying of clay samples

MILOŠ VASIĆ^{1*}, ZAGORKA RADOJEVIĆ¹ and ŽELJKO GRBAVČIĆ²

¹Institute for the Testing of Materials, Bulevar Vojvode Mišića 43, 11000 Belgrade,

Serbia and ²Faculty of Technology and Metallurgy, University of Belgrade,

Karnegijeva 4, 11000 Belgrade, Serbia

(Received 17 July, revised 10 October 2011)

Abstract: The aim of this study was to calculate the effective diffusion coefficient based on experimentally recorded drying curves for two masonry clays obtained from different localities. The calculation method and two computer programs based on the mathematical calculation of the Second Fick Law and the Crank Diffusion Equation were developed. Masonry product shrinkage during drying was taken into consideration for the first time and the appropriate correction was entered into the calculation. The results presented in this paper show that the values of the effective diffusion coefficient determined by the designed computer programs (with and without the correction for shrinkage) have similar values to those available in the literature for the same coefficient for different clays. Based on the mathematically determined prognostic value of the effective diffusion coefficient, it was concluded that, whatever the initial mineralogical composition of the clay, there is 90 % agreement of the calculated prognostic drying curves with the experimentally recorded ones. When a shrinkage correction of the masonry products is introduced into the calculation step, this agreement is even better.

Keywords: diffusion; drying; mathematical modeling; computer program.

INTRODUCTION

The studying of a drying process, due to its complexity, still attracts the attention of researchers around the world even today. The explanation of the drying process is reduced to the establishment of a series of theoretical and empirical drying models that show agreement, to a greater or lesser extent, with the experimental data. Complex processes of simultaneous mass and energy transfer, which are often non-stationary and the distinct nature of the properties of the material (hygroscopic, capillarity, pores size distribution, shrinkage effect, etc.) complicate even more the description of the drying process. For these reasons, a unique theo-

* Corresponding author. E-mail: milos.vasic@institutims.rs
doi: 10.2298/JSC110717191V

retical setting of drying, which would universally describe this process for different types of clay materials has not yet been developed.

The diffusion process viewed as the transport of matter due to the random motion of molecules is characteristic for a drying process. The transfer of moisture within the solid body at a certain temperature is realized due to the different moisture content in the interior and on the surface of a solid body. The mass transfer rate by diffusion is therefore proportional to the concentration gradient of the moisture content, with the diffusion coefficient being the proportionality factor. Knowing the diffusion coefficient is essential for a credible description of the mass transfer process, described by the Fick's Equation. The analytical solution of the general Fick's Law was described by Cranck in 1975.¹ Several different ways of solving the Fick's Equation were presented by Cranck:

- i) For the case when the diffusion coefficient is constant and the solid body isotropic;
- ii) For the case when the diffusion coefficient is not constant, together with special cases of non-Fickian diffusion and
- iii) For the case of diffusion in which a chemical reaction exists as well as the simultaneous diffusion of heat and moisture.

The drying process, in addition to pure diffusion, is characterized by the existence of other, secondary types of internal mass transfer, such as surface diffusion, Knudsen diffusion, capillary flow, evaporation and condensation, thermo-diffusion, *etc.*, which in small amounts influence the overall process of mass transfer.² Normally, a correction for secondary types of mass transfer is introduced into the calculation by replacing the pure diffusion coefficient with an effective diffusion coefficient.

In numerous papers, the results of drying kinetics obtained from different models for different materials, which include or neglect shrinkage of the material, are compared with the experimentally determined parameters of the drying kinetics.^{3–6} During the drying of certain materials such as: various agricultural products, various constructional products from wood, cement, hydraulic binders or clay, the shrinkage effect that occurs cannot be neglected, neither in practice nor in the mathematical models that are used to describe the drying process.

In most models that describe the drying process, shrinkage does not exist in the equations because the mathematical models that would include the shrinkage effect during drying are extremely complicated; hence, in the mathematical modeling process, it is the practice to assume that shrinkage does not exist or is negligible. Such models are usually applied on materials that exhibit a shrinkage effect and shrinkage deviations are usually corrected for by the introduction of correction factors.

A small number of papers that describe the drying process of ceramic materials and especially clay are available in the literature. Some data can be found

in the papers of Efremov⁷ (bricks), Chemkhi⁸, Zagrouba^{9,10} (clays), Skansi^{11,12}, Lalić¹³ (heavy clay tiles) and others.

The behaviors during the drying process of two different clays with different mineralogical compositions were considered in the present study. An appropriate shrinkage correction, caused by thickness shrinkage during drying, was introduced into the mathematical models for the calculation of the effective diffusion coefficient.

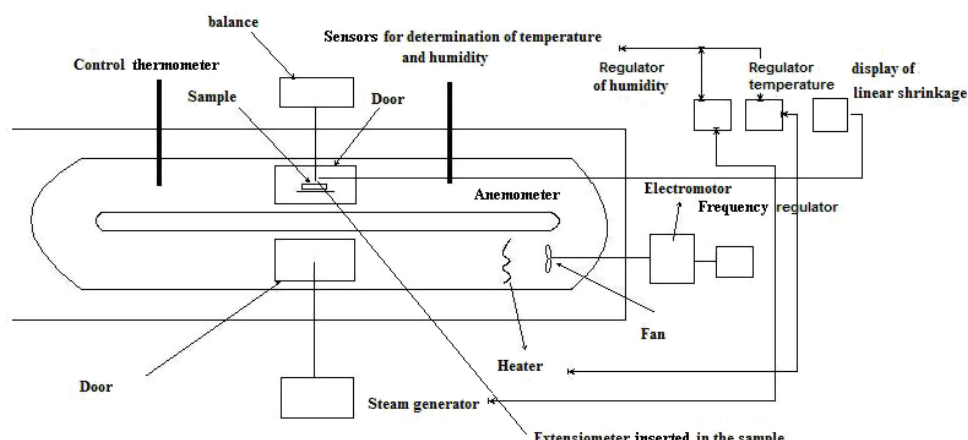
EXPERIMENTAL

Sample preparation

Two raw masonry clays from the localities Banatski Karlovac and Ćirilkovac were analyzed. After an initial characterization of these materials, which included chemical, mineralogical, X-ray diffraction (XRD) analysis, thermogravimetric analysis (TGA) and granulometric examination, the raw materials were subjected to further classical preparation. The raw material samples were first dried at 60 °C and then milled down in a laboratory perforated rolls mill. After that, the clays were moisturized and milled in a laboratory differential mill, first at a gap of 3 mm and then of 1 mm. Laboratory samples of size 120 mm×50 mm×14 mm were formed in a laboratory extruder "Hendle" type 4, under a vacuum of 0.8 bar. These samples were used in the further experimental work.

Drying experimental conditions

The behavior of the clay samples during drying was investigated by monitoring and recording the changes in weight and linear shrinkage of the test samples during drying in a laboratory dryer, especially created for this purpose, the schematic view of which is shown in Scheme 1.



Scheme 1. Laboratory recirculation dryer.

The laboratory recirculation dryer provides: regulation of the drying air temperature within 0–125 °C, with accuracy ± 0.2 °C; regulation of the relative humidity of the drying air within 20–100 %, with an accuracy of 0.2 %; velocity regulation of the drying air within 0–3.5 m s⁻¹, with an accuracy of 1 %; monitoring and recording of the weight of the drying

samples within 0–2000 g, with an accuracy of 0.01 g; monitoring and recording the linear shrinkage within 0–23 mm with an accuracy of 0.2 mm and continuous time monitoring during drying.

Data acquisition, continuous time monitoring and recording of the temperature and relative humidity of the drying medium and the linear shrinkage of the drying samples were realized automatically using PLC controllers and a standard Pentium IV computer.

Drying kinetic curves were recorded for the drying of the prepared heavy clay tiles (samples) in a laboratory recirculation dryer under the experimental conditions presented in Table I.

TABLE I. Experimental conditions

Experiment	Air velocity, $W / m s^{-1}$	Air temperature, $T / ^\circ C$	Air humidity, $V / \%$
Clay Banatski Karlovac (experiments from this work)			
1	1	40	60
2	3		
3	1	80	
4	3		
5	1	40	80
6	3		
7	1	80	
8	3		
Clay Čirilkovac (experiments taken from previous research phases ²¹)			
9	3	40	60
10		55	
11		70	
12			40

Theoretical principles

In order to determine the moisture diffusion in porous systems, it is necessary to use data analysis obtained from: drying, sorption kinetics and permeability measurements. An estimation of the diffusion coefficient can be obtained from drying curve by the slope method,^{14,15} or by comparing experimentally determined drying curves with curves obtained from the Fick Equations predicted analytically^{2,3,16} or numerically.^{6,17}

The drying curve of typical masonry clay consists of a first phase of drying, the constant velocity phase, and a phase of decreasing drying rate. In drying studies performed on different materials, diffusion is generally accepted as the main mechanism of moisture transport from the material interior to its surface. The restriction to one-dimensional diffusion gives a good approximation in many practical systems. Analytical solution of the Fick Equation are given for various geometrical shapes, assuming that the transport of moisture occurs by diffusion, that sample shrinkage is neglected and that diffusion coefficient and temperature have constant values. For the case of “thin plate” geometry, a solution was given by Crank,¹ that is represented by the expression:

$$MR = \frac{X - X_{eq}}{X_0 - X_{eq}} = \frac{8}{\pi^2} \sum_{n=0}^{\infty} \frac{1}{(2n+1)^2} \exp\left(-\frac{(2n+1)^2}{4} \frac{\pi^2 D_{eff} t}{l^2}\right) \quad (1)$$



where X_0 , X and X_{eq} represent, respectively, the initial, current and equilibrium moisture content, kg moisture kg^{-1} dry material, D_{eff} is the effective diffusion coefficient, $\text{m}^2 \text{s}^{-1}$, l is the half plate thickness and t is time, s. MR represents the moisture ratio and has no unit. Since clay products show dimensional change during drying, it was necessary to develop a model that would consider this phenomenon. By introducing into Eq. (1) the expression $l_{(t)}$, which represents the experimental dependence of the thickness of the tiles in time, Eq. (1) is corrected. It should be born in mind that this type of correction is not mathematically one hundred percent accurate because the resulting Eq. (1) was obtained using the assumption of unchangeable sample thickness. Formally speaking, a mathematically accurate correction can be obtained by entering the expression $l_{(t)}$ into the equation for the case of constant sample thickness, after an integration step. A small number of papers describing the sample dimensional correction can be found in literature. Some data can be found in the papers of Hassini,²⁰ and Disse.²¹ Da Silva^{18,19} presented in his studies a way of solving the diffusion equation for the case of spherical samples.

Program description

In order to solve Eq. (1), it is necessary to dispose with the experimental results and to have the experimentally determined dependence $MR_{exp}-t$. MR_{exp} represents the experimentally determined value of MR calculated from the experimentally measured data X_0 , X and X_{eq} . Eq. (1) can be converted into the form:

$$MR = \frac{8}{\pi^2} \sum_{n=N+1}^{\infty} \frac{1}{(2n+1)^2} \exp\left(-\frac{(2n+1)^2}{4}\pi^2 \frac{D_{eff}t}{x^2}\right) + \\ + \frac{8}{\pi^2} \sum_{n=0}^N \frac{1}{(2n+1)^2} \left(-\frac{(2n+1)^2}{4}\pi^2 \frac{D_{eff}t}{x^2}\right) \quad (2)$$

If the value of ε is defined as the relative error of neglecting terms higher than N in Eq. (2), the value of N can be determined and Eq. (2) is transformed from an infinite sum into a finite sum of N terms given by Eq. (3):

$$MR = \frac{8}{\pi^2} \sum_{n=0}^N \frac{1}{(2n+1)^2} \left(-\frac{(2n+1)^2}{4}\pi^2 \frac{D_{eff}t}{l^2}\right) \quad (3)$$

The value of $\varepsilon = 0.05$ was accepted for the further calculations in this paper. When $t = 0$, $MR = 1$ and Eq. (2) is transformed into Eq. (4). The value of N used in Eq. (3) can be determined from Eq. (4):

$$1 = \frac{8}{\pi^2} \sum_{n=0}^N \frac{1}{(2n+1)^2} + 0.05 \quad (4)$$

MR_{an} represents the analytically determined value calculated from Eq. (3). It is necessary to introduce the concept of a numerical counter i , which can have only integer values. The numerical counter i is defined for each value of the experimental pairs (MR_{exp}, t) . It starts from the value zero and increases by one until it reaches a final value, which is related to the last experimental pairs (MR_{exp}, t) . This concept enables the number of experimental pairs (MR_{exp}, t) from its first to its last value to be counted. In order to work properly, the program requires the initial value of the effective diffusion coefficient D_{eff} , and the ε value to be entered. Let the initial value of the effective diffusion coefficient D_{eff} be given the value of $1.0 \times 10^{-20} \text{ m}^2 \text{s}^{-1}$. Then, for each numerical counter value i , the program calculates the value χ^2 from Eq. (5):

$$\chi^2 = \sum_1^i (MR_{\text{exp},i} - MR_{\text{an},i})^2 \quad (5)$$

In the first cycle, $MR_{\text{an},1}$ is calculated according to Eq. (3) using the previously determined value of N and the initial value of D_{eff} . In the next cycle, the value of D_{eff} is doubled giving a new value for $MR_{\text{an},i}$ that is now used to calculate a new χ^2 according to Eq. (5). The program then compares the value of χ^2 obtained in the first cycle and the newly obtained χ^2 value. If the statement $\chi^2_{\text{first}} < \chi^2_{\text{second}}$ is satisfied, the program will continue the previously described cycle, otherwise the program will temporarily stop. Note: χ^2_{first} and χ^2_{second} refer to the last and the penultimate value of the cycle in which χ^2 is determined.

The last three values for D_{eff} and χ^2 are then recorded. The recorded D_{eff} interval is then divided into 100 parts. A hundredth part of this interval is defined as a step, s . The program commences the cycle again using the initial value for D_{eff} as $D_{\text{eff,third from end}} + s$. The cycle is repeated until the statement $\chi^2_{\text{first}} < \chi^2_{\text{second}} < 1.0 \times 10^{-10}$ is satisfied. In other words, the cycle is interrupted when the difference $\chi^2_{\text{second}} - \chi^2_{\text{first}}$ reaches 1.0×10^{-10} . The final D_{eff} value is then recorded. This value represents the finally calculated effective diffusion coefficient in $\text{m}^2 \text{ s}^{-1}$.

For long drying times, Eq. (1) can be transferred into Eq. (6):

$$MR = \frac{8}{\pi^2} \exp\left(\pi^2 \frac{D_{\text{eff}} t}{l^2}\right) \quad (6)$$

In a previous study,²¹ the effective diffusion coefficient was determined by the slope method from Eq. (7):

$$\ln\left(\frac{\pi^2 MR}{8}\right) = \ln(A) = -\pi^2 \frac{D_{\text{eff}}}{l^2} t \quad (7)$$

The case when there is shrinkage

For materials that show shrinkage during drying, Eq. (3) needs to be changed by the introduction of the expression $l_{(t)}$ into it. This expression represents the experimentally determined time dependence of the sample thickness. When this correction is entered, the previously described method for the determination of the effective diffusion coefficient can be used.

Two programs were designed to compute the effective diffusion coefficient. The first program did not include the shrinkage effect during drying into the computation algorithm while the second one did. Both programs were written in the Borland C program language on a standard Pentium IV computer (AMD 1200 MHz, 80GB HDD, 256 MB RAM memory) based of the previously described algorithm.

RESULTS AND DISCUSSION

Two models for predicting the drying behavior ($MR_{\text{an}}-t$ dependence) were obtained from these two programs. The first model did not include shrinkage (Model 1), while the second one (Model 2) did. Graphical views of the experimental and predicted drying behavior are presented in Figs. 1–3. The D_{eff} values obtained using the described programs and from the slope of Eq. (7) are presented in Table II.

From Table II, it can be clearly seen that in all experiments, the value of effective diffusion coefficient, D_{eff} , determined by Model 2 was lower than the value of the same coefficient determined by Model 1. On analyzing the experiments

1–8 (clay “Banatski Karlovac”), it can be seen that by increasing the velocity of the drying air from 1 to 3 m s⁻¹, the value of the effective diffusion coefficient also increased by up to 38 %.

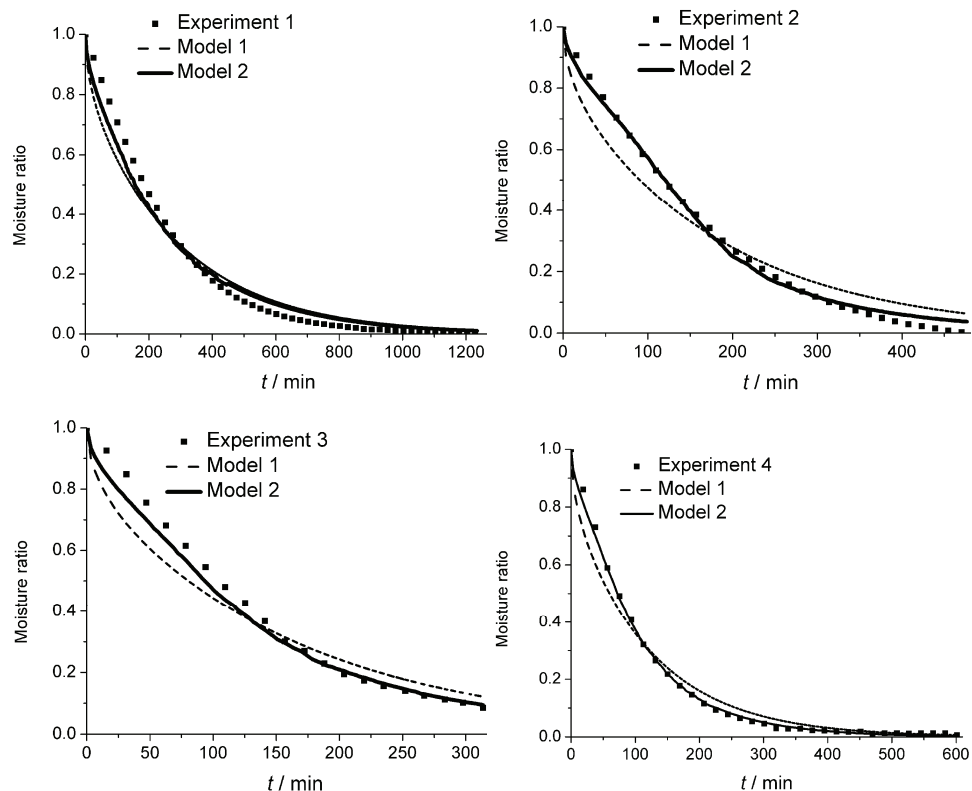


Fig. 1. Experimental and calculated moisture ratio vs. drying time for experiments 1–4.

The drying experiments from this and a previous study²¹ can be compared, because in both studies, the experimental conditions and the clay material (clay “Cirilkovac”) were the same.

A kinetic diagram analysis showed that the kinetic curves representing the model that neglects the shrinkage effect (Model 1) do not completely follow the configuration of the experimentally determined kinetic curves. Deviations of this model from the experimental drying curves are higher at the beginning of the drying process and after some time the deviations disappear. The moment of the disappearance matches the moment at which the sample continues to dry but without shrinkage. Drying kinetic curves of the model that includes shrinkage (Model 2) follow the configuration of the experimentally determined curves and their matching can be more than 95 %, as could be seen in experiments 2, 4 and 9–11. If minor deviations do exist, they are at the beginning of the drying process

and are most probably caused by the time interval which has to pass before stationary experimental conditions are fulfilled and the products are heated up to the required temperature in the dryer. The intersection point of the experimental drying curves and modeled drying curves is characterized as the critical point. The critical point is a characteristic kinetic parameter, which is important because it determines the moment after which the products no longer shrink.

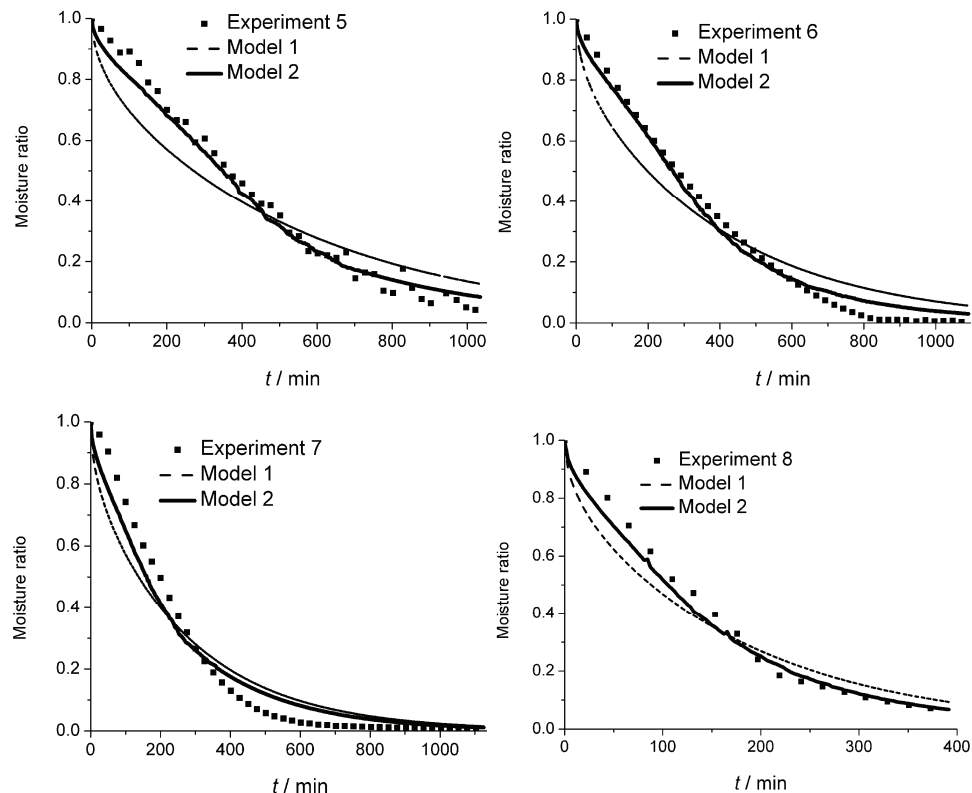


Fig. 2. Experimental and calculated moisture ratio vs. drying time for experiments 5–8.

From Table II, it could be concluded that value of the effective diffusion coefficient, D_{eff} determined using the model that included the sample shrinkage correction was lower than the corresponding value determined using the model that neglected sample shrinkage or the slope model. The data for D_{eff} determined by the slope model were higher than the data determined by the other two models. This is an expected result that is in agreement with the D_{eff} determination. This is additional proof that the model that included the shrinkage effect during drying gives more precise D_{eff} values. Only a few scientific papers^{8,11} in which the effective diffusion coefficients for masonry clay products were determined are available in the literature. In these papers, the D_{eff} values are in range of 10^{-7}

up to $10^{-12} \text{ m}^2 \text{ s}^{-1}$. This relatively large range for the D_{eff} values is connected with the different nature of the heavy clay and the different methods employed for their determination. The D_{eff} values presented in Table II lie below the previously mentioned range.

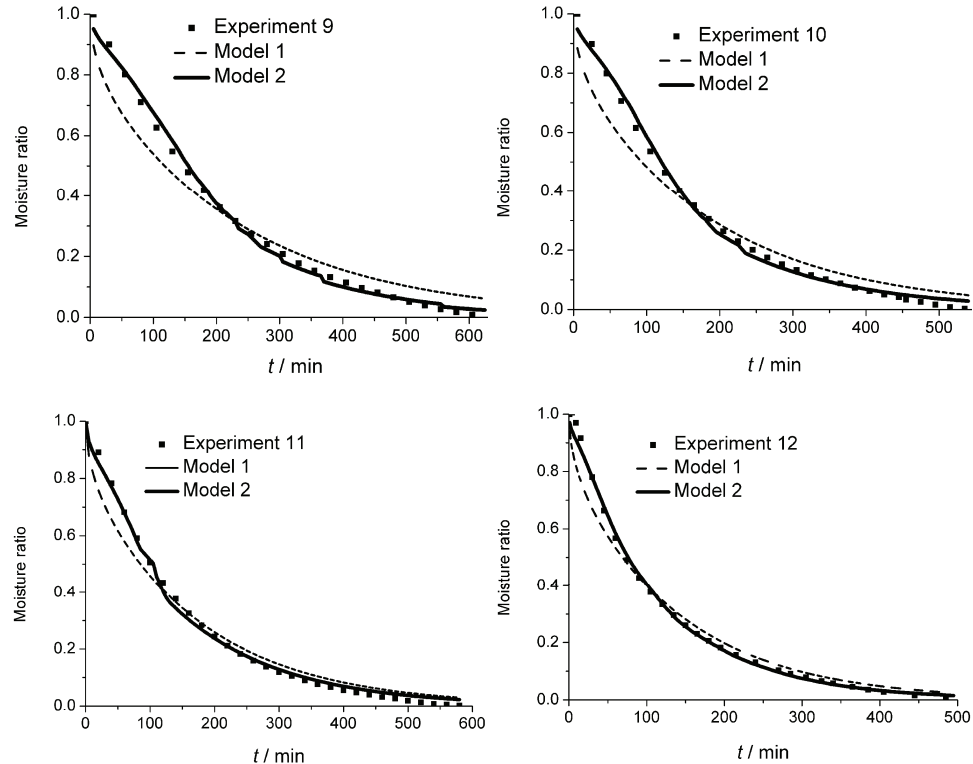


Fig. 3. Experimental and calculated moisture ratio vs. drying time for experiments 9–12.

TABLE II. Calculated values of the effective diffusion coefficient, $D_{\text{eff}} \times 10^9 / \text{m}^2 \text{ s}^{-1}$

Experiment	Model		
	1	2	Slope model
1	0.452	0.213	1.90
2	0.718	0.222	2.35
3	0.810	0.318	2.47
4	1.088	0.339	3.05
5	0.240	0.068	0.95
6	0.328	0.084	1.17
7	0.475	0.184	1.95
8	0.738	0.302	2.41
9	0.341	0.068	1.24
10	0.431	0.077	2.00
11	0.472	0.150	2.32
12	0.583	0.126	2.76

CONCLUSIONS

A new method and computer program for the determination of diffusion coefficients, which is based on the mathematical calculation of the Fick and Cranck Diffusion Equations, were developed. Two programs were designed to compute the effective diffusion coefficient. The first program (Model 1) did not include the shrinkage effect during drying in the computation algorithm, while the second one (Model 2) did. This was the first time in the mathematical modeling of the drying of masonry clay that a shrinkage correction was entered into the calculation step.

Kinetic diagram analysis showed that, irrespective of the nature the initial mineralogical composition of the clay, the kinetic curves representing the model that neglected the shrinkage effect (Model 1) did not fully follow the configuration of the experimentally determined kinetic curves, while in the case of the model that included shrinkage (Model 2), the resulting curves follows the experimental ones. From Figs. 1–3, it can be seen that the introduction of the shrinkage correction into Eq. (2) was entirely justified. The determined values of the effective diffusion coefficient were lower than the value that could be found in the literature. The values of the effective diffusion coefficient determined using the model that includes shrinkage were lower than the values determined using the model which neglected shrinkage or the values obtained using the slope method. The intersection point of the experimental drying curves and the modeled drying curves is characterized as the critical point.

Acknowledgement. This paper was realized under the project III 45008, which was financed by the Ministry of Education and Science of the Republic of Serbia.

ИЗВОД

ОДРЕЂИВАЊЕ ЕФЕКТИВНОГ КОЕФИЦИЈЕНТА ДИФУЗИЈЕ ПРИЛИКОМ СУШЕЊА УЗОРАКА ОД ГЛИНЕ

МИЛОШ ВАСИЋ¹, ЗАГОРКА РАДОЈЕВИЋ¹ и ЖЕЉКО ГРБАВЧИЋ²

¹Институција за испитивање мајтеријала, Булевар војводе Мишића 43, 11000 Београд

²Технолошко-металуршки факултет, Универзитет у Београду, Карнеџијева 4, 11000 Београд

Циљ овог рада је да се на примеру две опекарске глине са различитих локалитета одреди ефективни кофицијент дифузије на основу експериментално снимљених кривих сушења. Развијен је метод и направљена су два компјутерска програма за одређивање овог кофицијента, који се заснивају на математичком решавању Фикове, односно Кранкове дифузионе једначине. По први пут узето је у разматрање и скупљање опекарских производа у току сушења а одговарајућа корекција је унета у прорачун. Резултати показују да су вредности ефективног кофицијента дифузије одређени компјутерским програмима (са корекцијом и без корекције на скупљање опекарских производа) реда величине које су наведене у литератури за друге врсте опекарских глина. На основу математичким путем прогнозираних вредности ефективног кофицијента дифузије констатовано је, да без обзира на полазни минералошки састав опекарске сировине, постоји 90 % слагања прогнозираних

кривих сушења са експериментално снимљеним кривима сушења. За случај када је уведена у прорачуне и корекција на скупљање опекарских производа ово слагање је још веће.

(Примљено 17. јула, ревидирано 10. октобра 2011)

REFERENCES

1. J. Crank, *The mathematics of diffusion*, II ed., Oxford University Press, London, 1975
2. G. Efremov, T. Kudra, *Drying Technol.* **22** (2004) 2273
3. I. I. Ruiz-Lopez, M. A. Garcia-Alvarado, *J. Food Eng.* **79** (2007) 208
4. L. M. Batista, C. A. da Rosa, L. A. Pinto, *J. Food Eng.* **81** (2007) 127
5. J. A. Hernandez, G. Pavon, M. A. Garcia, *J. Food Eng.* **45** (2000) 1
6. K. J. Park, T. H. Ardito, A. P. Ito, K. J. B. Park, R. A. de Oliveira, M. Chiorato, *Drying Technol.* **25** (2007) 1313
7. G. I. Efremov, *Drying Technol.* **20** (2002) 55
8. S. Chemkhi, F. Zagrouba, *Desalination* **185** (2005) 491
9. D. Mihoubi, F. Zagrouba, M. Ben Amor, A. Bellagi, *Drying Technol.* **20** (2002) 465
10. F. Zagrouba, D. Mihoubi, A. Bellagi, *Drying Technol.* **20** (2002) 1895
11. A. Sander, D. Skansi, N. Bolf, *Ceram. Int.* **29** (2003) 641
12. S. Tomas, D. Skansi, M. Sokele, *Ceram. Int.* **20** (2004) 9
13. Ž. Lalić, M. Arsenović, Đ. Janacković, M. Vasić, Z. Radojević, *Rom. J. Mat.* **39** (2009) 175
14. N. Hamdami, J.-Y. Monteau, A. Le Bail, *J. Food Eng.* **62** (2004) 85
15. G. Efremov, M. Markowski, I. Bialobrzewski, M. Zielinska, *Int. Commun. Heat Mass Transfer* **35** (2008) 1069
16. , *Handbook of Industrial Drying*, III ed., A. S. Mujumdar, Ed., CRC Press, Boca Raton, FL, 2006
17. W. P. da Silva, J. W. Pecker, C. M. D. P. S. e Silva, D. D. P. S. e Silva, *J. Food Eng.* **95** (2009) 298
18. W. P. da Silva, J. W. Pecker, C. M. D. P. S. e Silva, J. P. Gomes, *J. Food Eng.* **98** (2010) 302
19. L. Hassini, S. Azzouz, R. Peczalski, A. Belghith, *J. Food Eng.* **79** (2007) 47
20. A. O. Dissa, H. Desmorieux, J. Bathiebo, J. Kouliadiati, *J. Food Eng.* **88** (2008) 429
21. Ž. Lalić, *M.Sc. Thesis*, Faculty of Technology and Metallurgy, University of Belgrade, Belgrade, 2006.



Decolorization of Reactive Black 5 using a dielectric barrier discharge in the presence of inorganic salts

BILJANA P. DOJČINOVIC^{1*}, GORAN M. ROGLIĆ², BRATISLAV M. OBRADOVIĆ³,
MILORAD M. KURAICA³, TOMISLAV B. TOSTI^{2#}, MARIJANA D. MARKOVIĆ^{2#}
and DRAGAN D. MANOJLOVIĆ²

¹Institute of Chemistry, Technology and Metallurgy, Center of Chemistry, Studentski trg
12–16, 11000 Belgrade, Serbia, ²Faculty of Chemistry, University of Belgrade,
P. O. Box 51, 11058 Belgrade, Serbia and ³Faculty of Physics, University
of Belgrade, P. O. Box 368, 11000 Belgrade, Serbia

(Received 29 June, revised 1 August 2011)

Abstract: Inorganic salts improve the coloration of textiles, which increases the pollution load of dye-house effluent in general. Decolorization of the reactive textile dye C.I. Reactive Black 5 was studied using Advanced Oxidation Processes (AOPs) in a non-thermal plasma reactor, based on the coaxial water falling film Dielectric Barrier Discharge (DBD). The initial dye concentration in the solution was 40.0 mg L⁻¹. The effects of the addition of different high concentrations of inorganic salt (NaCl, Na₂SO₄ and Na₂CO₃) on the degree of decolorization were studied. The dye solution was recirculated through the DBD reactor with an applied energy density of 45.0–315 kJ L⁻¹. The influence of residence time was investigated after 5 min and 24 h of plasma treatment. Decolorization of the dye was monitored spectrophotometrically. The pH value and the conductivity of the dye solution were measured after each recirculation. The most effective decolorization of over 90 % was obtained with the addition of NaCl (50 g L⁻¹) with an applied energy density of 135 kJ L⁻¹ and after a residence time of 24 h of plasma treatment. Decolorization of the solutions containing inorganic salts Na₂SO₄ and Na₂CO₃ were lower than for the solution without salt.

Keywords: decolorization; Reactive Black 5; inorganic salt; plasma treatment; dielectric barrier discharge; DBD reactor.

INTRODUCTION

Synthetic organic dyes are widely used as colorants in different industries, such as in the textile, leather tanning, paper, plastics, color photography, pharmaceutical, food and cosmetic industries. More than 0.7 million tons of synthetic

* Corresponding author. E-mail: bmatic@chem.bg.ac.rs

Serbian Chemical Society member.

doi: 10.2298/JSC110629179D

organic dyes are produced annually worldwide. It is reported that there are over 10,000 commercially available dyes that are classified by their application fields, namely acid, reactive, disperse, vat, metal complex, mordant, direct, basic and sulfur dyes.¹ Textile manufacture is one of the largest industrial producers of wastewater, which have high concentrations of organic and inorganic compounds and strong color, caused by residual dyes that were not fixed to the fibers during the dyeing process. Wastewaters from textile manufacture are characterized by highly fluctuating pH values, high chemical oxygen demand (COD), large amounts of non-biodegradable compounds, the presence of toxic substances, high temperature and large amounts of salt (ionic strength). Reactive dyes have been identified as the most environmentally problematic compounds in textile dye effluents. Research on textile effluent decolorization has been mostly focused on reactive dyes for several reasons. Firstly, reactive dyes are intensively used due to their superior performance and have an increasing market share, about 20–30 % of the total dye market, as they are used to dye cotton that contributes slightly less than half to the world's fiber consumption. Secondly, they are very soluble and approximately 10–15 % of the weight of applied reactive dyes is discharged from the dye houses. In addition, parts of the applied reactive dyes are wasted due to dye hydrolysis in the alkaline dye bath. Thirdly, conventional wastewater treatment plants, which rely on sorption and aerobic biodegradation, have a low removal efficiency for reactive and other anionic soluble dyes. Consequently, they lead to colored waterways, and public complaints, with the pollutants being transferred from one phase to another rather than being destroyed.^{2–7} Azo dyes constitute a major part (about 60 %) of all commercial reactive dyes employed in a dyeing process in the textile industry.⁸

Advanced oxidation processes (AOPs) are under investigation as alternative means of overcoming the limitations of the conventional techniques. Advanced oxidation processes were developed and used as potentially powerful methods capable of transforming pollutants into harmless substances. AOPs are based on the generation of very reactive non-selective transient oxidizing species, such as the hydroxyl radicals ($\cdot\text{OH}$) which were identified as the dominant oxidizing species, that attack organic compounds with high reaction rates.⁹ Amongst the many techniques employed in the AOP approach to industrial wastewater treatment are UV photolytic oxidation, the Fenton process, the photo-Fenton process, the ozonation process, sonolysis, the photocatalytic approach, radiation, supercritical water oxidation^{10,11} and non-thermal plasma technology^{12–17} induced degradation of organic pollutants. A literature survey revealed that there are a few studies on the effect of inorganic salts on the decolorization of textile dyes using advanced oxidation processes.^{18–21}

In the present study, decolorization was based on the dielectric barrier discharge (DBD) reactor, which is a typical non-equilibrium high-pressure AC gas

discharge. Various discharges in water were described in a review article by Bruggeman and Leys.²² A DBD is obtained between two electrodes, one of which at least is covered with a dielectric, by application of a high voltage AC to the electrodes. The dielectric is the key factor for the proper functioning of the discharge. It limits the charge transported in the discharge, *i.e.*, limits the current flow to the system, and distributes the discharge almost uniformly over the entire electrode area. A DBD is an excellent source of high-density energetic electrons, with energy between 1–10 eV. In humid air, a DBD can produce UV light and many reactive species, such as free electrons, negative ions, positive ions, uncharged short-lived radicals, H₂O₂ and O₃.^{23,24} It was shown that the principle reactive species involved in the degradation of organic compounds are •OH and H₂O₂.²⁵ •OH, especially, is known to play an important role in the degradation of organic compounds since its oxidation potential is higher than those of atomic oxygen and ozone.

In the present study, the decolorization of the commercial reactive azo dye C.I. Reactive Black 5 was studied using an advanced oxidation process (AOP) in a non-thermal plasma reactor based on coaxial dielectric barrier discharge (DBD).²⁶ A very similar coaxial DBD plasma reactor to that used in this research was recently developed for the treatment of various aqueous solutions,²⁷ and successfully tested for the removal of phenols from wastewater.^{28,29} An azo dye was chosen for study as azo dyes are the major colorants in the textile industry; they provide a wide spectrum of colors with outstanding colorfastness. However, azo dyes are the most toxic, mutagenic and carcinogenic of commercial dyes.³⁰

Initial dye concentration in the treated water solution was 40.0 mg L⁻¹. The effects of various conditions, such as applied energy density (45.0–315 kJ L⁻¹) and the presence high concentrations of an inorganic salt, *i.e.*, NaCl, Na₂SO₄ or Na₂CO₃, were studied.

EXPERIMENTAL

Materials

The textile dye, Reactive Black 5, was purchased from Clariant (Switzerland) and used without further purification. Reactive Black 5 is a dissociated anionic sulfonate in aqueous solution. The general characteristics of Reactive Black 5 are summarized in Table I. Other chemicals, purchased from Merck (Germany), were of analytical grade. All solutions were prepared using deionized water with conductivity between 1.0 and 1.5 µS cm⁻¹.

Instrument

The employed coaxial DBD was designed as an atmospheric non-thermal plasma reactor for the treatment of various water solutions.²⁶ In this reactor, water forms a falling film that is in direct contact with the plasma. The coaxial DBD is a source of a wide range of reactive species, created in both the gas and liquid phase. This discharge is able to produce O₃, H₂O₂, •OH and other active species. Ozone is considered as one of the most powerful molecule species because of its long lifetime and high oxidation potential. In such a discharge design, radicals are transferred from the plasma into the liquid phase, where reactions with pollutants occur.

cur. In addition, this discharge produces UV radiation, ions (*e.g.*, OH⁻, O₂⁻, O[·], O₂⁺, N₂⁺, N⁺, O⁺) and electrons. A schematic diagram of the experimental setup is shown in Fig. 1a. The cylindrical reactor is made of Pyrex glass with inner diameter of the tube 27.0 mm and length of 600 mm. The outer electrode is made of aluminum foil of length 400 mm glued to the outer side of the glass tube. The inner electrode is a glass cylinder with a diameter of 20.0 mm that is silver-plated on the inner side, Fig. 1a. The barrier discharge is generated between the inner glass and the outer glass tubes. When the discharge source works as a falling film reactor, water flows up through a vertical hollow glass tube and flows down making a thin dielectric film over the electrode, Fig 1a. The employed power supply was a high voltage transformer, which was fed by a frequency inverter, which allows variation of the sinusoidal voltage frequency up to 500 Hz. The frequency for the plasma reactor was set at the determined optimal value, 200 Hz. The discharge was generated within the 3.5 mm gap between the glass and the water layer by applying a voltage of 17 kV. To increase the total flow of the treated solution, three discharges are connected in parallel. The plug-in power for this system of discharges was 150 W.

TABLE 1. General characteristics of Reactive Black 5

Chemical structure	
Molecular formula	C ₂₆ H ₂₁ N ₅ Na ₄ O ₁₉ S ₆
Molecular weight	991.82
Synonyms	C.I. Reactive Black 5, Reactive Black 5, Reactive Black B, Remazol Black 5, Remazol Black B, Drimaren Black R/K-3B
C.I. (<i>Color Index</i>) name	C.I. Reactive Black 5
C.I. (<i>Color Index</i>) number	C.I. 20505
Application class	Cotton
Chemical class	Azo
CAS registry number	17095-24-8
λ _{max} / nm	590

A solution of dye was pumped to the top of the reactor through the inner electrodes using a peristaltic pump. From the top of the inner electrode, the solution flows down in a thin layer over the electrode. After treatment, the solution was collected in a reservoir at the bottom of the reactor. The total flow rate through the three parallel DBD reactors was 210 mL min⁻¹. The collected solution was introduced through the reactor for the next treatment in such way that the presently treated amount of solution was never mixed with the amount of solution treated in the previous pass. An energy density of ≈45 kJ L⁻¹ per one pass through the reactor was introduced in the solution. The introduced energy density was increased using multiple passes through the reactor. Each solution was recirculated seven times. In each series of experiments, the treatment was started with 2 L of dye solution (of a certain concentration and specified pH value). After each recirculation, 100 ml of the solution was sampled for analysis

after of 500 ml had passed through the DBD reactor. Each subsequent recirculation was realized immediately after completion of the previous one.

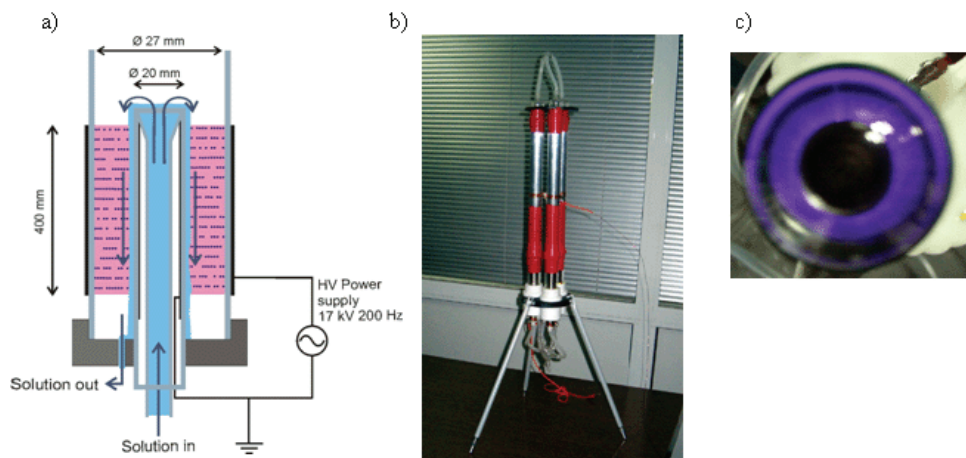


Fig. 1. a) Schematic of a coaxial DBD. b) Photo of three parallel-connected DBDs. c) Photo of the discharge viewed from the top. Dimensions: inner glass barrier (diameter 20.0 mm, length 500 mm, thickness 1.5 mm); outer glass barrier (diameter 30.0 mm, thickness 1.5 mm, length 600 mm); outer metal foil electrode (diameter 30.0 mm, length 400 mm).

Methods of analysis

The capability of the plasma reactor for decolorization of azo dye Reactive Black 5 was tested in triplicate. Each color solution was prepared by dissolving the commercial dye without preceding purification in deionized water. In all cases, water samples containing 40.0 mg L⁻¹ of dye were passed from one to seven times through the discharge. The decolorization efficiency is defined as the percent decrease in absorbance according to Eq. (1):

$$\text{Decolorization (\%)} = 100 \frac{A_0 - A}{A_0} \quad (1)$$

where A_0 is the absorbance at the maximum absorption wavelength (λ_{\max}) of the initial dye solution and A is the absorbance at the maximum absorption wavelength of the dye solution after the plasma treatment. The absorbance measurements were performed using a UV–Visible Cintra 6 spectrometer (GBC Scientific Equipment, Australia) 5 min and 24 h after the plasma treatment.

The effects of the addition of inorganic salts (NaCl, Na₂SO₄ and Na₂CO₃) on the decolorization efficiency of Reactive Black 5, $c_0 = 40.0$ mg L⁻¹, during the plasma treatment was tested. The concentrations of tested salts were: NaCl, 10 and 50 g L⁻¹, Na₂SO₄, 10 and 50 g L⁻¹ and Na₂CO₃, 0.1, 10 and 50 g L⁻¹. For comparison, the efficiency of decolorization without added salt was also determined. Decolorization efficiency was monitored 5 min and 24 h after the plasma treatment.

A solution of sodium chloride of concentration of 50 g L⁻¹ in the absence of dye was treated in the same way. After 5 min of plasma treatment, the concentrations of hypochlorite and hydrogen peroxide in the solution were determined. Ion chromatography was used to assay the appearance and quantity of hypochlorite formed. For this purpose, a Dionex ICS-3000

chromatographic set-up consisting of a single pump, a conductivity detector (ASRS ULTRA II (4 mm), recycle mode), an eluent generator (potassium hydroxide) with a Chromeleon® Chromatography Workstation and Chromeleon 6.7 Chromatography Management Software was employed. All the separation was performed using IonPac AS15 Analytical, 4 mm×250 mm and IonPac AG15 Guard, 4 mm×50 mm columns. The flow rate of the mobile phase was 1.20 mL min⁻¹ and the composition of mobile phase was changed during analysis in following order 0–15 min, 10 mM KOH; 15–25 min, 10–45 mM KOH; 25–26 min, 45 mM KOH; 26–31 min, 45–10 mM KOH; 31–36 min, 10 mM KOH. In addition, the following conditions were applied: column temperature 30 °C, conductivity cell temperature 35 °C and the suppressor current was 134 mA. The backpressure was ≈18 MPa.

A standard solution of hypochlorite was prepared fresh daily by diluting ≈15 % sodium hypochlorite solution, analytical grade (Carlo Erba, Italy), which was standardized by iodimetry.

The concentration of hydrogen peroxide was determined using the reaction of H₂O₂ with titanyl ions.³¹ The absorbance was measured at $\lambda = 407$ nm.

In addition, the pH of each solution was determined after each recirculation. The pH value was measured using a pH monitor (Microcomputer pH-vision 6071, JENCO Electronics Ltd., Taiwan). Five minutes after each recirculation, the conductivity of the treated solutions was determined using a Cond 330i/SET meter, WTW Wissenschaftlich, Germany.

RESULTS AND DISCUSSION

Given that different salts are added to the bath in textile industries in order to improve color fastness, the effects of Cl⁻, CO₃²⁻, HCO₃⁻, SO₄²⁻, H₂PO₄⁻ and NO₃⁻ on the dye decolorization rates were also investigated as some of these anions are thought to act as scavengers of •OH, thereby reducing their effective concentration in the solution. The addition of inorganic salts to the dye bath increases the pollution load of the effluent generated and has an effect on various effluent treatment processes.^{46–48} The influence of sodium sulfate, sodium chloride and sodium carbonate on DBD efficiency was studied.

The effect of the addition of NaCl

The influence of the sodium chloride concentration on the decolorization of Reactive Black 5 ($c_0 = 40.0$ mg L⁻¹) was measured as a function of the applied energy density. Two initial concentrations (10 and 50 g L⁻¹ NaCl) and the solution without added salt were examined. The results are shown in Fig. 2. The introduced energy was increased by multiple passes. For the dye solution without salt, the decolorization value measured 24 h after one pass through the DBD reactor reached the same value as the decolorization obtained in two passes (*i.e.*, an applied energy of 90 kJ L⁻¹) and measured after 5 min, Figs. 2 and 3. In all cases, decolorization after the first treatment (*i.e.*, 45 kJ L⁻¹) measured 5 min after passing through the DBD reactor was 30–45 % while 24 h after the plasma treatment, the decolorization had increased to 40–60 %, depending on the initial composition. This indicated that the effect of the plasma treatment could be intensified in aqueous solutions by the primary products formed during water treat-

ment. According to Magureanu *et al.*,⁴⁰ various oxidizing species are formed in plasma-treated aqueous solutions that contribute to the decomposition of organic dyes, but most of these oxidizers have very short lifetimes. Therefore, they can only react with the dye molecules while the solution flows through the DBD reactor. Ozone and hydrogen peroxide are the only oxidizers generated in the plasma, which are stable enough to react with the dye molecules outside of the plasma reactor, *i.e.*, later after the treatment. Reactions after plasma treatment can be partly attributed to reactions that are similar to the wet air oxidation and radiation. These reactions occur through the formation of alkyl and alkyl peroxy radicals, and hydroperoxides, with the latter being responsible for the auto-catalytic decomposition of organic compounds, as shown by Gözmen *et al.*³² and Rauf *et al.*³³

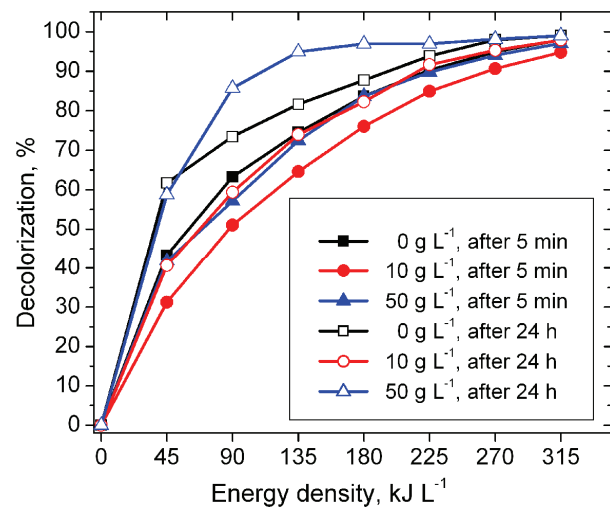


Fig. 2. Effect of the addition of NaCl on the efficiency of the decolorization of Reactive Black 5 ($c_0 = 40.0 \text{ mg L}^{-1}$, 5 min and 24 h after treatment).

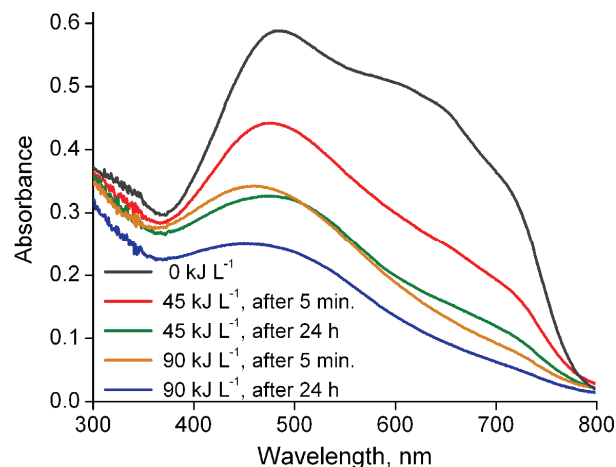


Fig. 3. The absorbance spectra of Reactive Black 5 without salt, recorded before and 5 min and 24 h after plasma treatment with an energy density 45 and 90 kJ L^{-1} .

For the continued process of decolorization during the residence time of the plasma-treated dye solution, molecular species (O_3 and H_2O_2) are primarily responsible, and possibly long-lived free radicals formed during plasma treatment. In the treated deionized water, the contents of O_3 and H_2O_2 were quantified 5 min after the treatment.^{26,28}

For all the introduced energy densities, 5 min after plasma treatment, the addition of NaCl (10 and 50 g L⁻¹) reduced the effect of decolorization as compared to the solution without salt. Higher reductions in decolorization (approximately 10 %) were observed in the solution with 10 g L⁻¹ salt. After 24 h of plasma treatment, with an applied energy density higher than 45 kJ L⁻¹, the resulting decolorization was largest for solution containing 50 g L⁻¹ NaCl. In this solution, with applied energy densities of 90 and 135 kJ L⁻¹, the decolorization was higher by 13 % compared to the solution with no added salt. In addition, the shape functions of the decolorization of the dye solution containing 50 g L⁻¹ NaCl, measured after 24 h of plasma treatment were different compared to all others. This significant increase in decolorization in this system can be explained by the formation of hypochlorite from the chloride ions during the plasma treatment. In order to confirm this explanation, the concentrations of hypochlorite and hydrogen peroxide in treated solution of NaCl (concentration: 50 g L⁻¹) were measured. During the first pass, the maximal concentration of hypochlorite of 3.46 mg L⁻¹ for 45 kJ L⁻¹ was obtained and with increasing energy density, its concentration decreased (finally, the concentration dropped to below the detection limit). On the other hand, the concentrations of hydrogen peroxide gradually increased and for an energy density of 315 kJ L⁻¹, a concentration of 6.52 mg L⁻¹ was attained. A possible explanation is that the chloride oxidation reaction was faster than hydrogen peroxide formation but it appeared that hypochlorite further reacted with the formed hydrogen peroxide, Eq. (2):



Hence, these two types of oxidation species cannot simultaneously exist in the solution.

Changes of the visible spectra of Reactive Black 5 solutions ($c_0 = 40.0$ mg L⁻¹) without salt after the plasma treatment for introduced energy densities of 45 and 90 kJ L⁻¹ are shown in Fig. 3. Spectra were recorded 5 min and 24 h after plasma treatment. The changes of the visible spectra of dye could be used to understand the dye degradation during the treatments. It can be seen that the absorbance was reduced over the whole spectra with increasing introduced energy. The decrease of absorbance in the visible part of the spectrum indicates the loss of the conjugated system in the compound.

A photograph of solutions of Reactive Black 5 ($c_0 = 40.0 \text{ mg L}^{-1}$) without the addition of salt 24 h after plasma treatment for energy densities from 0 to 315 kJ L^{-1} with an increment of 45 kJ L^{-1} are shown in Fig. 4.

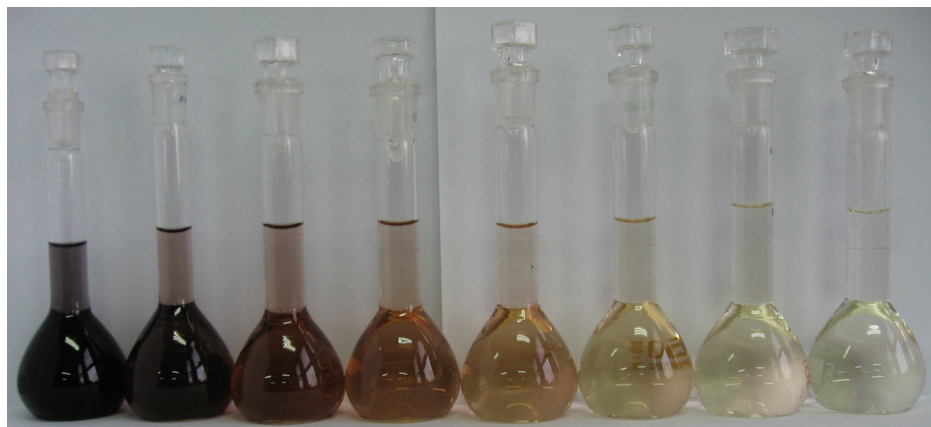


Fig. 4. Solutions of Reactive Black 5 ($c_0 = 40.0 \text{ mg L}^{-1}$) 24 h after of plasma treatment (energy density 0–315 kJ L^{-1} with increment of 45 kJ L^{-1} , from left to right).

The effect of the addition of Na_2SO_4

Large amounts of sulfate in the dye bath are generally essential for successful dyeing with reactive dyes, which results in high concentrations of sulfate in the effluent. To examine the effect of the Na_2SO_4 concentration on decolorization efficiency, solutions with different amounts of this salt were plasma treated. The color removal efficiency for an introduced energy density of 315 kJ L^{-1} decreased from 99 to 83 and 38 % after 24 h residence time with increasing Na_2SO_4 concentration from 0 to 10 and 50 g L^{-1} , respectively (Fig. 5). The highest concentration of salt (50 g L^{-1}) had the most negative effect on the decolorization. A possible explanation is that at high concentrations, the excess SO_4^{2-} reacts with the hydroxyl radicals to generate $\text{SO}_4^{\cdot-}$, which is less reactive than a hydroxyl radical,³⁴ Eq. (3). Thus, the excess SO_4^{2-} reduces the effect of the hydroxyl radicals:



The excess SO_4^{2-} reduces the photodegradation of the dye since $\text{SO}_4^{\cdot-}$ ($E^\ominus = 2.6 \text{ V}$) is less reactive than $\cdot\text{OH}$ ($E^\ominus = 2.7 \text{ V}$).³⁴

It is known that $\text{SO}_4^{\cdot-}$ and $\cdot\text{OH}$ react with organic compounds mainly by three mechanisms: hydrogen abstraction, hydrogen addition and electron transfer.³⁵ In general, $\text{SO}_4^{\cdot-}$ is more likely to participate in electron transfer reactions than $\cdot\text{OH}$, which is more likely to participate in hydrogen abstraction or addition reactions,^{36,37} and hence reactivity of $\cdot\text{OH}$ is less selective than $\text{SO}_4^{\cdot-}$.

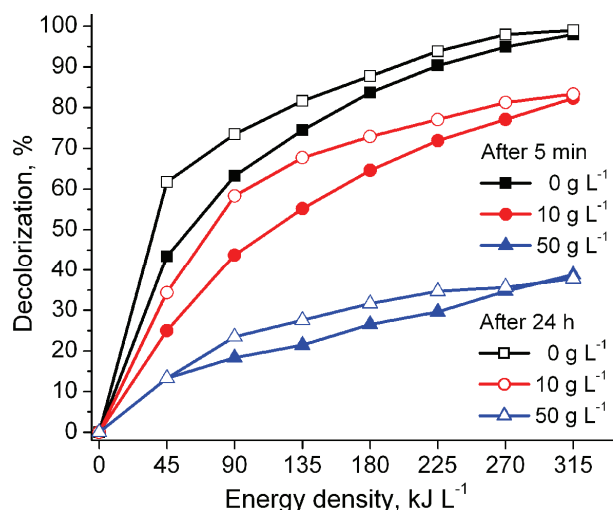


Fig. 5. The effect of adding Na_2SO_4 on the decolorization efficiency of Reactive Black 5 ($c_0 = 40.0 \text{ mg L}^{-1}$, 5 min and 24 h after treatment).

The effect of the addition of Na_2CO_3

The effect of addition of different concentrations of Na_2CO_3 on decolorization efficiency of Reactive Black 5 ($c_0 = 40.0 \text{ mg L}^{-1}$) is shown in Fig. 6. The tested concentrations of Na_2CO_3 were 0.1, 1 and 10 g L^{-1} . The results showed that the decolorization was inhibited in the presence of Na_2CO_3 in a dose dependent manner. Increasing amounts of salt in the dye solution resulted in decreasing efficiency of decolorization, *i.e.*, for an energy density of 315 kJ L^{-1} , on increasing the salt concentration from 0 to 10 g L^{-1} , the percentage decolorization decreased from 99 to 88 %. In addition, in the presence of Na_2CO_3 , the effect of increased decolorization 24 h after of plasma treatment was not ob-

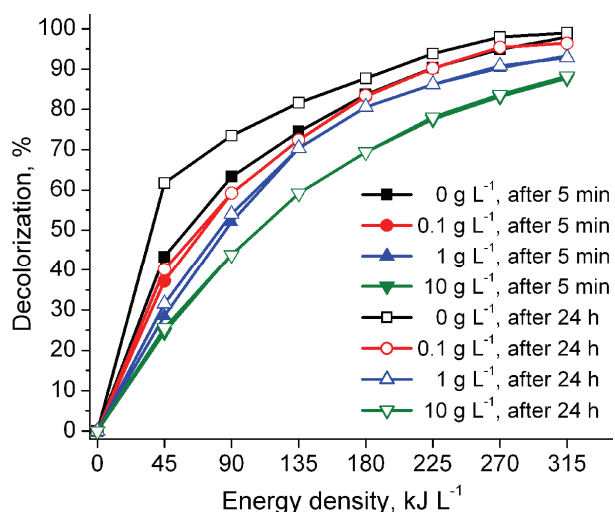


Fig. 6. The effect of addition of Na_2CO_3 on the decolorization efficiency of Reactive Black 5 ($c_0 = 40.0 \text{ mg L}^{-1}$, 5 min and 24 h after treatment).

served (contrary to the studied systems without sodium carbonate). Additionally, with increasing added Na_2CO_3 , the lower the efficiency of decolorization after 24 hours was more pronounced in comparison with the staining solution without salt the lower energy density, when the lowest energy was applied. Moreover, in the literature, CO_3^{2-} and *n*-butanol were used as $\cdot\text{OH}$ scavengers.³⁸

Effect of the salts on the pH during plasma treatment of the dye

The variations of pH values of the solutions containing the employed inorganic salts during the treatment process are shown in Fig. 7. The curves show that the pH value decreased considerably for all the tested systems, except for the solutions of the dye to which 1 and 10 g L⁻¹ Na_2CO_3 had been added. A certain contribution to the pH variation during the plasma treatment derived from sulfuric acid and carboxylic intermediates, produced from the degradation of dyes. The variation of pH value is probably caused by several specific acidic substances, such as nitric acid and nitrous acid, which are produced during the discharge process in air.²⁶ It can be concluded that the addition of Na_2CO_3 ($> 1\text{ g L}^{-1}$) had sufficient neutralization potential, so that the decolorization reaction in these systems during the subsequent recirculation was realized at almost the same pH (buffer system). Since the decolorization shape functions in all tested systems were very similar, it could be concluded that the pH of the solution during the plasma treatment did not affect the decolorization reaction.

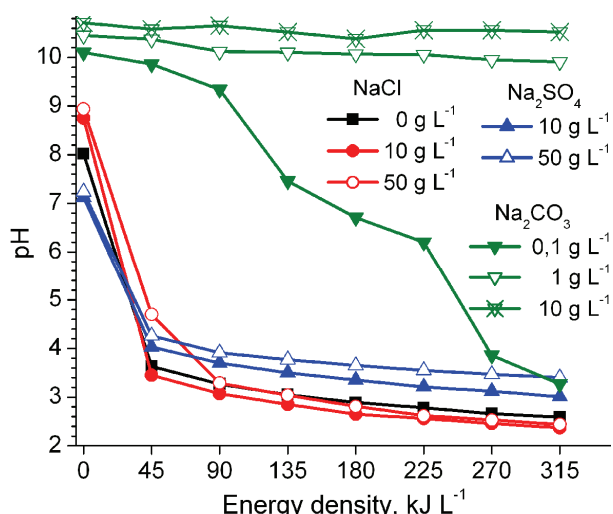


Fig. 7. The change in the pH values during the reaction process without and with salt after each recirculation (Reactive Black 5, $c_0 = 40.0 \text{ mg L}^{-1}$).

Effect of the salts on conductivity during plasma treatment of the dye

The variations in the conductivity of the solutions containing the examined inorganic salts during the treatment process are shown in Fig. 8. For the highest concentration of inorganic salts that were tested (1, 10 and 50 g L⁻¹), the

conductivity of the solution during the plasma treatment ($0\text{--}315 \text{ kJ L}^{-1}$) increased by about 30 %. The conductivity of the dye solution without salt during treatment increased 56 times, while in the system with $0.1 \text{ g L}^{-1} \text{ Na}_2\text{CO}_3$, the conductivity doubled. Based on these increases in conductivity in the matrix of inorganic salts during the plasma treatment, it could be concluded that the increases in the conductivity arose from the increase in the number of ionic species (organic intermediates, nitrates and nitrites that originated from the nitrogen in the air).

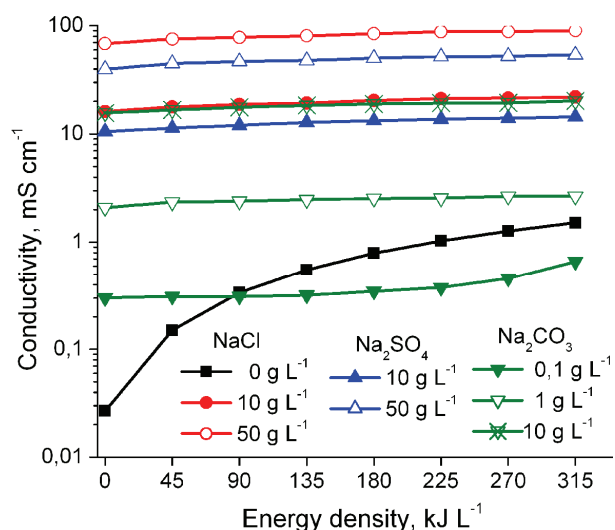


Fig. 8. The change in conductivity during the reaction process without and with salt after each recirculation (Reactive Black 5, $c_0 = 40.0 \text{ mg L}^{-1}$).

CONCLUSIONS

The results indicated that decolorization of the dyes was significantly limited in the presence of salts. Increasing the concentrations of inorganic salts in the water reduced the efficiency of decolorization of the dye, to varying degrees depending of the salt used. The most effective decolorization, of over 90 % was obtained with addition of $50 \text{ g L}^{-1} \text{ NaCl}$ with applied energy density of 135 kJ L^{-1} 24 h after plasma treatment. Decolorization in the presence of the inorganic salts Na_2SO_4 and Na_2CO_3 was lower than the solution without salt. The increased decolorization with addition $50 \text{ g L}^{-1} \text{ NaCl}$ was explained by the formation of hypochlorite from the chloride ions during the plasma treatment.

Finally, studies on dye oxidation in saline systems are not frequent; however, wastewater from the textile industries may contain appreciable levels of salts, which could impair the treatment processes, as confirmed in this work.

Acknowledgement. This work is supported by the Ministry of Education and Science of the Republic of Serbia.

ИЗВОД

ОБЕЗБОЈАВАЊЕ РЕАКТИВНОГ ЦРНОГ 5 ПОМОЋУ ДИЕЛЕКТРИЧНОГ БАРИЈЕРНОГ ПРАЖЊЕЊА У ПРИСУСТВУ НЕОРГАНСКИХ СОЛИ

БИЉАНА П. ДОЛЧИНОВИЋ¹, ГОРАН М. РОГЛИЋ², БРАТИСЛАВ М. ОБРАДОВИЋ³, МИЛОРАД М. КУРАИЦА³, ТОМИСЛАВ В. ТОСТИ², МАРИЈАНА Д. МАРКОВИЋ² и ДРАГАН Д. МАНОЛОВИЋ²

¹Институт за хемију, технологију и металургију, Центар за хемију, Студенички тир 12–16, 11000 Београд,

²Хемијски факултет, Универзитет у Београду, 11000 Београд и ³Физички факултет, Универзитет у Београду, 11000 Београд

Неорганские соли побољшавају бојење текстила. Повећана концентрација соли у отпадној води која потиче из текстилне индустрије додатно оптерећује отпадну воду у целини. У оквиру овог рада проучавано је обезбојавање реактивне текстилне боје реактивно црно 5 користећи унапређени оксидациони процес (AOP) помоћу коаксијалног реактора на бази нетермичке плазме. Реактор ради на принципу диелектричног баријерног пражњења (DBD), при чему је један слој диелектрика танак слој третирање воде који се константно обнавља (проточни тип реактора). Почетна концентрација боје у третираном раствору је била 40,0 mg L⁻¹. Проучаван је утицај различитих високих концентрација неорганских соли (NaCl, Na₂SO₄ и Na₂CO₃) на степен обезбојења. Раствор боје је седам пута рециркуласан кроз DBD реактор, што одговара примењеној густини енергије од 45 до 315 kJ L⁻¹. Проценат обезбојења раствора боје је мерење после 5 min и после 24 h од третмана плазмом. Обезбојавање боје је праћено помоћу спектрофотометријског мерења. После сваке рециркулације раствора боје мерење су промена pH вредности и проводљивост раствора. Најефикасније обезбојење од преко 90 % добијено је у систему са додатком 50 g L⁻¹ NaCl, при примењеној густини енергије од 45 kJ L⁻¹ и после 24 сата од плазма третмана. Обезбојења раствора боје који садрже неорганские соли Na₂SO₄ и Na₂CO₃ била су низа него код раствора боје без додатка соли.

(Примљено 29. јуна, ревидирано 1. августа 2011)

REFERENCES

1. K. Hunger, *Industrial Dyes: Chemistry, Properties, Applications*, Wiley VCH, Weinheim, 2003
2. P. C. Vandevivere, R. Bianchi, W. Verstraete, *J. Chem. Technol. Biotechnol.* **72** (1998) 289
3. J. Garcia-Montano, N. Ruiz, I. Munoz, X. Domenech, J. A. Garcia-Hortal, F. Torrades, J. Peral, *J. Hazard. Mater., A* **138** (2006) 218
4. A. Zille, T. Tzanov, G. M. Gübitz, A. Cavaco Paulo, *Biotechnol. Lett.* **25** (2003) 1473
5. T. Panswad, W. Luangdilok, *Water Res.* **34** (2000) 4177
6. J. T. Spadaro, L. Isabelle, V. Renganathan, *Environ. Sci. Technol.* **28** (1994) 1389
7. F. Harrelkas, A. Azizi, A. Yaacoubi, A. Benhammou, M. N. Pons, *Desalination* **235** (2009) 330
8. G. M. Walker, L. R. Weatherley, *Chem. Eng. J.* **84** (2001) 125
9. S. J. Masten, S. H. R. Davies, *Environ. Sci. Technol.* **28** (1994) 180A
10. P. R. Gogate, A. B. Pandit, *Adv. Environ. Res.* **8** (2004) 501
11. P. R. Gogate, A. B. Pandit, *Adv. Environ. Res.* **8** (2004) 553
12. Y. S. Mok, J. O. Jo, J. C. Whitehead, *Chem. Eng. J.* **142** (2008) 56
13. B. R. Locke, M. Sato, P. Sunka, M. R. Hoffmann, J. S. Chang, *Ind. Eng. Chem. Res.* **45** (2006) 882
14. B. Sun, M. Sato, J. S. Clements, *J. Phys. D: Appl. Phys.* **32** (1999) 1908
15. C. M. Du, T. H. Shi, Y. W. Sun, X. F. Zhuang, *J. Hazard. Mater.* **154** (2008) 1192



16. M. Magureanu, D. Piroi, N. B. Mandache, V. Parvulescu, *J. Appl. Phys.* **104** (2008) 103306
17. Z. Wang, D. Xu, Y. Chen, C. Hao, X. Zhang, *J. Electrostat.* **66** (2008) 476
18. A. Riga, K. Soutsas, K. Ntampaglis, V. Karayannidis, G. Papapolymerou, *Desalination* **211** (2007) 72
19. M. Sokmen, A. Ozkan, *J. Photochem. Photobiol., B* **147** (2002) 77
20. M. Muthukumar, N. Selvakumar, *Dyes Pigm.* **62** (2004) 221
21. D. R. Merouani, F. Abdelmalek, F. Taleb, M. Martel, A. Semmoud, A. Addou, *Arab. J. Chem.* (2011) doi: 10.1016/j.arabjc.2011.01.034
22. P. Bruggeman, C. Leys, *J. Phys., D* **42** (2009) 053001
23. X. Xu, *Thin Solid Films* **390** (2001) 237
24. U. Kogelschatz, *Plasma Chem. Plasma Process.* **23** (2003) 1
25. P. Lukes, M. Clupek, V. Babicky, V. Janda, P. Sunka, *J. Phys., D* **38** (2005) 409
26. B. P. Dojčinović, G. M. Roglić, B. M. Obradović, M. M. Kuraica, M. M. Kostić, J. Nešić, D. D. Manojlović, *J. Hazard. Mater.* (2011) doi:10.1016/j.jhazmat.2011.05.086
27. M. M. Kuraica, B. M. Obradović, D. Manojlović, D. R. Ostojić, J. Purić, *Vacuum* **73** (2004) 705
28. D. Manojlović, D. R. Ostojić, B. M. Obradović, M. M. Kuraica, V. D. Krsmanović, J. Purić, *Desalination* **213** (2007) 116
29. B. P. Dojčinović, D. Manojlović, G. M. Roglić, B. M. Obradović, M. M. Kuraica, J. Purić, *Vacuum* **83** (2008) 234
30. T. Zhou, X. Lu, J. Wang, F. S. Wong, Y. Li, *J. Hazard. Mater.* **165** (2009) 193
31. P. Lukes, M. Clupek, V. Babicky, P. Sunka, *Plasma Sources Sci. Technol.* **17** (2008) 1
32. B. Gözmen, B. Kayana, A. M. Gizir, A. Hesenov, *J. Hazard. Mater.* **168** (2009) 129
33. M. A. Rauf, S. Salman Ashraf, *J. Hazard. Mater.* **166** (2009) 6
34. M. Muruganandham, M. Swaminathan, *Dyes Pigm.* **68** (2006) 133
35. C. Liang, Z.-S. Wang, C. J. Bruell, *Chemosphere* **66** (2007) 106
36. F. Minisci, A. Citterio, C. Giordano, *Acc. Chem. Res.* **16** (1983) 27
37. G. R. Peyton, *Mar. Chem.* **41** (1993) 91
38. B. Sun, M. Sato, S. J. Clements, *J. Electrostat.* **39** (1997) 189.





Cadmium biosorption by baker's yeast in aqueous suspensions

KATALIN TÁLOS¹, TÍMEA PERNYESZI^{1*}, CORNELIA MAJDIK², ALZBETA HEGEDÜSOVA³ and CSILLA PÁGER¹

¹University of Pécs, Faculty of Science, Department of Analytical and Environmental Chemistry, 6 Ifjúság, H-7624 Pécs, Hungary, ²University Babeş-Bolyai, Faculty of Chemistry and Chemical Engineering, 11 Arany J., RO-400293 Cluj-Napoca, Romania and ³Department of Chemistry, Faculty of Natural Sciences, Constantine the Philosopher University, Tr. A. Hlinku 1, SK-949 01, Nitra, Slovakia

(Received 20 May, revised 30 August 2011)

Abstract: The biosorption of cadmium from artificial aqueous solutions using native baker's yeast was investigated. The highest metal uptake value was 110 mg g⁻¹ yeast in a suspension of 0.30 g L⁻¹. The effect of pH, initial cadmium concentration, adsorption time and biosorbent dosage on biosorption by baker's yeast was studied. The maximum biosorption capacity of yeast for cadmium was observed at pH 6.0. The adsorption equilibrium was reached within sixty minutes and the sorption process followed pseudo second-order kinetics. Cadmium biosorption isotherms were determined in the cadmium concentration range of 10–500 mg L⁻¹ at pH 6 in a suspension of 0.30 g L⁻¹. For evaluation of biosorption equilibrium, Langmuir and Freundlich equations were applied to the experimental data.

Keywords: cadmium; baker's yeast; biosorption; pH; kinetics; isotherm; biosorbent dosage.

INTRODUCTION

Heavy metal pollution has become one of the most serious environmental problems today. Cadmium is a heavy metal that poses serious health hazards through entry into the food chain by anthropogenic pathways. In the last decade, biosorption using microbial biomasses as sorbent materials has emerged as a cost-effective removal technique for the treatment of high volume and low concentration complex wastewaters containing heavy metal(s) at concentrations in the order of 1 to 100 mg L⁻¹ metal, compared to other processes such as chemical precipitation, evaporation, ion exchange and membrane separation. The conventional methods have disadvantages, including incomplete metal removal,

* Corresponding author. E-mail: ptimaea@ttk.pte.hu
doi: 10.2298/JSC110520181T

requirements for expensive equipment and monitoring systems, high reagent or energy requirements or generation of toxic sludge or other waste products that require disposal.^{1–3} The utilization of microorganisms (bacteria, fungi, yeast and algae) as biosorbents (biosorption) offers a potential alternative for heavy metal detoxification and the recovery and reuse of toxic/precious metals.⁴

In the concept of biosorption, several physical or chemical processes may be involved, such as physical and/or chemical adsorption, ion exchange, coordination, chelation and microprecipitation. Biomass cell walls, consisting mainly of polysaccharides, proteins and lipids, offer many functional groups, such as carboxylate, hydroxyl, sulfate, phosphate and amino groups, which can bind metal ions.^{2,5}

Some potential biomaterials with high metal-binding capacity have been identified in part. Algae, bacteria, fungi, yeast and waste microbial biomass from the fermentation and food industry are amongst them. For economic reasons, researchers have paid much attention to various by-products from the fermentation industry. The application of these waste microbes as biosorbents for the biosorption of heavy metals and radionuclides is to kill two birds with one stone because it uses waste to dispose of waste. The enterprises can sell their waste biomass and earn money, simultaneously, they can save the cost associated with disposing of the waste biomass they produced.^{2,5–9} A biomass used as a biosorbent must be selective and inexpensive.^{6,9} Among the promising biosorbents for heavy metal removal, *Saccharomyces cerevisiae* is still under consideration as a biomaterial due to its unique nature in spite of its mediocre capacity for metal uptake compared with other fungi. Yeast fungi are widely used for food and beverage production, are easily cultivated using cheap media, are also, as waste of the fermentation industry, a by-product produced in large quantities, and are easily manipulated at the molecular level.^{2,6–8} Yeasts have been studied in various forms, for example living cell/dead cell, intact cell/deactivated cell, immobilized cell/free cell, raw material/pretreated cell by physicochemical process, wild type/mutant cells, flocculent/non-flocculent cells, engineered/ non-engineered cells, lab culture/waste industrial cell, and cells from different industries.^{2,6–11}

However, little information exists on the use of commercial native baker's yeast as a biosorbent for metal removal. Yeast biosorption depends on several parameters, such as pH, the ratio of the initial metal ion and initial biomass concentrations, culture conditions, the presence of various ligands and competitive metal ions in solution, and on temperature to a limited extent.^{2,9,12–15}

The objectives of this study were:

- to test the recycling of native commercial baker's yeast biomass as a sorbent material for the immobilization of cadmium in polluted water,

- to evaluate using batch technique the influences of different experimental parameters, such as pH, sorption time, cadmium concentration and biosorbent dosage, on biosorption,
- to model cadmium biosorption kinetics by yeast using a second-order kinetic equation and
- to determine adsorption isotherms using batch technique and analyze the adsorption equilibrium using the Freundlich and Langmuir isotherm equations.

EXPERIMENTAL

Fungal biomass

The biosorbent was fresh and compressed baker's yeast (commercial yeast, "Budafok" Yeast and Spirit Factory, Budapest, Hungary). The baker's yeast was used as the sorbent material in natural commercial form. Its water content was 70 %. The determination of the water content was performed according to the protocol of the yeast factory (data obtained from the factory).

Chemicals

Cadmium nitrate ($\text{Cd}(\text{NO}_3)_2 \cdot 4\text{H}_2\text{O}$) (purity > 99 %) was purchased from Fluka (Switzerland) and used without further purification. The stock solution was prepared by dissolving 1.3718 g $\text{Cd}(\text{NO}_3)_2 \cdot 4\text{H}_2\text{O}$ in 1.0 L of distilled water. The test solutions were prepared by diluting 500 mg L^{-1} of stock solution to the desired concentrations. The cadmium concentration of the prepared test solutions varied between 5–500 mg L^{-1} in the sorption experiments. The pH of the suspensions was adjusted to the required value with 0.10 M HCl or 0.10 M NaOH solutions (Merck, Germany).

Analyses of cadmium

The concentration of cadmium was determined by atomic absorption spectrophotometry (Perkin–Elmer 2380) at 228.8 nm. The calibration of cadmium was made with standard cadmium solution (Scharlau, Germany) in the concentration range of 0–2.5 mg L^{-1} .

Effect of pH on the biosorption

The effect of pH on cadmium adsorption by baker's yeast was investigated using a 0.3 g L^{-1} suspension of baker's yeast and an initial cadmium concentration of 50 mg L^{-1} . The initial pH of the yeast suspension was 5.6, which was adjusted to the desired value in the range 2–11.

Zeta potential measurements

The zeta potential of aqueous suspensions of baker's yeast was measured with Zetameter instrument (Malvern Zetasizer nano ZS, UK). The suspensions were made from baker's yeast and distilled water. The suspensions contained 0.3 g L^{-1} yeast. After pH adjustment, the suspensions were stirred on a magnetic stirrer for 30 minutes and then the zeta potential was measured.

Kinetics study of biosorption

In the kinetics study of cadmium biosorption by baker's yeast, the concentrations of the metal ions were 5, 10, 25 and 50 mg L^{-1} at a suspension concentration of 0.30 g L^{-1} . The experimental time was 180 min. During the first 30 min of agitation at 250 rpm, samples were taken every 5 min, in the following 30 min every 10 min and in the following 2 h every 15 min. The samples were centrifuged at 5500 rpm for 10 min and the supernatants diluted for analysis by atomic absorption spectrophotometry.

Determination of biosorption isotherms

Biosorption experiments were performed in the batch mode for the determination of the adsorption isotherms. The concentrations of baker's yeast in the suspensions were 0.3, 0.6, 1.5 and 3.0 g L⁻¹. The initial concentration of cadmium was varied between 10–500 mg L⁻¹. A defined mass of biosorbent and a defined volume of cadmium solution were placed in a test-tube. The tubes were agitated on a shaker at 150 rpm at a constant temperature (22.5±1 °C). Samples were taken after 24 h and then spin-dried at 5500 rpm for 10 min. The supernatants were used for analysis of the residual amount of cadmium. The adsorbed amount of cadmium at time *t*, *q_t* (mg g⁻¹), was obtained as follows:

$$q_t = \frac{(c_0 - c_t)V}{m} \quad (1)$$

where *c₀* and *c_t* are the initial and at time *t* liquid phase cadmium concentrations (mg L⁻¹), *V* is the volume of the solution (L) and *m* is the mass of the dry biomass used (g).

Correspondingly, the adsorbed amount of cadmium at equilibrium, *q_e* (mg g⁻¹), is given by:

$$q_{eq} = \frac{(c_0 - c_{eq})V}{m} \quad (2)$$

where *c_{eq}* is the concentration of cadmium in the supernatant at equilibrium (mg L⁻¹).

RESULTS AND DISCUSSION

Effect of solution pH and zeta potential on the adsorption of cadmium

Previous studies on heavy metal biosorption showed that the pH value of the solution is an important factor in both the solution chemistry of the metal and the surface characteristics of the biosorbent.^{2,5,9,13–18} The effect of the initial pH on cadmium biosorption by yeast biomass is presented in Fig. 1. The biomass concentration was 0.30 g L⁻¹ and the initial metal concentration was 50.0 mg L⁻¹.

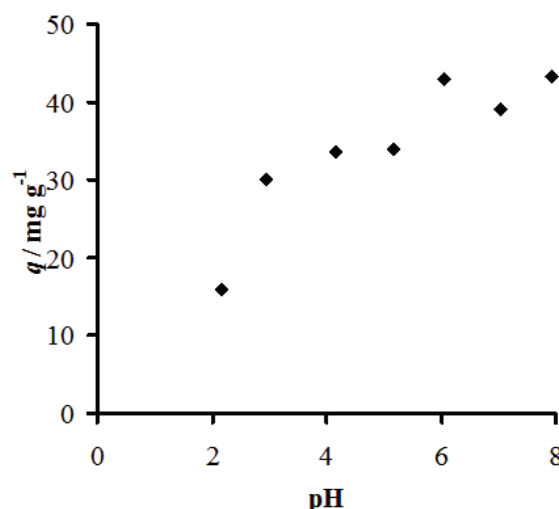


Fig. 1. The effect of pH on cadmium biosorption on baker's yeast. The biomass concentration was 0.30 g L⁻¹ and the initial cadmium concentration was 50 mg L⁻¹.

The cadmium biosorption capacity of biosorbent increased with increasing pH from 2.0 to 6.0. The highest metal uptake value obtained for cadmium was 42.9 mg g^{-1} . At the pH values of greater than pH 8.0, the cadmium ions precipitated as Cd(OH)_2 due to the increasing concentration of OH^- in the solution. For this reason, the experiments were not conducted at higher pH values. It is well known that at low pH values, cell wall ligands are closely associated with hydronium ions, which restrict the approach of positively charged metal ions because of the repulsive force. As the pH increases, more ligands carrying negative charges would be exposed, with the subsequent attraction of metal cations and biosorption onto the binding sites on the cell surface.⁷ The values of the zeta potential of the biomass at different pH values are shown in Fig. 2. The zeta potential value of the biomass was -0.61 mV at pH 2.2 and the overall surface of the biomass was negatively charged at the pH values between 2.2 and 11.0. The zeta potential values varied from -0.61 mV at pH 2.2 to -35.8 mV at pH 11.

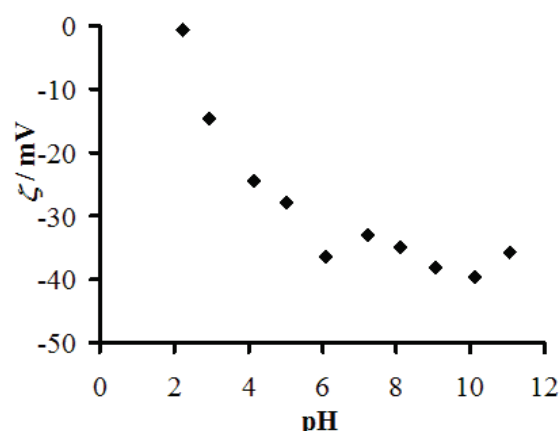


Fig. 2. Effect of pH on the zeta potential of baker's yeast cells in aqueous suspension. The biomass concentration was 0.30 g L^{-1} .

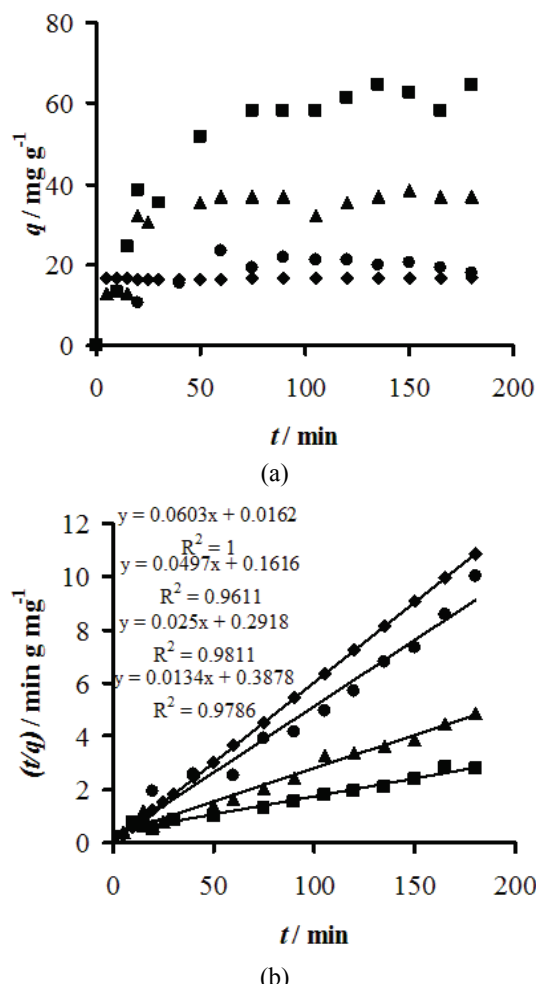
Several researchers have also investigated the effect of pH on the biosorption of cadmium by microbial biomass and similar results were reported. Shu-Juan *et al.* found that the adsorption rate of cadmium by *S. cerevisiae* from a brewery is low when the pH is lower than 4.0. Better adsorption results were obtained in the pH range of 4.0–7.0, and the percent adsorption reached 83.7 % when the pH was 6.0.¹⁸ Vasudevan *et al.*¹⁴ also reported that the cadmium ion adsorption capacity of a commercial yeast increased with increasing pH and it had a maximum at pH 6.5.¹⁴ Experiments were not conducted beyond pH 7.0 to avoid possible hydroxide precipitation.¹⁴ Göksungur *et al.*⁵ studied cadmium and lead biosorption by ethanol-treated waste baker's yeast. The maximum biosorption of the heavy metal ions by the yeast were observed at pH 6.0 for cadmium and at pH 5.0 for lead.²

Effect of contact time and initial cadmium concentration on biosorption

Adsorption equilibrium studies are important to determine the efficiency of adsorption. With the purpose of investigating the mechanism of biosorption and its potential rate-controlling steps that include mass transport and chemical reaction processes, kinetic models have been exploited to test the experimental data.

Adsorption kinetics is expressed as the solute removal rate that controls the residence time of the sorbate at the solid–solution interface.

The kinetics of cadmium adsorption was investigated using a concentration of baker's yeast in the suspension of 0.3 g L^{-1} at pH 6. The initial cadmium concentrations were 5.0, 12.5, 25.0 and 50.0 mg L^{-1} . The amounts of adsorbed cadmium against the adsorption time are presented in Fig. 3a. The biosorption



Figs. 3. a) The effect of the initial cadmium concentration on the kinetics of cadmium sorption by baker's yeast. b) Linearized pseudo second-order kinetic model for cadmium adsorption by baker's yeast at different initial cadmium concentrations. Initial concentrations: 5.0 (♦); 12.5 (●); 25.0 (▲); 50.0 mg L⁻¹ (■), temperature: 22.5 °C, biomass concentration: 0.30 g L⁻¹.

process of heavy metal by *S. cerevisiae* usually occurs rapidly.^{2,4,13,14} The adsorption rate was higher in the first thirty minutes and then decreased until equilibrium was reached. Similar trends were found by other workers.^{2,14} By investigating the biosorption of Cr(VI) and Fe(III) on *Streptococcus equisimilis*, *S. cerevisiae* and *Aspergillus niger*, Goyal *et al.*¹⁹ confirmed that metal uptake by the microorganisms proceeds in two stages: a passive uptake that occurs immediately and an active uptake that progresses slowly.¹⁹ The first stage is thought to be physical adsorption or ion exchange at the cell surface, reaching the adsorption equilibrium within 30–40 min at the end of the rapid physical adsorption. Vasudevan *et al.* found that the process of cadmium biosorption by inactive and protonated cells of *S. cerevisiae* was dependent on the availability of metal ion in aqueous solution or the metal ion concentration.¹⁴ However, the researchers suggested that the adsorption process occurred in four distinct steps and the rates for these steps decreased sequentially. The rate of cadmium (II) uptake in each case was pseudo second-order, with respect to the metal ion concentration. It should be noticed that the adsorption of cadmium increased with increasing sorption time.^{4,12}

When the initial cadmium concentration was 5.0 mg L⁻¹, the adsorption equilibrium was attained within 5 minutes, while when it was 12.5, 25.0 or 50.0 mg L⁻¹, equilibrium was reached within 60 min.

In adsorption equilibrium, at an initial cadmium concentration of 5.0 mg L⁻¹, the maximal adsorbed cadmium amount $q_{\text{eq,exp}}$ was 16.5 mg g⁻¹, at an initial concentration of 12.5 mg L⁻¹, $q_{\text{eq,exp}}$ was 20.1 mg g⁻¹, at initial concentration of 25.0 mg L⁻¹, $q_{\text{eq,exp}}$ was 36.5 mg g⁻¹ and at initial concentration of 50 mg L⁻¹, $q_{\text{eq,exp}}$ was 60.7 mg g⁻¹.

Kinetic modeling

The pseudo first- and second-order kinetic models are the most employed models to study the biosorption kinetics of heavy metals and to quantify the extent of uptake in biosorption kinetics.^{9,12,16,21} For an evaluation of the cadmium bioadsorption kinetics, two kinetic models were used to fit the experimental data at 5.0, 12.5, 25.0 and 50.0 mg L⁻¹ initial cadmium concentrations at pH 6. The pseudo first-order Lagergen model could not be applied to the experimental results of the kinetics of cadmium biosorption by baker's yeast, as the correlation coefficients for the pseudo first-order kinetics were lower than those for the pseudo second-order one. For this reason, the application of the pseudo second-order kinetic model will be pursued for an evaluation of the cadmium bioadsorption kinetics.

If the sorption rate is second-order, the pseudo second-order kinetic rate equation is expressed as:²²

$$\frac{dq}{dt} = k_{2,ad} (q_{eq} - q)^2 \quad (2)$$

where $k_{2,ad}$ is the rate constant of the second-order biosorption ($\text{g mg}^{-1}\cdot\text{min}^{-1}$). After integration, the following equation is obtained:

$$\frac{t}{q} = \frac{1}{k_{2,ad} q_{eq}^2} + \frac{t}{q_{eq}} \quad (3)$$

It should be noticed that for the utilization of this model, it is not necessary for the experimental value of q_{eq} to be pre-estimated. By plotting t/q against t for the initial concentrations (5.0, 12.5, 25.0, 50.0 mg L^{-1}), straight lines were obtained, as shown in Fig. 3b. The values of the second-order rate constants $k_{2,ad}$ and q_{eq} , determined from the slopes and intercepts of the plots, respectively, are presented in Table I.

TABLE I. The second-order adsorption rate constants of cadmium adsorption for different initial concentrations, at pH 6.0, temperature: 22.5 °C, biomass concentration: 0.30 g L^{-1}

$c_0 / \text{mg L}^{-1}$	$k_{2,ad} / \text{g mg}^{-1} \text{min}^{-1}$	$q_{eq,cal} / \text{mg g}^{-1}$	R^2	$q_{eq,exp} / \text{mg g}^{-1}$
5.0	0.22	16.6	1.000	16.5
12.5	1.5×10^{-2}	20.1	0.961	20.1
25.0	2.1×10^{-3}	40	0.981	36.5
50.0	4.6×10^{-4}	74.6	0.979	60.7

The correlation coefficients for the second-order kinetic model were close to 1.0 for all cases, and the theoretical values of q_{eq} also agreed well with the experimental data (Table I). The values of second-order rate constant $k_{2,ad}$ were in the range of 4.6×10^{-4} –0.22 $\text{g mg}^{-1}\cdot\text{min}^{-1}$. This suggests that the sorption of cadmium by baker's yeast follows second-order kinetics. The second-order kinetic parameters can be used to determine the equilibrium sorption capacity, the percent removal of cadmium, the rate constants and the initial sorption rate to facilitate bioreactor design.

Adsorption isotherms

The adsorption isotherms of cadmium adsorption by baker's yeast were determined in aqueous suspension using the batch technique. The adsorption isotherms of the adsorption of cadmium ions by baker's yeast in the initial concentration range of 10–500 mg L^{-1} are displayed in Fig. 4a. The adsorption isotherms determined in the low concentration range of 5–25 mg L^{-1} are shown in Fig. 4b. The biomass concentration was 0.30 g L^{-1} in both cases.

It can be observed from Figs. 4a and 4b that the uptake of cadmium by the biomass almost linearly increases with increasing initial cadmium concentration in solution. At an equilibrated concentration of 136.9 mg L^{-1} ($c_0 = 214 \text{ mg L}^{-1}$),

$q_{\text{eq,exp}} = 263.8 \text{ mg g}^{-1}$ and at ($c_0 = 52 \text{ mg L}^{-1}$) an equilibrated concentration of 32.6 mg L^{-1} ($c_0 = 52 \text{ mg L}^{-1}$), $q_{\text{eq,exp}} = 59.9 \text{ mg g}^{-1}$.

Equilibrium modeling

The analysis of equilibrium is important for developing a model that can be used for the design of biosorption systems. Several isotherm equations have been used for equilibrium modeling of biosorption systems.¹² Two classical adsorption models, Langmuir and Freundlich isotherms, are the most frequently employed. In this work, the Freundlich and Langmuir models were used to describe the relationship between the amounts of cadmium adsorbed and its equilibrium concentration in solution.

Freundlich isotherm

The Freundlich isotherm is capable of describing the adsorption of organic and inorganic compounds onto a wide variety of adsorbents, including biosorbents. The Freundlich Equation based on sorption onto a heterogeneous surface is:

$$q_{\text{eq}} = K_F c_{\text{eq}}^{1/n} \quad (4)$$

where K_F and n are the Freundlich constants, which are indicators of the adsorption capacity and adsorption intensity of the sorbent. Eq. (4) can be linearized in logarithmic form as follows:

$$\log q_{\text{eq}} = \log K_F + \frac{1}{n} \log c_{\text{eq}} \quad (5)$$

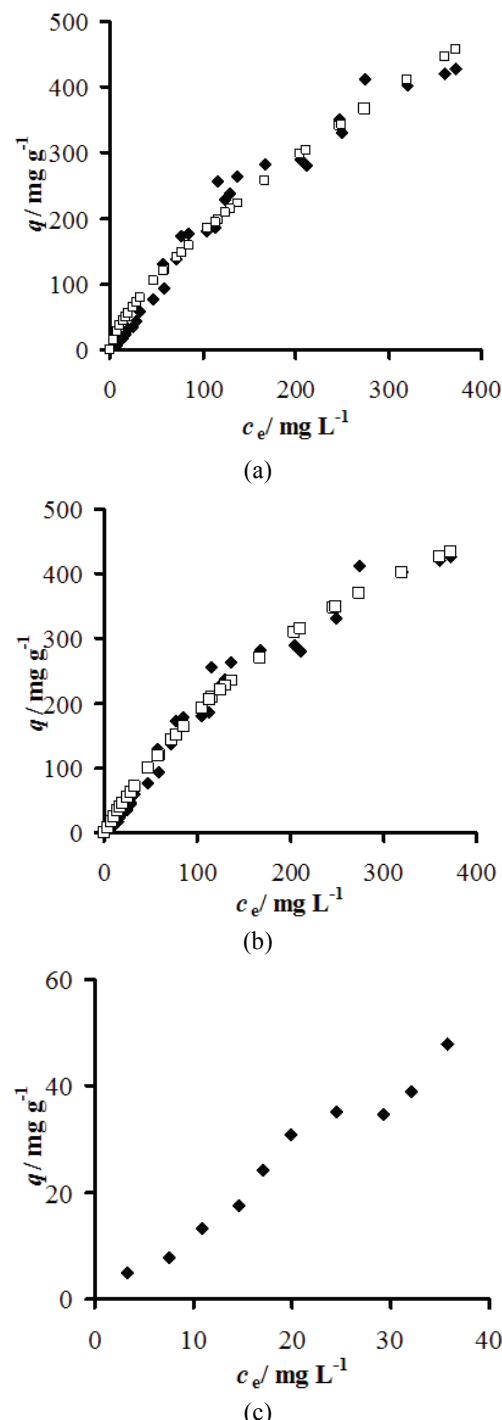
A plot of $\log q_{\text{eq}}$ vs. $\log C_{\text{eq}}$ has a slope with the value of $1/n$ and an intercept of $\log K_F$. $\log K_F$ is equivalent to $\log q_{\text{eq}}$ when $1/n$ equals unity. However, in other case, when $1/n \neq 1$, the K_F value depends on the units in which q_{eq} and C_{eq} are expressed. The experimental cadmium adsorption and non-linearly fitted (using Gnuplot software) by Freundlich model isotherms can be seen in Fig 4a. The values of K_F and n calculated are $6.5 \text{ [(mg g}^{-1}) (\text{mg L}^{-1})]^n$ and 1.4 , respectively (Table II).^{12,23}

Langmuir Isotherm

The Langmuir Isotherm is valid for monolayer adsorption onto a surface with a finite number of identical sites. It is given as:

$$q_{\text{eq}} = \frac{Q^0 b c_{\text{eq}}}{1 + b c_{\text{eq}}} \quad (6)$$

where c_{eq} and q_{eq} are equilibrium concentration (mg L^{-1}) and the amount adsorbed at equilibrium time (mg g^{-1}), respectively. Q^0 and b are Langmuir



Figs. 4. Adsorption isotherms of cadmium by baker's yeast from aqueous solutions at a biomass concentration of 0.30 g L^{-1} and initial cadmium concentrations in the range a) $0\text{--}500 \text{ mg L}^{-1}$ ♦ – experimental data, □ – non-linear fitted data using the Freundlich Equation; b) ♦ – experimental data, □ – non-linear fitted data using the Langmuir Equation; c) adsorption isotherm in the initial concentration range of $5\text{--}25 \text{ mg L}^{-1}$.

constants related to the capacity and energy of adsorption, respectively. The linearized form of the Langmuir Equation is:

$$\frac{c_{\text{eq}}}{q_{\text{eq}}} = \frac{1}{Q^0 b} + \frac{c_{\text{eq}}}{Q^0} \quad (7)$$

Q^0 and b can be determined from a linear plot of $c_{\text{eq}}/q_{\text{eq}}$ vs. c_{eq} .⁸

The experimental cadmium adsorption and the non-linearly fitted (using Gnuplot software) by the Langmuir model isotherm can be seen in Fig. 4b. The calculated values of b and Q^0 are 2.8×10^{-3} L mg⁻¹ and 852.6 mg g⁻¹, respectively (Table II). The calculated monomolecular adsorption capacity Q^0 is fits well to the experimental value.

TABLE II. Bioadsorption isotherm constants for the biosorption of cadmium onto baker's yeast

Isotherm	$K_F / [(\text{mg g}^{-1})(\text{mg L}^{-1})]^n$	n	$b / \text{L mg}^{-1}$	$Q^0 / \text{mg g}^{-1}$
Langmuir	—	—	2.8×10^{-3}	852.6
Freundlich	6.5	1.4	—	—

Biosorption yield

The biosorption yields are presented against the suspension concentrations at an initial cadmium concentration of 50.0 mg L⁻¹ in Fig. 5. The biomass concentrations were 0.30, 0.60, 1.5 and 3.0 g L⁻¹. Increasing of biomass concentration from 0.30 to 3.0 g L⁻¹ caused the biosorption yield to increase up to 38 %. Above a biomass concentration of 1.5 g L⁻¹, the biosorption yield did not change significantly.

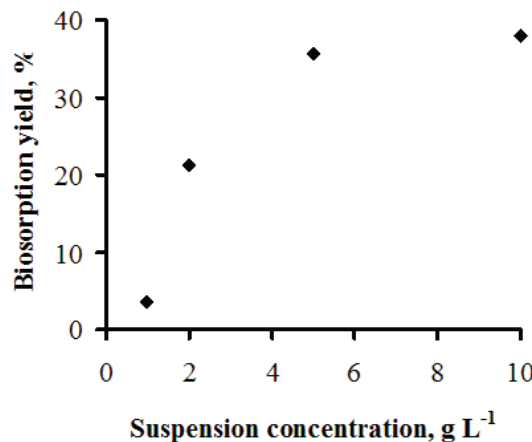


Fig. 5. Effect of the suspension concentration of biomass on cadmium biosorption onto baker's yeast. The initial cadmium concentration was 50.0 mg L⁻¹.

CONCLUSIONS

The biosorption properties of waste baker's yeast (*S. cerevisiae*) were studied for cadmium removal from aqueous suspension. The initial heavy metal concentration, pH of the solution and contact time were found to have an effect on the bioadsorption capacity of the biomass. The maximal biosorption capacity was determined at pH of 6.0. With increasing initial cadmium concentration and contact time, the amount of cadmium adsorbed increased as well. The biosorption kinetics followed pseudo second-order kinetics. The Freundlich Equation and the Langmuir adsorption model were used for a mathematical description of the biosorption of cadmium onto native baker's yeast. It was found that the adsorption equilibrium data fitted well to the Freundlich and Langmuir Models. With increasing biomass concentration, the adsorption efficiency increased significantly up to a biomass dosage of 1.5 g L^{-1} . It seems that the use of readily available waste baker's yeast from the fermentation industry offers an alternative in the removal of metals from contaminated waters.

Acknowledgements. Timea Pernyeszi, Katalin Tálos and Alžbeta Hegedűsova gratefully acknowledge support for this research from the Hungarian–Slovak Intergovernmental & Cooperation Program (APVV SK–HU 0018-08, SK-18/2008) between the University of Pécs and Constantine the Philosopher University for 2009–2011. Timea Pernyeszi, Katalin Tálos and Cornelia Majdik gratefully acknowledge support for this research from the Hungarian–Romanian Intergovernmental and Cooperation Program between University of Pécs and University of Babes-Bolyai for 2008–2009 (RO-15/2007).

И З В О Д

БИОСОРПЦИЈА КАДМИЈУМА ПЕКАРСКИМ КВАСЦЕМ У ВОДЕНОЈ СУСПЕНЗИЈИ

KATALIN TÁLOS¹, TÍMEA PERNYESZI¹, CORNELIA MAJDIK², ALZBETA HEGEDŰSOVA³ и CSILLA PÁGER¹

¹*University of Pécs, Faculty of Science, Department of Analytical and Environmental Chemistry, 6 Ifjúság,
H-7624 Pécs, Hungary*, ²*University Babes-Bolyai, Faculty of Chemistry and Chemical Engineering, 11 Arany
J., RO-400293 Cluj-Napoca, Romania* и ³*Department of Chemistry, Faculty of Natural Sciences, Constantine
the Philosopher University, Tr. A. Hlinku 1, SK-949 01, Nitra, Slovakia*

Испитана је биосорпција кадмијума из вештачких водених растворова помоћу изворног пекарског квасца. Највиша вредност преузете количине била је 110 mg g^{-1} у сусpenзији од $0,30 \text{ g L}^{-1}$. Истраживани су утицаји pH, почетне концентрације кадмијума, адсорpcionог времена и дозе биосорбента на биосорпцију помоћу пекарског квасца. Максимални капацитет биосорпције кадмијума квасцем био је уочен на pH 6. Адсорpcionа равнотежа је била достигнута након 60 min, а процес сорпције је пратио кинетику псевдо-другог реда. Изотерме биосорпције кадмијума одређене су у опсегу концентрација кадмијума од 10 до 500 mg L^{-1} при pH 6 у сусpenзији од $0,30 \text{ g L}^{-1}$. За процену равнотеже биосорпције, на експерименталне податке су примењене Лангмирове и Фроиндлихове једначине.

(Примљено 20. маја, ревидирано 30. августа 2011)

REFERENCES

1. Z. Aksu, G. Egretli, T. Kutsal, *J. Environ. Health* **34** (1999) 295



2. Y. Göksungur, S. Üren, U. Güvenc, *Bioresour. Technol.* **96** (2005) 103
3. P. A. Marques, J. A. Pinheiro, M. F. Rosa, *Desalination* **214** (2007) 343
4. F. Veglio, F. Beolchini, *Hydrometallurgy* **44** (1997) 301
5. Y. Göksungur, S. Üren, U. Güvenc, *Turk. J. Biol.* **27** (2003) 23
6. A. Kapoor, T. Viraraghavan, *Bioresour. Technol.* **53** (1995) 195
7. F. Ghorbani, H. Younesi, S. M. Ghasempouri, A. A. Zinatizadeh, M. Amini, A. Daneshi, *Chem. Eng. J.* **145** (2008) 267
8. P. Marques, H. M. Pinheiro, M. F. Rosa, *Desalination* **214** (2007) 343
9. J. Wang, C. Chen, *Biotechn. Adv.* **24** (2006) 427
10. W. Jianlong, *Process Biochem.* **37** (2002) 847
11. A. Menegário, P. S. Tonello, S. F. Durrant, *Anal. Chim. Acta* **683** (2010) 107
12. J. Febrianto, A. N. Kosasih, J. Sunarso, Y. H. Ju, N. Indraswati, S. Ismadji, *J. Hazard. Mater.* **162** (2009) 616
13. P. Marques, H. M. Pinheiro, J. A. Teixeira, M. F. Rosa, *Desalination* **124** (1999) 137
14. P. Vasudevan, V. Padmavathy, S. C. Dhingra, *Bioresour. Technol.* **89** (2003) 281
15. Sz. Tonk, A. Măicăneanu, C. Indolean, S. Burca, C. Majdik, *J. Serb. Chem. Soc.* **76** (2011) 363
16. Z. Aksu, *Sep. Purif. Technol.* **21** (2001) 285
17. A. Çabuk, T. Akar, S. Tunali, S. Gedikli, *Chem. Eng. J.* **131** (2007) 293
18. D. Shu-Juan, W. De-Zouo, Z. Dong-Qin, J. Chun-Yun, W. Yu-Juan, L. Wen-gang, *Trans. Non-Ferrous Metals Soc. China* **18** (2008) 1008
19. N. Goyal, S. C. Jain, U. C. Banerjee, *Adv. Environ. Res.* **7** (2000) 311
20. D. Brady, J. R. Duncan, *Appl. Microbiol. Biotechnol.* **41** (1994) 149
21. C. C. V. Cruz, A. C. A. da Costa, C. A. Henriques, A. S. Luna, *Bioresour. Technol.* **91** (2004) 249
22. Z. Aksu, S. Tezer, *Process Biochem.* **36** (2000) 431
23. A. Delle Site, *J. Phys. Chem. Ref. Data* **30** (2001) 187.



J. Serb. Chem. Soc. 77 (4) 563–567 (2012)

Journal of the Serbian Chemical Society

JSCS@tmf.bg.ac.rs • www.shd.org.rs/JSCS

UDC 543+061.3(4)

EuCheMS news



DIVISION OF ANALYTICAL CHEMISTRY
EUROPEAN ASSOCIATION FOR CHEMICAL AND
MOLECULAR SCIENCES

EUCHEMS NEWS

European Analytical Column No. 40

Analytical chemistry in Europe – education, research, publications and conferences

(January 2012)

JIRI BAREK¹, REINER SALZER², PAUL WORSFOLD³
and JENS E. T. ANDERSEN^{4*}

¹Charles University in Prague, Faculty of Science, Department of Analytical Chemistry, Albertov 6, CZ 128 43 Prague 2, Czech Republic, ²Dresden University of Technology, Department of Chemistry and Food Chemistry, D 01062 Dresden, Germany, ³School of Geography, Earth and Environmental Sciences, University of Plymouth, Plymouth PL4 8AA, UK and ⁴Department of Chemistry, Technical University of Denmark, Building 207, 2800 Lyngby, Denmark

COMMENT

Introduction

Modern analytical methods are indispensable in many disciplines, including medicine, biology and environmental protection, as well as being fundamental to chemistry and chemical technology. Nearly 50% of EU laws and regulations require strict analytical measurements to monitor compliance. Prof M. Grasserbauer expressed this eloquently at EUROANALYSIS XIII in 2004 in Salamanca in his statement that “Analytical Chemistry is indispensable to democratic governance”. This is supported by the number of batch analyses per year carried out in Europe (*ca.* 10¹⁰) and the astronomical amount of data resulting from continuous analytical monitoring. Nearly 70% of European chemists consider chemical analysis as either the main or an extremely important part of their job description. In the field of Analytical Chemistry more than 100,000 papers are generated in Europe alone every year. Therefore it is not surprising that Analytical Science was proclaimed as a breakthrough science by EuCheMS. It is clearly stated in its documents that the need for analytical measurements arises in all research

*Corresponding author. E-mail: jeta@dac-euchems.org; jeta@kemi.dtu.dk

disciplines, industrial sectors and human activities that entail the need to know not only the identities and amounts of chemical components in a mixture, but also how they are distributed in space and time. Recent developments in this area have underpinned major advances in the biosciences, such as genome mapping and diagnostics. Further developments will improve our capability for real time and remote analysis and miniaturisation will enhance our ability to undertake *in situ* and *in vivo* analysis. Increasing globalisation of analytical chemistry, together with the increasing range of tasks within its remit, put an escalating burden on analytical chemists with regard to education, research and development of new analytical methods and approaches, their publication and, above all, their practical application in everyday life. The activities of EuCheMS-DAC [1] are focused in this direction and can provide helpful support in addressing these demanding challenges as demonstrated in the following paragraphs. In our opinion the main task of DAC is to promote analytical chemistry, *e.g.* by attracting more young people to study this exciting field of chemistry and increasing general awareness of the importance of the subject.

Teaching of analytical chemistry

In spite of its growing importance, chairs of Analytical Chemistry are not very common in the older EU countries and the outlook in the newer EU countries is also not too optimistic. Therefore, most people working in the field of analytical chemistry are not graduates from departments specialising in analytical chemistry education. Learning by doing is a well-known slogan in our rapidly changing world but it would probably be useful, and indeed beneficial, for society to educate graduates who are fit for their job at an early stage. DAC has traditionally paid great attention to appropriate education in the subject, which resulted in the Eurocurriculum of Analytical Chemistry. This Eurocurriculum was supported and approved by all EuCheMS member societies and a well-known and well accepted textbook has been written on the basis of this Eurocurriculum [2]. Further developments in this field resulted in Eurocurriculum II [3]. This document incorporates the requirements of the Bologna Process [4] and is a very good starting point for all further effort in this field. For many years the comprehensive biennial analytical congress EUROANALYSIS (the flagship DAC event) has fostered a special session devoted to education, and such a session will be incorporated in EUROANALYSIS XVII, which will be held on August 23-25, 2013 in Warsaw, Poland [5]. From this point of view the activities of the DAC Study Group Education are very important and can greatly contribute to further improvements in analytical chemistry education. However, a crucial role in this process must inevitably be played by individual teachers of the subject, *i.e.* individual analytical chemists who love, and can enthuse about, their science. Such people are encouraged to submit contributions to the special ses-

sion describing their experiences, in particular in areas such as “Pitfalls in Education in Analytical Chemistry” and “Models for Education in Analytical Chemistry”.

The constant evolution and fine tuning of the education of analytical chemists in Europe is important from the perspective of *e.g.* student exchanges, joint PhD projects and ERASMUS exchange programmes. In this regard it is necessary to mention the extensive activities of the European Chemistry Thematic Network Association (ECTNA) [6] which have resulted in the Chemistry Euro-bachelor and Chemistry Euromaster labels and - since this year – the Chemistry Doctorate Eurolabel [7]. DAC is ready to support any effort in this field because without appropriate education there will not be a bright future for analytical chemistry in Europe.

Research in analytical chemistry

Many recent developments in analytical chemistry have been connected more with technical and/or technological progress than with new discoveries. The centre of gravity has moved from chemistry to physics (the construction and development of expensive instrumentation based more on physical than chemical principles) and to biology (the application of biological principles for analyte recognition and the construction of smart sensors). The increasing cost of sophisticated instrumentation simultaneously generates a pressure to develop simple and inexpensive methods suitable for large scale monitoring. Fundamentally new principles useful for analytical chemistry can be expected to originate at the interface between various disciplines and the communication between scientists from different disciplines is of paramount importance in this regard. These changes in research directions also require changes in our educational practice [8]. DAC assists in this process by organising the biennial EUROANALYSIS conference and inviting people to attend from different fields that are important for the further development of Analytical Chemistry.

Publication in analytical chemistry

As in all branches of sciences, analytical chemists are under increasing pressure to generate quantifiable outputs (*i.e.* increasing number of papers in high impact factor journals) which serve as a basis for their evaluation, further grant support, etc. It remains questionable if this pressure really improves science in general and analytical chemistry in particular as it can lead to an increasing number of papers of decreasing quality. Moreover, the increasing volume of published data makes it very difficult to follow recent developments, even in a relatively narrow field of research. New journals (especially web-based) are introduced nearly every week. Analytical chemists, as members of the world-wide scientific community, have to follow these trends in order not to lose research income and scientific status. Nonetheless it is important that a balance is found

and that outputs are targeted at appropriate journals (with particular reference to their scope), demonstrate clear novelty AND added value compared with published work and include robust method validation.

The role of EuCheMS-DAC

As stated above, DAC is very active, especially in the field of education of Analytical Chemistry and in the organisation and support of analytical chemistry oriented events such as conferences, seminars and meetings. Our Polish colleagues are very active in their preparations for the above mentioned EUROANALYSIS conference in Warsaw. A listing of other interesting conferences sponsored by DAC can be found on its web pages [1]. Among these is the 12th Eurasia Conference on Chemical Sciences on April 16–20, 2012 at Corfu, Greece [9]. Analytical Chemistry will also be well represented at the 4th EuCheMS Chemistry Congress in Prague, Czech Republic, on August 26–30, 2012 [10]. The analytical programme will include sessions on electroanalytical methods, separation methods, spectroscopic methods and chemometrics, as well as application based contributions, *e.g.*, in environmental analysis and bioanalysis, and will be of interest to a broad spectrum of Analytical Chemists. In addition, the 1st International Conference on Analytical Chemistry (ROICAC 2012) will be held in Targoviste, Romania on September 18–21, 2012 [11].

INFORMATION FROM THE EUCHEMS DIVISION OF ANALYTICAL CHEMISTRY

The 2011 Annual Meeting (42nd Meeting of EuCheMS-DAC) was held in Belgrade, Serbia, the venue for Euroanalysis XVI. Sixteen EuCheMS Societies were represented. Two DAC Steering Committee Meetings were held during the year: London on April 5th 2011 and Belgrade on 9th September 2011. The Royal Society of Chemistry and the Serbian Chemical Society are thanked for their hospitality. The Steering Committee membership for 2012 is: Paul Worsfold (Chair, Royal Society of Chemistry), Jens Andersen (Secretary, Danish Chemical Society), Wolfgang Buchberger (Austrian Society for Analytical Chemistry), Slavica Ražić (Serbian Chemical Society), Jiri Barek (Czech Chemical Society) and Maciej Jarocz (Polish Chemical Society). The Secretary of DAC will retire by the end of 2012 and Wolfgang Buchberger has kindly agreed to become the new Secretary. The 2012 Annual Meeting will be held in Prague on 26th August 2012. Two DAC Steering Committee Meetings will be held during 2012, one in Warsaw and one in Prague (co-incident with ECC4).

Euroanalysis XVI was held in Belgrade, Serbia, September 11–15, 2011. The Chairpersons were Prof Dr Slavica Ražić and Prof Dr Ivanka Popović. This was a highly successful Conference and attracted 600 participants. Further details can be found at www.euroanalysis2011.rs. The Robert Kellner Lecture (RKL) jury selected Prof Jonas Bergquist from Uppsala University for the 2011 RKL award and the lecture was delivered as a Plenary Lecture in Belgrade. The 2011

EuCheMS Lecture was also presented as a Plenary Lecture in Belgrade by Prof Alfredo Sanz-Medel from the University of Oviedo, Spain.

Euroanalysis XVII will be held in Warsaw, Poland, August 25–29, 2013 and the Chairperson is Prof Dr Maciej Jarosz. Further details can be found at www.euroanalysis2013.pl. Euroanalysis XVIII will be held in Bordeaux, France in 2015 under the auspices of the Société Chimique de France. The Chairpersons are Prof Philippe Garrigues and Dr Christian Rolando.

DAC will have 5 active Study Groups in 2012:

- “Education in Analytical Chemistry”; Head: Prof Reiner Salzer.
- “Quality Assurance and Accreditation”; Head: Dr Jens Andersen. Prof Hendrik Emons will act as DAC liaison person to CITAC. Dr Heiner Korte will chair a sub-committee of this Study Group to provide feedback on the proposed changes to SI units.
- “History”; Head: Prof Duncan Burns.
- “Bioanalytics”; Head: Prof George Horvai.
- “European AC on the web”; Head: Prof Bo Karlberg.

A Task Force on “Chemometrics” will also operate in 2012, headed by Prof Roma Tauler.

The following meetings/networks will be organised in co-operation with EuCheMS-DAC:

- 13th Conference on Instrumental Analysis (JAI), EXPOQUIMIA, 14–16 November, 2011, Barcelona, Spain.
- 12th Eurasia Conference on Chemical Sciences, April 16–20, 2012, Corfu, Greece.
- Analysdagarna, 11–13 June, 2012, Uppsala, Sweden.
- European Chemistry and Chemical Engineering Education Network (EC2E2N, www.ec2e2n.net).

REFERENCES

1. <http://www.dac-euchems.org>
2. Analytical Chemistry - A Modern Approach to Analytical Science. 2nd Edition Edited by R. Kellner, J.-M. Mermet, M. Otto, M. Valcárcel, H.M. Widmer. Wiley-VCH 2004
3. R. Salzer, *Anal. Bioanal. Chem.* **378** (2004) 28 (see http://www.dac-euchems.org/reports/education/eurocurriculum_II.pdf)
4. <http://www.ond.vlaanderen.be/hogeronderwijs/bologna/>
5. <http://www.euroanalysis2013.pl/>
6. <http://ectn-assoc.cpe.fr/network/index.htm>
7. <http://ectn-assoc.cpe.fr/eurobachelor/>
8. R. Salzer, *Analyt. Bioanalyt. Chem.* **402** (2012) 25
9. <http://eurasia12.uoi.gr/>
10. <http://euchems-prague2012.cz/>
11. <http://www.icstm.ro/ICAC2012>.

